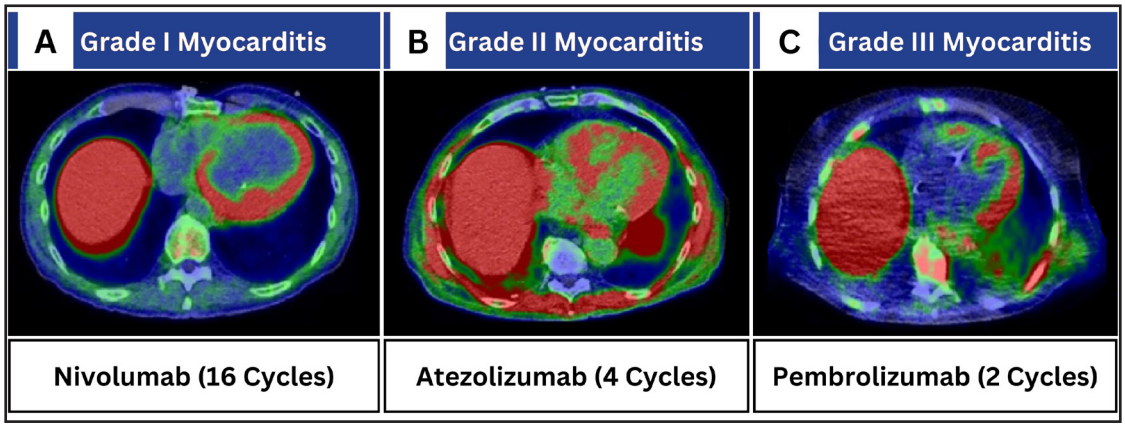
E-ISSN: 2147-1959

# MIRT

## Molecular Imaging and Radionuclide Therapy

October 2025 Volume 34 Issue 3 www.tsnm.org




"Official Journal of the Turkish Society of Nuclear Medicine"

galenos yayınevi

TURKISH SOCIETY OF NUCLEAR MEDICINE 1975

# MIRT

## Molecular Imaging and Radionuclide Therapy



**The Ownership: Turkish Society of Nuclear Medicine (TSNM)**
Turkish Society of Nuclear Medicine
Address: Aziziye Mah. Pilot Sk. 10/12,
Çankaya/Ankara, Türkiye
e-mail: dernekmerkezi@tsnm.org ·
Tel: +90 312 441 00 45

**Publishing Manager**
**Prof. Elif Özdemir, MD.**
Ankara Yıldırım Beyazıt University Faculty of Medicine, Department of Nuclear Medicine; Ankara Bilkent City Hospital, Clinic of Nuclear Medicine, Ankara, Türkiye
E-mail: ozdemire80@gmail.com
ORCID ID: 0000-0002-9142-8752

**Editor in Chief**
**Prof. Murat Fani Bozkurt, MD, FEBNM**
FEBNM Hacettepe University, Medical School, Department of Nuclear Medicine, Ankara, Türkiye
E-mail: fanibozkurt@gmail.com
ORCID ID: 0000-0003-2016-2624

**Associate Editors**
**Prof. Nalan Selçuk, MD.**
Yeditepe University, Medical School, Department of Nuclear Medicine, İstanbul, Türkiye
E-mail: nalanselcuk@yeditepe.edu.tr
ORCID ID: 0000-0002-3738-6491

**Prof. Çiğdem Soydal, MD.**
FEBNM, Ankara University Medical School, Department of Nuclear Medicine, Ankara, Türkiye
Email: csoydal@yahoo.com; csoydal@ankara.edu.tr
ORCID ID: 0000-0002-6199-8551

**Statistics Editors**
**Prof. Gül Ergör, MD.**
Dokuz Eylül University, Medical School, Department of Public Health, İzmir, Türkiye
E-mail:gulergor@deu.edu.tr

**Prof. Sadettin Kılıçkap, MD.**
Hacettepe University, Medical School, Department of Preventive Oncology, Ankara, Türkiye
E-mail: skilickap@yahoo.com

**English Language Editor**
**Galenos Publishing House**



## Scientific Advisory Board

**Ayşegül Akgün**
Ege University, Medical School, Department of Nuclear Medicine, İzmir, Türkiye
**Esma Akın**
The George Washington University, Medical School, Department of Diagnostic Radiology, Wahington DC, USA
**Akram Al-Ibraheem**
King Hussein Cancer Center (KHCC), Department of Nuclear Medicine, Amman, Jordan
**Claudine Als**
Hopitaux Robert Schuman Zitha Klinik, Médecine Nucléaire, Luxembourg
**Corinna Altini**
Nuclear Medicine Unit, AOU Policlinic of Bari – University of Bari "Aldo Moro", Bari, Italy
**Vera Artiko**
Clinical Center of Serbia, Center for Nuclear Medicine, Belgrade, Serbia
**Nuri Arslan**
University of Health Sciences Türkiye, Gülhane Medical School, Gülhane Training and Research Hospital, Clinic of Nuclear Medicine, Ankara, Türkiye
**Lütfiye Özlem Atay**
Gazi University Faculty of Medicine, Department of Nuclear Medicine, Ankara, Türkiye
**Marika Bajc**
Lund University Hospital, Clinic of Clinical Physiology, Lund, Sweden
**Lorenzo Biassoni**
Great Ormond Street Hospital for Children NHS Foundation Trust, Department of Radiology, London, United Kingdom
**Hans Jürgen Biersack**
University of Bonn, Department of Nuclear Medicine, Clinic of Radiology, Bonn, Germany
**M. Donald Blaufox**
Albert Einstein College of Medicine, Department of Radiology, Division of Nuclear Medicine, New York, USA.
**Patrick Bourguet**
Centre Eugène Marquis Department of Nuclear Medicine, Clinic of Radiology, Rennes, France
**Murat Fani Bozkurt**
FEBNM Hacettepe University, Medical School, Department of Nuclear Medicine, Ankara, Türkiye
**A. Cahid Civelek**
NIH Clinical Center, Division of Nuclear Medicine, Bethesta, USA
**Arturo Chiti**
Humanitas University, Department of Biomedical Sciences; Humanitas Clinical and Research Center, Clinic of Nuclear Medicine, Milan, Italy
**Josep Martin Comin**
Hospital Universitari de Bellvitge, Department of Nuclear Medicine, Barcelona, Spain
**Alberto Cuocolo**
University of Naples Federico II, Department of Advanced Biomedical Sciences, Napoli, Italy
**Tevfik Fikret Çermik**
University of Health Sciences Türkiye, İstanbul Training and Research Hospital, Clinic of Nuclear Medicine, İstanbul, Türkiye
**Angelika Bischof Delaloye**
University Hospital of Lausanne, Department of Radiology, Lausanne, Switzerland
**Mustafa Demir**
İstanbul University, Cerrahpaşa Medical School, Department of Nuclear Medicine, İstanbul, Türkiye
**Hakan Demir**
Kocaeli University Medical School, Department of Nuclear Medicine, Kocaeli, Türkiye
**Peter Josef Ell**
University College Hospital, Institute of Nuclear Medicine, London, United Kingdom
**Tanju Yusuf Erdil**
Marmara University, Pendik Training and Research Hospital, Clinic of Nuclear Medicine, İstanbul, Türkiye
**Türkan Ertay**
Dokuz Eylül University, Medical School, Department of Nuclear Medicine, İzmir, Türkiye
**Jure Fettich**
University Medical Centre Ljubljana, Department for Nuclear Medicine, Ljubljana, Slovenia
**Christiane Franzius**
Klinikum Bremen Mitte Center, Center for Modern Diagnostics, Bremen, Germany

# MIRT

## Molecular Imaging and Radionuclide Therapy



**Lars Friberg**
University of Copenhagen Bispebjerg Hospital, Department of Nuclear Medicine, Copenhagen, Denmark
**Jørgen Frøkiær**
Aarhus University Hospital, Clinic of Nuclear Medicine and PET, Aarhus, Denmark
**Maria Lyra Georgosopoulou**
University of Athens, 1st Department of Radiology, Aretaieion Hospital, Radiation Physics Unit, Athens, Greece
**Gevorg Gevorgyan**
The National Academy of Sciences of Armenia, H. Buniatian Institute of Biochemistry, Yerevan, Armenia
**Seza Güleç**
Florida International University Herbert Wertheim College of Medicine, Departments of Surgery and Nuclear Medicine, Miami, USA
**Liselotte Højgaard**
University of Copenhagen, Department of Clinical Physiology, Nuclear Medicine and PET, Rigshospitalet, Copenhagen, Denmark
**Ora Israel**
Tel Aviv University Sackler Medical School, Assaf Harofeh Medical Center, Clinic of Otolaryngology-Head and Neck Surgery, Haifa, Israel
**Csaba Juhasz**
Wayne State University Medical School, Children's Hospital of Michigan, PET Center and Translational Imaging Laboratory, Detroit, USA
**Gamze Çapa Kaya**
Dokuz Eylül University, Medical School, Department of Nuclear Medicine, İzmir, Türkiye
**Metin Kır**
Ankara University, Medical School, Department of Nuclear Medicine, Ankara, Türkiye
**Irena Dimitrova Kostadinova**
Alexandrovska University Hospital, Clinic of Nuclear Medicine, Sofia, Bulgaria
**Lale Kostakoğlu**
The Mount Sinai Hospital, Clinic of Nuclear Medicine, New York, USA
**Rakesh Kumar**
All India Institute of Medical Sciences, Department of Nuclear Medicine, New Delhi, India
**Georgios S. Limouris**
Athens University, Medical School, Department of Nuclear Medicine, Athens, Greece
**Luigi Mansi**
Second University of Naples, Medical School, Department of Nuclear Medicine, Naples, Italy
**Yusuf Menda**
University of Iowa Health Care, Carver College of Medicine, Department of Radiology, Iowa City, USA
**Vladimir Obradović**
University of Belgrade, Faculty of Organizational Sciences, Department of Human Development Theory, Business Administration, Organizational Studies, Belgrade, Serbia
**Zehra Özcan**
Ege University Faculty of Medicine, Department of Nuclear Medicine, İzmir, Türkiye
**Yekta Özer**
Hacettepe University, Faculty of Pharmacy, Department of Radiopharmaceutical, Ankara, Türkiye
**Francesca Pons**
Hospital Clinic, Clinic of Nuclear Medicine, Barcelona, Spain
**Monica Rossleigh**
Sydney Children's Hospital, Clinic of Nuclear Medicine, Sydney, Australia
**Dragana Sobic Saranovic**
University of Belgrade, Medical School, Departments of Radiology, Oncology and Cardiology, Belgrade, Serbia
**Mike Sathekge**
University of Pretoria, Steve Biko Academic Hospital, Department of Nuclear Medicine, Pretoria, South Africa
**Kerim Sönmezoğlu**
İstanbul University, Cerrahpaşa Medical School, Department of Nuclear Medicine, İstanbul, Türkiye
**Zsolt Szabo**
The Johns Hopkins Hospital, Divisions of Radiology and Radiological Science, Baltimore, USA
**Istvan Szilvasi**
Semmelweis University, Medical School, Department of Nuclear Medicine, Budapest, Hungary
**Berna Okudan Tekin**
Ankara Numune Trainig and Research Hospital, Clinic of Nuclear Medicine, Ankara, Türkiye
**Mathew L. Thakur**
Thomas Jefferson University, Department of Radiology, Pennsylvania, USA
**Bülent Turgut**
Cumhuriyet University, Medical School, Department of Nuclear Medicine, Sivas, Türkiye
**Turgut Turoğlu**
Marmara University, Medical School, Department of Nuclear Medicine, İstanbul, Türkiye
**Gülin Uçmak**
University of Health Sciences Türkiye, Ankara Oncology Training and Research Hospital, Clinic of Nuclear Medicine, Ankara,Türkiye
**Doğangün Yüksel**
Pamukkale University, Medical School, Department of Nuclear Medicine, Denizli, Türkiye



**Turkish Society of Nuclear Medicine**
Cinnah Caddesi Pilot Sokak No: 10/12 Çankaya 06650 Ankara, Türkiye **Phone:** +90 312 441 00 45 **Fax:** +90 312 441 12 95 **Web:** www.tsnm.org **E-mail:** dernekmerkezi@tsnm.org
*"Formerly Turkish Journal of Nuclear Medicine"*

Reviewing the articles' conformity to the publishing standards of the Journal, typesetting, reviewing and editing the manuscripts and abstracts in English, creating links to source data, and publishing process are realized by Galenos.

**Publisher Contact**
**Address:** Molla Gürani Mah. Kaçamak Sk. No: 21/1 34093 İstanbul, Türkiye
**Phone:** +90 (530) 177 30 97 / +90 (539) 307 32 03
**E-mail:** info@galenos.com.tr/yayin@galenos.com.tr
**Web:** www.galenos.com.tr
**Publisher Certificate Number:** 14521

**Online Publication Date:** October 2025
**ISSN:** 2146-1414 **E-ISSN:** 2147-1959
International scientific journal published quarterly.

# MIRT

## Molecular Imaging and Radionuclide Therapy

Please refer to the journal's webpage **(https://mirt.tsnmjournals.org/)** for "Aims and Scope", "Instructions to Authors" and "Ethical Policy".

The editorial and publication process of Molecular Imaging and Radionuclide Therapy are shaped in accordance with the guidelines of ICMJE, WAME, CSE, COPE, EASE, and NISO. The journal is in conformity with the Principles of Transparency and Best Practice in Scholarly Publishing.

Molecular Imaging and Radionuclide Therapy is indexed in **Pubmed, Pubmed Central (PMC), Emerging Sources Citation Index (ESCI), TUBITAK-ULAKBIM, Scopus, Gale/Cengage Learning, EBSCO databases, ProQuest Health & Medical Complete, CINAHL, Embase, J-Gate, IdealOnline, Türkiye Atıf Dizini-Turkiye Citation Index, Turk Medline, Hinari, GOALI, ARDI, OARE, AGORA** and **CNKI**.

The journal is published electronically.

**Owner:** Turkish Society of Nuclear Medicine

**Responsible Manager:** Murat Fani Bozkurt

MIRT
Molecular Imaging and Radionuclide Therapy

CONTENTS

## Special Editorial Series: Tribute to Global Contributors of Nuclear Medicine

168 Dr. A. Cahid Civelek Exemplifies the Act of Integrating Patient Care, Staff Education, Research, and Global Knowledge Sharing

*Dr. A. Cahid Civelek, Hasta Bakımı, Personel Eğitimi, Araştırma ve Küresel Bilgi Paylaşımını Bir Araya Getirme Başarısı Gösteren Örnek Bir Akademisyendir*

Hong Zhang; Hangzhou, China

## Original Articles

173 Performance of $^{68}$Ga-PSMA PET/CT in Metastatic Prostate Cancers at the Time of Diagnosis and Correlation with Obesity

*Tanı Anında Metastatik Prostat Kanserlerinde $^{68}$Ga- PSMA PET/BT'nin Performansı ve Obezite ile Korelasyonu*

Özge Ulaş, Zekiye Hasbek; Tokat, Sivas, Türkiye

180 Investigation of the Partial Volume Effect in Pre-Dosimetry of Liver Tumors for $^{90}$Y Radioembolization: A Phantom Study

*$^{90}$Y Radyoembolizasyon Tedavisinde Karaciğer Tümörleri Pre-Dozimetri'de Kısmi Hacim Etkisinin İncelenmesi: Bir Fantom Çalışması*

Ayşe Dilaver Akar, Nami Yeyin, Sinem Akyol, Özge Demir, Eylem Gülce Çoker, Mustafa Demir; İstanbul, Türkiye

188 The PSMA-PET Conundrum: A Survey of UK Prostate Cancer Surgeons and Their Use of PSMA-PET Prior to Radical Prostatectomy

*PSMA-PET Bilmecesi: Birleşik Krallık'taki Prostat Kanseri Cerrahları ve Radikal Prostatektomi Öncesi PSMA-PET Kullanımları Üzerine Bir Anket*

Rustam Nariman Karanjia, Pallab Kumar Sarkar, Humayun Bashir, Sashi S Kommu; Canterbury, United Kingdom

194 A Disease Progression Predictor by Quantitative Assessment of the Hepatic Accumulation on Postablative Iodine-131 Whole-Body Image in Differentiated Thyroid Cancer

*Diferansiye Tiroid Kanserinde Postablatif İyot-131 Diferansiye Tiroid Kanserinde Postablatif İyot-131 Tüm Vücut Görüntüsünde Hepatik Tutulumun Kantitatif Değerlendirmesiyle Hastalık İlerlemesinin Öngörülmesi*

Michihiro Nakayama, Kenta Nomura, Sho Kamieda, Ippei Yoshida, Atsushi Fujiya1, Takahiro Uno2, Atsutaka Okizaki; Asahikawa, Japan

202 $^{18}$F-FDG PET/CT Parameters and Standard Uptake Values Predicting Contralateral Lung Metastasis in Lung Cancer

*Akciğer Kanserinde Karşı Akciğer Parankim Metastazını Öngörmeye Yarayan $^{18}$F-FDG PET/BT Parametreleri*

Büşra Özdemir Günay, Funda Üstün; Giresun, Edirne, Türkiye

213 Radiation-induced Xerostomia: Evaluation with $^{18}$F-FDG PET/CT

*Radyoterapi İlişkili Kserostominin $^{18}$F-FDG PET/BT ile Değerlendirilmesi*

Gözde Mütevelizade, Bilal Çağrı Bozdemir, Nazım Aydın, Ahmet Furkan Süner, Ömür Karakoyun Çelik, Yasemin Parlak, Ecem Çorlu, Özgür Yıldırım, Mustafa Kahya, Gizem Bakıcıerler, Gül Gümüşer, Elvan Sayıt; Manisa, İstanbul, Zonguldak, Türkiye

## Interesting Images

221 Penile Metastasis from Prostate Cancer: Detection on $^{18}$F-PSMA-1007 PET/CT

*Prostat Kanserinden Kaynaklanan Penis Metastazı: $^{18}$F-PSMA-1007 PET/BT ile Saptanması*

Hend Komber, Ayah Nawwar, Julie Searle, Iain Lyburn; Bristol, Cheltenham, Gloucestershire, Wiltshire, UK; Cairo, Egypt

MIRT
Molecular Imaging and Radionuclide Therapy

CONTENTS

**224** Triple Tumors Uncovered: Insights from $^{68}$Ga PSMA PET-CT
*Üç Tümörün Ortaya Çıkarılması: $^{68}$Ga PSMA PET-BT'den Elde Edilen Bilgiler*
Sana Munir Gill, Aamna Hassan, Waqas Ahmad, Islah Ud Din; Lahore, Pakistan; Columbia, Canada

**228** The Role of Bone Scintigraphy in Detection of Disseminated Coccidioides Fungemia
*Dissemine Coccidioidies Fungemisinin Saptanmasında Kemik Sintigrafisinin Rolü*
Turgut Bora Cengiz, Caroline Diane Wilson; Winston-Salem, USA

**231** Extensive Malignant Thrombus Revealed by $^{18}$F-FDG PET/CT in Patient with Papillary Thyroid Cancer
*Papiller Tiroid Karsinomlu Hastada $^{18}$F-FDG PET/BT ile Saptanan Yaygın Malign Trombüs*
Merve Nida Calderon Tobar, Lütfü Perktaş, Hasan Önner, Gonca Kara Gedik; Konya, Türkiye

**234** Analysis of Imaging Findings in a Patient with Squamous Cell Carcinoma of the External Auditory Canal Metastatic to the Dura with Trigeminal Nerve Involvement
*Trigeminal Sinir Tutulumuyla Birlikte Duraya Metastatik Dış Kulak Yolu Skuamöz Hücreli Karsinomu Olan Bir Hastada Görüntüleme Bulgularının Analizi*
Güler Silov, İsmet Miraç Çakır, Hande Arslan, Asuman Çelik, Aslı Ayan; Samsun, Ankara, Türkiye

**239** Unveiling the Diagnostic Mystery: $^{18}$F-FDG PET and Bone Scan Negative in Bone Metastases of Lobular Breast Cancer: A Case Report
*Tanısal Gizemin Çözülmesi: Lobüler Meme Kanseri Kemik Metastazlarında $^{18}$F-FDG PET ve Kemik Taraması Negatif: Bir Olgu Sunumu*
Sharjeel Usmani, Khulood Al Riyami, Anjali Jain, Asiya Al Busaidi, Paul Dumasig, Vipin V Jayakrishnan, Subhash Kheruka, Najeeb Ahmed; Maskat, Oman; Cottingham, UK

**242** Gluteal Muscle Metastasis of Papillary Thyroid Cancer with Increased Somatostatin Receptor Expression in $^{68}$Ga-DOTATATE PET/MRI
Papiller Tiroit Kanserinin Gluteal Kas Metastazında Artmış Somatostatin Ekspresyonunun $^{68}$Ga-DOTATATE PET/MR Görüntüsü
Ali Kibar, Sertaç Asa, Lebriz Uslu-Beşli, Mine Önenerk, Sait Sağer, Kerim Sönmezoğlu, Haluk Burçak Sayman; İstanbul, Türkiye

**246** An Interesting Case of Fornix Rupture Discovered Accidentally on Bone Scintigraphy
*Kemik Sintigrafisinde Tesadüfen Saptanan İlginç Bir Forniks Rüptürü Olgusu*
Salah Nabih Oueriagli, Ayoub Dribla, Omar Ait Sahel, Yassir Benameur, Abderrahim Doudouh; Rabat, Morocco

**249** Rare Acute Polyarticular Gout Disease Detected with $^{18}$F-FDG PET/CT
*$^{18}$F-FDG PET/BT ile Tespit Edilen Nadir Akut Poliartiküler Gut Hastalığı*
Zehranur Tosunoğlu, Ayşe Nur Toksöz Yıldırım, Esra Arslan, Göksel Alçın, Elife Akgün; İstanbul, Türkiye

**252** $^{18}$F-FDG PET/CT Detection of Extensive Pleural Metastasis in Rare Malignancy Thymoma
*Nadir Bir Malignite Olan Timomada Yaygın Plevral Metastazın $^{18}$F-FDG PET/BT ile Tespiti*
Mehmet Oğuz Kartal, Berna Okudan; Elazığ, Ankara, Türkiye

## Letter to the Editor

**255** Comment on the Use of the ThyPRO Questionnaire in Turkish Populations: Methodological Consideration
*ThyPRO Anketinin Türk Popülasyonlarında Kullanımına İlişkin Yorum: Metodolojik Değerlendirme*
Aziz Gültekin; Denizli, Türkiye

MIRT
Molecular Imaging and Radionuclide Therapy

CONTENTS

## Review

256 False Positive Findings of $^{68}$Ga-DOTATOC PET/CT: A Systematic Review

*$^{68}$Ga-DOTATOC PET/BT'nin Yanlış Pozitif Bulguları: Sistematik Derleme*

*Dhuha Al-Adhami, Ahmed Saad Abdlkadir, Sze Ting Lee, Punit Sharma, Naser Obeidat, Hassan Al-Alawi, Mai Hong Son, Aysar Khalaf, Akram Naif Al-Ibraheem; Amman, Irbid, Jordan; Melbourne, Australia; Kolkata, India; Karbala, Iraq; Hanoi, Vietnam*

## Indexes

2025 Referee Index / 2025 Hakem Dizini

2025 Author Index / 2025 Yazar Dizini

2025 Subject Index / 2025 Konu Dizini

*Special Editorial Series: Tribute to Global Contributors of Nuclear Medicine*
*Mol Imaging Radionucl Ther 2025;34:168-172* *DOI:10.4274/mirt.galenos.2025.57614*

# Dr. A. Cahid Civelek Exemplifies the Act of Integrating Patient Care, Staff Education, Research, and Global Knowledge Sharing

## *Dr. A. Cahid Civelek, Hasta Bakımı, Personel Eğitimi, Araştırma ve Küresel Bilgi Paylaşımını Bir Araya Getirme Başarısı Gösteren Örnek Bir Akademisyendir*

*Hong Zhang*

*Zhejiang University School of Medicine, The Second Affiliated Hospital of Zhejiang University School of Medicine, Clinic of Nuclear Medicine, Hangzhou, China*

**Keywords:** Dr. A. Cahid Civelek, nuclear medicine, clinical innovation, global collaboration
**Anahtar kelimeler:** Dr. A. Cahid Civelek, nükleer tıp, klinik yenilik, küresel iş birliği

Among the many bright and successful academic physicians, some stand out for their deep commitment to teaching and sharing their knowledge, experience, and unique skills with others, locally and internationally. These individuals dedicate their academic time, energy, and efforts to this purpose without expecting anything in return. Their only reward is the satisfaction of witnessing their learners and mentees thrive in their academic careers.

I am pleased to introduce A. Cahid Civelek Doctor of Medicine (MD), a colleague, friend, and close supporter of Chinese nuclear medicine who is a professor in the Department of Radiology and Radiological Science of the Johns Hopkins University School of Medicine (Figure 1). Cahid's distinguished nuclear medicine and medical education career began in January 1982 when he joined Johns Hopkins as a Nuclear Medicine resident (1,2).

Since 2003, Dr. Civelek has served as a full professor of nuclear medicine at various institutions. Dr. Civelek is recognized for his accomplishments as a clinician-researcher and clinician-educator.

Dr. Civelek is an internationally recognized expert and educator in nuclear cardiology, nuclear oncology, theranostics, and general nuclear medicine. His scholarship in these areas has been achieved through peer-reviewed publications and numerous presentations in international settings.

## Introduction

Dr. Civelek earned his medical degree at the İstanbul University School of Medicine and completed his nuclear medicine residency at Hacettepe University Medical Center in Ankara. He joined Johns Hopkins to pursue a research fellowship funded by a scholarship he received from the International Atomic Energy Agency (IAEA, Vienna, Austria). After completing training and fellowship in 1984, Dr. Civelek was recruited to the full-time faculty in nuclear

**Address for Correspondence:** Hong Zhang, Zhejiang University School of Medicine, The Second Affiliated Hospital of Zhejiang University School of Medicine, Clinic of Nuclear Medicine, Hangzhou, China
**E-mail:** hzhang21@zju.edu.cn **ORCID ID:** orcid.org/0000-0002-4084-5150
**Received:** 18.04.2025 **Accepted:** 15.07.2025 **Publication Date:** 08.10.2025

**Cite this article as:** Zhang H. Dr. A. Cahid Civelek exemplifies the act of integrating patient care, staff education, research, and global knowledge sharing. Mol Imaging Radionucl Ther. 2025;34:168-172.

Copyright© 2025 The Author. Published by Galenos Publishing House on behalf of the Turkish Society of Nuclear Medicine.
This is an open access article under the Creative Commons Attribution-NonCommercial-NoDerivatives 4.0 (CC BY-NC-ND) International License.

medicine at Johns Hopkins. He was promoted to Associate Professor in 1995 and remained at Hopkins until 2003 (1).

During his early career at Johns Hopkins, Dr. Civelek laid a solid professional foundation through outstanding contributions to clinical and research programs. He subsequently assumed key leadership roles, including the Director of Nuclear Cardiology, Program Director of the Nuclear Medicine Residency Program, and Medical Director of the Nuclear Medicine Technologist Program, while also serving as an Interim Clinical Director. Before his appointment as Professor and Director of Nuclear Medicine and positron emission tomography (PET) at the University of Louisville in 2008, Dr. Civelek had served as a Professor and Director of Nuclear Medicine in Saint Louis University Medical School Hospital.

Dr. Civelek held the position of Clinical Director for the Nuclear Medicine Division at the NIH Clinical Center and subsequently advanced to the role of Deputy Director. Before that, he spent two years at the Department of Radiology and Imaging Sciences at the NIH Clinical Center, specifically in the section of body magnetic resonance imaging (MRI) and MRI-PET. During this time, he also held a visiting faculty position at the Department of Radiology at Johns Hopkins School of Medicine. In January 2018, he was recruited to Johns Hopkins full-time back.

He is a fellow of the American College of Nuclear Medicine, a fellow and founding member of the American Society of Nuclear Cardiology, and a fellow of The American College of Angiology.

Dr. Civelek has mentored numerous physicians in nuclear medicine across the U.S. and internationally, with trainees specializing in both nuclear cardiology and nuclear oncology. As a world-renowned expert in Nuclear Medicine, he has been invited to deliver lectures at medical centers on nuclear medicine, focused on nuclear cardiology, nuclear oncology-theranostics/PET/CT, and PET-MRI.

Dr. Civelek is dedicated to advancing the development of nuclear medicine, cardiology, and oncology. He focuses on pioneering new tumor-targeting radiopharmaceuticals for imaging and therapy, while advocating for high-quality clinical trials and enhancing patient care and safety standards.

He is a devoted patient advocate. He is committed to improving the efficiency of clinical operations and, notably, patient safety. As in his previous practices, he has been improving and implementing new patient safety measures (3). For example, the patient dose reduction program he applied has resulted in nearly a 50% reduction in the injected radiotracer doses and (computed tomography) CT doses, without compromising diagnostic accuracy (4,5).

**Research Scholarship and Accomplishments**

As a junior faculty member, Dr. Civelek became interested in nuclear cardiology. At that time, the standard of care for nuclear cardiac stress testing involved planar nuclear imaging. A significant improvement in accuracy came with the introduction of single photon emission computed tomography (SPECT), which produced cross-sectional images analogous to the more familiar X-ray CT. When the second SPECT machine in the United States was installed at Johns Hopkins, Dr. Civelek took the opportunity to become an expert in the installation and running of SPECT for clinical applications in nuclear cardiology, participating in some of the earliest work in cardiac SPECT (6,7) and describing specific imaging signs for more accurate diagnosis of coronary artery disease (8).

Early SPECT machines were developed primarily for myocardial imaging, but Dr. Civelek felt such a technological advance should also be used in other clinical problems. One such area is minimally invasive parathyroid surgery for primary hyperparathyroidism, where success demands accurate preoperative localization of a parathyroid adenoma; scintigraphy is the most common localization method. Starting with his clinical observations, Dr. Civelek demonstrated in a large prospective study that a single-phase delayed SPECT study was more accurate than dual-phase planar imaging and equivalent to dual-phase SPECT. This study streamlined the parathyroid imaging protocol and led to a highly cited publication (9).

Since those early cardiac SPECT days, Dr. Civelek's career has continued to evolve successfully alongside the inevitable technological advances in nuclear medicine. These changes shifted his interest from nuclear cardiology to nuclear oncology, the latter involving PET cancer detection and, more recently, the combination of PET with CT or MRI (PET/CT and PET-MR, respectively) (10). During these changes, Dr. Civelek has maintained his practice of drawing from clinical practice to find practical applications of new radiotracers and imaging protocols. For example, he has investigated new PET/CT radiotracers to image non-small cell lung cancer (11,12), the simultaneous injection of two tumor-seeking radiotracers (13), and the utilization of $^{68}$Ga-DOTATATE to detect pheochromocytoma and paraganglioma (14). Dr. Civelek's work with $^{68}$Ga-DOTATATE exemplifies his quick adaptation to innovations in the field, since it is one of the more recent clinical PET radiotracers approved for nuclear oncology.

**Clinical Practice Scholarship and Accomplishments**

Dr. Civelek is a busy clinical nuclear medicine physician who spends 80 to 90% of his time providing patient care in all stations of nuclear medicine, including general nuclear

medicine, nuclear cardiology, PET/CT, nuclear oncology, and theragnostics. Despite his accomplishments in research and education, he considers himself to be foremost a clinician with the ultimate responsibility of providing high-quality, expert clinical care. Even as a junior faculty member at Johns Hopkins, he became the "go-to'' for nuclear cardiology. He received specific referrals from established Hopkins physicians to perform nuclear cardiac stress tests on their patients and themselves when necessary.

In keeping with his clinical emphasis, he is an expert and "go-to" person for troubleshooting patient-related clinical problems. Dr. Civelek's willingness to address whatever problems arise is reflected by the diverse topics of some of his publications and invited talks. His emphasis on providing high-quality care has led him to be recruited to lead nuclear medicine divisions at three different institutions the University of Saint Louis, the University of Louisville, and the National Institutes of Health Clinical Center in Bethesda.

## Education Scholarship and Accomplishments

Dr. Civelek sees the education of nuclear medicine trainees as an integral part of clinical practice, and he continues to devote significant time and effort to supervising residents and fellows daily. His broad and deep knowledge of all aspects of nuclear medicine is respected and appreciated by trainees, advisees, and his clinical colleagues. These traits and his clinical emphasis make him the ideal person to be the Director of our nuclear medicine residency and PET/CT fellowship programs.



**Figure 1.** Professor Dr. A. Cahid Civelek
The use of the images was made with the explicit consent of Dr. A. Cahid Civelek

While his educational influence starts with those around him, his efforts receive attention from a broader audience. For example, in the early days of SPECT, his troubleshooting skills led him to travel to institutions around the United States of America to help install their new SPECT gamma camera equipment.

## Reputation and Recognition

Dr. Civelek's scholarship, clinical skills, and educational acumen have been recognized nationally and internationally. His initial interest and expertise in nuclear cardiology led him to be one of the founding members of the American Society of Nuclear Cardiology, the primary organization for this subspecialty. He has also been asked to serve on multiple committees associated with the Society of Nuclear Medicine and Molecular Imaging, the world's primary organization for nuclear medicine. He has served on many editorial boards and has received multiple editorial awards for his peer-review contributions.

However, Dr. Civelek's most significant impact has been his educational outreach on the international stage, which includes Türkiye his native country and especially China. His regular trips to China include Nanjing University, one of the nine elite universities in China's C9 "Ivy" League (Figure 2). The invitation eventually grew to a regular string of invitations, leading to a "tour" of multiple academic venues in China. In 2012, Dr. Civelek assisted in revising

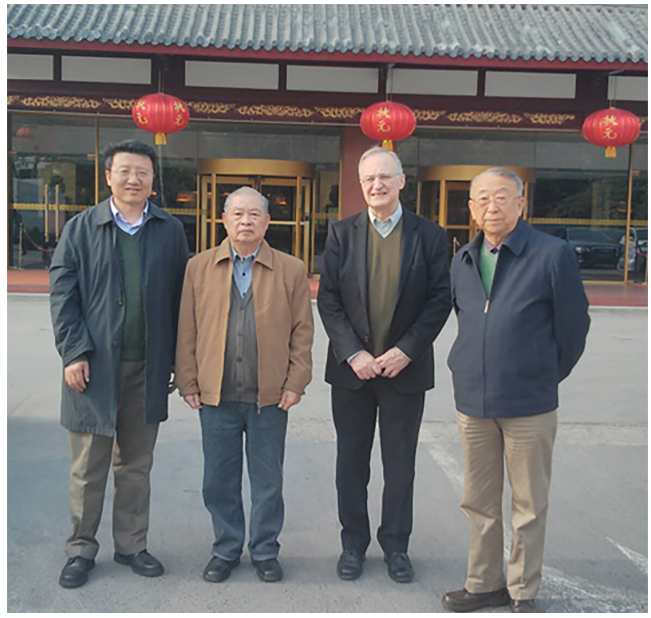


**Figure 2.** Nanjing 2013: From left to right: Professor Drs. Xiao-Feng Li, Xiu Jie Liu, A. Cahid Civelek, Jixiao Ma. At the front of the Nanjing Hotel
The use of the images was made with the explicit consent of Dr. A. Cahid Civelek

the primary nuclear medicine textbook in the Chinese language, funded by the International Atomic Energy Agency. Recognizing his contributions, he was asked to coauthor the textbook's foreword. Also, in 2012, Dr. Civelek was appointed a member of the Advisory Board of the Center of Excellence in Medical Molecular Imaging of Zhejiang Province. This center is part of the Institute of Nuclear Medicine and Molecular Imaging of Zhejiang University (another "C9'' university), one of the few leading institutes of molecular imaging in China. In 2016, Nanjing University recognized his academic influence by conferring the title of Visiting Professor (Figure 3). Unlike the term "visiting professor" in the United States of America, which implies a temporary interaction, the title of Visiting Professor at Nanjing University is permanent, akin to an honorary faculty appointment. It requires submitting academic credentials and requesting recommendation letters from academic referees.

Dr. Civelek has made significant accomplishments in clinical nuclear medicine, including extensive scholarship and recognition for international educational outreach.

He played a pivotal role in helping implement and strengthen China's global scientific collaboration in nuclear medicine and molecular imaging. (15).

Dr. Civelek was first introduced to Chinese Medicine and culture when he met Dr. Xiu Jie Liu, MD, and Dr. Jiang, at Johns Hopkins Nuclear Medicine in 1982 during their training. His friendship with Dr. Liu was deep and uninterrupted until Dr. Liu's passing on January 1, 2023, due to complications associated with COVID-19.




**Figure 3.** A commemorative photograph capturing Dr. A. C. Civelek during the official ceremony in November 26, 2016 at Nanjing University Medical School, Nanjing, China, where he was formally awarded the title of professor.
Dr. Civelek alongside the university's dignitaries, including the Dean and President of Nanjing University Medical School
The use of the images was made with the explicit consent of Dr. A. Cahid Civelek

In October 1985, Dr. Civelek made his first visit to China. During his stay, he delivered lectures on SPECT Myocardial perfusion imaging (MPI) at the FuWai Hospital of the Chinese Academy of Medical Sciences, the world's largest center for cardiovascular diseases. After spending a few days in Beijing, he visited the second affiliated hospital of China Medical University in Shenyang. He spent two weeks helping Dr. Zhuguo Pei (who passed away several years ago), his colleagues, and their technical staff in establishing their SPECT MPI program. During his stay, Dr. Civelek delivered multiple daily lectures and guided the staff on nuclear cardiology imaging and its potential pitfalls.

Dr. Civelek became a mentor to Dr. Feng Wang and later a colleague after being introduced by Drs. Liu and Jixiao Ma. He continued to collaborate and support Dr. F. Wang and his department through lectures, short visits to his department, and mentoring several graduate students from Nanjing University Hospital.

Over the years, Dr. Civelek has visited many university hospitals in China, delivering numerous lectures, and, at times, even visiting multiple cities during a single trip.

Dr. Civelek also developed a long-lasting collaboration and friendship with Professor Mei Tian and Hong Zhang, who are leaders at Zhejiang University, Hangzhou. He joined and contributed to their international scientific meetings (Figure 4) by delivering lectures at many HIMIC conferences, most recently HIMIC-2024 (16). In 2024, Professors Feng Wang and Civelek at Nanjing University received the Foreign Researcher Award from the Chinese government.

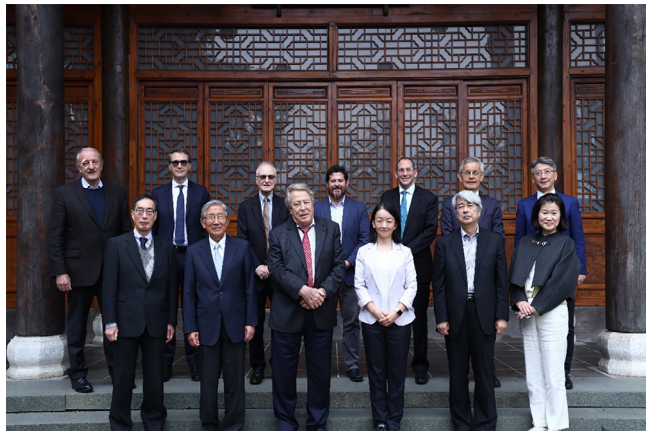


**Figure 4.** Hangzhou International Molecular Imaging (HIMIC2024):
First Row from left to right: Prof. Koji Murakami, Keigo Endo, Heinrich Schelbert, Mei Tian, Yasuyoshi Watanabe, Mijin Yun. Second Row from left to right: Prof. Markus Schwaiger, Arturo Chiti, Cahid Civelek, Charles Manning, Ulaner Gary, Nagara Tamaki, Hong Zhang. At the front of Moganshan Li Shan Yun Ju Hotel
The use of the images was made with the explicit consent of Dr. A. Cahid Civelek

Dr. A. Cahid Civelek is a beacon of excellence, seamlessly blending patient care, staff education, groundbreaking clinical research, and a commitment to sharing knowledge globally.

## References


1. Wagner HN. A personal history of nuclear medicine. London: Springer. 2006.
2. Linton OW, Gayler BW. Johns Hopkins Radiology, 1896-2010. Baltimore, Md: Johns Hopkins Radiology, Johns Hopkins Hospital. 2011.
3. Civelek AC. Patient safety and privacy in the electronic health information era: Medical and beyond. Clinical Biochemistry. 2009;42:298-299.
4. Talbott S, Bhatt G, Li XF, Civelek AC. Dose related decreased image quality of CT doesn't degrade the diagnostic quality of PET-CT. J Nucl Med. 2014;55 (Supplement 1):423-423.
5. Civelek AC, Talbott S. A new paradigm: How to reduce the medically induced patient radiation burden without compromising the image quality. J Nucl Med. 2011;52 (Supplement 1):1018-1018.
6. Clausen M, Bice AN, Civelek AC, Hutchins GM, Wagner HN Jr. Circumferential wall thickness measurements of the human left ventricle: reference data for Thallium 201 single-photon emission computed tomography. Am J Cardiol. 1986;58:827-883.
7. Clausen M, Civelek AC, Bice A, Petronis J, Koller D, Loncaric S, Weiss J, Wagner HN Jr. Comparison of short axis circumferential profiles by Tl-201 myocardial SPECT and 2D-echocardiography in normal volunteers. Radiology. 1988;168:723-726.
8. Civelek AC, Shafique I, Brinker JA, Durski K, Weiss JL, Links JM, Natarajan TK, Ozguven MA, Wagner HN Jr. Reduced left ventricular cavitary activity ("black hole sign") in Thallium-201 SPECT perfusion images of antero-apical transmural myocardial infarction. The Am J Cardiol. 1991;68:1132-1137.
9. Civelek AC, Ozalp E, Donovan P, Udelsman R. Prospective evaluation of delayed technetium-99m sestamibi SPECT scintigraphy for preoperative localization of primary hyperparathyroidism. Surgery. 2002;131:149-157.
10. Civelek A C, Niglio S A, Malayeri A A, Lin J, Gurram S, Chalfin HJ, Turkbey B, Valera V, Steinberg SM, Apolo AB. Clinical value of 18FDG PET/MRI in muscle-invasive, locally advanced, and metastatic bladder cancer. Urologic oncology: Seminars and Original Investigations. Elsevier. 2021;39:787.e17-787. e21.
11. Huang T, Civelek AC, Li J, Jiang H, Ng CK, Postel GC, Shen B, Li XF. Tumor microenvironment–dependent 18F-FDG, 18F-fluorothymidine, and 18F-misonidazole uptake: a pilot study in mouse models of human non–small cell lung cancer. J Nucl Med. 2012;53:1262-1268.
12. Huang T, Civelek AC, Zheng H, Ng CK, Li J, Postel GC, Shen B, Li XF. 18F-misonidazole PET imaging hypoxia in micrometastases and macroscopic xenografts of human non-small cell lung cancer: correlating with autoradiographic and histological findings. Am J Nucl Med Mol Imaging. 2013;3:142-153.
13. Li XF, Huang T, Jiang H, Wang X, Shen B, Wang X, Ng CK, Postel GC, Civelek AC. Combined injection of (18)F-fluorodeoxyglucose and 3'-Deoxy-3'- [(18)F] fluorothymidine PET achieves more complete identification of viable lung cancer cells in mice and patients than individual radiopharmaceutical: a proof-of-concept study. Transl Oncol. 2013;6:775-783.
14. Jha A, Ling A, Millo C, Gupta G, Lin FI, Herscovitch P, Adams KT, Wakim P, Taïeb D, Kebebew E, Lodish M, Civelek AC, Pacak K. Superiority of 68Ga-DOTATATE over 18F-FDG and anatomic imaging in the detection of succinate dehydrogenase mutation (SDHx)-related pheochromocytoma and paraganglioma in the pediatric population. Eur J Nucl Med Mol Imaging. 2018;45:787-797.
15. Tian M, Chai ZF, Chen L, Chiti A, Civelek C A, Endo K, Gary U, Jin L, Manning C, Murakami K, Schelbert H, Schwaiger M, Tamaki N, Tan WH, Watanabe Y, Yun MJ, Zhang H. Moganshan international consensus on further strengthening global scientific collaboration in the field of molecular imaging. EJNMMI. 2025:1-4.
16. Zhang Z, Winston GP, Zhao HT, Oei EH, Ai Q, Loffroy R, Lin T, Shen Y, Ng CK, Liu H, Civelek AC, Han Z, He YM, Ji LY, Wáng YX. Focus on China: should clinicians engage in research? and lessons from other countries. Quant Imaging Med Surg. 2014;4:413-425.

*Original Article*

*Mol Imaging Radionucl Ther 2025;34:173-179* *DOI:10.4274/mirt.galenos.2025.46762*

# Performance of $^{68}$Ga-PSMA PET/CT in Metastatic Prostate Cancers at the Time of Diagnosis and Correlation with Obesity

## *Tanı Anında Metastatik Prostat Kanserlerinde $^{68}$Ga- PSMA PET/BT'nin Performansı ve Obezite ile Korelasyonu*

**Özge Ulaş[1], Zekiye Hasbek[2]**

[1]*Tokat Gaziosmanpaşa University Faculty of Medicine, Department of Nuclear Medicine, Tokat, Türkiye*
[2]*Sivas Cumhuriyet University Faculty of Medicine, Department of Nuclear Medicine, Sivas, Türkiye*

## Abstract

**Objective:** The aim of this study was to evaluate the relationship between Galium-68 prostate-specific membrane antigen positron emission tomography combined with computed tomography ($^{68}$Ga-PSMA PET/CT) quantitative parameters and patient obesity, prostate-specific antigen (PSA) levels, and metastasis type in prostate cancer.

**Methods:** In the present study, we included 112 patients diagnosed with prostate cancer between 2020 and 2024. These patients underwent $^{68}$Ga-PSMA PET/CT imaging for staging purposes, with locoregional or distant metastasis detected in the imaging results.

**Results:** No significant correlation was observed between body mass index (BMI) classification and prostate gland maximum standard uptake values ($SUV_{max}$), metabolic tumor volume (MTV), total lesion glycolysis (TLG), standardized uptake value lean (SUL), or $SUV_{mean}$ values. A weak inverse correlation was found between BMI and PSA levels (p=0.08, r=-0.248), with PSA values decreasing as patient weight increased. The presence of locoregional disease or distant metastasis was not significantly associated with prostate gland $SUV_{max}$, MTV, TLG, $SUV_{mean}$, or SUL values (p=0.25; 0.667; 0.667; 0.244; 0.126, respectively). However, a significant association was detected between PSA levels and distant metastases or locoregional disease (p=0.02), with higher PSA values observed in patients with distant metastases compared to those with locoregional disease. Additionally, significant correlations were found between the D'Amico risk classification and the prostate gland $SUV_{max}$, TLG, SUL, and $SUV_{mean}$ values (p=0.035, 0.037, 0.012, 0.028, respectively).

**Conclusion:** PSA levels may assist in estimating whether metastases are local or distant. However, due to the weak inverse correlation between BMI and PSA, it is important that low PSA levels may not necessarily indicate localized disease during clinical evaluation.

**Keywords:** Prostate cancer, $^{68}$Ga-PSMA PET/CT, PSA, BMI, D'Amico risk classification

## Öz

**Amaç:** Bu çalışmanın amacı prostat kanserlerinde Gallium-68 prostat spesifik membran antijeni pozitron emisyon tomografisi/bilgisayarlı tomografi ($^{68}$Ga-PSMA PET/BT) kantitatif değerleri ile, hastanın obezitesi, prostat spesifik antijen (PSA) değerleri ve metastaz tipi ilişkisini değerlendirmekti.

**Yöntem:** Bu çalışmaya 2020-2024 tarihleri arasında prostat kanseri tanısı almış ve evreleme amacıyla $^{68}$Ga-PSMA PET/BT görüntülemesi yapılan ve görüntülemede lokorejyonel veya uzak metastaz tespit edilen 112 hasta dahil edildi.

**Address for Correspondence:** Özge Ulaş, Tokat Gaziosmanpaşa University Faculty of Medicine, Department of Nuclear Medicine, Tokat, Türkiye
**E-mail:** ozgeulas23@gmail.com **ORCID ID:** orcid.org/0000-0002-8687-5769
**Received:** 13.01.2025 **Accepted:** 15.06.2025 **Epub:** 11.08.2025 **Publication Date:** 08.10.2025

**Cite this article as:** Ulaş Ö, Hasbek Z. Performance of $^{68}$Ga-PSMA PET/CT in metastatic prostate cancers at the time of diagnosis and correlation with obesity. Mol Imaging Radionucl Ther. 2025;34:173-179.

Copyright© 2025 The Author. Published by Galenos Publishing House on behalf of the Turkish Society of Nuclear Medicine.
This is an open access article under the Creative Commons Attribution-NonCommercial-NoDerivatives 4.0 (CC BY-NC-ND) International License.

## Öz

**Bulgular:** Hastaların beden kitle indeks sınıflaması ile prostat bezimaksimum standart tutulum değeri ($SUV_{max}$), metabolik tümör hacmi (MTV), toplam lezyon glikolizi (TLG), standardize edilmiş alım değeri (SUL) ve $SUV_{mean}$ değerleri arasında anlamlı ilişki bulunamadı. Hastaların vücut kitle indeksi (VKİ) ile PSA değeri arasında VKİ vardı (p=0,08, r=-0,248). Hastalarda kilo arttıkça PSA değerlerinde azalma tespit edildi. Hastaların lokorejyonel hastalığı ya da uzak metastazı olmasının, prostat bezi $SUV_{max}$, MTV, TLG, $SUV_{mean}$ ve SUL değerleri ile anlamlı bir ilişkisi bulunamadı (p=0,25, p=0,667, p=0,244 p=0,126, p=0,057). Bununla birlikte, hastaların uzak metastaz olması veya lokorejyonel hastalığı olması ile PSA değerleri arasında anlamlı bir ilişki vardı (p=0,02). Uzak metastazı olan hastada lokorejyonel hastalığa göre PSA değerleri daha yüksek bulundu. D'Amico risk sınıflaması ile, prostat bezi $SUV_{max}$, TLG, SUL ve $SUV_{mean}$ arasında da anlamlı ilişki vardı (p=0,035, p=0,037, p=0,12, p=0,028).

**Sonuç:** PSA değerleri metastazların lokal mi yoksa uzak mı olduğunu tahmin etmemize yardımcı olabilir. Ancak VKİ ile PSA üzerinde düşük düzeyde ters korelasyon olması sebebiyle, düşük PSA düzeylerinin obez hastalarda lokal hastalık ile sınır olmayabileceği klinik değerlendirmede mutlaka göz önünde bulundurmalıyız.


**Anahtar kelimeler:** Prostat kanseri, $^{68}$Ga-PSMA PET/BT, PSA, BMI, D'Amico risk sınıflaması

## Introduction

Prostate cancer is the second most common cancer among men and the second leading cause of cancer-related mortality (1). Although it is often curable, the presence of metastasis at the time of diagnosis or during the course of treatment significantly worsens both treatment response and prognosis (2). Consequently, the identification of metastasis at diagnosis and staging has become a critical factor in determining treatment strategies for prostate cancer. Transrectal ultrasound, thoracoabdominal computed tomography (CT), multiparametric magnetic resonance imaging, and bone scintigraphy are commonly employed for initial clinical staging. The primary aim of clinical staging in prostate cancer is to assess the disease burden and to guide the selection of the most appropriate treatment plan for each patient.

For many years, clinical staging systems based on prostate-specific antigen (PSA) levels, Gleason score, and radiological imaging systems have been used to guide treatment planning. However, Gallium-68 ($^{68}$Ga) prostate specific membrane antigen (PSMA) positron emission tomography/CT (PET/CT) has emerged as the most reliable method for staging, particularly in detecting distant metastases. This nuclear medicine imaging modality is especially recommended for patients with intermediate- to high-risk prostate cancer. PSMA is a transmembrane protein consisting of 750 amino acids, significantly expressed in prostate cancer and metastases (3). As a result, it is frequently utilized in imaging for the detection of both primary tumors and metastatic lesions in prostate cancer.

This study aimed to evaluate the effectiveness of $^{68}$Ga-PSMA PET/CT in detecting primary tumors and metastatic lesions in patients with metastatic prostate cancer and to investigate its correlation with obesity.

## Materials and Methods

In this study, 112 patients diagnosed with prostate cancer between 2020 and 2024 who underwent $^{68}$Ga-PSMA PET/CT imaging for staging purposes and in whom locoregional or distant metastasis was detected on imaging were included. Patients with no metastasis detected on $^{68}$Ga-PSMA PET/CT were excluded from the study. All patients underwent biopsy from all quadrants of the prostate gland, and patients who had not received any treatment (hormonotherapy, radiotherapy, chemotherapy) or surgery were included in the imaging study. PSA values in the last month were recorded.

$^{68}$Ga-PSMA PET/CT images were evaluated by 2 experienced nuclear medicine specialists and $^{68}$Ga-PSMA PET/CT data were recorded. Informed consent forms were obtained from the patients.

The Faculty of Medicine Dean's Office at Tokat Gaziosmanpaşa University and The University's Ethics Committee approved our study on (number: 831116987-522, date: 12.09.2024).

### $^{68}$Ga-PSMA PET/CT Imaging Protocol

During the $^{68}$Ga-PSMA PET/CT examinations, patients were administered an average of 111-185 Megabecquerel (3-5 mCi) of $^{68}$Ga-PSMA. The examination included a low-dose CT scan, followed by a PET scan conducted 45-60 minutes after the injection, taking about 10 minutes in total. The CT data were used for anatomical correlation and attenuation correction, while the PET scans were employed to compute the maximum standardized uptake values ($SUV_{max}$).

The $SUV_{max}$ was calculated by drawing regions of interest from the whole prostate tissue and metastatic tissue, which were considered to have the highest PSMA expression, and this value was recorded. Semi-automatic volumetric quantification of individual lesions and each patient was performed using a volume measurement software named

positron emission tomography volume computer assisted reading, which can measure metabolic tumor volume (MTV) as well as the $SUV_{max}$ or $SUV_{mean}$. Total lesion glycolysis (TLG) is a quantitative value obtained from the product of $SUV_{max}$ and MTV.

The images were evaluated by two experienced nuclear medicine specialists.

### Statistical Analysis

SPSS version 24 software was used for statistical analysis. The median value was used to express descriptive quantitative data, while percentages were used to express qualitative data. Fisher's exact test and chi-square test were used to compare variables. Analytical techniques (Kolmogorov-Smirnov/Shapiro-Wilk tests) and visual methods (histograms and probability graphs) were used to assess whether the variables showed a normal distribution. Descriptive analyses were performed using the median and interquartile range for non-normally distributed variables. When analyzing data that was not normally distributed, the Mann-Whitney U test was employed. While investigating the associations between non-normally distributed and/or ordinal variables, the correlation coefficients and their significance were calculated using the Spearman's correlation coefficient test. A p-value of less than 0.05 was considered to indicate a statistically significant result.

### Prostate Biopsy Protocol

All patients were started on antibiotics for prophylaxis one day before the procedure. On the day before the biopsy, 500 mg of ciprofloxacin was administered orally in the morning and evening. Antibiotics were continued in the morning and evening for 3 days after the procedure. The day before the biopsy, rectal cleansing was achieved using an enema. A 12-quadrant biopsy was taken from the prostate gland. The biopsy needle and automatic biopsy gun used were Angiotech Tru-Core I (Florida, USA).

## Results

The study included 112 patients, with a mean age of 70.5 years (range: 31-85 years). The mean PSA level was 46.35 ng/dL, which ranged from 2.15 to 5000 ng/dL. Among the patients, 13 (11.6%) had a Gleason score of 6, 27 (24.1%) of 7, 32 (28.6%) of 8, 25 (22.3%) of 9, and 15 (13.4%) of 10. For ISUP scoring, 13 patients (11.6%) had a score of 6, 6 patients (5.4%) hadscore of 7 (3+4), 22 patients (19.6%) had score of 7 (4+3), 31 patients (27.7%) had score of 8, and 40 patients (35.7%) had a score of 9-10.

According to the D'Amico risk classification, the number of low-risk patients was 3 (2.7%) medium-risk patients was 6 (5.4%) high-risk patients was 103 (92%).

According to body mass index (BMI), 1 patient (0.9%) was underweight, 35 patients (31.3%) were normal-weight, 49 patients (43.8%) were overweight, 22 patients (19.6%) were obese, and 5 patients (4.5%) were severely obese. The PSA value of the only underweight patient was 149 ng/dL. The mean PSA value of 35 normal-weight patients was 100 ng/dl. 49 overweight patients had a mean PSA value of 45.9 ng/mL. The 22 obese patients had a mean PSA value of 19.93 ng/dL, and 5 extremely obese patients had a mean PSA value of 82.6 ng/dL. A low correlation was observed between PSA values and BMI in the patients (p=0.08, r=-0.248).

The $SUV_{max}$ for the prostate gland was 38.9 in the only underweight patient. Among 35 normal-weight patients, the median $SUV_{max}$ value was 16.2 (ranging from 3.9 to 55.8). For the 49 overweight patients, the median $SUV_{max}$ was 15.4 (with a range of 1 to 123).

The 22 obese patients exhibited a median $SUV_{max}$ value of 12.75 (ranging from 3.9 to 40.5), while the 5 extremely obese patients had a median $SUV_{max}$ value of 40.2 (ranging from 8.7 to 55.6). No significant correlation was observed between the $SUV_{max}$ value of the prostate gland and BMI (p=0.128) (Table 1). There was also no significant correlation between prostate gland MTV, TLG, SUL, and $SUV_{mean}$ (p=0.363, p=0.558, p=0.247, p=0.085).

**Table 1. Relationship between BMI and prostate gland $SUV_{max}$ and PSA value**

| | BMI | | | | | p-value |
|---|---|---|---|---|---|---|
| | Underweight <18.5 | Normal 18.5-24.9 | Overweight 25- 29.9 | Obese 30- 34.9 | Extremely obese 35- 39.9 | |
| Prostate gland $SUV_{max}$ (median) (min-max) | 38.9 | 16.2 (3.9-55.8) | 15.4 (1-123) | 12.75 (3.9-40.5) | 40.2 (8.7-55.6) | p=0.128 |
| PSA value ng/dL | 149 ng/dL | 100 ng/dL | 45.9 ng/dL | 19.93 ng/dL | 82.6 ng/dL | p=0.008 r=-0.248 |

BMI: Body mass index, $SUV_{max}$: Maximum standard uptake values, PSA: Prostate-specific antigen

There was no correlation between BMI and D'Amico classification. Of the 3 low-risk patients, 1 (33.3%) was obese and 2 (66.7%) were overweight. Of the 6 patients with medium risk, 2 (33.3%) were normal weight, 2 (33.3%) were overweight, and 2 (33.3%) were obese. Of 103 high-risk patients, 1 (1%) was underweight, 33 (32%) were normal weight, 45 (43.7%) were overweight, 19 (18.4%) were obese, and 5 (4.9%) were extremely obese (p=0.467) (Table 2).

A correlation was observed between D'Amico risk groups and prostate $SUV_{max}$ values (p=0.035). In the low-risk group, the median $SUV_{max}$ value of the prostate gland was 6.8 (ranging from 6.4 to 8.7), while in the medium-risk group, it was 6.2 (ranging from 3.9 to 34.8), and in the high-risk group, it was 16.6 (ranging from 1 to 123). The $SUV_{max}$ values of the prostate gland were elevated in the high-risk group. There were also significant associations between D'Amico risk classification and prostate gland TLG, SUL and $SUV_{mean}$ (p=0.037, p=0.012, p=0.028). However, there was no significant association between prostate gland MTV value and D'Amico classification (p=0.366).

Seventy-six patients with distant metastases had a mean PSA level of 63 ng/dL (range: 2.15-5000 ng/dL). No significant correlation was observed between PSA value and prostate gland $SUV_{max}$, MTV, TLG, SUL, and $SUV_{mean}$ (p=0.881, p=0.602, p=0.630, p=0.995, p=0.875). Thirty-six patients with locoregional metastases had a mean PSA value of 31.15 ng/mL (range: 3-495 ng/mL). The PSA value was significantly higher for patients with distant metastasis compared to patients with locoregional metastasis only (p=0.02).

Thirty-six patients (32.1%) had locoregional metastases while 76 patients (67.9%) had distant metastases. Thirty-eight patients (33.9%) had only bone metastases. Fourteen patients (12.5%) had bone and distant lymph node metastases. There were 4 patients (3.6%) with solid organ metastases only. There were 6 patients (5.4%) with both bone and solid organ metastases. One patient (0.9% of the cohort) had solid organ and distant lymph node metastasis. Six patients (5.4%) had only distant metastasis to lymph nodes. Five patients (4.5%) had bone, distant lymph node, and solid organ metastases.

According to D'Amico's classification, 31 out of 36 patients (86.1%) with locoregional disease were classified as high-risk, 2 patients (5.6%), were classified as low-risk, and 3 patients (8.3%), were categorized as intermediate-risk. Among the 76 patients with distant metastasis, 72 patients (94.8%) were classified as high-risk, 3 patients (3.9%) as intermediate-risk, and 1 patient (1.3%) as low-risk. Of the 38 patients with only bone metastases, 37 patients (97.4%) were in the high-risk group, and 1 patient (2.6%) was in the low-risk group. No patients were classified within the intermediate-risk group. All 14 patients with both bone and distant lymph node metastases were classified as high-risk, as were all 4 patients with only solid organ metastases. Among the 6 patients with both bone and solid organ metastases, 5 patients (83.3%) were in the high-risk group, 1 patient (16.7%) was in the intermediate-risk group, and none were classified as low-risk. Only 1 patient with both solid organ and distant lymph node metastasis was classified as high-risk. Of the 8 patients with only distant lymph node metastasis, 6 (75%) were in the high-risk group, and 2 (25%) were in the intermediate-risk group. No significant correlation was observed between D'Amico risk groups and metastasis localization (p=0.452).

Furthermore, no significant correlation was observed between D'Amico classification and the presence of distant metastasis or locoregional disease (p=0.257). The presence of locoregional disease or distant metastasis was not significantly associated with prostate gland $SUV_{max}$, MTV, TLG, $SUV_{mean}$ and SUL values (p=0.25, p=0.667, p=0.667, p=0.244, p=0.126, p=0.057). However, a significant correlation was observed between the presence of distant metastasis or locoregional disease and PSA levels (p=0.02). The average PSA value for the 76 patients with distant metastasis was 63 ng/mL (range: 2.15-5000 ng/mL), whereas the average PSA value for the 36 patients with locoregional disease was 31.15 ng/mL (range: 3-495 ng/mL).

**Table 2. Relationship between BMI and D'Amico risk classifications**

| | **BMI** | | | | | **p-value** |
|---|---|---|---|---|---|---|
| D'Amico risk classifications | Underweight <18.5 | Normal 18.5-24.9 | Overweight 25-29.9 | Obese 30-34.9 | Extremely obese 35-39.9 | |
| Low-risk | 0 (0%) | 0 (0%) | 2 (66.7%) | 1 (33.3%) | 0 (0%) | p=0.467 |
| Medium-risk | 0 (0%) | 2 (33.3%) | 2 (33.3%) | 2 (33.3%) | 0 (0%) | |
| High-risk | 1 (1%) | 33 (32%) | 45 (43.7%) | 19 (18.4%) | 5 (4.9%) | |

BMI: Body mass index

## Discussion

The D'Amico classification is the most widely used system for assessing metastatic risk in prostate cancer. $^{68}$Ga-PSMA PET/CT is the most sensitive imaging modality for staging prostate cancer, especially in patients classified as intermediate to high risk. The majority of our patients were classified as high-risk all of whom exhibited metastases on $^{68}$Ga-PSMA PET/CT. Although not statistically significant, metastases were detected in 3 patients classified as the low-risk group and 6 patients in the intermediate-risk group; however, not all patients in these groups were metastatic. No significant correlation was observed between metastasis location and the D'Amico risk classification. However, a significant correlation was observed between D'Amico risk classification and the $SUV_{max}$ values of the prostate gland. Significant associations were also observed between the D'Amico risk classification and TLG, $SUV_{mean}$, and SUL values. As the risk classification increased, PSMA uptake in the prostate gland correspondingly increased. Our literature review revealed that similar studies investigating the relationship between the D'Amico risk classification and prostate gland $SUV_{max}$ values in prostate cancer patients have likewise reported significant findings. Significant associations were also observed between the D'Amico risk classification and TLG, $SUV_{mean}$, and SUL values. In the same study, a significant relationship was reported between the D'Amico risk classification and both $SUV_{max}$ and MTV. However, in our study, no significant correlation was found between the D'Amico classification and MTV (4).

For instance, Koerber et al. (5), in a study involving 104 patients, demonstrated that PSMA uptake levels increased with higher D'Amico risk classifications. Similarly, Ekmekçioğlu et al. (6) and Liu et al. (7) reported findings consistent with ours, showing increased PSMA uptake levels in the prostate gland in patients in the high-risk group.

No significant correlation was observed between PSA values and quantitative PET/CT measurements of the prostate gland in our study. However, Jafari et al. (8) reported a significant correlation between PSA levels and all PET/CT parameters. This discrepancy may be attributed to all patients in our study having metastatic disease.

No significant correlation was observed between the presence of distant metastasis or locoregional disease and prostate gland $SUV_{max}$ values. However, the general trend of higher $SUV_{max}$ values in high-risk patients suggests that an increased $SUV_{max}$ may be associated with a greater likelihood of metastasis. However, no significant correlation was found between $SUV_{max}$ values and the presence of local versus distant metastases. Similarly, no significant associations were observed between other PET/CT parameters and either local or distant metastasis. Our literature review did not reveal any previous studies specifically addressing this topic. Therefore, we believe that the findings of our study provide valuable and novel insights.

However, we observed a significant association between PSA levels and the presence of distant metastasis or locoregional disease. Blackwell et al. (9) demonstrated that preoperative serum PSA values had predictive value for determining tumour burden and stage. Another study reported that the probability of lymph node involvement is less than 1% n patients with PSA levels below 20 ng/mL, suggesting that radiological imaging for staging could be minimized in this group (10). In our study, all patients were metastatic, with a median PSA level of 31.15 ng/dL in patients with locoregional metastasis and 63 ng/dL in those with distant metastasis.

The majority of our patients being overweight and obese suggested that obesity was associated with prostate cancer. However, no significant correlation was observed between BMI and prostate gland PET/CT values. According to a meta-analysis study, obesity was associated with an increased risk of prostate cancer in Europe (11). Several large cohort studies also observed a stronger association between increasing BMI and prostate cancer risk (12,13,14). However, some studies did not find an association between BMI and certain health outcomes related to obesity (15,16). Considering these contradictory results, a recent meta-analysis revealed that prostate cancer was weakly associated with an increased risk related to obesity (11). In addition, since our study included patients with locally advanced and distant metastases, and the majority of them were overweight, we think that obesity may contribute to the aggressiveness of prostate cancer. The mechanisms showing that obesity causes aggressive prostate cancer were described in Allot et al.'s (17). They suggested that low PSA levels, resulting from hemodilution due to increased blood volume in obese men, may delay or prevent prostate biopsy, potentially leading to the diagnosis of more aggressive prostate cancer (18). Additionally, the difficulty of performing digital rectal examination and the increased prostate volume in obese men may contribute to delayed cancer detection during biopsy (19,20).

Obese men had significantly lower PSA values compared to lean, and normal-weight men. Consistent with our findings, Vidal et al. (21) also reported lower PSA levels in obese and overweight patients compared with normal-weight patients. Other studies have indicated that obesity

is associated with reduced PSA levels, which may in turn decrease the rate of cancer detection (22,23). Further research is warranted to better understand this relationship.

### Study Limitation

The limited number of patients and the retrospective nature of the study are among the limitations of our study. In addition, not all metastases could be confirmed histopathologically.

## Conclusion

There are numerous treatment options for prostate cancer, with staging being the most critical factor in determining effective management. Consequently, the detection and localization of metastases are of paramount importance. In our study, we would like to emphasize that metastasis is present in a large proportion of patients in the high-risk class in the D'Amico risk classification. However, considering the possibility of distant metastasis in the low- and intermediate-risk class, $^{68}$Ga-PSMA PET/CT may also be recommended in the staging of these patients. We would like to emphasize that although PSA values carry important information about the stage of the disease, they may not reflect the reality in overweight or obese patients and should be taken into consideration in clinical evaluation.

### Ethics

**Ethics Committee Approval:** The Faculty of Medicine Dean's Office at Tokat Gaziosmanpaşa University and The University's Ethics Committee approved our study on (number: 831116987-522, date: 12.09.2024).

**Informed Consent:** Our study was retrospective, and informed consent was obtained from the patients.

### Footnotes

### Authorship Contributions

Concept: Z.H., Design: Z.H., Data Collection or Processing: Ö.U., Analysis or Interpretation: Z.H., Literature Search: Ö.U., Z.H., Writing: Ö.U., Z.H.

**Conflict of Interest:** No conflict of interest was declared by the authors.

**Financial Disclosure:** The authors declared that this study has received no financial.

## References

1. SEER Cancer Statistics Review (CSR) 1975-2016. 2019
2. Sartor O, de Bono JS. Metastatic prostate cancer. N Engl J Med. 2018;378:645-657.
3. Mease RC, Foss CA, Pomper MG. PET imaging in prostate cancer: focus on prostate-specific membrane antigen. Curr Top Med Chem. 2013;13:951-962.
4. Lv J, Yu H, Yin H, Shi Y, Shi H. A single-center, multi-factor, retrospective study to improve the diagnostic accuracy of primary prostate cancer using [$^{68}$Ga]Ga-PSMA-11 total-body PET/CT imaging. Eur J Nucl Med Mol Imaging. 2024;51:919-927.
5. Koerber SA, Utzinger MT, Kratochwil C, Kesch C, Haefner MF, Katayama S, Mier W, Iagaru AH, Herfarth K, Haberkorn U, Debus J, Giesel FL. $^{68}$Ga-PSMA-11 PET/CT in newly diagnosed carcinoma of the prostate: correlation of ıntraprostatic PSMA uptake with several clinical parameters. J Nucl Med. 2017;58:1943-1948.
6. Ekmekcioglu O, Yavuzsan AH, Arican P, Kirecci SL. Is there a nonnegligible effect of maximum standardized uptake value in the staging and management of prostate cancer with $^{68}$Ga-prostate-specific membrane antigen positron emission tomography/computerized tomography imaging? A single-center experience. J Cancer Res Ther. 2021;17:1351-1357.
7. Liu C, Liu T, Zhang N, Liu Y, Li N, Du P, Yang Y, Liu M, Gong K, Yang X, Zhu H, Yan K, Yang Z. $^{68}$Ga-PSMA-617 PET/CT: a promising new technique for predicting risk stratification and metastatic risk of prostate cancer patients. Eur J Nucl Med Mol Imaging. 2018;45:1852-1861.
8. Jafari E, Dadgar H, Zarei A, Samimi R, Manafi-Farid R, Divband G, Assadi M. The role of [68Ga] Ga-PSMA PET/CT in primary staging of newly diagnosed prostate cancer: predictive value of PET-derived parameters for risk stratification through machine learning. Clin Transl Imaging. 2024;12:669-682.
9. Blackwell KL, Bostwick DG, Myers RP, Zincke H, Oesterling JE. Combining prostate specific antigen with cancer and gland volume to predict more reliably pathological stage: the influence of prostate specific antigen cancer density. J Urol. 1994;151:1565-1570.
10. Huncharek M, Muscat J. Serum prostate-specific antigen as a predictor of staging abdominal/pelvic computed tomography in newly diagnosed prostate cancer. Abdom Imaging. 1996;21:364-367.
11. MacInnis RJ, English DR. Body size and composition and prostate cancer risk: systematic review and meta-regression analysis. Cancer Causes Control. 2006;17:989-1003.
12. Veierød MB, Laake P, Thelle DS. Dietary fat intake and risk of prostate cancer: a prospective study of 25,708 Norwegian men. Int J Cancer. 1997;73:634-638.
13. Engeland A, Tretli S, Bjørge T. Height, body mass index, and prostate cancer: a follow-up of 950000 Norwegian men. Br J Cancer. 2003;89:1237-1242.
14. Hasbek Z, Yılmaz M, Uçar M, Hasbek ME. Prostate cancer and obesity. CMJ. 2024;46:118-120.
15. Schuurman AG, Goldbohm RA, Dorant E, van den Brandt PA. Anthropometry in relation to prostate cancer risk in the netherlands cohort study. Am J Epidemiol. 2000;151:541-549.
16. Nilsen TI, Vatten LJ. Anthropometry and prostate cancer risk: a prospective study of 22,248 Norwegian men. Cancer Causes Control. 1999;10:269-275.
17. Allott EH, Masko EM, Freedland SJ. Obesity and prostate cancer: weighing the evidence. Eur Urol. 2013;63:800-809.
18. Grubb RL 3rd, Black A, Izmirlian G, Hickey TP, Pinsky PF, Mabie JE, Riley TL, Ragard LR, Prorok PC, Berg CD, Crawford ED, Church TR, Andriole GL Jr; PLCO Project Team. Serum prostate-specific antigen hemodilution among obese men undergoing screening in the Prostate, Lung, Colorectal, and Ovarian Cancer Screening Trial. Cancer Epidemiol Biomarkers Prev. 2009;18:748-751.
19. Chu DI, De Nunzio C, Gerber L, Thomas JA 2nd, Calloway EE, Albisinni S, Senocak C, McKeever MG, Moreira DM, Tubaro A, Moul JW, Freedland SJ, Bañez LL. Predictive value of digital rectal examination for prostate cancer detection is modified by obesity. Prostate Cancer Prostatic Dis. 2011;14:346-353.

20. Freedland SJ, Platz EA, Presti JC Jr, Aronson WJ, Amling CL, Kane CJ, Terris MK. Obesity, serum prostate specific antigen and prostate size: implications for prostate cancer detection. J Urol. 2006;175:500-504.
21. Vidal AC, Howard LE, Moreira DM, Castro-Santamaria R, Andriole GL, Freedland SJ. Obesity increases the risk for high-grade prostate cancer: results from the REDUCE study. Cancer Epidemiology, Biomarkers & Prevention. 2014;23:2936-2942.
22. Barqawi AB, Golden BK, O'Donnell C, Brawer MK, Crawford ED. Observed effect of age and body mass index on total and complexed PSA: analysis from a national screening program. Urology. 2005;65:708-712.
23. Baillargeon J, Pollock BH, Kristal AR, Bradshaw P, Hernandez J, Basler J, Higgins B, Lynch S, Rozanski T, Troyer D, Thompson I. The association of body mass index and prostate-specific antigen in a population-based study. Cancer. 2005;103:1092-1095.

*Original Article*

*Mol Imaging Radionucl Ther 2025;34:180-187* *DOI:10.4274/mirt.galenos.2025.77200*

# Investigation of the Partial Volume Effect in Pre-Dosimetry of Liver Tumors for $^{90}$Y Radioembolization: A Phantom Study

## *$^{90}$Y Radyoembolizasyon Tedavisinde Karaciğer Tümörleri Pre-Dozimetri'de Kısmi Hacim Etkisinin İncelenmesi: Bir Fantom Çalışması*

**Ayşe Dilaver Akar[1], Nami Yeyin[2], Sinem Akyol[2], Özge Demir[3], Eylem Gülce Çoker[1], Mustafa Demir[2]**

[1]*İstanbul Aydın University, Graduate Education Institute, Health Physics Program, İstanbul, Türkiye*
[2]*İstanbul University-Cerrahpaşa, Cerrahpaşa Faculty of Medicine, Department of Nuclear Medicine, İstanbul, Türkiye*
[3]*İstanbul University-Cerrahpaşa, Cerrahpaşa Faculty of Medicine, Department of Chemical Engineering, İstanbul, Türkiye*

## Abstract

**Objectives:** Yttrium-90 ($^{90}$Y) radioembolization has become increasingly important in the treatment of liver tumors. This study aims to experimentally determine the extent to which small liver tumors are affected by the partial volume effect (PVE) in single photon emission computed tomography/computed tomography (SPECT/CT) scintigraphy using technetium-99m-macroaggregated albumin (Tc-99m-MAA), and to investigate the impact of PVE on tumor dosimetry and image quality.

**Methods:** In this experimental study, a custom-designed liver phantom containing four tumor mimics with diameters of 1 cm, 2 cm, 3 cm, and 5 cm was used. The tumor and liver parenchyma volumes were filled with Tc-99m at a ratio of 4.86: 1. The phantom was imaged in a water tank using SPECT/CT according to standard clinical protocols. Volumetric regions of interest were drawn for each lesion and tumor volumes, contrast values (C), contrast to noise ratios (CNR), and absorbed tumor doses were calculated from the counts obtained. Since this study does not involve live subjects and was conducted solely on a phantom model, ethical approval, informed consent, and consent forms are not required for this study.

**Results:** Tumor diameters measured on SPECT/CT images matched those obtained from both CT images and the actual dimensions. The contrast values calculated from the SPECT/CT images for lesions with diameters of 2 cm and 5 cm were 2.03 and 3.89, respectively. Similarly, the corresponding CNR values were 8.64 and 21.07. Tumor-to-normal tissue ratios were 2.03 and 3.89 for the 2 cm and 5 cm lesions, respectively.

For the 2 cm lesion, the actual and SPECT/CT-derived absorbed doses were 15.3 Gy and 7.87 Gy, respectively. For the 5 cm lesion, these values were 15.4 Gy and 13.38 Gy, respectively. The absorbed tumor doses significantly decreased as tumor diameter decreased due to the influence of PVE.

**Conclusion:** Tumors smaller than 2 cm in diameter were markedly affected by the PVE. Considering the influence of PVE, or applying appropriate corrections in dosimetric calculations, is of critical importance for improving the accuracy of dosimetry results.

**Keywords:** $^{90}$Y radioembolization therapy, Tc-99m-MAA dosimetry, partial volume effect, tumor imaging, image quality

**Address for Correspondence:** Eylem Gülce Çoker, İstanbul Aydın University, Graduate Education Institute, Health Physics Program, İstanbul, Türkiye
**E-mail:** demirm@iuc.edu.tr **ORCID ID:** orcid.org/0000-0001-6361-9458
**Received:** 14.02.2025 **Accepted:** 18.06.2025 **Epub:** 13.08.2025 **Publication Date:** 08.10.2025

**Cite this article as:** Dilaver Akar A, Yeyin N, Akyol S, Demir Ö, Çoker EG, Demir M. Investigation of the partial volume effect in pre-dosimetry of liver tumors for $^{90}$Y radioembolization: a phantom study. Mol Imaging Radionucl Ther. 2025;34:180-187.

Copyright© 2025 The Author. Published by Galenos Publishing House on behalf of the Turkish Society of Nuclear Medicine.
This is an open access article under the Creative Commons Attribution-NonCommercial-NoDerivatives 4.0 (CC BY-NC-ND) International License.

## Öz

**Amaç:** Karaciğer tümörlerine yönelik ittriyum-90 ($^{90}$Y) radyoembolizasyon tedavisinin önemi giderek artmaktadır. Bu çalışmanın amacı, teknesyum-99m-makroagregat albümin (Tc-99m-MAA) kullanılarak yapılan tek foton emisyonlu tomografi/bilgisayarlı tomografi (SPECT/BT) sintigrafisinde küçük karaciğer tümörlerinin kısmi hacim etkisinden (PVE) etkilenme düzeylerinin deneysel olarak belirlenmesi ve PVE'nin tümör dozları ile görüntü kalitesi üzerindeki etkisinin araştırılmasıdır.

**Yöntem:** Bu deneysel çalışmada, çapları 1 cm, 2 cm, 3 cm ve 5 cm olan dört taklit tümör içeren özel tasarlanmış bir karaciğer fantomu kullanıldı. Tümör/karaciğer parankim dokusunu temsil eden hacimler Tc-99m ile 4,86/1 oranında dolduruldu. Fantom, rutin klinik protokollere uygun olarak bir su tankı içinde SPECT/BT ile görüntülendi. Lezyonlardan hacimsel ilgi alanları çizilerek elde edilen sayımlardan lezyon hacimleri, kontrastlar (C), kontrast/gürültü oranları (CNR) ve tümör dozları hesaplandı.

**Bulgular:** SPECT/BT görüntülerinde tümör çapları, BT görüntülerinden ölçüldü ve gerçek değerlerle aynı ölçülerde bulundu. 2 cm ve 5 cm çaplı lezyonlar için SPECT/BT görüntülerinden hesaplanan kontrast değerleri sırasıyla 2,03 ve 3,89 bulundu. Benzer şekilde CNR değerleri sırasıyla 8,64 ve 21,07 bulundu. Tümör/normal doku (oranları 2 cm ve 5 cm çaplı lezyonlar için sırasıyla 2,03 ve 3,89 bulundu.

2 cm çaplı lezyon için reel ve SPECT/BT'den hesaplanan absorbe dozlar sırasıyla 15,3 Gy ve 7,87 Gy bulundu. 5 cm çaplı lezyon için reel ve SPECT/BT'den hesaplanan absorbe dozlar sırasıyla 15,4 Gy ve 13,38 Gy bulundu. PVE'ye bağlı olarak tümör çapı azaldıkça tümör dozlarının da önemli oranda azaldığı belirlendi.

**Sonuç:** Çapı 3 cm'den küçük olan tümörler PVE' den belirgin şekilde etkilenmiştir. Dozimetri hesaplamalarında PVE etkisinin göz önünde bulundurulması veya gerekli düzeltmelerin uygulanması, dozimetri sonuçlarının doğruluğunu artırmak açısından büyük önem taşımaktadır.


**Anahtar kelimeler:** $^{90}$Y mikroembolizasyon tedavisi, Tc-99m-MAA dozimetrisi, kısmi hacim etkisi, tümör görüntüleme, görüntü kalitesi

## Introduction

Yttrium-90 ($^{90}$Y) transarterial radioembolization is an important treatment option for liver malignancies, including hepatocellular carcinoma and liver metastases originating from colorectal cancer (1,2,3). Primary and secondary liver tumors (Tm) that are not amenable to surgery can be treated through the transarterial administration of $^{99}$Y-labeled microspheres. While 80-100% of liver Tm are supplied arterially via the hepatic artery, 60-70% of the normal liver parenchyma receives blood from the portal vein. When microspheres are administered via catheter into the hepatic artery, they predominantly accumulate in the peripheral areas of the tumor regions with higher perfusion thus theoretically enabling the delivery of high radiation doses to the tumor while sparing the normal parenchymal tissue.

Prior to treatment, technetium-99m-macroaggregated albumin (Tc-99m-MAA), is administered by the interventional radiology department to predict the biodistribution of $^{99}$Y microspheres. Following angiography, hepatic artery perfusion scintigraphy is performed to assess any extrahepatic leakage of the radiotracer and to evaluate the distribution of radioactivity within the tumor (4,5). The Tc-99m-MAA photon emission computed tomography/computed tomography (SPECT/CT) scan, performed intra-arterially prior to $^{99}$Y microsphere therapy, is used to determine the hepatopulmonary shunt fraction and to exclude potential reflux of radioactive material into the bowel, stomach, or pancreas (6). The distribution of microspheres in the capillary bed as seen on Tc-99m SPECT/CT imaging closely resembles the distribution of $^{99}$Y microspheres during actual treatment; therefore, this imaging method is used in dosimetric studies (7).

Partial volume effect (PVE) is a phenomenon that arises when small lesions appear larger and with lower activity on scintigraphy due to the limited spatial resolution of the imaging system. If the imaged object or region is smaller than twice the full width at half maximum (FWHM) in the x, y, and z axes of the system, the activity within the lesion will be underestimated and its visual clarity diminished (8). PVE is a complex process influenced by several factors, including tumor size and shape, background activity in surrounding tissues, the spatial resolution of the imaging system, voxel size, and imaging modality. One of the primary causes of blurring in three-dimensional imaging is limited spatial resolution. Signal intensity within voxels represents tissue properties. Even when the spatial resolution of the imaging system is optimal, PVE may occur if lesion size is small. Additionally, smaller voxel sizes contribute to an increase in PVE (9).

The aim of this study is to: identify the perfused regions and their activity distribution in SPECT/CT scintigraphy using Tc-99m-MAA; experimentally determine the degree to which small liver Tm are affected by PVE; and investigate the impact of PVE on tumor dosimetry and image quality (IQ).

## Materials and Methods

This study was conducted at the Department of Nuclear Medicine, İstanbul University-Cerrahpaşa Faculty of Medicine. The liver phantom used in the study was

designed based on the model described by Yeyin et al. (10). Additionally, lesions specific to this study were added to the phantom (Figure 1).

### Liver Phantom and Water Tank

The model designed for this study consists of two main components: the liver and the water tank. The materials used in the phantom were selected in collaboration with the Department of Chemical Engineering. The liver was produced using a 3D printer and additive manufacturing technique (Fused Deposition Modeling), with a filament material called polylactic acid (PLA), which has a density of 1.24 g/cm³. Both the outer wall of the liver parenchyma and the outer shells of the simulated Tm were made of PLA, each with a thickness of 1.5 mm. The dimensions of the liver phantom are 112 mm × 191 mm, and its empty weight is 350 grams. The diameters of the four simulated lesions in the phantom are 1 cm, 2 cm, 3 cm, and 5 cm, with internal volumes that need checking against spherical volume calculations for consistency. The volume representing the liver parenchyma is 615 cm³. The second component of the phantom set, the water tank, has a depth of 20 cm and dimensions of 25 × 30 cm. The water tank and its mounting apparatus are made of Plexiglas, with no metal components used. The water filled in the tank simulates the photon scattering environment that may arise from organs and tissues other than the liver.

### Phantom Operating Principle and Functionality

Our model includes four separate cylindrical tumor cavities within the liver phantom. These Tm can be filled with Tc-99m at either the same or different concentrations. Additionally, the cavity representing the liver parenchyma can be filled with a radioactive substance through a separate cap. After the phantoms are placed in the tank, they are fixed with plastic screws. Once the tank is filled with water, it can be positioned for imaging.

### Imaging Protocol

SPECT/CT imaging was performed using a Siemens Symbia T16 SPECT/CT device equipped with a low-energy high-resolution collimator and dual detectors (Figure 2). After the Tm and all the compartments representing liver parenchymal tissue were filled with Tc-99m at a concentration of 2.13 µCi/mL, SPECT/CT imaging was performed. The routine clinical protocol was used for imaging. Low-dose CT scanning was performed with 120 kV and 100 mAs. The parameters used for SPECT/CT imaging were 140 keV, 15% dual-energy window, 128 × 128 matrix, 40 projections per scan, non-circular continuous orbit, and 20 seconds exposure time per SPECT projection. SPECT/CT data were reconstructed using the ordered subsets expectation maximization (3D) method with eight iterations and eight subsets. A 6 mm Gaussian filter was used for scatter correction based on the dual-energy window and attenuation correction based on CT data.

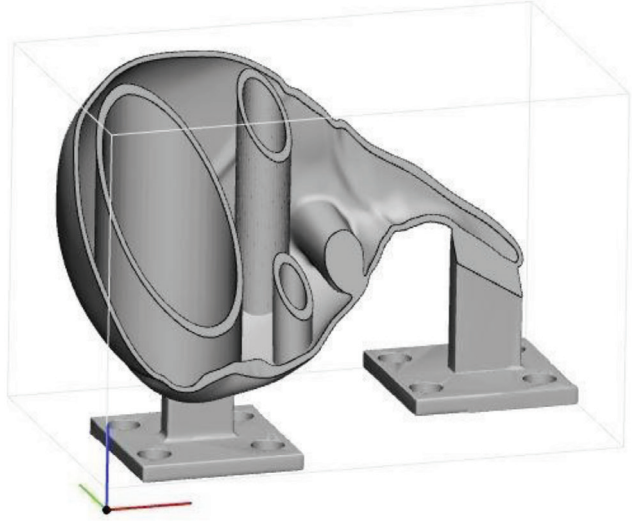


**Figure 1.** 3D image of the liver phantom and the fixation feet inside the water tank




**Figure 2.** Position of the liver phantom in the SPECT/CT device within the water tank

### SPECT/CT Image Quality Quantification

To assess SPECT/CT IQ volumetric regions of interest (VOIs) were drawn on the SPECT/CT images. Based on the counts within the VOIs, tumor-to-normal tissue ratio (T/N), contrast (C), and contrast-to-noise ratio (CNR) were calculated (11).

$$C = \frac{Nl - Nbg}{Nbg} \quad (1)$$

Nl = Counts within the lesion VOI, Nbg = Counts within the background

$$CNR = \frac{C}{COV} \quad (2)$$

C: Contrast, COV: The coefficient of variation is given by

$$COV = \frac{\sigma bg}{Nbg}$$

σbg is the standard deviation of the background VOI.

### Organ and Tumor Doses

Based on the activity amounts of the Tc-99m radioisotope filled into the phantom, the actual doses for both the tumor and the liver were calculated and considered as reference doses. The internal volumes of the phantom were assumed to correspond to the volume of the Tc-99m solution within the phantom. In the dosimetric calculations based on SPECT/CT images, the masses of organs and Tm were determined from CT-derived volume measurements.

The administered activity (A) was calculated using Equation 3, and the absorbed dose (D) was calculated using Equation 4 (12).

$$A\ (GBq)_{Total} = A\ (GBq)_{Normal\ liver\ tissue} + A\ (GBq)_{Tumor} \quad (3)$$

A $(GBq)_{Total}$: The amount of activity filled into the phantom's simulated lesions and the compartments representing the liver parenchymal tissue.

$$D\ (Gy)_{Tumor} = \frac{49.38\ A_{total}\ (1-LSF)}{\frac{1}{\frac{T}{N}}\left(m_{Normal\ liver\ tissue} + \frac{T}{N} m_{Tumor}\right)} \quad (4)$$

D $(Gy)_{Tumor}$: Tumor dose

LSF: Lung shunt fraction (assumed to be zero), T/N: Tumor-to-normal tissue activity ratio, m: Mass (kg)

## Results

Following the filling of all compartments representing Tm and normal liver parenchyma with Tc-99m at a concentration of 2.13 μCi/mL, SPECT/CT imaging was performed. In the scintigraphic cross-sectional images obtained after scanning, the outer boundaries of the lesions were clearly visible (Figure 3). The actual tm of 1 cm, 2 cm, 3 cm, and 5 cm were found to match with the tms measured on SPECT/CT images. For CNR calculation, 12 equally sized VOIs were drawn from the SPECT/CT and Planar images shown in Figure 3. The significance between VOI counts was compared using the Mann-Whitney U test. A significant difference was found between the two VOI groups at p=0.015.

The contrast and CNR values calculated from the SPECT/CT images are presented in Table 1. The T/N activity ratios and tumor doses are shown in Table 2. Based on the actual Tc-99m activity values administered to the phantom, the

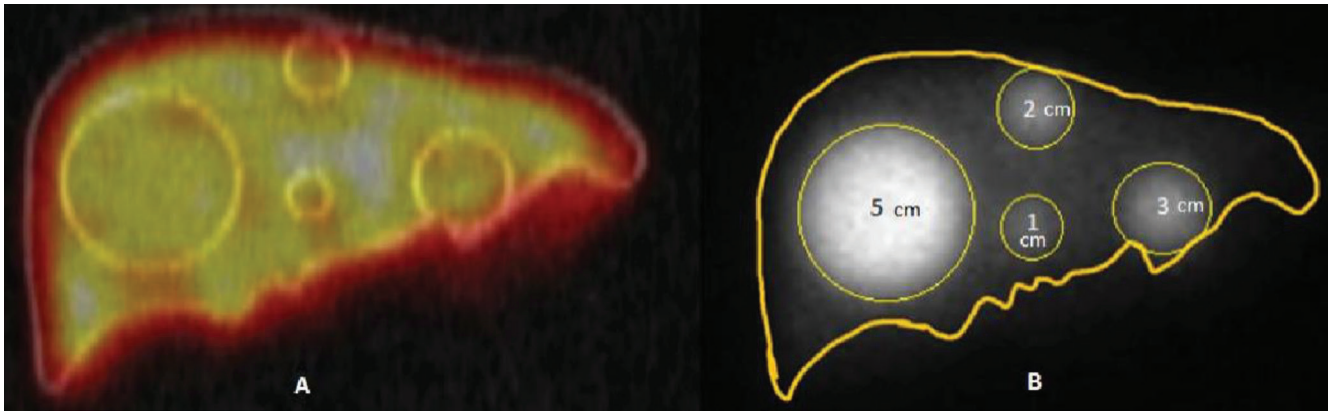



**Figure 3.** SPECT/CT fusion VOI images showing the CT image of the lesions (A). In the planar image, the numbers inside the ROIs represent the lesion diameters (B)

T/N ratio was kept constant at 4.86:1. However, it was observed that the T/N ratios increased with increasing tumor diameter (tm) in the SPECT/CT images. The tumor volumes calculated from the SPECT/CT images were found to be 16 $cm^3$, 20 $cm^3$, 30 $cm^3$, and 205 $cm^3$. The correlation between tumor volumes and tumor doses is presented in Figure 4.

The correlation between the tumor doses calculated from SPECT/CT images and the CNR values is shown in Figure 5. It was observed that CNR values increased with increasing tumor dose. However, for the tumor with a volume of 30 $cm^3$, the increase in CNR value appeared to be disproportionate compared to the others. The correlation between the tumor doses and contrast values calculated from the SPECT/CT images is presented in Figure 6. It was determined that contrast values also increased with tumor dose, and that there was a strong correlation between them.

## Discussion

In this study, PVE investigation was conducted using a specially designed liver phantom that included four simulated Tm with diameters of 1 cm, 2 cm, 3 cm, and 5 cm, as well as a separate compartment representing normal liver parenchyma. In scintigraphic imaging, PVE is a well-known phenomenon that particularly affects the visibility of small-volume lesions and leads to significant errors in dosimetric calculations based on scintigraphic

**Table 1. Contrast, CNR, and noise values calculated from SPECT/CT**

| Tumor diameter (cm) | Contrast (SPECT/CT) | CNR (SPECT/CT) |
|---|---|---|
| 1 | 1.64 | 5.5 |
| 2 | 2.03 | 8.64 |
| 3 | 2.24 | 9 |
| 5 | 3.89 | 21.07 |

CNR: Contrast to noise ratio, SPECT/CT: Single photon emission computed tomography/computed tomograp

**Table 2. Lesion diameter, scintigraphic T/N ratios, and calculated tumor doses in the actual T/N (4.86/1)**

| Tumor diameter (cm) | T/N (SPECT/CT) | Actual doses calculated from phantom activites (Gy) | Tumor dose calculated from SPECT/CT (Gy) | Tumor dose decreas rates (%) |
|---|---|---|---|---|
| 1 | 1.65 | 14.9 | 6.04 | 59.3 |
| 2 | 2.03 | 15.3 | 7.87 | 48.6 |
| 3 | 2.24 | 16.3 | 9.66 | 40.8 |
| 5 | 3.89 | 15.4 | 13.38 | 7.97 |

SPECT/CT: Single photon emission computed tomography/computed tomograp, T/N: Tumor-to-normal tissue ratio,

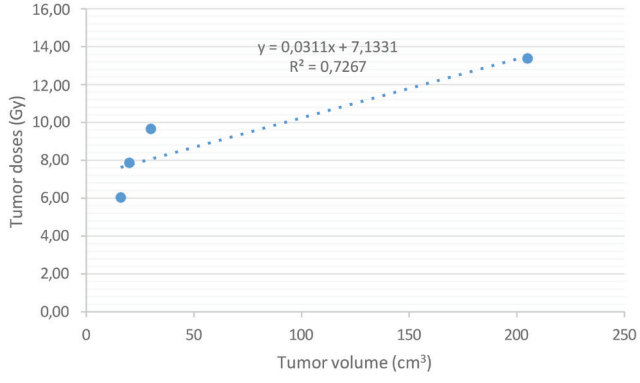



**Figure 4.** Tumor volume-tumor dose correlation obtained from SPECT/CT images

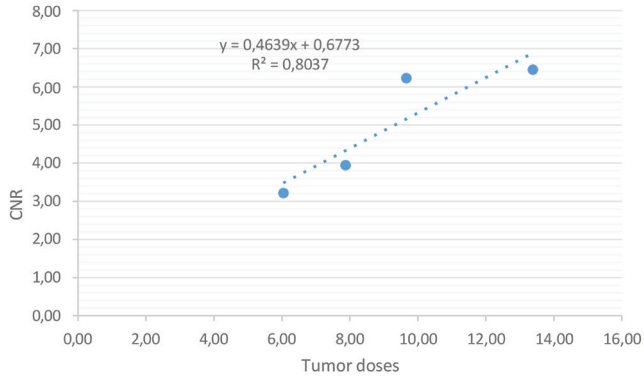



**Figure 5.** Tumor dose/CNR correlation calculated from SPECT/CT

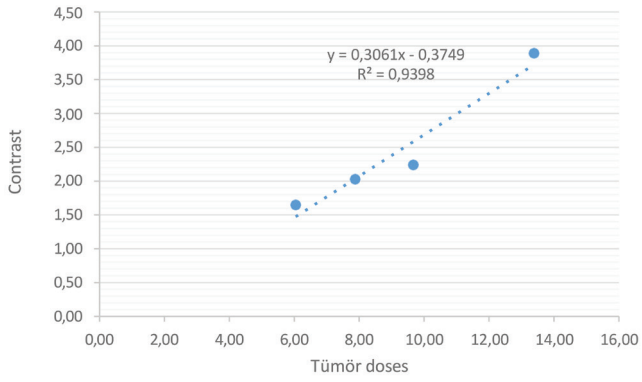



**Figure 6.** Tumor dose-contrast correlation in SPECT/CT

images (13,14,15). This study found that Tm with diameters <3 cm were significantly affected by PVE, and the impact of PVE diminished as tumor size increased.

In recent years, $^{99}$Y microsphere therapy has become a widely used, effective, and safe radionuclide therapy option for primary and metastatic liver Tm. The success of this therapy depends on accurate calculation, of tumor dose, which is determined by various parameters. Prior to administration of $^{99}$Y microspheres to the patient, dosimetry is performed using Tc-99m-MAA with SPECT/CT imaging. When dosimetric calculations rely solely on SPECT images, the regions of interest VOIs may appear larger than their actual size due to radiotracer spill-out (16,17). PVE in SPECT imaging arises from the system's limited spatial resolution. It is also influenced by whether corrections such as reconstruction algorithms and collimator-detector response have been applied. PVE includes both partial volume loss and spillover from neighboring regions, and particularly for structures smaller than 2-3 times of the system's FWHM (18).

Recently, 3D-printed phantoms made of PLA material have been used. It has been reported that PLA phantoms can be filled with Tc-99m and lutetium-177 radionuclides, which are mixed with water, allowing the acquisition of their scintigraphic images. These images can then be analyzed for scatter and photon attenuation effects (19).

Studies on PVE correction in scintigraphic imaging have shown that restoration filters based on frequency-distance relationships or approaches using spatial resolution modeling depending on distance in iterative reconstruction can reduce PVE; however, complete recovery of activity is not always achievable (20,21).

Factors degrading IQ and reducing the absorbed dose to lesions have been analyzed by Pacilio et al. (21) using Monte Carlo simulations. PVE was identified as one of the most significant degrading effects in scintigraphic images, with activity loss exceeding 20% in 1.8 cm lesions. It was reported that lesions smaller than 2 cm should be excluded from voxel-based dosimetry because accurate corrections cannot be performed (22). Cheng et al. (23) reported that PVE can significantly impact the accuracy of voxel-based dosimetry due to high noise in the images, and recommended increasing the number of iterations and subsets in image reconstruction. Additionally, they noted that high activity concentration may partially correct PVE. It has also been reported that pre- or post-filtering reduces spatial resolution and increases PVE, therefore, image filtering is not recommended (8).

In studies related to PVE and scintigraphic IQ, it has been reported that contrast and CNR values, which are methods used to evaluate IQ, are affected by PVE (24). A more detrimental effect than bias caused by PVE is the significant variability PVE introduces in lesion uptake. This variability can lead to substantial differences in measured tumor uptake, depending on tumor characteristics (e.g., size and shape), technical specifications of the tomography (e.g., spatial resolution), processing methods (e.g., reconstruction algorithms), and measurement procedures. Moreover, this variability hinders the feasibility of meta-analyses based on published data, posing substantial challenges for future clinical studies (25).

Kerckhaert et al. (26) evaluated IQ using an NEMA IQ phantom with Tc-99m-MAA and reported CNR values of 7.26 and 10.3 for 10 mm and 37 mm diameter lesions, respectively. In our study, tumor doses showed good correlation with tumor volumes ($R^2$=0.7267). Similarly, strong correlations were observed between tumor dose and CNR ($R^2$=0.8), and tumor dose and contrast ($R^2$=0.94). For lesions with diameters of 2 cm and 5 cm, contrast and CNR values were found to be 2.03 and 3.89, respectively. These results indicate a 1.9-fold improvement in contrast and a 2.43-fold improvement in CNR, respectively, in the 5 cm lesion. The actual and SPECT/CT-derived absorbed doses for the 2 cm lesion were 15.3 Gy and 7.87 Gy while for the 5 cm lesion, they were 15.4 Gy and 13.38 Gy, respectively. These findings highlight that the error due to PVE in dose estimation decreases with increasing lesion size.

Roesink JM et al. (27) who studied the effect of PVE on tumor dose, reported that tumor doses decreased as PVE increased. Consistently, in this study, it was observed that the T/N ratios decreased with decreasing tumor size on SPECT/CT images, likely due to the effect of partial volume effect PVE.

### Study Limitations

This study presents data for a single model device. It does not include data from other brands or models of gamma cameras

## Conclusion

To significantly reduce the bias caused by the partial volume effect, simple but imperfect correction methods currently being utilized. Until a widely accepted correction technique is routinely implemented, great care should be taken to standardize the acquisition, processing, and analysis of imaging data. In this context, it was concluded that Tms smaller than 2 cm are significantly affected by PVE, and applying necessary corrections in dosimetric calculations will have a decisive impact on the accuracy of dosimetric results.

### Ethics

**Ethics Committee Approval:** Since the study was conducted solely on a phantom model and did not involve any human subjects, ethical approval, informed consent, and volunteer consent forms were not required

**Informed Consent:** Since this study does not involve live subjects and was conducted solely on a phantom model, ethical approval, informed consent, and consent forms are not required.

### Footnotes

### Authorship Contributions

Surgical and Medical Practices: A.D.A., M.D., Concept: A.D.A., N.Y., S.A., Ö.D., M.D., Design: A.D.A., S.A., M.D., Data Collection or Processing: A.D.A., M.D., Analysis or Interpretation: A.D.A., M.D., Literature Search: A.D.A., N.Y., S.A., M.D., Writing: A.D.A., Ö.D., M.D.

**Conflict of Interest:** No conflict of interest was declared by the authors.

**Financial Disclosure:** The authors declared that this study has received no financial support.

## References

1. Geschwind JF, Salem R, Carr BI, Soulen MC, Thurston KG, Goin KA, Van Buskirk M, Roberts CA, Goin JE. Yttrium-90 microspheres for the treatment of hepatocellular carcinoma. Gastroenterology. 2004;127:S194-S205.
2. Silva LP, Paiva E, Trombini H. Heterogeneity in dose distribution in Yttrium-90 and Holmium-166 microspheres radioembolization of hepatic tumors. Radiation Physics and Chemistry. 2025;230:1-7.
3. Salem R, Lewandowski RJ, Gates VL, Nutting CW, Murthy R, Rose SC, Soulen MC, Geschwind JF, Kulik L, Kim YH, Spreafico C, Maccauro M, Bester L, Brown DB, Ryu RK, Sze DY, Rilling WS, Sato KT, Sangro B, Bilbao JI, Jakobs TF, Ezziddin S, Kulkarni S, Kulkarni A, Liu DM, Valenti D, Hilgard P, Antoch G, Muller SP, Alsuhaibani H, Mulcahy MF, Burrel M, Real MI, Spies S, Esmail AA, Raoul JL, Garin E, Johnson MS, Benson AB 3rd, Sharma RA, Wasan H, Lambert B, Memon K, Kennedy AS, Riaz A; Technology assessment committee; ınterventional oncology task force of the society of ınterventional radiology. Research reporting standards for radioembolization of hepatic malignancies. J Vasc Interv Radiol. 2011;22:265-278.
4. Salem R, Thurston KG. Radioembolization with 90Yttrium microspheres: a state-of-the-art brachytherapy treatment for primary and secondary liver malignancies. Part 1: technical and methodologic considerations. J Vasc Interv Radiol. 2006;17:1251-1278.
5. Miller FH, Lopes Vendrami C, Gabr A, Horowitz JM, Kelahan LC, Riaz A, Salem R, Lewandowski RJ. Evolution of radioembolization in treatment of hepatocellular carcinoma: a pictorial review. Radiographics. 2021;41:1802-1818.
6. Lambert B, Mertens J, Sturm EJ, Stienaers S, Defreyne L, D'Asseler Y. 99mTc-labelled macroaggregated albumin (MAA) scintigraphy for planning treatment with 90Y microspheres. Eur J Nucl Med Mol Imaging. 2010;37:2328-2333.
7. Jadoul A, Bernard C, Lovinfosse P, Gérard L, Lilet H, Cornet O, Hustinx R. Comparative dosimetry between $^{99m}$Tc-MAA SPECT/CT and $^{90}$Y PET/CT in primary and metastatic liver tumors. Eur J Nucl Med Mol Imaging. 2020;47:828-837.
8. Dawson LA, Ten Haken RK. Partial volume tolerance of the liver to radiation. Semin Radiat Oncol. 2005;15:279-283.
9. Chiesa C, Sjogreen-Gleisner K, Walrand S, Strigari L, Flux G, Gear J, Stokke C, Gabina PM, Bernhardt P, Konijnenberg M. EANM dosimetry committee series on standard operational procedures: a unified methodology for $^{99m}$Tc-MAA pre- and $^{90}$Y peri-therapy dosimetry in liver radioembolization with $^{90}$Y microspheres. EJNMMI Phys. 2021;8:77.
10. Yeyin N, Kesmezacar FF, Tunçman D, Demir Ö, Uslu-Beşli L, Günay O, Demir M. Hepatopulmonary shunt ratio verification model for transarterial radioembolization. Curr Radiopharm. 2024;17:276-284.
11. Dieckens D, Lavalaye J, Romijn L, Habraken J. Contrast-noise-ratio (CNR) analysis and optimisation of breast-specific gamma imaging (BSGI) acquisition protocols. EJNMMI Res. 2013;3:21.
12. Dezarn WA, Cessna JT, DeWerd LA, Feng W, Gates VL, Halama J, Kennedy AS, Nag S, Sarfaraz M, Sehgal V, Selwyn R, Stabin MG, Thomadsen BR, Williams LE, Salem R; American Association of Physicists in Medicine. Recommendations of the American Association of Physicists in Medicine on dosimetry, imaging, and quality assurance procedures for 90Y microsphere brachytherapy in the treatment of hepatic malignancies. Med Phys. 2011;38:4824-4845.
13. Thurnheer R, Engel H, Weder W, Stammberger U, Laube I, Russi EW, Bloch KE. Role of lung perfusion scintigraphy in relation to chest computed tomography and pulmonary function in the evaluation of candidates for lung volume reduction surgery. Am J Respir Crit Care Med. 1999;159:301-310.
14. Elschot M, Nijsen JF, Lam MG, Smits ML, Prince JF, Viergever MA, van den Bosch MA, Zonnenberg BA, de Jong HW. ($^{99}$m)Tc-MAA overestimates the absorbed dose to the lungs in radioembolization: a quantitative evaluation in patients treated with $^{166}$Ho-microspheres. Eur J Nucl Med Mol Imaging. 2014;41:1965-1975.
15. Tafti BA, Padia SA. Dosimetry of Y-90 microspheres utilizing Tc-99m SPECT and Y-90 PET. Semin Nucl Med. 2019;49:211-217.
16. Kafrouni M, Allimant C, Fourcade M, Vauclin S, Guiu B, Mariano-Goulart D, Ben Bouallègue F. Analysis of differences between 99m Tc-MAA SPECT-and 90 Y- microsphere PET-based dosimetry for hepatocellular carcinoma selective internal radiation therapy. EJNMMI Research. 2019;9:1-9.
17. Du Y, Tsui BM, Frey EC. Partial volume effect compensation for quantitative brain SPECT imaging. IEEE Trans Med Imaging. 2005;24:969-976.
18. Grings A, Jobic C, Kuwert T, Ritt P. The magnitude of the partial volume effect in SPECT imaging of the kidneys: a phantom study. EJNMMI Phys. 2022;9:18.
19. Pretorius PH, King MA, Pan TS, de Vries DJ, Glick SJ, Byrne CL. Reducing the influence of the partial volume effect on SPECT activity quantitation

with 3D modelling of spatial resolution in iterative reconstruction. Phys Med Biol. 1998;43:407-420.

20. Yokoi T, Shinohara H, Onishi H. Performance evaluation of OSEM reconstruction algorithm incorporating three-dimensional distance-dependent resolution compensation for brain SPECT: a simulation study. Ann Nucl Med. 2002;16:11-18.
21. Pacilio M, Ferrari M, Chiesa C, Lorenzon L, Mira M, Botta F, Becci D, Torres LA, Perez MC, Gil AV, Basile C, Ljungberg M, Pani R, Cremonesi M. 3D dosimetry treatment planning with 99mTc macroaggregated albumin SPECT in radioembolization with 90Y microspheres: a Monte Carlo study of the impact on absorbed dose distributions of attenuation and scatter corrections using the patient relative calibration methodology. Med Phys. 2016;43:4053-4064.
22. Chiesa C, Mira M, Maccauro M, Spreafico C, Romito R, Morosi C, Camerini T, Carrara M, Pellizzari S, Negri A, Aliberti G, Sposito C, Bhoori S, Facciorusso A, Civelli E, Lanocita R, Padovano B, Migliorisi M, De Nile MC, Seregni E, Marchianò A, Crippa F, Mazzaferro V. Radioembolization of hepatocarcinoma with (90)Y glass microspheres: development of an individualized treatment planning strategy based on dosimetry and radiobiology. Eur J Nucl Med Mol Imaging. 2015;42:1718-1738.
23. Cheng L, Hobbs RF, Segars PW, Sgouros G, Frey EC. Improved dose-volume histogram estimates for radiopharmaceutical therapy by optimizing quantitative SPECT reconstruction parameters. Phys Med Biol. 2013;58:3631-3647.
24. Kästner D, Braune A, Brogsitter C, Freudenberg R, Kotzerke J, Michler E. Gamma camera imaging characteristics of $^{166}$Ho and $^{99m}$Tc used in selective ınternal radiation therapy. EJNMMI Phys. 2024;11:35.
25. Soret M, Bacharach SL, Buvat I. Partial-volume effect in PET tumor imaging. J Nucl Med. 2007;48:932-945.
26. Kerckhaert CEM, de Jong HWAM, Meddens MBM, van Rooij R, Smits MLJ, Rakvongthai Y, Dietze MMA. Subtraction of single-photon emission computed tomography (SPECT) in radioembolization: a comparison of four methods. EJNMMI Phys. 2024;11:72.
27. Roesink JM, Moerland MA, Hoekstra A, Van Rijk PP, Terhaard CH. Scintigraphic assessment of early and late parotid gland function after radiotherapy for head-and-neck cancer: a prospective study of dose-volume response relationships. Int J Radiat Oncol Biol Phys. 2004;58:1451-1460.

*Original Article*

*Mol Imaging Radionucl Ther 2025;34:188-193* *DOI:10.4274/mirt.galenos.2025.78700*

# The PSMA-PET Conundrum: A Survey of UK Prostate Cancer Surgeons and Their Use of PSMA-PET Prior to Radical Prostatectomy

## *PSMA-PET Bilmecesi: Birleşik Krallık'taki Prostat Kanseri Cerrahları ve Radikal Prostatektomi Öncesi PSMA-PET Kullanımları Üzerine Bir Anket*

*Rustam Nariman Karanjia[1], Pallab Kumar Sarkar[1], Humayun Bashir[2], Sashi S Kommu[1]*

[1]*Kent and Canterbury Hospital, East Kent Hospitals University NHS Foundation Trust, Clinic of Urology, Canterbury, United Kingdom*
[2]*Kent and Canterbury Hospital, East Kent Hospitals University NHS Foundation Trust, Clinic of Nuclear Medicine, Canterbury, United Kingdom*

### Abstract

**Objectives:** Prostate-specific membrane antigen-positron emission tomography (PSMA-PET) has significantly improved sensitivity and specificity for detecting metastatic disease in prostate cancer compared to traditional computed tomography and bone scans. It is now recommended by the European Association of Urology for staging intermediate and high-risk disease, however, there are no recommendations on its incorporation into practice due to lack of long-term survival data. We aimed to identify the current use of PSMA-PET in high-volume prostate cancer centres to see whether there is standardisation in its use and interpretation prior to robotic-assisted laparoscopic prostatectomy (RALP).

**Methods:** An anonymised SurveyMonkey® was sent to multiple high-volume surgeons across the United Kingdom (UK), with all questions optional. Participants were asked about their personal practices for PSMA-PET staging, for both intermediate and high-risk disease, and how it would change their management if considering RALP.

**Results:** Thirty-one participants responded across 17 different UK centres. 11/31 (35%) used PSMA-PET a lone as primary staging for high-risk prostate cancer, with 6/30 (20%) using it for intermediate staging as well. Of the 23 surgeons that routinely perform lymph node dissection (LND) in high-risk cases, 13/23 (57%) would obviate performing it if the PSMA was negative. If a patient was found to have positive nodes on PSMA-PET, 12/31 (39%) surgeons will still offer RALP. Individual answers also varied within same centres.

**Conclusion:** The current interpretation of PSMA-PET for staging and treatment before RALP varies widely amongst surgeons, particularly regarding LND. A national consensus statement is needed to help standardise treatment practice for patients until robust long-term survival data exists.

**Keywords:** Prostate, PSMA, nuclear

### Öz

**Amaç:** Prostat spesifik membran antijen-pozitron emisyon tomografisi (PSMA-PET), prostat kanserinde metastatik hastalığı tespit etmede geleneksel bilgisayarlı tomografi ve kemik taramalarına kıyasla duyarlılığı ve özgüllüğü önemli ölçüde artırmıştır. Şu anda Avrupa Üroloji Derneği tarafından orta ve yüksek riskli hastalıkların evrelemesi için önerilmektedir, ancak uzun dönem sağkalım verilerinin eksikliği nedeniyle uygulamaya

**Address for Correspondence:** Rustam Nariman Karanjia, Kent and Canterbury Hospital, East Kent Hospitals University NHS Foundation Trust, Clinic of Urology, Canterbury, United Kingdom
**E-mail:** r.karanjia@nhs.net **ORCID ID:** orcid.org/0000-0001-8944-2208
**Received:** 15.10.2024 **Accepted:** 29.06.2025 **Epub:** 13.08.2025 **Publication Date:** 08.10.2025

**Cite this article as:** Karanjia R, Kumar Sarkar P, Bashir H, S Kommu SS. The PSMA-PET conundrum: a survey of UK prostate cancer surgeons and their use of PSMA-PET prior to radical prostatectomy. Mol Imaging Radionucl Ther. 2025;34:188-193.

Copyright© 2025 The Author. Published by Galenos Publishing House on behalf of the Turkish Society of Nuclear Medicine.
This is an open access article under the Creative Commons Attribution-NonCommercial-NoDerivatives 4.0 (CC BY-NC-ND) International License.

dahil edilmesine dair bir öneri bulunmamaktadır. Robotik yardımlı laparoskopik prostatektomi (RALP) öncesinde kullanımında ve yorumlanmasında standardizasyon olup olmadığını görmek için yüksek hacimli prostat kanseri merkezlerinde PSMA-PET'in mevcut kullanımını belirlemeyi amaçladık.

**Yöntem:** Birleşik Krallık (UK) genelindeki birçok yüksek hacimli merkezde çalışan cerrahlara, tüm soruların isteğe bağlı olarak doldurulduğu anonim bir SurveyMonkey® anketi gönderildi. Katılımcılara, hem orta hem de yüksek riskli hastalıklar için PSMA-PET evrelemesi konusundaki kişisel uygulamaları ve RALP düşünülürse tedavilerini nasıl değiştireceği soruldu.

**Bulgular:** On yedi farklı UK merkezinden 31 katılımcı yanıt verdi. Otuz bir katılımcıdan 11'i (%35) yüksek riskli prostat kanseri için birincil evreleme olarak yalnızca PSMA-PET'i kullanırken, 30'unun 6'sı (%20) orta riskli evreleme için de PSMA-PET'i kullandığını belirtti. Yüksek riskli olgularda rutin olarak lenf nodu diseksiyonu (LND) uygulayan 23 cerrahın 13'ü (%57), PSMA negatifse bunu yapmaktan kaçınacağını belirtti. Bir hastada PSMA-PET'te pozitif nodüller bulunursa, 31 cerrahtan 12'si (%39) yine de RALP önereceğini belirtti. Bireysel yanıtlar da aynı merkezler arasında farklılık gösterdi.

**Sonuç:** Robotik yardımlı RALP öncesi evreleme ve tedavi için PSMA-PET'in mevcut yorumu, özellikle LND konusunda, cerrahlar arasında büyük ölçüde farklılık göstermektedir. Sağlam uzun vadeli sağkalım verileri elde edilene kadar hastalar için tedavi uygulamalarının standartlaştırılmasına yardımcı olmak amacıyla ulusal bir mutabakat beyanına ihtiyaç duyulmaktadır.

**Anahtar kelimeler:** Prostat, PSMA, nükleer

## Introduction

Accurate staging of prostate cancer is paramount to informed decision-making prior to offering radical treatment. Until 2024, European Association of Urology (EAU) recommended conventional staging for both intermediate and high-risk patients using cross-sectional abdominopelvic imaging and nuclear medicine bone scans (1). However, this imaging lacks sensitivity and specificity for diagnosing extra-prostatic disease, even in high-risk cases. Prostate-specific membrane antigen positron emission tomography (PSMA-PET) as an alternative staging modality has gained popularity in recent years, due to its increased diagnostic accuracy and reduced number of equivocal findings (2). In 2023, the National Comprehensive Cancer Network updated its guidelines to recommend the use of PSMA-PET as first-line imaging for primary staging of prostate cancer (3,4). In 2024, EAU endorsed its use, where available, for primary staging of both intermediate and high-risk disease (1). However, solely based on PSMA-PET, they could not offer a clear recommendation on its interpretation and on the application regarding radical treatment, including robotic-assisted laparoscopic prostatectomy (RALP), due to a lack of long-term randomized control trial (RCT) survival data.

Amidst the prevailing uncertainty we aimed to identify the utilization and interpretation of PSMA-PET prior to RALP amongst different United Kingdom (UK), centres and whether this was broadly similar or lacked standardisation. We designed and distributed a bespoke online survey regarding the use of PSMA-PET in primary prostate cancer staging to various high-volume pelvic oncology surgeons working across in the UK.

## Materials and Methods

A bespoke and anonymised SurveyMonkey® was distributed to high-volume prostate cancer surgeons across the UK in October 2023. Participants were asked nine questions (Table 1) about their hospital practices for PSMA-PET staging, in both intermediate and high-risk disease, how it would change their management if considering RALP. All questions were optional and collated anonymously.

### Statistical Analysis

Statistical analysis was not required for data interpretation.

## Results

Thirty-one participants responded across 17 different UK centres (Figure 1). 18/31 (58%) worked in centres annually performing over 200 RALPs; 30/31 (97%) performed at least 50. There was large heterogeneity in the use of PSMA-PET for staging: 11/31 (35%) used PSMA-PET alone as primary staging for high-risk prostate cancer, with 6/30 (20%) using it for intermediate staging as well. For those who used conventional staging rather than PSMA-PET, 14/31 (45%) used computed tomography (CT) and bone scans for high-risk staging, with 6/31 (19%) used only bone scans. In intermediate imaging, 16/30 (53%) used bone scans only, while 8/30 (26%) used both CT and bone scans (Figure 2).

Of the 23 surgeons that routinely perform lymph node dissection (LND) in high-risk cases, 13/23 (57%) would obviate performing it if the PSMA was negative. If a patient was found to have positive nodes on PSMA-PET, 12/31 (39%) surgeons would still offer radical prostatectomy as a treatment option and 12/29 (41%) would use the PSMA-PET images to guide their LND (Figure 3). Individual answers also varied within same centres. 14/31 (45%) routinely use the Briganti nomogram to predict lymph node involvement, and 24/31 (77%) would support the trial with RALP and subsequent SABR for a single positive node in the field of pelvic node extirpation.

| Table 1. Nine questions asked to high-volume RALP surgeons in the UK | | |
|---|---|---|
| | **Question** | **Options** |
| Question 1 | Which hospital do you work in? | - |
| Question 2 | Approximately how many RALPs does your hospital perform each year? | a) 0-49<br>b) 50-99<br>c) 100-149<br>d) 150-199<br>e) 200+ |
| Question 3 | How do you currently stage high-risk prostate cancer in your hospital? | a) CT and bone scan<br>b) Bone scan only<br>c) PSMA-PET only |
| Question 4 | How do you currently stage intermediate-risk Gleason 4+3 prostate cancer in your hospital? | a) CT and bone scan<br>b) Bone scan only<br>c) PSMA-PET only |
| Question 5 | Does a negative PSMA-PET change your decision to do a lymph node dissection in an otherwise high risk patient? | a) Yes - It obviates the need to perform it<br>b) No - I would still perform it if deemed necessary<br>c) I do not routinely perform lymph node dissection |
| Question 6 | Would you still perform radical prostatectomy in patients with positive nodes on PSMA-PET, and otherwise favourable factors? | a) Yes - With lymph node dissection<br>b) Yes - Without lymph node dissection<br>c) Rarely |
| Question 7 | If yes, do you use PSMA-PET images to help guide lymph node dissection? | a) Yes<br>b) No |
| Question 8 | Do you routinely use the Briganti nomogram to predict likelihood of lymph node involvement? | a) Yes<br>b) No |
| Question 9 | For high risk patients, with a solitary positive node in the field of pelvic nodal extirpation, would you consider a trial in which RALP is performed and SABR offered to the node in a multimodal setting? | a) Yes<br>b) No |
| PSMA-PET: Prostate-specific membrane antigen-positron emission tomography, CT: Computed tomography, RALP: Robotic-assisted laparoscopic prostatectomy | | |

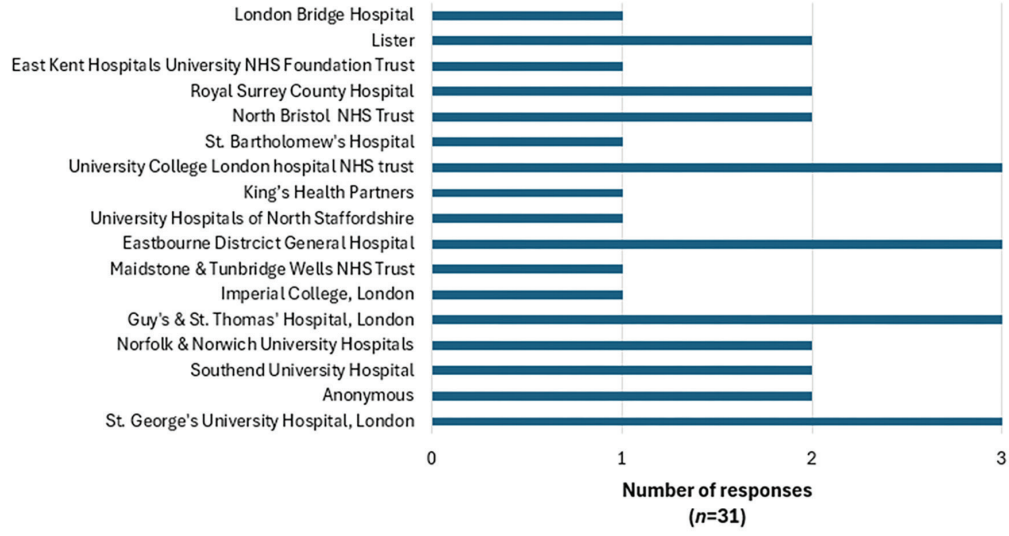



**Figure 1.** Responses by hospital

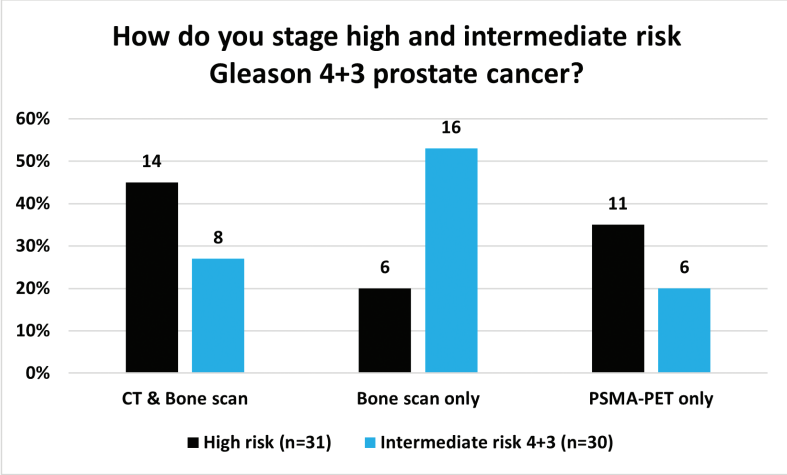



**Figure 2.** Use of PSMA-PET as staging prior to RALP
PSMA-PET: Prostate-specific membrane antigen-positron emission tomography, RALP: Robotic-assisted laparoscopic prostatectomy, CT: Computed tomography

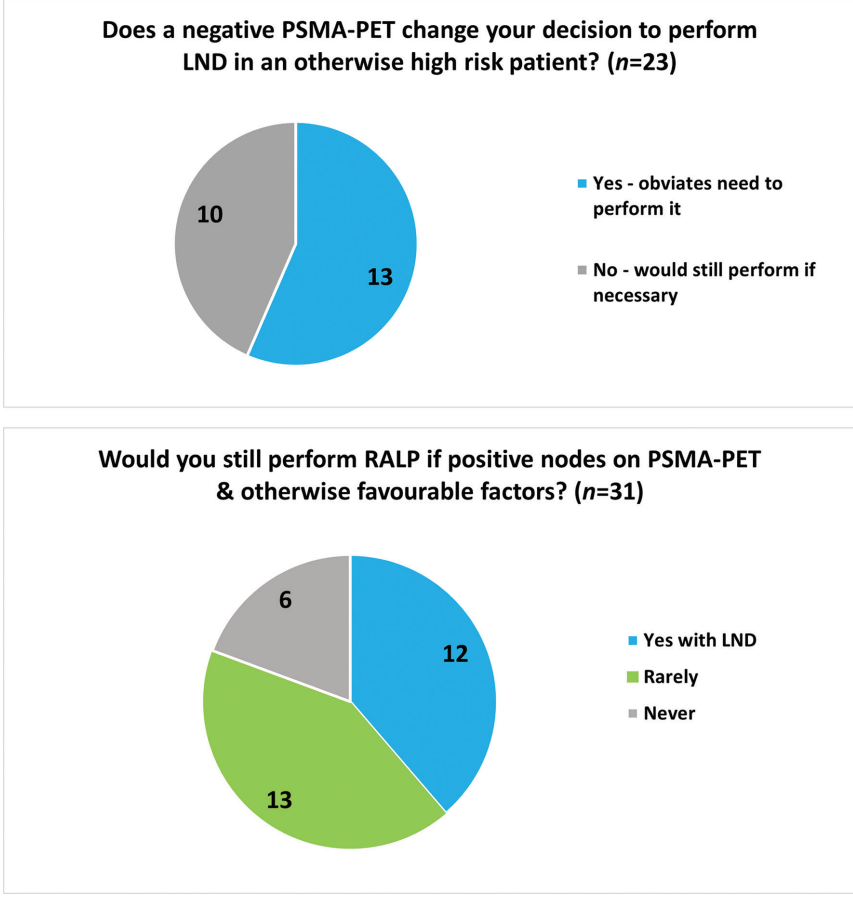



**Figure 3.** Use of PSMA-PET in treatment prior to RALP
PSMA-PET: Prostate-specific membrane antigen-positron emission tomography, RALP: Robotic-assisted laparoscopic prostatectomy, LND: Lymph node dissection

## Discussion

The role of PSMA-PET is an evolving one: only in 2024 have the EAU finally recommended the use of PSMA-PET in staging of intermediate and high-risk prostate cancer. However, they fall short of a recommendation regarding treatment due to a lack of long-term survival data from RCTs (1). This leaves clinicians in a conundrum: staging with PSMA-PET is now recommended, but the interpretation and application of PSMA-PET prior to treatment remain unclear. It is therefore unsurprising to see the large heterogeneity in our survey on the use of PSMA-PET prior to RALP. This reflects both the diagnostic uncertainty of PSMA-PET in its ability to exclude metastatic disease and the potential survival benefit of radical treatment based on PSMA-PET rather than conventional staging. This subsequently impacts several clinical decisions for surgeons prior to RALP, in particular, the clinical utility of performing LND. EAU advise that LND in high-risk patients may be useful for staging, although systematic reviews have shown they are not associated with improved oncological outcomes (5). Given its lack of therapeutic benefit and significant associated morbidity, many clinicians are reluctant to perform the procedure. Interestingly, approximately half of respondents felt confident they could avoid LND if they usually performed it, as long as the PSMA-PET was negative. In addition, 12/31 (39%) respondents were still happy to offer RALP with LND if a patient had positive nodal disease detected on PSMA-PET, a response which also does not suggest consensus. Previous studies have suggested that PSMA-PET could be used to guide LND (6), and several respondents perform the procedure, despite no recommendation. Whilst there is no long-term data to support biochemical recurrence-free survival or overall survival benefit, there is a possibility targeted LND, using PSMA-PET, may change this.

### Study Limitations

It is worth noting, our survey was conducted in October 2023, prior to the EAU recommending PSMA-PET for staging. It is therefore likely heterogeneity with PSMA-PET staging may have improved as its nationwide availability improved. At the time of writing, no recommendations on the interpretation of PSMA-PET prior to RALP are available, and our results are therefore likely to be representative. Historically, PET has been a unique modality; its utilization is dictated more by "availability" than by the pace at which "favourable evidence" can be collated. This realization amplifies the need for consensus among practitioners.

## Conclusion

The lack of recommendations regarding interpretation of PSMA-PET in primary staging of prostate cancer has resulted in large heterogeneity in practice when offering radical prostatectomy. National consensus, achieved through expert opinion, is needed to standardise care for patients and ensure similar practice across the UK until robust long-term data assessing its role in prostate cancer exist.

### Ethics

**Ethics Committee Approval:** Not required.

**Informed Consent:** This article was an anonymous survey of surgeons, not patients. Because there are no patients included in the paper, patient consents and ethical approval were not required.

### Footnotes

### Authorship Contributions

Surgical and Medical Practices: R.N.K., P.K.S., H.B., S.S.K., Concept: R.N.K., P.K.S., H.B., S.S.K., Design: R.N.K., P.K.S., H.B., S.S.K., Data Collection or Processing: R.N.K., P.K.S., H.B., S.S.K., Analysis or Interpretation: R.N.K., P.K.S., H.B., S.S.K., Literature Search: R.N.K., P.K.S., H.B., S.S.K., Writing: R.N.K., P.K.S., H.B., S.S.K.

**Conflict of Interest:** No conflict of interest was declared by the authors.

**Financial Disclosure:** The authors declared that this study has received no financial support.

## References

1. EAU Guidelines - Uroweb [Internet]. Available from: https://uroweb.org/guidelines
2. Hofman MS, Lawrentschuk N, Francis RJ, Tang C, Vela I, Thomas P, Rutherford N, Martin JM, Frydenberg M, Shakher R, Wong LM, Taubman K, Ting Lee S, Hsiao E, Roach P, Nottage M, Kirkwood I, Hayne D, Link E, Marusic P, Matera A, Herschtal A, Iravani A, Hicks RJ, Williams S, Murphy DG; proPSMA Study Group Collaborators. Prostate-specific membrane antigen PET-CT in patients with high-risk prostate cancer before curative-intent surgery or radiotherapy (proPSMA): a prospective, randomised, multicentre study. Lancet. 2020;395:1208-1216.
3. Jochumsen MR, Bouchelouche K. PSMA PET/CT for primary staging of prostate cancer - an updated overview. Semin Nucl Med. 2024;54:39-45.
4. Schaeffer EM, Srinivas S, Adra N, An Y, Barocas D, Bitting R, Bryce A, Chapin B, Cheng HH, D'Amico AV, Desai N, Dorff T, Eastham JA, Farrington TA, Gao X, Gupta S, Guzzo T, Ippolito JE, Kuettel MR, Lang JM, Lotan T, McKay RR, Morgan T, Netto G, Pow-Sang JM, Reiter R, Roach M, Robin T, Rosenfeld S, Shabsigh A, Spratt D, Teply BA, Tward J, Valicenti R, Wong JK, Berardi RA, Shead DA, Freedman-Cass DA. NCCN guidelines® insights: prostate cancer, version 1.2023. J Natl Compr Canc Netw. 2022;20:1288-1298.

5. Fossati N, Willemse PM, Van den Broeck T, van den Bergh RCN, Yuan CY, Briers E, Bellmunt J, Bolla M, Cornford P, De Santis M, MacPepple E, Henry AM, Mason MD, Matveev VB, van der Poel HG, van der Kwast TH, Rouvière O, Schoots IG, Wiegel T, Lam TB, Mottet N, Joniau S. The benefits and harms of different extents of lymph node dissection during radical prostatectomy for prostate cancer: a systematic review. Eur Urol. 2017;72:84-109.

6. Maurer T, Robu S, Schottelius M, Schwamborn K, Rauscher I, van den Berg NS, van Leeuwen FWB, Haller B, Horn T, Heck MM, Gschwend JE, Schwaiger M, Wester HJ, Eiber M. $^{99m}$Technetium-based prostate-specific membrane antigen-radioguided surgery in recurrent prostate cancer. Eur Urol. 2019;75:659-666.

*Original Article*

*Mol Imaging Radionucl Ther 2025;34:194-201* *DOI:10.4274/mirt.galenos.2025.71542*

# A Disease Progression Predictor by Quantitative Assessment of the Hepatic Accumulation on Postablative Iodine-131 Whole-Body Image in Differentiated Thyroid Cancer

## *Diferansiye Tiroid Kanserinde Postablatif İyot-131 Tüm Vücut Görüntüsünde Hepatik Tutulumun Kantitatif Değerlendirmesiyle Hastalık İlerlemesinin Öngörülmesi*

*Michihiro Nakayama[1], Kenta Nomura[2], Sho Kamieda[1], Ippei Yoshida[1], Atsushi Fujiya[1], Takahiro Uno[2], Atsutaka Okizaki[1]*

*Asahikawa Medical University Faculty of Medicine, Department of Radiology, Asahikawa, Japan*
*Asahikawa Medical University Hospital, Division of Radiology, Asahikawa, Japan*

## Abstract

**Objectives:** A Iodine-131 ($^{131}$I) whole body scan (WBS) is performed to evaluate the treatment response after radioactive iodine (RAI) therapy. Despite the clinical relevance of RAI-refractory differentiated thyroid cancer, a consensus on its precise definition remains lacking.

This study investigates the potential utility of hepatic $^{131}$I accumulation as an early predictor for tumor recurrence or progression after RAI administration.

**Methods:** Of 814 patients receiving care at our institution, we enrolled 225 patients who exhibited no accumulation of RAI in the remnant tissues or other lesions on $^{131}$I WBS. We quantified the hepatic uptake ratio [defined as (hepatic uptake/background uptake (H/B)] from WBS. All patients were categorized into group A (H/B ≤1.5) and group B (H/B >1.5), and we assessed between-group differences. The Kaplan-Meier method and Log-rank test were used to analyze the progression-free survival (PFS). Using the Cox proportional hazards model, we identified independent prognostic factors from among the seven known prognostic factors, i.e., H/B, thyroglobulin, sex, age, stage, total $^{131}$I dose, and final therapeutic dose.

**Results:** The 5-year and median PFS were 98.8% and 114.7 months in group A (n: 171) compared with 24.1% and 42.7% months in group B (n: 54), respectively. Group B showed a significant correlation with poor prognosis ($p<0.00001$). Of the seven prognostic factors, H/B exhibited the highest impact on patient outcomes (hazards ratio for recurrence/disease progression, 42.156; 95% confidence interval: 8.750-203.106).

**Conclusion:** Quantitative evaluation of hepatic uptake on $^{131}$I WBS provides a marker that may help identify patients with differentiated thyroid cancer who are at a high risk of disease progression/recurrence immediately after RAI therapy.

**Keywords:** Radioactive iodine-refractory differentiated thyroid cancer, hepatic accumulation, radioactive iodine therapy, thyroglobulin, metabolically persistent disease

**Address for Correspondence:** Kenta Nomura, Asahikawa Medical University Hospital, Division of Radiology, Asahikawa, Japan
**E-mail:** kenta.rpg7vsd@gmail.com **ORCID ID:** orcid.org/0009-0008-5386-2575
**Received:** 30.04.2025 **Accepted:** 04.07.2025 **Epub:** 01.08.2025 **Publication Date:** 08.10.2025

**Cite this article as:** Nakayama M, Nomura K, Kamieda S, Yoshida I, Fujiya A, Uno T, Okizaki A. A disease progression predictor by quantitative assessment of the hepatic accumulation on postablative iodine-131 whole-body image in differentiated thyroid cancer. Mol Imaging Radionucl Ther. 2025;34:194-201.

Copyright© 2025 The Author. Published by Galenos Publishing House on behalf of the Turkish Society of Nuclear Medicine.
This is an open access article under the Creative Commons Attribution-NonCommercial-NoDerivatives 4.0 (CC BY-NC-ND) International License.

## Öz

**Amaç:** Radyoaktif iyot (RAİ) tedavisinden sonra tedaviye yanıtı değerlendirmek için İyot-131 ($^{131}$I) tüm vücut taraması (WBS) yapılır. RAİ-refrakter diferansiye tiroid kanseri klinik önemine rağmen, kesin tanımı konusunda bir fikir birliği henüz yoktur.

Bu çalışma, RAİ uygulamasından sonra tümör nüksü veya ilerlemesi için erken bir tahmin edici olarak hepatik $^{131}$I tutulumunun potansiyel faydasını araştırmaktadır.

**Yöntem:** Kurumumuzda tedavi gören 814 hastadan, $^{131}$I WBS'de artık dokularda veya diğer lezyonlarda RAİ birikimi görülmeyen 225 hastayı çalışmaya dahil ettik. Hepatik alım oranını [(hepatik alım/arka plan alımı (H/B)] WBS'den nicelendirdik. Tüm hastaları grup A (H/B ≤1,5) ve grup B (H/B >1,5) olarak kategorize ettik ve gruplar arası farklılıkları değerlendirdik. Progresyonsuz sağkalımı (PFS) analiz etmek için Kaplan-Meier yöntemi ve Log-rank testi kullanıldı. Cox orantılı risk modelini kullanarak, bilinen yedi prognostik faktör arasından bağımsız prognostik faktörleri belirledik: H/B, tiroglobulin, cinsiyet, yaş, evre, toplam $^{131}$I dozu ve son tedavi dozu.

**Bulgular:** Grup A'da (n: 171) 5 yıllık ve ortanca PFS sırasıyla %98,8 ve 114,7 ay iken, grup B'de (n: 54) sırasıyla %24,1 ve %42,7 ay idi. Grup B, kötü prognozla anlamlı bir korelasyon gösterdi (p<0,00001). Yedi prognostik faktör arasında H/B, hasta sonuçları üzerinde en yüksek etkiyi gösterdi (nüks/hastalığın ilerlemesi için risk oranı, 42,156; %95 güven aralığı: 8,750-203,106).

**Sonuç:** $^{131}$I tüm vücut taramasında karaciğer tutulumunun kantitatif değerlendirmesi, RAİ tedavisinden hemen sonra hastalık ilerlemesi/nüksü riski yüksek olan diferansiye tiroid kanserli hastaların belirlenmesine yardımcı olabilecek bir belirteç sağlar.


**Anahtar kelimeler:** Radyoaktif iyota-dirençli diferansiye tiroid kanseri, karaciğer birikimi, radyoaktif iyot tedavisi, tiroglobulin, metabolik olarak kalıcı hastalık

## Introduction

Thyroid cancer is the leading endocrine malignancy with a growing incidence in recent years (1,2). Total thyroidectomy is the gold standard for most patients with differentiated thyroid cancer (DTC) (3,4,5). Radioactive iodine (RAI) therapy is reportedly effective for patients with risk factors for recurrence (6,7). Patients who respond to RAI therapy exhibit excellent 10-year survival (92%) (8,9,10), compared with patients who do not respond to RAI therapy (10-year survival, 19%).

Although there is no standardized definition of radioactive iodine-refractory DTC (RR-DTC) at present, a general consensus exists that any patient with a known cancer lesion that does not display accumulation of RAI on Iodine-131 ($^{131}$I) whole body scan (WBS), or experiences growth of a lesion despite RAI uptake 6-12 months after RAI therapy, is considered RR-DTC (11,12,13,14). Until recently, limited effective treatment options were available for patients with RR-DTC besides suppression of thyroid-stimulating hormone. Presently, molecular-targeted therapy for RR-DTC is initiated in patients who exhibit disease progression within 12 months after diagnosis (15,16); however, such an approach may delay treatment.

The metabolism of organic iodine results in its hepatic uptake, which is captured on $^{131}$I WBS and is also considered to show retention in thyrogenic cells. Previously, we reported that patients who exhibit positive results on $^{131}$I WBS have a quantitatively high hepatic uptake/background uptake (H/B) (17). As the quantitative assessment of the hepatic uptake on $^{131}$I WBS could reflect cancer status, we quantitatively assessed the hepatic uptake in patients who exhibited negative results on $^{131}$I WBS, that is, those who had no clinically identified lesions that displayed $^{131}$I uptake. This study intends to ascertain whether the risk of recurrence and disease progression can be predicted. Accordingly, the present study seeks to identify a hepatic uptake-based indicator on $^{131}$I WBS for early assessment of the likelihood of disease progression or relapse following RAI administration.

## Materials and Methods

### Study Design

This study protocol adhered to the Declaration of Helsinki and was approved by the Asahikawa Medical University Research Ethics Committee (number: 15198, date: 09.03.2016). The requirement of informed consent was waived by the Ethics Committees because of the retrospective and non-invasive study design.

### Study Population

Eight hundred fourteen consecutive patients were treated at our hospital. Two experienced nuclear medicine specialists independently evaluated that all patients enrolled in this study did not exhibit accumulation of RAI in the remnant tissues or other lesions on $^{131}$I WBS after 4-day-treatment. Exclusion criteria based on previous studies (17) were inadequate biochemical and/or imaging parameters, presence of hepatic metastases and/or impaired liver function, or insufficient follow-up (<6 months). All patients had previously undergone total thyroidectomy, and were administered RAI therapy (3.70-5.55 GBq) following a minimum 2-week withdrawal from thyroid hormone replacement. Patients were considered to have completed ablation if they had no elevated thyroglobulin (Tg) levels

and no imaging or clinical evidence suggestive of persistent or recurrent disease during a follow-up period of at least 6 months.

### Image Protocols

We acquired $^{131}$I WBS images with a therapeutic radioactive dose 4 days after the RAI administration. Imaging was performed using a dual-head gamma camera with high-energy, medium-sensitivity collimators. The equipment used was Millennium VG (GE Medical Systems, Tokyo, Japan).

In the WBS, an anterior image was acquired at a speed of 15 cm/min, using a 256 1024 matrix and a 364-keV photopeak with a 20% window.

### Region of Interest Setting and H/B Calculation

We set a region of interest (ROI) on the liver in the WBS anterior view. To reduce variability related to bone marrow activity among individuals, a background ROI was first positioned in the cranial region. Two board-certified nuclear medicine physicians then manually delineated the liver and background ROIs based on visual assessment. The H/B ratio defined as the hepatic accumulation divided by background accumulation was obtained from $^{131}$I whole-body scintigraphy. The final H/B value was calculated as the mean of the two values independently determined by the blinded observers. Next, computed tomography images were also examined to support accurate ROI placement.

Previously, the receiver operating characteristic (ROC) curve was evaluated from the H/B values of the group that needed retreatment (abnormal accumulation in the neck and lung metastasis in $^{131}$I WBS) and the group ascertained to not require retreatment; the optimal cut off value evaluated from the ROC curve was H/B ≤1.5, and the diagnostic ability of retreatment with this cut-off value was 99.4% sensitivity and 98.4% specificity (17). Thus, in this study, we evaluated the prognosis of RR-DTC by classifying patients, judged as accumulation-negative by $^{131}$I WBS, based on the hepatic accumulation using this cut off value. We divided the study population into two groups based on our previous study: group A (H/B ≤1.5) and group B (H/B >1.5), and assessed between-group differences.

### Statistical Analysis

In this study, we conducted statistical analyses using XLSTAT software (Addinsoft, Paris, France). We used the mean values of H/B for the analyses. Using the Kaplan-Meier method, we plotted the progression-free survival (PFS) curves. We then compared the groups using the Log-rank test to evaluate differences in survival outcomes. Additionally, the Cox proportional hazards model was used to determine independent prognostic factors among the already known factors (H/B, Tg, sex, age, stage, total $^{131}$I dose, and final therapeutic dose). We considered $p<0.05$ as statistically significant.

## Results

Of 814 patients treated at our institution during the study period, we enrolled 225 patients who tested negative for $^{131}$I on WBS and were available for follow-up. An overview of patients' demographics, histologic subtypes, and tumor-node-metastasis (TNM) staging is presented in Table 1. A study using TNM version 8 (2017) pathological classification of thyroid tumors was performed (18). The median duration of follow-up was 114.7 months in group A [95% confidence interval (CI): 112.3-117.2] and 42.7 months in group B (95% CI: 31.9-53.5), as shown in Figure 1. The PFS rate at 5 years was 98.8% in group A compared to 24.1% in group B, with a statistically significant difference (Log-rank test, $p<0.00001$). Additionally, Tg, H/B, and age correlated with an increased hazard for the PFS. The analysis of the correlation between recurrence/disease progression and the seven prognostic factors using the Cox proportional hazards model revealed that H/B exhibited the highest impact on patient outcomes (hazard ratio: 42.156, 95% CI: 8.750-203.106; Table 2).

**Table 1. The characteristics of the study population disaggregated by the study group (n: 225)**

| Characteristic | Group A (H/B ≤1.5) | Group B (H/B >1.5) |
|---|---|---|
| **Gender** | | |
| Female | 114 | 42 |
| Male | 57 | 12 |
| Age (y) | 58.9±14.1 | 61.9±13.2 |
| **Histological subtype** | | |
| Papillary thyroid cancer | 166 | 53 |
| Follicular thyroid cancer | 5 | 1 |

| Table 1. Continued | | |
|---|---|---|
| **Characteristic** | **Group A (H/B ≤1.5)** | **Group B (H/B >1.5)** |
| **TNM stage** | | |
| Stage 1 | 18 | 0 |
| Stage 2 | 5 | 1 |
| Stage 3 | 37 | 7 |
| Stage 4A | 74 | 23 |
| Stage 4B | 5 | 4 |
| Stage 4C | 32 | 19 |
| **Thyroglobulin (ng/mL)** | 83.5±191.6 | 231.5±286.5 |
| **Number of times of treatment** | 2.2±0.7 | 2.5±1.2 |
| **$^{131}$I dose in final RAI therapy (mCi)** | 142.8±15.5 | 144.8±8.8 |
| TNM: Tumor, node, and metastasis, H/B: Hepatic uptake ratio, RAI: Radioactive iodine, $^{131}$I: Iodine-131 | | |

| Table 2. The incidence of recurrence or metastases in relation to clinical, imaging, and biological variables | | | | | | |
|---|---|---|---|---|---|---|
| **Variable** | **Regression coefficient** | **Standard error** | **p value** | **Hazard ratio** | **95% CI for hazard ratio** | |
| | | | | | **Lower** | **upper** |
| Tg: ≥35 ng/mL vs. <35 ng/mL | 1.017 | 0.445 | <0.03 | 2.765 | 1.157 | 6.610 |
| H/B: >1.5 vs. ≤1.5 | 3.741 | 0.802 | <0.0001 | 42.156 | 8.750 | 203.106 |
| Female vs. male | 0.204 | 0.410 | N.S. | 1.226 | 0.549 | 2.739 |
| Age: >55 vs. ≤55 | 1.375 | 0.509 | <0.01 | 3.954 | 1.458 | 10.724 |
| Number of times of treatment: ≥4 (total 600 mCi) vs. <4 | 0.819 | 0.524 | N.S. | 2.269 | 0.812 | 6.342 |
| Stage: 4C vs. 1-3, 4A and 4B | 0.309 | 0.387 | N.S. | 1.362 | 0.638 | 2.908 |
| $^{131}$I dose of final RAI therapy: 150 mCi vs. <50 mCi | 0.320 | 0.356 | N.S. | 1.377 | 0.685 | 2.768 |
| H/B: Hepatic uptake ratio, Tg: Thyroglobulin, CI: Confidence interval, RAI: Radioactive iodine, N.S.: Not significant, $^{131}$I: Iodine-131 | | | | | | |

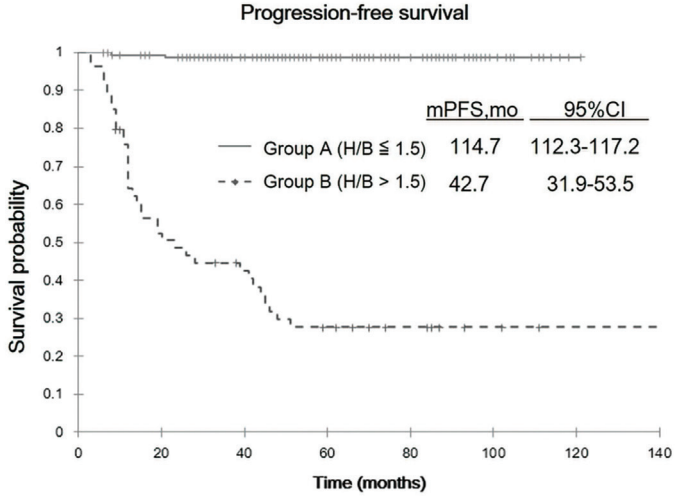



**Figure 1.** The Kaplan-Meier curves for the progression-free survival in groups A and B
CI: Confidence interval, H/B: Hepatic uptake ratio, mPFS: Mean progression-free survival

## Discussion

Recent developments in medical technology have facilitated a paradigm shift in the approach to cancer treatment; that is, a shift from individual decision making by physicians to a collaborative, multidisciplinary team approach. The treatment of thyroid cancer is no exception. With the advent of molecular-targeted drugs, patients with RR-DTC who previously had limited treatment options can now hope for better outcomes. The revised American Thyroid Association management guidelines (2015) highlight the significance of treatment response reclassification (19).

The SELECT and DECISION trials have already established the efficacy of molecular-targeted drugs; however, appropriate discretion should be exercised during the selection of candidate patients because of various potential adverse effects such as hypertension, hand-foot syndrome, and bleeding. Molecular-targeted drugs are suggested for advanced RR-DTC as well. The SELECT and DECISION trials defined RR-DTC as cancer progression (based on imaging findings and changes in serum levels of Tg and anti-Tg antibody) despite treatment with RAI at a cumulative dose of at least 22.2 GBq (600 mCi). The DECISION trial enrolled patients with RR-DTC who exhibited cancer progression within the past 14 months, whereas the SELECT trial enrolled those who presented cancer progression within the past 12 months (15-20).

Presently, there are no means available to estimate the prognosis of patients with RR-DTC, except close monitoring of their clinical course. Of note, not all patients with RR-DTC experience rapid deterioration; indeed, cancer progression is rather slow in many patients. Molecular-targeted therapy in such patients might be more harmful than beneficial. However, some patients have recurrent metastatic differentiated cancer that displays rapid progression and is eventually fatal. Hence, observation should be minimized before starting molecular-targeted drugs in these patients.

Per the American Thyroid Association guidelines, kinase inhibitor therapy should be considered for patients with RR-DTC who have metastatic, rapidly progressive, symptomatic, and/or imminently threatening disease not otherwise amenable to local control using other approaches (19). The National Comprehensive Cancer Network Guidelines (version 2.2015) recommend considering lenvatinib or sorafenib for progressive and/or symptomatic diseases with iodine-refractory metastases, except central nervous system metastases (21). Nevertheless, candidates should be comprehensively counseled on the risks and benefits of these therapies. Owing to the high frequency of adverse events, meticulous patient selection is imperative. Nonetheless, early detection and prompt intervention for RR-DTC are preferable due to the substantial therapeutic benefits of these agents (22).

The hepatic uptake on $^{131}$I WBS might reflect the thyroid cancer status. Hepatic uptake on WBS occurs primarily due to the uptake of thyroxin, as organic iodine is typically metabolized in the liver, and inorganic iodine is eliminated from the kidneys via urine. Thus, the postoperative hepatic uptake on $^{131}$I WBS for thyroid cancer is indicative of the possible presence of thyrogenic cells. In the literature, the reported efficacy of the hepatic uptake exhibited much variability, which was perhaps attributable to the visual assessment of the hepatic uptake. Following total thyroidectomy, any remaining thyroid tissue or DTC tissues are key sites for iodine metabolism. A hallmark of DTC is its ability to actively accumulate iodine for thyroid hormone synthesis (19).

Iodine metabolism begins with the transport of iodide from the bloodstream into thyroid follicular cells. This process, which occurs against both chemical and electrical gradients, is mediated by the sodium-iodide symporter located on the basolateral membrane of these cells (23). The second step involves the synthesis and secretion of Tg. Tg molecules contain approximately 140 tyrosine residues that act as precursors in thyroid hormone biosynthesis. In the next stage, iodide is enzymatically oxidised. Once inside the follicular cells, the iodide is transported towards the apical membrane and enters the follicular lumen. Iodination of the tyrosine residues on Tg occurs. The coupling of two diiodotyrosine (DIT) residues yields thyroxine (T4), while the combination of a monoiodotyrosine and a DIT yields triiodothyronine (T3). These hormones cross the basal membrane and enter the bloodstream. In the liver, T4 is rapidly converted to its active form, T3, by enzymatic deiodination. (24,25). This process is referred to as "radioactive iodide trapping" in the liver of RAI therapy-treated patients and is assumed to be a mechanism for hepatic accumulation (Figure 2).

Reportedly, the $^{131}$I dose exhibits a positive correlation with the hepatic uptake grade (26,27,28,29). Typically, the radioiodine dose is determined according to the tumor, node, and metastasis stage. However, Jeon et al. (7) reported that patients with distant metastases who were administered 200 mCi exhibited low hepatic uptake, corroborating our findings. These findings indicate that elevated radioiodine dose does not directly correlate with higher hepatic uptake (30).

This study suggests that elevated H/B in patients who test negative on $^{131}$I WBS designates the presence of organic iodine metabolized in the liver. The metabolic images of these patients might reflect the presence of a tumor (i.e.,

"metabolically persistent disease") (Figure 3). Although our study is single-center, the findings suggest that patients with elevated H/B tend to develop recurrence or disease progression during follow-up. Conversely, patients with low H/B do not experience disease progression, even if they have distant metastasis, perhaps, additional treatment is not needed in such patients.

The use of molecular-targeted drugs might not be practical in treatment-resistant patients, when they are asymptomatic. However, it is imperative to initiate treatment in a timely manner because the cancer is often quite advanced when symptoms manifest. Perhaps H/B could enable the identification of candidates for aggressive use of molecular-targeted drugs, especially when the selection of the optimal therapeutic option is not straightforward. Of note, no additional capital investment is needed, for the H/B assessment, because it can be ascertained with $^{131}$I WBS, which is already used for assessing treatment efficacy. Hence, no physical or financial burden exists on patients. Perhaps clearly defining the H/B indications might decrease medical expenses in the future.

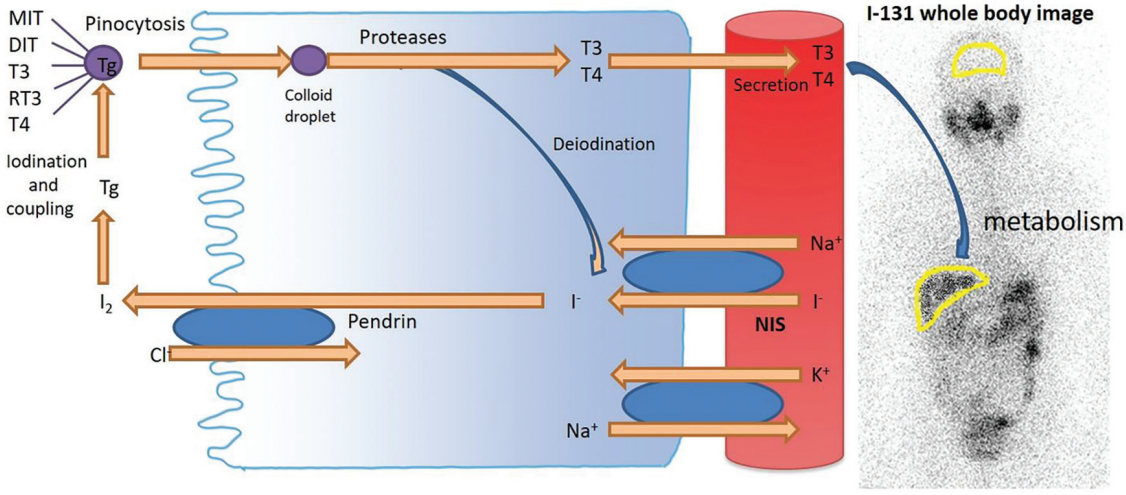



**Figure 2.** The thyroid hormone synthesis and the mechanism of liver accumulation in $^{131}$I WBS
DIT: Diiodotyrosine, MIT: Monoiodotyrosine, NIS: Sodium iodide symporter, T3: Triiodothyronine, T4: Thyroxine, RT3: Reverse T3, WBC: Whole body scan

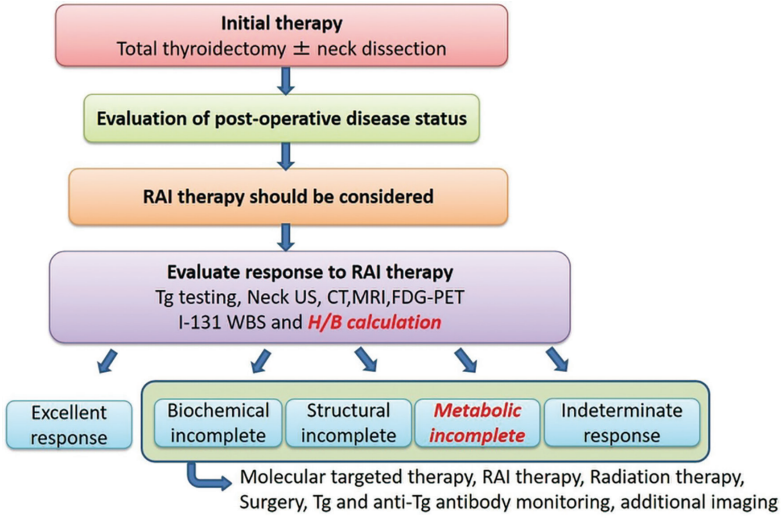



**Figure 3.** Clinical decision-making and management of patients with differentiated thyroid cancer after total thyroidectomy
CT: Computed tomography, FDG-PET: fluorodeoxyglucose positron emission tomography, H/B: Hepatic uptake ratio, MRI: Magnetic resonance imaging, US: Ultrasonography, RAI: Radioactive iodine, Tg: Thyroglobulin, WBS: Whole body scan, I-131: Iodine-131

### Study Limitations

This study has several limitations. First, this is a single-center study. The optimized selection of the cut-off H/B could vary for each facility. Thus, it is essential to discuss and further clarify the optimized selection of the cut-off H/B. Additionally, it would be crucial to provide a recommended time window for $^{131}$I WBS after RAI therapy, and discuss the potential impact of the time interval between $^{131}$I WBS and RAI therapy on the results in multiple institutions. Hence, prospective research data from various institutions are warranted to validate the proposed idea.

## Conclusion

In conclusion, this study suggests that H/B could be a useful marker that facilitates optimal treatment decision making and maximizes drug efficacy. Of note, H/B can be determined at various facilities by using the existing equipment. With the advent of molecular-targeted drugs, multidisciplinary healthcare teams comprising surgeons, medical oncologists, endocrinologists, and radiologists will be needed for thyroid cancer treatment. Furthermore, the use of H/B could help maximize the efficacy of molecular-targeted drugs, which are speculated to be used extensively in the near future, thereby further enhancing the outcomes in patients with thyroid cancer.

### Ethics

**Ethics Committee Approval:** This study protocol adhered to the Declaration of Helsinki and was approved by the Asahikawa Medical University Research Ethics Committee (number: 15198, date: 09.03.2016).

**Informed Consent:** The requirement of informed consent was waived by the Ethics Committees because of the retrospective and non-invasive study design.

### Acknowledgment

This work was supported by JSPS KAKENHI Grant Number JP16K20745.

### Footnotes

### Authorship Contributions

Surgical and Medical Practices: M.N., K.N., S.K., Concept: M.N., K.N. Design: K.N. Data Collection or Processing: A.F., T.U., Analysis or Interpretation: S.K., I.Y., A.O., Literature Search: M.N., K.N., Writing: M.N.

**Conflict of Interest:** No conflict of interest was declared by the authors.

**Financial Disclosure:** The authors declared that this study has received no financial support.

## References

1. American Cancer Society. Cancer facts & figures 2025. Atlanta: American Cancer Society. 2025:24-25. Avaible from: https://www.cancer.org/content/dam/cancer-org/research/cancer-facts-and-statistics/annual-cancer-facts-and-figures/2025/2025-cancer-facts-and-figures-acs.pdf
2. Burns WR, Zeiger MA. Differentiated thyroid cancer. Semin Oncol. 2010;37:557-566.
3. Carvalho MR, Ferreira TC, Leite V. Evaluation of whole-body retention of iodine-131 ((131)I) after postoperative remnant ablation for differentiated thyroid carcinoma - thyroxine withdrawal versus rhTSH administration: A retrospective comparison. Oncol Lett. 2012;3:617-620.
4. Rosenbaum MA, McHenry CR. Contemporary management of papillary carcinoma of the thyroid gland. Expert Rev Anticancer Ther. 2009;9:317-329.
5. Morrison SA, Suh H, Hodin RA. The surgical management of thyroid cancer. Rambam Maimonides Med J. 2014;5:e0008.
6. Mazzaferri EL, Jhiang SM. Long-term impact of initial surgical and medical therapy on papillary and follicular thyroid cancer. Am J Med. 1994;97:418-428.
7. Jeon MJ, Kim WG, Choi YM, Kwon H, Lee YM, Sung TY, Yoon JH, Chung KW, Hong SJ, Kim TY, Shong YK, Song DE, Kim WB. Features predictive of distant metastasis in papillary thyroid microcarcinomas. Thyroid. 2016;26:161-168.
8. Durante C, Haddy N, Baudin E, Leboulleux S, Hartl D, Travagli JP, Caillou B, Ricard M, Lumbroso JD, De Vathaire F, Schlumberger M. Long-term outcome of 444 patients with distant metastases from papillary and follicular thyroid carcinoma: benefits and limits of radioiodine therapy. J Clin Endocrinol Metab. 2006;91:2892-2899.
9. Scott E, Learoyd D, Clifton-Bligh RJ. Therapeutic options in papillary thyroid carcinoma: current guidelines and future perspectives. Future Oncol. 2016;12:2603-2613.
10. Tuttle RM, Ball DW, Byrd D, Dilawari RA, Doherty GM, Duh QY, Ehya H, Farrar WB, Haddad RI, Kandeel F, Kloos RT, Kopp P, Lamonica DM, Loree TR, Lydiatt WM, McCaffrey JC, Olson JA Jr, Parks L, Ridge JA, Shah JP, Sherman SI, Sturgeon C, Waguespack SG, Wang TN, Wirth LJ. National Comprehensive Cancer Network. Thyroid carcinoma. J Natl Compr Canc Netw. 2010;8:1228-1274.
11. Robbins RJ, Wan Q, Grewal RK, Reibke R, Gonen M, Strauss HW, Tuttle RM, Drucker W, Larson SM. Real-time prognosis for metastatic thyroid carcinoma based on 2-[18F]fluoro-2-deoxy-D-glucose-positron emission tomography scanning. J Clin Endocrinol Metab. 2006;91:498-505.
12. Schlumberger M, Tubiana M, De Vathaire F, Hill C, Gardet P, Travagli JP, Fragu P, Lumbroso J, Caillou B, Parmentier C. Long-term results of treatment of 283 patients with lung and bone metastases from differentiated thyroid carcinoma. J Clin Endocrinol Metab. 1986;63:960-967.
13. Yen TC, Lin HD, Lee CH, Chang SL, Yeh SH. The role of technetium-99m sestamibi whole-body scans in diagnosing metastatic Hürthle cell carcinoma of the thyroid gland after total thyroidectomy: a comparison with iodine-131 and thallium-201 whole-body scans. Eur J Nucl Med. 1994;21:980-983.
14. Narayanan S, Colevas AD. Current standards in treatment of radioiodine refractory thyroid cancer. Curr Treat Options Oncol. 2016;17:30.
15. Schlumberger M, Tahara M, Wirth LJ, Robinson B, Brose MS, Elisei R, Habra MA, Newbold K, Shah MH, Hoff AO, Gianoukakis AG, Kiyota N, Taylor MH, Kim SB, Krzyzanowska MK, Dutcus CE, de las Heras B, Zhu J, Sherman SI. Lenvatinib versus placebo in radioiodine-refractory thyroid cancer. N Engl J Med. 2015;372:621-630.
16. Faugeras L, Pirson AS, Donckier J, Michel L, Lemaire J, Vandervorst S, D'Hondt L. Refractory thyroid carcinoma: which systemic treatment to use? Ther Adv Med Oncol. 2018;10:1758834017752853.

17. Nakayama M, Okizaki A, Sakaguchi M, Ishitoya S, Uno T, Sato J, Takahashi K. A quantitative evaluation of hepatic uptake on I-131 whole-body scintigraphy for postablative therapy of thyroid carcinoma. Medicine (Baltimore). 2015;94:e1191.
18. Amin MB, Greene FL, Edge SB, Compton CC, Gershenwald JE, Brookland RK, Meyer L, Gress DM, Byrd DR, Winchester DP. The eighth edition AJCC cancer staging manual: continuing to build a bridge from a population-based to a more "personalized" approach to cancer staging. CA Cancer J Clin. 2017;67:93-99.
19. Haugen BR, Alexander EK, Bible KC, Doherty GM, Mandel SJ, Nikiforov YE, Pacini F, Randolph GW, Sawka AM, Schlumberger M, Schuff KG, Sherman SI, Sosa JA, Steward DL, Tuttle RM, Wartofsky L. 2015 american thyroid association management guidelines for adult patients with thyroid nodules and differentiated thyroid cancer: the american thyroid association guidelines task force on thyroid nodules and differentiated thyroid cancer. Thyroid. 2016;26:1-133.
20. Brose MS, Nutting CM, Jarzab B, Elisei R, Siena S, Bastholt L, de la Fouchardiere C, Pacini F, Paschke R, Shong YK, Sherman SI, Smit JW, Chung J, Kappeler C, Peña C, Molnár I, Schlumberger MJ; DECISION investigators. Sorafenib in radioactive iodine-refractory, locally advanced or metastatic differentiated thyroid cancer: a randomised, double-blind, phase 3 trial. Lancet. 2014;384:319-328.
21. NCCN Clinical practice guidelines in oncology, thyroid carcinoma. 2015. Available from: https://pancan.org/facing-pancreatic-cancer/patient-services/nccn-guidelines/?gad_source=1&gad_campaignid=21995416780&gbraid=0AAAAD8O9VKyvXQarifK4YA-rcw8DUw5i&gclid=EAIaIQobChMI6qHBirvVjgMV7KSDBx17ygvbEAAYASAAEgIyyPD_BwE
22. Ito Y, Suzuki S, Ito K, Imai T, Okamoto T, Kitano H, Sugitani I, Sugino K, Tsutsui H, Hara H, Yoshida A, Shimizu K. Tyrosine-kinase inhibitors to treat radioiodine-refracted, metastatic, or recurred and progressive differentiated thyroid carcinoma [Review]. Endocr J. 2016;63:597-602..
23. Khurana I. Textbook of medical physiology. India: reed elsevier. Endocrinal System.2006;710-715.
24. Bianco AC, Salvatore D, Gereben B, Berry MJ, Larsen PR. Biochemistry, cellular and molecular biology, and physiological roles of the iodothyronine selenodeiodinases. Endocr Rev. 2002;23:38-89.
25. Pal GK. Textbook of medical physiology. India: ahuja publishing house. Endocrine Physiology. 2007;3:346.
26. Ziessman HA, Bahar H, Fahey FH, Dubiansky V. Hepatic visualization on iodine-131 whole-body thyroid cancer scans. J Nucl Med. 1987;28:1408-1411.
27. Tatar FA, Morita E, Ituarte PH, Cavalieri RR, Duh QY, Price DC, Siperstein AE, Clark OH. Association between residual thyroid carcinoma and diffuse hepatic uptake of 131I following radioiodine ablation in postoperative total thyroidectomy patients. World J Surg. 2001;25:718-722.
28. Blum M. Hepatic visualization after 131I in patients with thyroid carcinoma. N Engl J Med. 1977;296:634.
29. Hung BT, Huang SH, Huang YE, Wang PW. Appropriate time for post-therapeutic I-131 whole body scan. Clin Nucl Med. 2009;34:339-342.
30. Kim K, Kim SJ, Kim IJ, Kim YK, Kim BS, Pak K. Clinical significance of diffuse hepatic visualization and thyroid bed uptake on post-ablative iodine-131 whole body scan in differentiated thyroid cancer. Onkologie. 2012;35:82-86.

*Original Article*

*Mol Imaging Radionucl Ther 2025;34:202-212* *DOI:10.4274/mirt.galenos.2025.48379*

# $^{18}$F-FDG PET/CT Parameters and Standard Uptake Values Predicting Contralateral Lung Metastasis in Lung Cancer

## *Akciğer Kanserinde Karşı Akciğer Parankim Metastazını Öngörmeye Yarayan $^{18}$F-FDG PET/BT Parametreleri*

**Büşra Özdemir Günay[1], Funda Üstün[2]**

[1]*Giresun Training and Research Hospital, Clinic of Nuclear Medicine, Giresun, Türkiye*
[2]*Trakya University Faculty of Medicine, Department of Nuclear Medicine, Edirne, Türkiye*

## Abstract

**Objectives:** Contralateral lung parenchymal metastasis (CLM), less common than expected in lung cancer, and its exact mechanism is still unknown. To determine the additional value of $^{18}$F-fluorodeoxyglucose positron emission tomography/computed tomography ($^{18}$F-FDG PET/CT) in determining CLM, its causes, and predictive factors in lung cancer.

**Methods:** The data were evaluated by comparing the group with CLM and the group without CLM but with distant metastasis to other organs, two groups known as the M1 classification according to the 9$^{th}$ tumor-node-metastasis classification in lung cancer. Histopathological data, follow-up, and $^{18}$F-FDG PET/CT findings, including primary tumor lobe, segment, size, pleural effusion, additional metastasis, and their maximum standardized uptake value ($SUV_{max}$) values were recorded, and survival analyses were performed.

**Results:** CLM developed in 125 cases. Eighty-one individuals had contralateral metastases at diagnosis, and 44 developed CLM during follow-up. Distant metastases were present in 100 patients; there was no CLM in the control group. While there was no statistical difference between the two groups in terms of the $SUV_{max}$, mean standardized uptake, and metabolic tumor volume values, the presence of satellite nodules and metastatic nodules in other lobes in the same lung were found to be significantly higher in the CLM group (p=0.007; p<0.001). Also, in the CLM group, ipsilateral nodules had significantly higher SUV values than the control group (3.47 g/mL in the CLM group vs 2.81 g/mL in the control group; p=0.046). Pleural metastasis and effusion were more common in the CLM group (p=0.003; p=0.036). The mean SUV values in pleural metastases and pleural effusions in the CLM group were statistically significantly higher (p=0.048 and p=0.037). In statistical analyses, satellite nodules increase the probability of CLM fourfold, while ipsilateral other lobe nodules in the same lung increase it by 5.527 times (p=0.012; R=-0.2752 and p=0.005; R=-0.3672). Additionally, the absence of necrosis in the initial tumor raises the probability of metastasis to the contralateral lung by 3.326 times during follow-up (p=0.015; R=0.2656).

**Conclusion:** The study emphasized the role of ipsilateral nodules, pleural effusion, and pleural metastasis in predicting CLM using $^{18}$F-FDG PET/CT imaging.

**Keywords:** $^{18}$F-FDG PET/CT, lung cancer, contralateral spread, contralateral lung metastasis, pleural spread

**Address for Correspondence:** Büşra Özdemir Günay, Giresun Training and Research Hospital, Clinic of Nuclear Medicine, Giresun, Türkiye
**E-mail:** busraozdemir39@gmail.com **ORCID ID:** orcid.org/0000-0001-8540-0115
**Received:** 17.02.2025 **Accepted:** 24.08.2025 **Publication Date:** 08.10.2025

**Cite this article as:** Özdemir Günay B, Üstün F. $^{18}$F-FDG PET/CT parameters and standard uptake values predicting contralateral lung metastasis in lung cancer. Mol Imaging Radionucl Ther. 2025;34:202-212.

Copyright© 2025 The Author. Published by Galenos Publishing House on behalf of the Turkish Society of Nuclear Medicine.
This is an open access article under the Creative Commons Attribution-NonCommercial-NoDerivatives 4.0 (CC BY-NC-ND) International License.

## Öz

**Amaç:** Akciğer kanserinde kontralateral akciğer parankim metastazı (CLM), beklenenden daha az görülmekte olup kesin mekanizması hala bilinmemektedir. Bu çalışmada, akciğer kanserinde CLM'nin belirlenmesinde $^{18}$F-florodeoksiglukoz pozitron emisyon tomografisi/bilgisayarlı tomografinin ($^{18}$F-FDG PET/BT) ek değerini, nedenlerini ve prediktif faktörlerini ortaya koymak amaçlandı.

**Yöntem:** Veriler, CLM görülen grup ile CLM olmayan ancak diğer organlara uzak metastazı bulunan grup karşılaştırılarak değerlendirildi. Bu iki grup, akciğer kanserinde 9. tümör-nod-metastaz sınıflamasına göre M1 sınıflaması olarak tanımlanmaktadır. Histopatolojik veriler, takip bulguları ve primer tümör lobu, segmenti, boyutu, plevral efüzyon, ek metastazlar ile maksimum standardize tutulum değeri ($SUV_{max}$) dahil olmak üzere $^{18}$F-FDG PET/BT bulguları kaydedildi ve sağkalım analizleri yapıldı.

**Bulgular:** Toplam 125 olguda CLM gelişti. Seksen bir hastada tanı sırasında kontralateral metastaz saptandı, 44 hastada ise takip sırasında CLM gelişti. Kontrol grubunda ise 100 hastada uzak metastaz varken CLM saptanmadı. İki grup arasında $SUV_{max}$, ortalama standardize tutulum ve metabolik tümör hacmi değerleri açısından istatistiksel fark bulunmazken, aynı akciğerdeki diğer loblarda bulunan satellit nodüller ve metastatik nodüller CLM grubunda anlamlı derecede daha fazlaydı (p=0,007; p<0,001). Ayrıca CLM grubunda ipsilateral nodüllerin SUV değerleri, kontrol grubuna göre anlamlı derecede yüksekti (CLM grubunda 3,47 g/mL; kontrol grubunda 2,81 g/mL; p=0,046). Plevral metastaz ve plevral efüzyon CLM grubunda daha sık görüldü (p=0,003; p=0,036). CLM grubunda plevral metastaz ve plevral efüzyonların ortalama SUV değerleri de istatistiksel olarak anlamlı derecede daha yüksekti (p=0,048 ve p=0,037). İstatistiksel analizlerde, satellit nodüller CLM olasılığını 4 kat artırırken, aynı akciğerin diğer lobundaki ipsilateral nodüller bu olasılığı 5,527 kat artırdı (p=0,012; R=-0,2752 ve p=0,005; R=-0,3672). Ayrıca, başlangıç tümöründe nekroz bulunmaması, takip sürecinde kontralateral akciğere metastaz gelişme olasılığını 3,326 kat artırdı (p=0,015; R=0,2656).

**Sonuç:** Çalışma, $^{18}$F-FDG PET/BT görüntüleme kullanılarak CLM öngörülmesinde ipsilateral nodüllerin, plevral efüzyonun ve plevral metastazın önemini vurgulamaktadır.


**Anahtar kelimeler:** $^{18}$F-FDG PET/BT, akciğer kanseri, kontralateral yayılım, kontralateral akciğer metastazı, plevral yayılım

## Introduction

Lung cancer is the second most frequent type of cancer worldwide, behind breast cancer in terms of incidence (1). The majority of lung cancer patients are diagnosed with metastatic disease, which considerably affects their prognosis. The 5-year survival rate for lung cancer is roughly 20%, indicating the percentage of patients who live at least five years after diagnosis (2). This low survival rate highlights the critical need for early detection and more effective treatments, as advanced-stage disease is much harder to treat successfully. The tumor-node-metastasis (TNM) staging system is the most-used approach for staging and directing treatment choices in primary lung cancer (3).

Several studies have demonstrated the advantages of $^{18}$F-fluorodeoxyglucose positron emission tomography/computed tomography ($^{18}$F-FDG PET/CT) over standard conventional imaging methods in lung cancer, and the guidelines of the National Comprehensive Cancer Network recommend $^{18}$F-FDG PET/CT imaging for the evaluation of patients in all stages of lung cancer (4,5). The presence of a metastatic nodule and its location affect the patient's stage, while metastasis to the opposite lung, pericardium, or pleura is considered a distant metastatic disease (6). According to the 9$^{th}$ edition of the TNM classification, the M1a category includes patients with specific characteristics such as malignant pleural or pericardial effusion, and contralateral lung metastasis (CLM). Survival rates decrease significantly in cases of CLM; however, it is still better compared to patients with distant metastases to other organs (3,7). Early detection and precise characterization of the metastatic pathways of CLM can result in improved survival rates. Early detection allows for prompt intervention, which may halt or reduce the progression of metastatic disease. Furthermore, identifying the exact metastatic pathways in CLM enables the development of targeted therapies and personalized treatment regimens.

In cases of lung cancer, CLM may not exhibit distinct clinical or radiological signs, as typically observed in metastases to other organs. Nonetheless, evidence suggests that surgical resection of contralateral metastatic lesions could contribute to improved overall survival outcomes. CLM poses significant challenges in determining optimal treatment protocols due to its association with poor prognosis. Consequently, early detection of CLM through accurate imaging is crucial for guiding treatment decisions. While conventional imaging modalities such as CT and magnetic resonance imaging have demonstrated limited sensitivity and specificity in identifying CLM, $^{18}$F-FDG PET/CT has shown superior diagnostic capability (3,4,5). $^{18}$F-FDG PET/CT not only enhances the detection of metastatic lesions but also provides critical insights into tumor grading and metastatic potential, making it a valuable tool in the clinical management of lung cancer (4,5).

The aim of this study is to determine the critical $^{18}$F-FDG PET/CT characteristics that, in the preoperative phase of lung cancer patients, can predict CLM. In cases where there are organ metastases outside the lung parenchyma, these parameters would be methodically compared with

surgical and histological findings. The best cut-off levels will be determined by examining standard uptake value maximum ($SUV_{max}$) values in order to improve diagnostic precision. By evaluating $^{18}$F-FDG PET/CT's effectiveness as a non-invasive diagnostic tool, the evaluation seeks to enhance clinical judgment in the treatment of lung cancer.

## Materials and Methods

### Patients

Retrospective analysis was performed on 225 cases between October 2015 and December 2021. Of these, 125 had been diagnosed with lung cancer and had CLM in $^{18}$F-FDG PET/CT imaging at diagnosis and during follow-up (CLM group), and 100 had distant metastases, CLM during the follow-up (control group).

Gender, age at the time of diagnosis, postoperative histopathological data, $^{18}$F-FDG PET/CT findings including primary tumor lobe, segment, size, tumor contours, necrosis, pleural effusion, pleural involvement, mediastinal invasion, thorax wall invasion, ipsilateral lung metastasis, and additional metastasis were recorded. Patients TNM stages were recorded based on $^{18}$F-FDG PET/CT.

We compared data from 44 patients who developed CLM in follow up, and 100 patients who had distant metastases (control group) to determine which factors predict contralateral metastasis. In addition, imaging and $^{18}$F-FDG PET/CT findings that could predict the possibility of metastasis were analyzed in groups with and without CLM.

This study was performed in accordance with the ethical concepts of the October 2013 Helsinki Declaration and approved by the institutional ethical review board Ethics Committee of Scientific Research, Dean's Office, Faculty of Medicine, Trakya University (number: TUTF BAEK-2020/299, date: 24.08.2020).

### Imaging and Image Analysis

All patients fasted for at least 4 hours until reaching a blood sugar level lower than 170 mg/dL before the injection of $^{18}$F-FDG, and oral contrast was administered. Approximately 3.7 MBq/kg of $^{18}$F-FDG was injected intravenously into the patients. After one hour, $^{18}$F-FDG PET/CT scans were performed from the skull to the mid-thigh, 3 min per bed position, and with iterative reconstruction using a combined PET/CT system (Discovery STE; GE Medical Systems, Milwaukee, WI). $^{18}$F-FDG PET/CT fusion images were created, and axial, coronal, and sagittal images were reformatted.

$^{18}$F-FDG PET/CT images were interpreted in PET VCAR software (GE Healthcare) by a nuclear medicine physician without any information about the patient.

$^{18}$F-FDG PET/CT images showing greater FDG uptake than normal organs or surrounding tissues were classified as metastatic lesions. In the case of lung nodules, the CT component was evaluated and any suspicious opacity was determined as a possible lung metastasis. By reviewing follow-up $^{18}$F-FDG PET/CT, CT, and magnetic resonance images, as well as histological analysis and treatment response, a consensus was reached on the classification of lesions as metastatic.

The $SUV_{max}$, mean standardized uptake ($SUV_{mean}$), and metabolic tumor volume (MTV) values were calculated for primary tumors and metastatic lesions. Regions of interest of the lesions were reviewed using a threshold of 42% of the tumor $SUV_{max}$ or greater.

### Statistical Analysis

Statistical analyses were conducted using SPSS version 25 (SPSS, Inc., Chicago, IL). Student's t-tests were used to analyze paired samples. Categorical variables were compared using the $\chi^2$ and Fisher's exact tests. Pearson's r correlation coefficient and Spearman's rank correlation coefficient were used to analyze the relationship between continuous variables. One-way ANOVA or Kruskal-Wallis tests were used to compare groups, followed by Tukey post-hoc tests for continuous variables. All p values less than 0.05 were considered statistically significant. Kaplan-Meier estimations were used to create survival curves.

## Results

### Patient and Tumor Characteristics

The study included 225 patients undergoing $^{18}$F-FDG PET/CT (30 females, 195 males). The mean age at the time of diagnosis was 61.8±9.2 (38-85) years in the contralateral lung parenchyma group (CLM group) and 61.4±8.2 (30-78) years in the control group. Histopathological diagnoses were 57 adenocarcinomas, 50 squamous cell carcinomas, 6 large cell carcinomas, and 12 small cell carcinomas in the CLM group. 47 adenocarcinomas, 30 squamous carcinomas, 4 large cell carcinomas, and 19 small cell carcinomas were observed in the control group, respectively. There was no association found between tumor histology and CLM (p=0.156). Table 1 provides details of patient and tumor characteristics. When patients were staged based on $^{18}$F-FDG PET/CT findings, 43 patients had M1a, 16 had M1b, and 66 of them had M1c disease in the CLM group.

In a subgroup of 44 patients, who developed CLM during follow-up, the mean age in this group was 62.4±10.2 (38-83). Nineteen adenocarcinomas, 23 squamous cell carcinomas, 1 large cell carcinoma, and 1 small cell

carcinoma were observed in CLM in the follow-up group. There was no significant variance between the histological categories in terms of the development of CLM during follow-up (p=0.231).

Primary tumors' locations are defined as lobes and segments based on the CT component of $^{18}$F-FDG PET/CT. Primary tumors could not be evaluated due to prior surgery in 7 patients in the CLM group and 8 patients in the control group. When the location of the primary lung tumor and metastasis to the contralateral lung parenchyma were assessed, there was no statistically significant correlation between tumor localization and metastasis (p=0.314). In addition, when we differentiated primary tumors that originated from either the lower lobe or the upper lobe, no significant difference was found in terms of the risk of metastasis to the opposite lung parenchyma (0.176). Throughout the follow-up, there was no significant correlation between tumor localization and the development of opposite parenchymal metastases (p=0.320 and p=0.241).

### $^{18}$F-FDG PET/CT Findings

The metabolic parameters of primary tumors of the 225 patients were evaluated. The mean $SUV_{max}$, $SUV_{mean}$, and MTV of the primary tumors were 14.9 g/mL, 8.8 g/mL, and 52.75 $cm^3$, respectively. $SUV_{max}$, $SUV_{mean}$, and MTV of the main tumor on $^{18}$F-FDG PET/CT did not differ significantly between the CLM group and the group that developed metastasis during follow-up compared to the control groups (p=0.187; p=0.167; p=0.873 in CLM group and p=0.274; p=0.212; p=0.104 in the CLM in follow-up group).

In the CLM group, there were 24 patients with mediastinal invasion and 7 patients with thoracic wall invasion, compared to 19 patients with mediastinal invasion and 4 patients with thoracic wall invasion in the control group (p=0.545 and p=0.426). Thirty-one patients in the control group, and 44 patients in the CLM group had necrotic components in their primary tumors (p=0.347).

Metastatic nodules are categorized based on $^{18}$F-FDG PET/CT as one nodule, oligo-metastatic nodules, and multiple nodules. Thirty-three patients had a single nodule in the contralateral lung, 63 patients had oligo-metastatic nodules, and 29 patients had multiple contralateral nodules in $^{18}$F-FDG PET/CT. Mean dimensions of the contralateral nodules was 14.6±6.9 mm (2.3 to 29 mm) and mean $SUV_{max}$ of the contralateral nodules was 4.6±4.4 (min 0.4 and max 29.9 g/mL).

In the CLM group, 65 (52%) patients had satellite nodules that were metastatic nodules in the same lobe as the primary. Additionally, 65 (52%) patients had metastatic nodules in the ipsilateral other lobe, with a mean dimension of 12.2±4.3 mm and a mean $SUV_{max}$ of 3.47 g/mL. In the control group, 34 (34%) patients had satellite nodules and 20 (20%) patients had nodules in the ipsilateral lobe with a mean dimension of 13.9±3.4 mm, a mean $SUV_{max}$ of 2.81 g/mL. A satellite nodule and an ipsilateral nodule were observed to be significantly more common in the CLM group than in the control group (p=0.007 and p<0.001, respectively). There was no difference in the mean dimension of ipsilateral nodules between the two groups (p=0.432), but in the CLM group, ipsilateral nodules had significantly higher SUV values than the control group (p=0.046).

Figure 1 shows a patient who had both an ipsilateral satellite nodule and a metastatic nodule in the contralateral lung at the time of diagnosis. $SUV_{max}$ of the patient's primary lesion was 9.7 g/mL, ipsilateral nodules $SUV_{max}$ was 5.2 g/mL, and contralateral nodules $SUV_{max}$ was 3.1 g/mL.

Among the concomitant findings, pleural metastases were found in 55 patients in the CLM group and in 25 patients

**Table 1. Patients and tumor characteristics**

| | CLM group (n: 125) | Control group (n: 100) |
|---|---|---|
| **Gender** | | |
| Male | 106 | 89 |
| Female | 19 | 11 |
| **Age** | 61.8±9.2 | 61.4±8.2 |
| **Pathology** | | |
| Adenocarcinoma | 57 | 47 |
| Squamous cell carcinoma | 50 | 30 |
| Large cell carcinoma | 6 | 4 |
| Small cell carcinoma | 12 | 19 |

CLM: Contralateral lung parenchymal metastasis

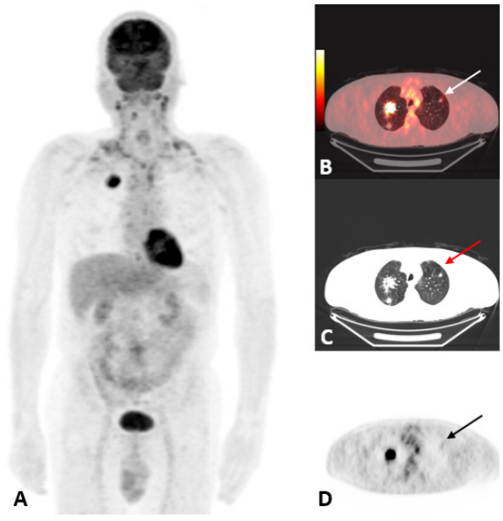



**Figure 1.** (A-D) A patient who had both an ipsilateral satellite nodule and a metastatic nodule in the contralateral lung at the MIP image (A) and and this patient's contralateral lung metastasis (arrows) (B-D) at the time of diagnosis. $SUV_{max}$ of the primary lesion was 9.7 g/mL

$SUV_{max}$: Standardized uptake value, MIP: Maximum intensity projection

in the control group (p=0.003). Pleural effusion was found in 42 patients in the CLM group and in 21 patients in the control group (p=0.025). The findings are summarized in Table 2. The mean SUV values in pleural metastases in the CLM group were 5.42 g/mL, and a statistically significant difference was found in the mean SUV values in the non-CLM group, with 4.17 g/mL (p=0.048). Similarly, the mean SUV value in the CLM group with pleural effusion was 3.25 g/mL while the SUV value in the non-CLM group with pleural effusion was 2.11g/mL. A statistically significant difference was found (p=0.037).

When the patients were grouped according to the stages of the mediastinal lymph nodes, there were 7 patients in the N1 stage, 27 patients in the N2 stage and 54 patients in the N3 stage in the CLM group, while there were 5 patients in the N1 stage, 25 patients in the N2 stage and 47 patients in the N3 stage in the control group. Mediastinal lymph node positivity and stage were not significantly correlated with CLM (p=0.547).

A total of 41 (32.8%) patients showed PET-positive bone metastases, with an average $SUV_{max}$ of 11.8±6.4. Thirty-one (24.8%) patients had PET-positive adrenal metastasis, with an average $SUV_{max}$ of 7±4.8. A total of 18 patients (14.4%) showed PET-positive liver metastases, with an average

**Table 2. Characteristics of primary tumor, ipsilateral metastatic nodules and pleural involvement between two group and their p values**

| | CLM group | Control group | p |
|---|---|---|---|
| **Mediastinal invasion** | | | NS |
| Negative | 94 | 73 | |
| Positive | 24 | 19 | |
| **Thoracic wall invasion** | | | NS |
| Negative | 111 | 88 | |
| Positive | 7 | 4 | |
| **Necrosis** | | | NS |
| Negative | 74 | 61 | |
| Positive | 44 | 31 | |
| **Pleural metastasis** | | | 0.003* |
| Negative | 70 | 75 | |
| Positive | 55 | 25 | |
| **Pleural effusion** | | | 0.025* |
| Negative | 83 | 79 | |
| Positive | 42 | 21 | |
| **Ipsilateral lung metastasis** | | | |
| Same lobe | 65 | 34 | 0.007* |
| Other lobe | 65 | 30 | <0.001* |

*: statistically significant, CLM: Contralateral lung parenchymal metastasis, NS: Not significant

$SUV_{max}$ of 11.5±6. Thirteen patients (10.4%) had brain metastases, and six (4.8%) had soft tissue metastases.

When distant node metastasis was evaluated, twenty-six (20.8%) had neck lymph node metastasis and twenty-two (17.6%) had abdominal lymph node metastasis, with an average $SUV_{max}$ of 6.7±4.6. All these findings did not significantly correlate with the CLM.

When the characteristics of the group that developed CLM during follow-up were compared to the control group, no significant difference was found between histopathological subtypes in terms of developing CLM during follow-up (r=0.1321, p=0.231).

Similar to the CLM group, no significant difference was detected in terms of $SUV_{max}$, $SUV_{mean}$, and MTV values of the primary lesions between CLM in the follow-up group and the control group (p=0.274; p=0.212 and p=0.104).

Among the evaluated parameters: mediastinal lymph node metastasis stage (p=0.547), supraclavicular lymph node metastasis (p=0.422) and metastasis to the other neck lymph nodes (p=0.877), and presence of abdominal lymph node metastasis (p=0.381) did not contribute significantly to predicting contralateral lung parenchymal metastasis during follow-up. Also, the presence of distant metastases such as bone (p=0.858), liver (p=0.291), adrenal (p=0.264), soft tissue (p=0.064), brain metastases (p=0.614) and their SUV values did not contribute significantly to predicting CLM during follow up.

The factors predicting the development of CLM in the follow-up were as follows;

1- Satellite nodules in the same lobe raise the probability of CLM by fourfold [p=0.012; R=-0.2752; 95% confidence interval (CI): 0.082-0.767].

2- Nodules in the other ipsilateral lobe raise the probability of CLM by 5.527 times (p=0.005; R=-0.3672; 95% CI: 0.042-0.563).

3- The absence of necrotic features in the initial tumor increases the likelihood of metastasis to the contralateral lung parenchyma by 3.326 times (p=0.015; R=0.2656; 95% CI: 1.236-8.950).

There was no significant difference between the two groups when the other associated findings were compared. The findings are summarized in Table 3.

### Overall Survival

Median follow up time was 19.9 months (minimum: 1, maximum: 123). In the follow-up, 110 (88%) patients died in the CLM group and 94 (94%) patients died in the control group.

**Table 3. Characteristics of primary tumor, ipsilateral metastatic nodules, pleural involvement and their p values between CLM in follow up and control group**

| | CLM in follow up group | Control group | p |
|---|---|---|---|
| **Mediastinal invasion** | | | |
| Negative | 40 | 73 | NS |
| Positive | 4 | 19 | |
| **Thoracic wall invasion** | | | |
| Negative | 44 | 88 | NS |
| Positive | 0 | 4 | |
| **Necrosis** | | | 0.015* |
| Negative | 36 | 61 | |
| Positive | 8 | 31 | |
| **Pleural metastasis** | | | NS |
| Negative | 37 | 75 | |
| Positive | 7 | 25 | |
| **Pleural effusion** | | | NS |
| Negative | 36 | 79 | |
| Positive | 8 | 21 | |
| **Ipsilateral lung metastasis** | | | |
| Same lobe | 16 | 34 | 0.012* |
| Other lobe | 10 | 30 | 0.005* |

*: statistically significant, CLM: Contralateral lung parenchymal metastasis, NS: Not significant

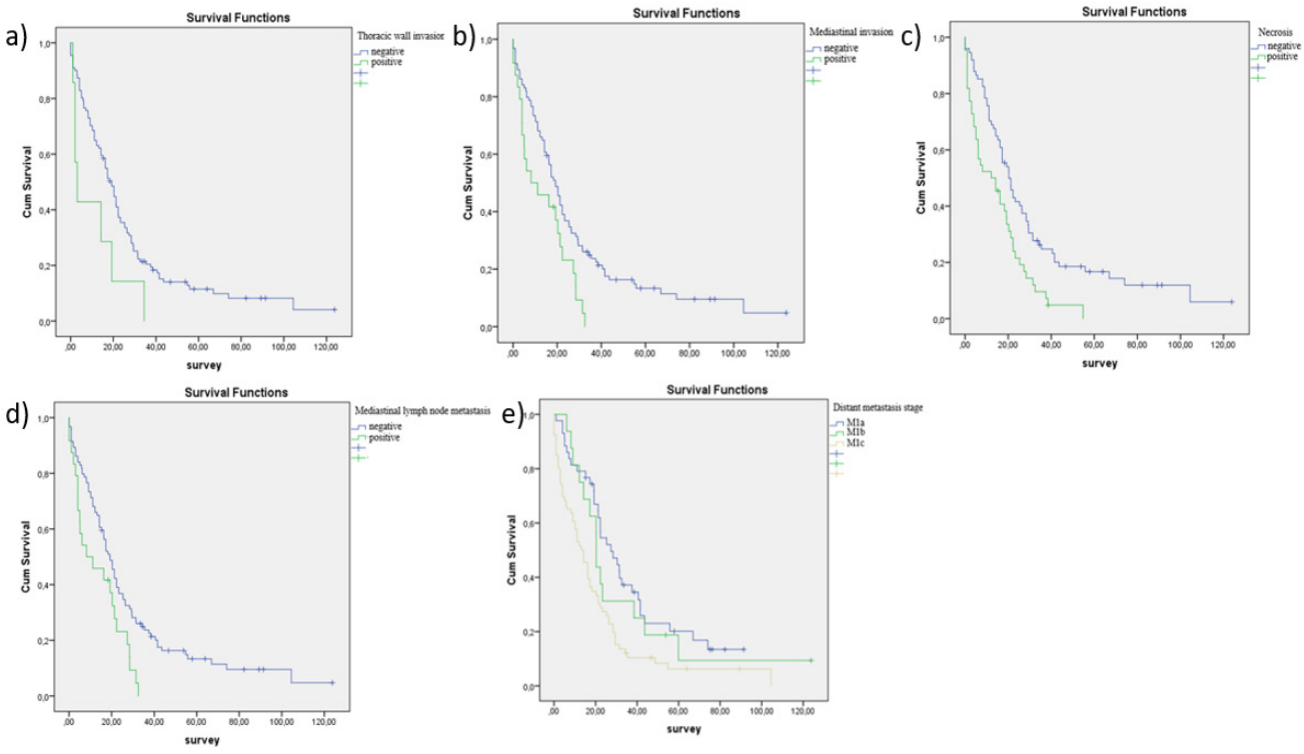



**Figure 2.** (A-E) Survival curves shown based on the significant predictors

When divided based on distant metastases, in the CLM group, 43 patients were at the M1a stage, 16 patients were at the M1b stage, and 66 patients were at the M1c stage. In the control group, 22 patients were found in the M1b stage and 78 patients were found in the M1c stage.

The median duration of life was 35.7 months in the M1a group, which had only CLM. In the M1b group, which had distant metastases to a single organ, median lifetime was 33.2 months, and in the M1c group, which had multiple distant metastases, the median lifetime was 20.1 months. The M1b and M1a groups did not show any significant differences in survival (p=0.497); however, there was a significant difference in survival between the M1a and M1c groups (p=0.001).

When analyzed separately, the overall 1-year survival rate was 0.65 and 5-year survival rate was 0.08 in the CLM group. The 1-year survival rate was 0.44 and the 5-year survival rate was 0.02 in the control group, respectively. In terms of overall survival, there was a substantial difference between the CLM group and the control group (p<0.001). The average survival of patients with CLM was 28.3 months, and the control group was 15.5 months.

In the CLM group, only small cell lung cancer showed a significantly shorter survival time compared to adenocarcinoma and squamous cell carcinoma (p=0.001). There was no association in survival for other subtypes.

The factors significantly correlated with patient survival include thoracic wall invasion (p=0.044, a), mediastinal invasion (p=0.008, b), presence of necrosis in primary tumor (p=0.001, c), mediastinal lymph node involvement (p=0.030, d), and stage of distant metastasis (p=0.002, e). In Figure 2, survival curves are shown based on the significant predictors.

When we analyzed the association between contralateral nodule features and survival, there was no significant difference in surveillance regarding the number, size, or $SUV_{max}$ of contralateral parenchymal metastases (p=0.698; p=0.447; p=0.352).

## Discussion

This study aims to identify $^{18}$F-FDG PET/CT features that predict CLM in lung cancer patients. For several years, researchers have extensively investigated the phenomenon of CLM lung cancer, proposing various hypotheses

regarding its mechanisms of dissemination. Notably, Ferguson et al. (8) reported that CLM occurs infrequently, even in cases where there is mediastinal involvement. This finding suggests that the pathways of metastatic spread to the contralateral lung may differ from those to other organs, underscoring the need for further research to elucidate the specific biological and pathological processes governing CLM. By accurately diagnosing the tumor grade and contralateral development, $^{18}$F-FDG PET/CT helps improve the clinical care for patients.

Onuigbo (9) examined the spread of lung cancer and the mechanisms underlying CLM. The article highlights several key factors: anatomically, both lungs share a similar microenvironment; the contralateral lung is one of the closest organs to the primary tumor; and the lungs receive their blood supply directly from the aorta. Additionally, both lungs are interconnected through venous and lymphatic collaterals. Despite these considerations, Onuigbo (9) proposed a novel explanation for the relatively infrequent occurrence of metastasis to the contralateral lung: although cancer cells do reach the opposing lung, they disappear before they can adhere and establish a metastatic focus.

In our study, satellite nodules in the same lobe with the primary and metastatic nodules in the ipsilateral other lobe were frequently observed in CLM, suggesting that not only tumor grade or burden but also specific routes might affect metastasis to the contralateral lung. The mechanism by which the contralateral lung is spread to could be the reason for the frequent occurrence of CLM. This finding may be consistent with the view stated in Onuigbo's study (9), that although cancer cells reach the opposite lung, they disappear without being able to establish there. In addition, studies on lymphatic drainage have shown that the visceral lymphatic circulation connects the two lungs (10). In the study we performed, $SUV_{max}$ values for satellite nodules or nodules in the same lobe that developed CLM were 3.47 g/mL. Quantifying $SUV_{max}$ values of ipsilateral nodules in $^{18}$F-FDG PET/CT scans may help predict CLM by identifying high tumor burden that could metastasize between lungs. This measurement is crucial because it enables us to better identify the tumor's biological behavior and spread potential. Specifically, elevated FDG uptake identified using $^{18}$F-FDG PET/CT indicates a more aggressive biological behavior of the tumor or a greater number of tumor cells disseminated through the lung lymphatics, raising the likelihood of metastasis to the opposing lung. Because of the useful information $^{18}$F-FDG PET/CT offers in the assessment of metastatic spread, it is an essential tool in the clinical decision-making process and plays a significant role in directing patient care.

Patients with lung cancer who have pleural effusion frequently have advanced disease and a bad prognosis (11). According to a study, 20% of cases of lung cancer and pleural effusion are discovered at the time of diagnosis (12). In our study, 28% of patients with lung cancer had pleural effusions, and 66.6% of these individuals had CLM. A meta-analysis by Treglia et al. (13) demonstrated that $^{18}$F-FDG PET/CT has 86% sensitivity and 80% specificity in detecting pleural abnormalities.

The diagnostic accuracy of malignant and benign pleural effusions was evaluated by $^{18}$F-FDG PET/CT imaging, more specifically by calculating $SUV_{max}$. In the study by Simsek et al. (14), the specificity and positive predictive value for $SUV_{max}$ >1.3 were found to be 100%, although the sensitivity was suboptimal. Furthermore, Nakajima et al. (15) emphasize that cytological evaluations cannot provide a definitive diagnosis in up to 30% of cases, and that imaging methods, especially $^{18}$F-FDG PET/CT, should be relied upon for more accurate differentiation. In our investigation, the $SUV_{max}$ values of pleural effusions associated with CLM were assessed as 3.25 g/mL, whereas the $SUV_{max}$ values of pleural effusions unassociated with CLM were measured as 2.11 g/mL, indicating a clinically significant difference. Furthermore, our findings contribute to the current literature by revealing that greater SUV values of a pleural effusion are related to an increased likelihood of malignant pleural effusion and a higher risk of developing CLM. These findings make an important contribution to conventional imaging and cytological sampling procedures.

This emphasizes how crucial it is to incorporate metabolic data into the therapeutic setting in order to improve the precision of diagnosis. Because $^{18}$F-FDG PET/CT can objectively detect metabolic activity by SUV values, it offers a non-invasive method of evaluating tumor aggressiveness and survival.

Pleural involvement in lung cancer has been recognized as a substantial risk factor for CLM. It promotes tumor cell spread through the lymphatic system and pleural space, increasing the risk of metastasis to the opposite lung. Lymphatic routes may allow tumor cells on the pleural surface to spread to the contralateral lung and diaphragm. According to studies metastasis usually starts with ipsilateral pleural involvement, then spreads to the contralateral pleura, and finally invades the contralateral lung parenchyma, without any blood vessel involvement (9,10,16,17).

In Rashidi et al.'s (18) experimental study, lung cancer cells have been reported to migrate to the diaphragmatic surface via lymphatic pathways in the ipsilateral lung. Most of the cells reached the contralateral diaphragmatic

surface, and only a small percentage proceeded through the bronchovascular pedicle to reach the contralateral lung parenchyma.

Several studies have shown that the presence of pleural effusion and pleural metastases increases the incidence of metastatic lesions in the contralateral lung parenchyma (19,20,21,22). In our study, we found that the incidence of metastasis in the contralateral lung parenchyma was higher in cases with ipsilateral pleural involvement consistent with the literature. According to these data, pleural involvement in lung cancer patients can be regarded as a significant indicator that worsens the prognosis of the illness and raises the possibility of metastatic dissemination. Evidence suggests that pleural effusion and pleural metastases have been associated with an increased risk of metastatic lesions in the contralateral lung parenchyma. However, the intensity of this link differs between studies, emphasizing the need for further research to understand the underlying mechanisms and therapeutic implications.

The relationship between necrotic tissue and lung cancer involves various biological mechanisms that affect tumor behavior and treatment outcomes (23). Necrosis in tumor cells could influence the tumor microenvironment, immune response, and treatment efficacy, although its effect on prognosis and therapy results in lung cancer is unknown (24). Future research should look into how necrosis influences drug delivery, immune cell infiltration, and inflammation, potentially affecting therapeutic responses. Our study indicated that the risk of metastasis to the contralateral lung parenchyma increased 3.326 times during the follow-up period in tumors without necrosis compared to primary necrotic lung masses. This suggests that tumors with less necrosis may have a more robust vascular network, which may facilitate the continued growth of the tumor and the spread of malignant cells to distant sites. The lack of necrosis within the primary tumor may indicate that the tumor is in a well-vascularized environment, which supports its sustainable growth and metastasis potential. In this context, the low amount of necrotic tissue and the high presence of viable tissue may play a more important role tumor grade and prognosis, and may determine the course of the disease and response to treatment. Onuigbo (17) explained in their study on lung cancer that the lower incidence of metastasis to the opposite lung parenchyma could be attributed to significant necrosis development in tumor cells that reach the pleura of the opposite lung through the lymphatic route. This could be because these tumors were sensitive to factors secreted during necrosis. As a result, the primary tumor's sensitivity to these factors may lead to the elimination of metastatic cells by the contralateral lung before they can establish lesions during their invasion of the other lung.

Apart from conventional imaging findings, $^{18}$F-FDG PET/CT provides information about tumor biology and tumor heterogeneity, by showing necrotic tissue. Although there are no specific data on tumor heterogeneity in our study, the effect of the presence of necrosis on CLM has been clearly demonstrated. Tumor heterogeneity may have an important role in predicting CLM, and future studies on this subject are needed. Besides high $SUV_{max}$ values in tumors, necrotic areas may be associated with an increased risk of metastasis, and this finding is of great importance in evaluation both metabolic imaging and CLM.

Previous studies primarily aimed to determine whether a nodule detected in the contralateral lung is malignant. Two of these studies found that malignant contralateral nodules are typically adenocarcinomas (25,26). In contrast, Carretta et al. (27) observed no significant association between the initial tumor histology and the presence of metastatic nodules in the lung. Similarly, our study suggests that histopathological subtypes did not affect CLM or the development of metastasis during follow-up.

The lobe or segment location of original tumors did not correlate with the location where CLM were more frequently identified in our investigation. On the other hand, Huang et al. (28) showed that initial tumors in the upper lobe were associated with metastases in the upper lobe of the contralateral lung in patients with adenocarcinoma. Larger prospective studies are required to validate these results, and elucidate the significance of various subtypes, especially those that concentrate on pure histopathological subtypes.

Sánchez de Cos Escuín et al. (29) demonstrated in a previous study that the number of CLM, whether single or multiple, has no effect on survival. In a study by Rami-Porta and Eberhardt (16) that examined the IASLC database, the researchers hypothesized that the presence of multiple metastatic nodules may have a worse prognosis than the presence of a single nodule, but it did not create a statistically significant result due to the low number of patients. In our study, no significant correlation was found between the number of CLM and survival. There was no association between survival and the size or $SUV_{max}$ values of metastatic nodules in the contralateral lung. To the best of our knowledge, this is the first study to assess the association between the number of contralateral metastatic lung nodules as well as their $SUV_{max}$ values with survival.

### Study Limitations

As a limitation of the study, because it was conducted retrospectively, we included patients with proven contralateral metastases, resulting in selection bias. Not all lesions could be correlated histopathologically as metastatic in the contralateral lung. However, additional imaging and clinical follow-ups aid in the characterization of the lesions. Since the treatments received by the patients were not evaluated in this study, data related to treatment could not be presented in the survival analyses. Nevertheless, the strengths of the study include the interpretation of all $^{18}$F-FDG PET/CT, imaging, and all pathologies, at our university hospital. Further prospective studies are needed to confirm our findings and identify predictive factors.

## Conclusion

In conclusion, the study indicated the importance of ipsilateral nodules, pleural effusion, and pleural metastasis in utilizing $^{18}$F-FDG PET/CT imaging to predict CLM. These results demonstrate the significance of $^{18}$F-FDG PET/CT as a useful diagnostic tool for locating and evaluating lung cancer patients' metastatic pathways, which helps with more precise prediction of outcomes and treatment planning. In the management of lung cancer, more investigation and validation of these prognostic indicators may improve clinical expertise and patient outcomes.

### Acknowledgment

The authors thank MD, Prof. Necdet Süt for his contribution to the statistical analyses. Also, I would like to thank my husband MD, Burak Günay for his support and always being there for me.

### Ethics

**Ethics Committee Approval:** This study was performed in accordance with the ethical concepts of the October 2013 Helsinki Declaration and approved by the institutional ethical review board Ethics Committee of Scientific Research, Dean's Office, Faculty of Medicine, Trakya University (number: TUTF BAEK- 2020/299, date: 24.08.2020).

**Informed Consent:** Retrospective study.

### Footnotes

### Authorship Contributions

Surgical and Medical Practices: F.Ü., Concept: B.Ö.G., F.Ü., Design: F.Ü., Data Collection or Processing: B.Ö.G., Analysis or Interpretation: B.Ö.G., Literature Search: B.Ö.G., F.Ü., Writing: B.Ö.G., F.Ü.

**Conflict of Interest:** No conflict of interest was declared by the authors.

**Financial Disclosure:** The authors declared that this study has received no financial support.

## References

1. Sung H, Ferlay J, Siegel RL, Laversanne M, Soerjomataram I, Jemal A, Bray F. Global Cancer Statistics 2020: GLOBOCAN estimates of incidence and mortality worldwide for 36 cancers in 185 countries. CA Cancer J Clin. 2021;71:209-249.
2. Akdemir ÜÖ, Aydos U. Role of fluorodeoxyglucose positron emission tomography/computed tomography imaging in diagnosis and staging of lung cancer. Nucl Med Semin. 2018;4:6-17.
3. Kandathil A, Kay FU, Butt YM, Wachsmann JW, Subramaniam RM. Role of FDG PET/CT in the eighth edition of TNM staging of non-small cell lung cancer. Radiographics. 2018;38:2134-2149.
4. Deppen SA, Blume JD, Kensinger CD, Morgan AM, Aldrich MC, Massion PP, Walker RC, McPheeters ML, Putnam JB Jr, Grogan EL. Accuracy of FDG-PET to diagnose lung cancer in areas with infectious lung disease: a meta-analysis. JAMA. 2014;312:1227-1236.
5. Kubota K, Matsuno S, Morioka N, Adachi S, Koizumi M, Seto H, Kojo M, Nishioka S, Nishimura M, Yamamoto H. Impact of FDG-PET findings on decisions regarding patient management strategies: a multicenter trial in patients with lung cancer and other types of cancer. Ann Nucl Med. 2015;29:431-441.
6. Eberhardt WE, Mitchell A, Crowley J, Kondo H, Kim YT, Turrisi A 3rd, Goldstraw P, Rami-Porta R; International association for study of lung cancer staging and prognostic factors committee, advisory board members, and participating institutions. the IASLC lung cancer staging project: proposals for the revision of the m descriptors in the forthcoming eighth edition of the TNM classification of lung cancer. J Thorac Oncol. 2015;10:1515-1522.
7. Shin J, Keam B, Kim M, Park YS, Kim TM, Kim DW, Kim YW, Heo DS. Prognostic impact of newly proposed m descriptors in TNM classification of non-small cell lung cancer. J Thorac Oncol. 2017;12:520-528.
8. Ferguson MK, DeMeester TR, DesLauriers J, Little AG, Piraux M, Golomb H. Diagnosis and management of synchronous lung cancers. J Thorac Cardiovasc Surg. 1985;89:378-385.
9. Onuigbo WI. Anomalous lung cancer cell carriage: a historical review with present prospects. Int J Surg. 2014;12:734-746.
10. Riquet M. Bronchial arteries and lymphatics of the lung. Thorac Surg Clin. 2007;17:619-638.
11. Skok K, Hladnik G, Grm A, Crnjac A. Malignant pleural effusion and its current management: a review. Medicina (Kaunas) 2019;55:490.
12. Lombardi G, Zustovich F, Nicoletto MO, Donach M, Artioli G, Pastorelli D. Diagnosis and treatment of malignant pleural effusion: a systematic literature review and new approaches. Am J Clin Oncol. 2010;33:420-423.
13. Treglia G, Sadeghi R, Annunziata S, Lococo F, Cafarotti S, Prior JO, Bertagna F, Ceriani L, Giovanella L. Diagnostic performance of fluorine-18-fluorodeoxyglucose positron emission tomography in the assessment of pleural abnormalities in cancer patients: a systematic review and a meta-analysis. Lung Cancer. 2014;83:1-7.
14. Simsek FS, Yuksel D, Yaylali O, Aslan HS, Kılıçarslan E, Bir F, Arslan M, Can FE, Ugurlu E. Can PET/CT be used more effectively in pleural effusion evaluation? Jpn J Radiol. 2021;39:1186-1194.
15. Nakajima R, Abe K, Sakai S. Diagnostic ability of FDG-PET/CT in the detection of malignant pleural effusion. Medicine (Baltimore). 2015;94:e1010.

16. Rami-Porta R, Eberhardt WEE. Clinical implications of the innovations in the primary tumour and metastasis of the 8th edition of the TNM classification for lung cancer. J Thorac Dis. 2018;10(Suppl 22):2682-2685.
17. Onuigbo WI. Contralateral pulmonary metastases in lung cancer. Thorax. 1974;29:132-133.
18. Rashidi B, Moossa AR, Hoffman RM. Specific route mapping visualized with GFP of single-file streaming contralateral and systemic metastasis of Lewis lung carcinoma cells beginning within hours of orthotopic implantation [correction of implantion]. J Cell Biochem. 2013;114:1738-1743.
19. Kruse M, Sherry SJ, Paidpally V, Mercier G, Subramaniam RM. FDG PET/CT in the management of primary pleural tumors and pleural metastases. AJR Am J Roentgenol. 2013;201:W215-W226.
20. Mordant P, Rivera C, Legras A, Le Pimpec Barthes F, Riquet M. Current readings: the most influential and recent studies regarding resection of lung cancer in m1a disease. Semin Thorac Cardiovasc Surg. 2013;25:251-255.
21. Zutić H. [Bronchial carcinoma–an overview]. Med Arh. 1999;53(3 Suppl 1):27-31.
22. Svaton M, Havel D, Buresova M, Baxa J, Hosek P. Percutaneous transthoracic needle biopsy of lung lesions is a safe method associated with a very low risk of pleural recurrence. Biomed Pap Med Fac Univ Palacky Olomouc Czech Repub. 2025;169:21-25.
23. Butter R, Halfwerk H, Radonic T, Lissenberg-Witte B, Thunnissen E. The impact of impaired tissue fixation in resected non-small-cell lung cancer on protein deterioration and DNA degradation. Lung Cancer. 2023;178:108-115.
24. Kludt C, Wang Y, Ahmad W, Bychkov A, Fukuoka J, Gaisa N, Kühnel M, Jonigk D, Pryalukhin A, Mairinger F, Klein F, Schultheis AM, Seper A, Hulla W, Brägelmann J, Michels S, Klein S, Quaas A, Büttner R, Tolkach Y. Next-generation lung cancer pathology: development and validation of diagnostic and prognostic algorithms. Cell Rep Med. 2024;5:101697.
25. Ruppert AM, Lerolle U, Carette MF, Lavole A, Khalil A, Bazelly B, Antoine M, Cadranel J, Milleron B. Coexisting pulmonary nodules in operable lung cancer: prevalence and probability of malignancy. Lung Cancer. 2011;74:233-238.
26. Riihimäki M, Hemminki A, Fallah M, Thomsen H, Sundquist K, Sundquist J, Hemminki K. Metastatic sites and survival in lung cancer. Lung Cancer. 2014;86:78-84.
27. Carretta A, Ciriaco P, Canneto B, Nicoletti R, Del Maschio A, Zannini P. Therapeutic strategy in patients with non-small cell lung cancer associated to satellite pulmonary nodules. Eur J Cardiothorac Surg. 2002;21:1100-1104.
28. Huang YH, Hsu KH, Tseng JS, Chen KC, Su KY, Chen HY, Chang CS, Chen JJ, Yu SL, Chen HW, Yang TY, Chang GC. Predilection of contralateral upper lung metastasis in upper lobe lung adenocarcinoma patients. J Thorac Dis. 2016;8:86-92.
29. Sánchez de Cos Escuín J, Abal Arca J, Melchor Íñiguez R, Miravet Sorribes L, Núñez Ares A, Hernández Hernández JR, García Arangüena L, Núñez Delgado M, Pavón Fernández MJ, Francisco Corral G, de Esteban Júlvez L, González Budiño MT, Abad Cavaco F, Ansótegui Barrera E, Andreo García F, Serra Mitjans M, Hernández Rodríguez H. Tumor, node and metastasis classification of lung cancer–M1a versus M1b–analysis of M descriptors and other prognostic factors. Lung Cancer. 2014;84:182-189.

*Original Article*

*Mol Imaging Radionucl Ther 2025;34:213-220* *DOI:10.4274/mirt.galenos.2025.04696*

# Radiation-induced Xerostomia: Evaluation with $^{18}$F-FDG PET/CT

## *Radyoterapi İlişkili Kserostominin $^{18}$F-FDG PET/BT ile Değerlendirilmesi*

*Gözde Mütevelizade[1], Bilal Çağrı Bozdemir[1], Nazım Aydın[2], Ahmet Furkan Süner[3], Ömür Karakoyun Çelik[4], Yasemin Parlak[1], Ecem Çorlu[4], Özgür Yıldırım[4], Mustafa Kahya[4], Gizem Bakıcıerler[4], Gül Gümüşer[1], Elvan Sayıt[1]*

[1]*Celal Bayar University Faculty of Medicine, Department of Nuclear Medicine, Manisa, Türkiye*
[2]*University of Health Sciences Türkiye, Prof. Dr. Cemil Taşcıoğlu City Hospital, Clinic of Nuclear Medicine, İstanbul, Türkiye*
[3]*Ministry of Health of the Republic of Türkiye, Çaycuma District Health Directorate, Zonguldak, Türkiye*
[4]*Celal Bayar University Faculty of Medicine, Department of Radiation Oncology, Manisa, Türkiye*

## Abstract

**Objectives:** To investigate the relationship between radiation dose, metabolic changes in the salivary glands assessed by $^{18}$F-fluorodeoxyglucose positron emission tomography/computed tomography ($^{18}$F-FDG PET/CT), and xerostomia severity in patients with head and neck cancer following radiotherapy (RT).

**Methods:** We retrospectively analyzed 107 patients treated with intensity-modulated RT or volumetric modulated arc therapy for head and neck malignancies. Clinical xerostomia severity was evaluated at the time of post-treatment PET/CT. Mean gland doses and dose–volume parameters (V10–V50) were extracted from treatment plans. Metabolic changes were evaluated by $^{\Delta}$maximum standardized uptake value and $^{\Delta}$mean standardized uptake value between pre and post treatment PET/CT scans. The relationships between clinical, dosimetric, and metabolic variables were examined.

**Results:** Moderate-to-severe xerostomia occurred in 63.6% of patients. Both higher T and N stage were significantly associated with greater xerostomia severity ($p<0.05$). Patients with nodal metastases on pretreatment PET/CT demonstrated a higher prevalence of xerostomia. Dose–volume parameters (V10–V30 for parotids, V50 for submandibular glands) were significantly correlated with symptom severity. $^{\Delta}$SUV values were significantly associated with both mean dose and dose–volume parameters, particularly in the left parotid gland, where patients receiving >30 Gy showed markedly greater metabolic decline. Parotid glands demonstrated stronger dose-dependent metabolic changes compared with submandibular glands, consistent with their higher radiosensitivity.

**Conclusion:** Despite the use of advanced RT techniques, xerostomia remains a frequent toxicity. $^{18}$F-FDG PET/CT reliably captured dose-dependent salivary gland impairment and reflected the impact of tumor burden on toxicity risk. These findings underscore the complementary role of PET-derived biomarkers as integrative tools for predicting salivary dysfunction beyond conventional dosimetric parameters.

**Keywords:** $^{18}$F-FDG PET/CT, head and neck cancer, radiotherapy, xerostomia

**Address for Correspondence:** Gözde Mütevelizade, Celal Bayar University Faculty of Medicine, Department of Nuclear Medicine, Manisa, Türkiye
**E-mail:** gozdemutevelizadee@gmail.com **ORCID ID:** orcid.org/0000-0001-5986-8777
**Received:** 27.08.2025 **Accepted:** 04.09.2025 **Publication Date:** 08.10.2025

**Cite this article as:** Mütevelizade G, Bozdemir BÇ, Aydın N, Süner AF, Karakoyun Çelik Ö, Parlak Y, Çorlu E, Yıldırım Ö, Kahya M, Bakıcıerler G, Gümüşer G, Sayıt E. Radiation-induced xerostomia: evaluation with $^{18}$F-FDG PET/CT. Mol Imaging Radionucl Ther. 2025;34:213-220.

Copyright© 2025 The Author. Published by Galenos Publishing House on behalf of the Turkish Society of Nuclear Medicine.
This is an open access article under the Creative Commons Attribution-NonCommercial-NoDerivatives 4.0 (CC BY-NC-ND) International License.

## Öz

**Amaç:** Bu çalışmada, baş ve boyun kanseri nedeniyle radyoterapi (RT) uygulanan hastalarda, tükrük bezlerine ait radyasyon dozu, $^{18}$F-florodeoksiglukoz pozitron emisyon tomografisi/bilgisayarlı tomografi ($^{18}$F-FDG PET/BT) ile değerlendirilen metabolik değişiklikler ve kserostomi şiddeti arasındaki ilişki araştırıldı.

**Yöntem:** Baş ve boyun kanseri tanısı ile RT alan 107 hasta retrospektif olarak incelendi. Post-RT PET/BT sırasında klinik kserostomi semptomları değerlendirildi. Tedavi planlarından ortalama bez dozları ve doz–hacim parametreleri (V10–V50) elde edildi. Pre- ve post-RT PET/BT arasındaki $^{\Delta}$maksimum standart tutulum değeri ve $^{\Delta}$ortalama standart tutulum değeri değerleri hesaplanarak metabolik değişiklikler değerlendirildi. Klinik, dozimetrik ve metabolik değişkenler arasındaki ilişkiler incelendi.

**Bulgular:** Hastaların %63,6'sında orta ve şiddetli kserostomi saptandı. İleri T ve N evreleri kserostomi şiddeti ile anlamlı ilişkiliydi ($p<0,05$). Pre-RT PET/BT'de nodal metastazı olan hastalarda şiddetli kserostomi daha sık izlendi. Parotis bezleri için V10–V30, submandibuler bezler için V50 parametreleri semptom şiddeti ile anlamlı ilişkiliydi. $^{\Delta}$SUV değerleri ortalama doz ve doz–hacim parametreleri ile korelasyon gösterdi; özellikle sol parotiste >30 Gy alan hastalarda belirgin metabolik azalma gözlendi. Parotis bezleri, submandibuler bezlere kıyasla daha güçlü doz bağımlı metabolik değişiklikler sergiledi.

**Sonuç:** Gelişmiş RT tekniklerine rağmen kserostomi sık görülen bir yan etki olmaya devam etmektedir. 18F-FDG PET/BT, tükrük bezlerindeki doz bağımlı fonksiyon kaybını güvenilir şekilde gösterebilmekte ve tümör yükünün toksisite riskine etkisini yansıtmaktadır. Bu bulgular, PET tabanlı biyogöstergelerin geleneksel dozimetrik parametrelerin ötesinde kserostomi riskinin öngörülmesinde tamamlayıcı rol oynayabileceğini ortaya koymaktadır.


**Anahtar kelimeler:** $^{18}$F-FDg PET/BT, baş ve boyun kanseri, radyoterapi, kserostomi

## Introduction

Radiotherapy (RT) remains a fundamental treatment method for head and neck cancers (HNC), either as a primary treatment or in combination with chemotherapy (CT) and/or surgery. However, radiation-induced damage to surrounding normal tissues is a major limitation, with xerostomia being one of the most frequent and distressing side effects. Moreover, RT affects the composition of saliva, resulting in a thicker and more viscous secretion (1). Xerostomia occurs due to radiation-induced dysfunction of the salivary glands. Despite advances in RT techniques, radiation-induced damage to normal tissues remains a major concern. One of the most debilitating and common late toxicities is xerostomia, which substantially impairs patients' quality of life by affecting speech, mastication, taste, oral hygiene, and overall nutritional status (2). Stimulated salivary production is largely derived from the parotid glands, contributing approximately 60-70% of total saliva, whereas resting (unstimulated) salivary flow predominantly originates from the submandibular and sublingual glands as well as numerous minor oral salivary glands (3). This physiological distinction underlines the different clinical impact of radiation-induced dysfunction in these glands.

Previous studies have shown that both the occurrence and severity of xerostomia are closely associated with the mean radiation dose delivered to the parotid and submandibular glands. The parotid glands appear particularly radiosensitive due to their predominantly serous acinar structure. Dose–response relationships have demonstrated that when the mean dose to the parotid glands is maintained below approximately 26 Gy and to the submandibular glands below approximately 40 Gy, the incidence of xerostomia is significantly reduced. Furthermore, prospective data indicate that, provided these thresholds are not exceeded, a gradual recovery of salivary gland function may occur within two years following RT. In contrast, doses beyond these limits are often associated with persistent dysfunction and chronic symptoms. According to the Quantitative Analyses of Normal Tissue Effects in the Clinic (QUANTEC) guidelines, these thresholds form the basis of widely applied dose–volume constraints for organs at risk (OARs) in head and neck RT (3,4,5,6).

In addition to its established role in staging and treatment response assessment in HNC, $^{18}$F-fluorodeoxyglucose positron emission tomography/computed tomography ($^{18}$F-FDG PET/CT) can also provide insights into radiation-induced changes in normal tissues. PET-derived metabolic parameters, such as maximum standardized uptake value ($SUV_{max}$) and mean standardized uptake value ($SUV_{mean}$), may therefore serve as objective biomarkers of salivary gland function and radiation-related injury (7). Nevertheless, the association between metabolic changes in salivary glands, radiation dose exposure, and clinical xerostomia symptoms has not been fully elucidated.

The present study aimed to investigate the relationship between radiation doses delivered to the salivary glands, metabolic changes assessed by pre- and post-RT $^{18}$F-FDG PET/CT parameters, and the correlation of these factors with the severity of xerostomia symptoms in patients with head and neck malignancies.

## Materials and Methods

### Patient Selection

This retrospective study included 107 patients with histopathologically confirmed head and neck malignancies who underwent $^{18}$F-FDG PET/CT in our institution between 2018 and 2023 for disease staging and subsequent treatment response evaluation after curative RT. Patients with distant metastases at baseline, a history of another malignancy, or prior surgical treatment for HNC were excluded. Patients with incomplete clinical, pathological, or imaging data were also not included in the analysis. None of the patients received any treatment specifically for xerostomia between the two PET/CT scans. The study protocol was reviewed and approved by the Health Sciences Ethics Committee of Manisa Celal Bayar University Faculty of Medicine (number: 20.478.486/3287, date: 16.07.2025). Written informed consent was obtained from all subjects.

### PET/CT Acquisition and Image Analysis

All patients fasted for at least 4-6 hours prior to the examination, and serum glucose levels were confirmed to be <200 mg/dL before tracer administration. The standard intravenous dose of 370-555 MBq (10-15 mCi) of $^{18}$F-FDG was injected, followed by a resting period of approximately 60 minutes in a quiet room. Imaging was performed using a General Electric Discovery IQ 3-Ring hybrid PET/CT scanner (GE Healthcare, Milwaukee, USA). A low-dose CT scan (16-slice; 120 kVp; 90 mA) was acquired first for attenuation correction and anatomical reference. Subsequently, PET data were obtained from the skull base to the mid-thigh in the supine position, with an acquisition time of 2 minutes per bed position (typically 8–10 beds per patient). PET images were reconstructed with the Q. Clear penalized-likelihood algorithm (β-value 500) to improve image quality. Images were generated on a 192 × 192 matrix with a field of view of 70 cm and a slice thickness of 3.26 mm, yielding a voxel size of approximately 3.65 mm³. Fusion PET/CT images were reviewed in axial, sagittal, and coronal planes using maximum intensity projection and attenuation-corrected datasets.

For quantitative analysis, regions of interest were manually drawn over the bilateral parotid and submandibular glands on attenuation-corrected PET/CT images. $SUV_{max}$ and $SUV_{mean}$ values were measured for each gland on both the pre-RT and the post-RT PET/CT scans. The second (post-RT) PET/CT examination was performed 3–6 months after completion of RT. Differences between pre-RT and post-RT values were calculated and expressed as $^{\Delta}SUV_{max}$ and $^{\Delta}SUV_{mean}$. At the time of the post-RT PET/CT examination, xerostomia-related symptoms were assessed using the Turkish validated version of the University of Washington Quality of Life Questionnaire version 4 (8). Based on patient-reported responses to the xerostomia domain, patients were categorized into three groups: no symptoms, mild symptoms, and moderate-to-severe symptoms.

### Radiotherapy and Dosimetric Evaluation

All patients received curative-intent RT using intensity-modulated radiotherapy (IMRT) or volumetric modulated arc therapy (VMAT) techniques delivered with an Elekta Versa HD linear accelerator (Elekta AB, Stockholm, Sweden), according to institutional protocols. Treatment planning was performed on CT images, with target volumes and OARs delineated in accordance with international contouring guidelines (Figure 1). Dose–volume histograms were generated for each plan (Figure 2).

For dosimetric analysis, the mean radiation doses delivered to the bilateral parotid and submandibular glands were recorded. In addition, volumetric parameters were calculated to quantify the percentage of gland volume receiving specified dose levels. For the parotid glands,

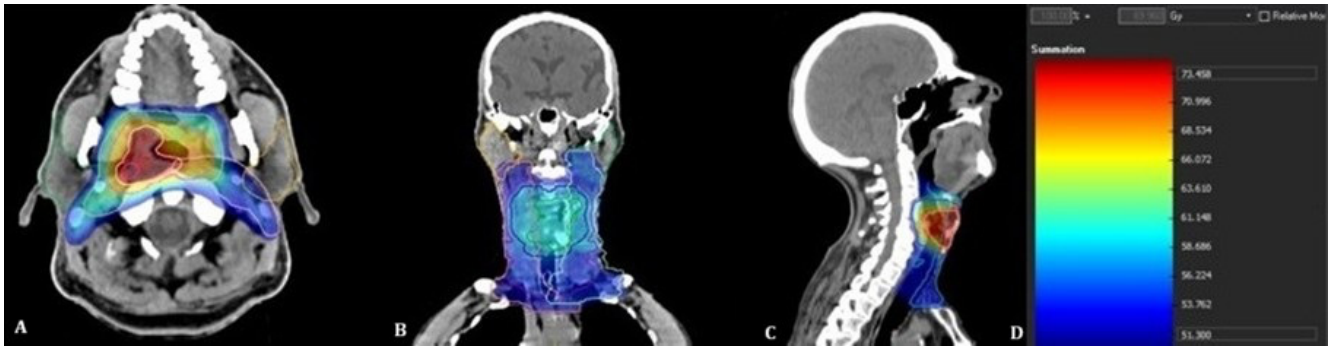



**Figure 1.** Representative radiotherapy planning computed tomography images of a patient with a right posterolateral oropharyngeal tumor. (A) Axial, (B) coronal, and (C) sagittal slices demonstrate in the slices target volumes and dose distributions, with delineation of parotid and submandibular glands as organs at risk. (D) Corresponding dose-color scale

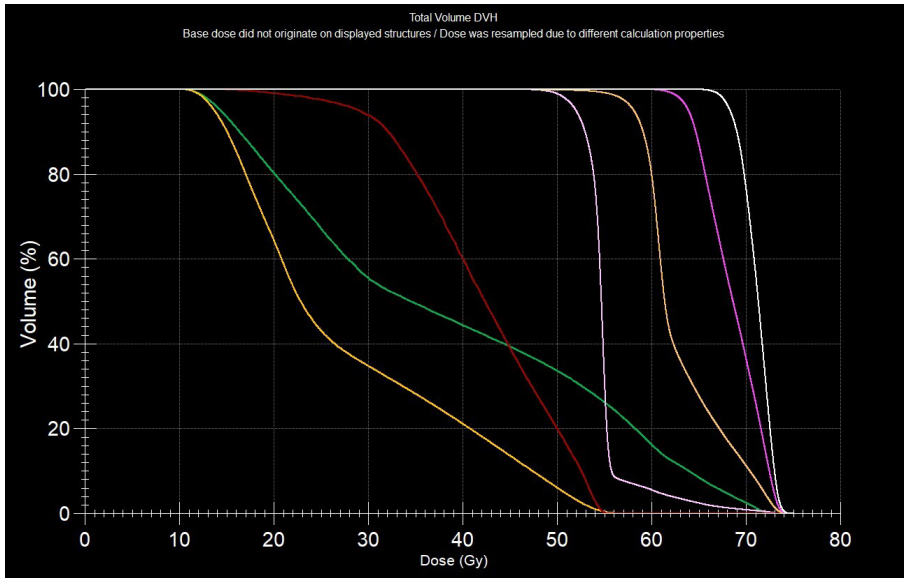



**Figure 2.** Representative dose–volume histogram from the same patient shown in Figure 1. Due to the right posterolateral location of the oropharyngeal tumor, the right parotid gland (green line) received substantially higher radiation doses compared with the contralateral parotid gland (yellow line). Dose–volume histograms of target volumes are also displayed for reference
DVH: Dose–volume histogram

V10, V20, and V30 were determined, representing the proportions of gland volume exposed to ≥10 Gy, ≥20 Gy, and ≥30 Gy, respectively. For the submandibular glands, V50 was calculated as the proportion of gland volume exposed to ≥50 Gy. These parameters, together with mean gland doses, were subsequently analyzed in relation to xerostomia severity and PET-derived metabolic changes ($^{\Delta}SUV_{max}$ and $^{\Delta}SUV_{mean}$).

### Statistical Analysis

Descriptive statistics were expressed as mean, standard deviation, and range for continuous variables, and as frequency and percentage for categorical variables. The association between xerostomia severity and continuous parameters such as age was assessed using Spearman's rank correlation test. Correlations between PET/CT-derived metabolic parameters ($^{\Delta}SUV_{max}$, $^{\Delta}SUV_{mean}$) and both mean doses and dose–volume parameters (V10, V20, V30 for the parotid glands and V50 for the submandibular glands) were also evaluated using Spearman's rank correlation. Differences in $^{\Delta}SUV$ values across xerostomia severity groups (0, 1, 2) were analyzed with the Kruskal-Wallis test. Categorical variables, including sex, tumor stage, and lateralization, were compared with xerostomia severity using the chi-square test. For cut-off analysis, patients were stratified according to a 30 Gy threshold for parotid mean dose, and intergroup differences were assessed using the Mann–Whitney U test. Statistical analyses were performed using SPSS version 26.0 (IBM Corp., Armonk, NY, USA), and a p-value <0.05 was considered statistically significant.

## Results

A total of 107 patients who underwent RT for head and neck malignancies were included in the study. The cohort consisted of 95 men (88.8%) and 12 women (11.2%), with a mean age of 61.3 years (range: 25–84 years). Primary tumor sites were the larynx (n=63), nasopharynx (n=13), oral cavity (n=11), hypopharynx (n=8), oropharynx (n=6), paranasal sinus (n=3), and HNC of unknown primary (n=3). In 56 patients (52.3%), the tumor was located in the midline, while 26 patients (24.3%) had left-sided and 25 patients (23.4%) had right-sided tumors. At the time of post-RT PET/CT imaging, xerostomia symptoms were absent in 9 patients (8.4%), mild in 30 patients (28.0%), and moderate-to-severe in 68 patients (63.6%) (Table 1).

Additional analyses were performed to evaluate the association between xerostomia severity and baseline clinical variables. Older age was significantly correlated with higher xerostomia severity (p=-0.27, p=0.005). Sex and tumor lateralization (right, left, or midline) were not significantly related to xerostomia severity (p>0.05). In contrast, both T stage and N stage were significantly associated with xerostomia, with more advanced stages corresponding to more moderate-to-severe symptoms (p<0.001 and p=0.004, respectively).

| Table 1. Distribution of descriptive characteristics | |
|---|---|
| **Variable** | **n (%) or mean ± SD (range)** |
| **Total patients** | 107 |
| **Age (years)** | 61.3±10.9 (25–84) |
| **Sex** | Male: 95 (88.8%)<br>Female: 12 (11.2%) |
| **Primary tumor lateralization** | Midline: 56 (52.3%)<br>Left: 26 (24.3%)<br>Right: 25 (23.4%) |
| **T stage** | T1: 8 (7.5%)<br>T2: 14 (13.1%)<br>T3: 35 (32.7%)<br>T4: 49 (45.8%) |
| **N stage** | N0: 46 (43.0%)<br>N1: 17 (15.9%)<br>N2: 32 (29.9%)<br>N3: 11 (10.3%) |
| **Mean radiation dose (Gy)** | Right parotid: 24.8<br>Left parotid: 26.2<br>Right submandibular: 52.5<br>Left submandibular: 52.7 |
| **Xerostomia severity** | None: 9 (8.4%)<br>Mild: 30 (28.0%)<br>Moderate-to-severe: 68 (63.6%) |
| SD: Standard deviation | |

A significant relationship was observed between tumor lateralization and N stage (p=0.0046), largely driven by the predominance of N0 cases in midline tumors. When right- and left-sided tumors were compared, no statistically significant differences were observed in N stage distribution (p=0.478). However, right-sided tumors more frequently presented as N0 (28.0%) compared with left-sided tumors (19.2%), whereas higher nodal stages were relatively more common in left-sided tumors. When patients were stratified according to primary tumor site, those with oropharyngeal, oral cavity, nasopharyngeal, or hypopharyngeal cancers exhibited a markedly higher rate of moderate-to-severe xerostomia compared with patients with laryngeal, paranasal sinus, or HNC of unknown primary origin (92.1% vs. 47.8%, p<0.001).

The mean radiation doses delivered to the salivary glands were 24.8 Gy, 26.2 Gy, 52.5 Gy, and 52.7 Gy for the right parotid, left parotid, right submandibular, and left submandibular glands, respectively. Statistically significant associations were observed between the mean doses to the salivary glands and the severity of xerostomia symptoms (p<0.05). In addition to mean gland doses, volumetric dose parameters were also analyzed. Kruskal-Wallis tests demonstrated that V10, V20, and V30 for both parotid glands, as well as V50 for both submandibular glands, were significantly associated with xerostomia severity (all p<0.001).

Pre-treatment $SUV_{max}$ and $SUV_{mean}$ values of the salivary glands showed no significant association with xerostomia severity (all p>0.05). $^{\Delta}SUV_{max}$ and $^{\Delta}SUV_{mean}$ values of the parotid and submandibular glands were calculated between pre- and post-RT PET/CT scans (Figure 3). When compared across xerostomia severity groups, statistically significant associations were observed only for the left parotid gland (p=0.031 and p=0.044, respectively). In contrast, no significant associations were found for the right parotid or for either submandibular gland (all p>0.05).

Significant correlations were observed between $^{\Delta}SUV$ values and radiation dose metrics of the salivary glands. For the parotid glands, $^{\Delta}SUV_{max}$ and $^{\Delta}SUV_{mean}$ demonstrated moderate inverse correlations with both mean dose and dose–volume parameters (V10, V20, V30), with the strongest associations observed in the left parotid gland (p=-0.34 to -0.44, p<0.05). For the submandibular glands, weaker but statistically significant correlations were identified between $^{\Delta}SUV$ values and V50 (p=-0.20 to -0.31,

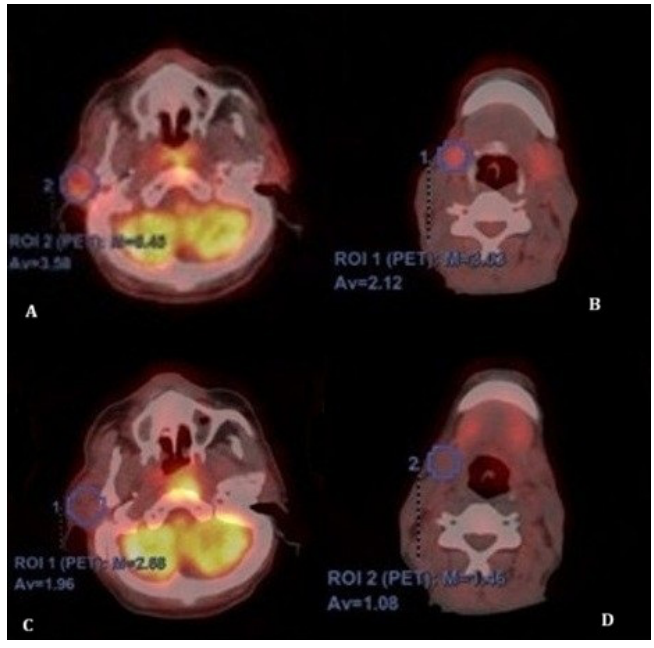



**Figure 3.** Representative pre-and post-radiotherapy $^{18}$F-fluorodeoxyglucose positron emission tomography/computed tomography images from a patient included in the study. (A, B) Pre-treatment scans demonstrate preserved metabolic activity in the parotid and submandibular glands. (C, D) Follow-up scans performed 3-6 months after radiotherapy show a marked reduction in tracer uptake within the glands, reflecting radiation-induced functional impairment. Regions of interest (ROIs) used for maximum standardized uptake value and mean standardized uptake value measurements are indicated
PET: Positron emission tomography

p<0.05). These findings indicate that larger gland volumes exposed to higher radiation doses were associated with greater reductions in metabolic activity. When patients were stratified according to a 30 Gy cut-off for parotid dose–volume parameters, statistically significant differences were found only in the left parotid gland, where both $^{\Delta}SUV_{max}$ (p=0.013) and $^{\Delta}SUV_{mean}$ (p=0.024) showed greater reductions in the high-dose group.

## Discussion

Despite the widespread adoption of advanced RT techniques such as IMRT and image-guided RT, xerostomia remains among the most common and distressing late toxicities in patients with HNC, significantly diminishing quality of life. Studies have consistently shown that sparing the major salivary glands, particularly by maintaining mean parotid doses below 26 Gy and submandibular doses below 40-50 Gy, can effectively reduce the incidence and severity of xerostomia, without compromising tumor control (4,9,10,11). In line with this evidence, the present study aimed to explore the relationship between radiation dose to the salivary glands, metabolic changes visualized on $^{18}$F-FDG PET/CT, and the clinical manifestation of xerostomia in patients treated for head and neck malignancies.

In our study cohort, 63.6% of patients developed moderate-to-severe xerostomia following RT, despite the use of advanced techniques such as IMRT and VMAT. This finding underscores the persistent clinical burden of xerostomia as a late toxicity in HNC treatment. Notably, the observed prevalence rate is in line with previously reported data, where the incidence of moderate-to-severe xerostomia ranged between 40% and 70%, even in studies employing parotid-sparing RT approaches (9, 12).

Our results demonstrated that patients with moderate-to-severe xerostomia had significantly higher mean radiation doses to both the parotid and submandibular glands. This finding reinforces the well-established dose–response relationship between salivary gland irradiation and the development of xerostomia. Moiseenko et al. (4) demonstrated a clear correlation between increased mean dose and higher patient-reported xerostomia severity. Our findings are consistent with these results and highlight the importance of adhering to gland-specific dose constraints during treatment planning.

The relatively high prevalence of moderate-to-severe xerostomia in our cohort is likely attributable to the high rate of nodal involvement as detected on pretreatment $^{18}$F-FDG PET/CT with 60 out of 106 patients (56.6%) presenting with nodal metastases (N1–N3). Patients with advanced N-stage disease often require more extensive target volumes and elective nodal irradiation, which reduces the possibility of sparing adjacent salivary glands, particularly the parotid and submandibular glands (13). In addition, T-stage was significantly associated with xerostomia severity in our cohort, with more advanced stages corresponding to more severe symptoms. Taken together, these findings suggest that tumor burden, reflected by both primary tumor size and nodal involvement, plays a critical role in salivary gland toxicity by limiting the feasibility of gland preservation during RT.

In our cohort, older age was significantly associated with higher xerostomia severity (p=0.005). This finding is consistent with the results of Beetz et al. (13), who reported that patients aged over 70 years had a substantially increased risk of persistent xerostomia despite meeting QUANTEC dose constraints, reflecting the limited recovery potential of elderly salivary glands. However, Pan et al. (14) did not identify age as a significant predictor of xerostomia in their study, which included nasopharyngeal carcinoma patients, where the median patient age was relatively young (47 years). Overall, these observations suggest that age is an important clinical factor influencing salivary gland recovery, although its impact may vary depending on patient demographics and tumor distribution.

When stratified by primary tumor site, the severity of xerostomia differed markedly across subsites. Moderate-to-severe xerostomia was observed in all patients with oropharyngeal and oral cavity cancers (100%) and in the majority of those with nasopharyngeal (84.6%) and hypopharyngeal (87.5%) primaries. In contrast, the prevalence was significantly lower in patients with laryngeal cancers (49.2%) and in those with paranasal sinus tumors (exact prevalence not specified, p<0.001). These findings underscore the importance of tumor location in determining the risk of xerostomia. Beetz et al. (13) reported that parotid-sparing with IMRT was considerably more difficult in oropharyngeal and oral cavity cancers due to their proximity to the major salivary glands. Likewise, nasopharyngeal and hypopharyngeal tumors frequently require large bilateral nodal irradiation volumes, further limiting the potential for gland sparing. However, laryngeal tumors are generally located in the midline and in a more caudal position, thereby reducing dose exposure to the parotid and submandibular glands, and resulting in a substantially lower prevalence of xerostomia compared with nasopharyngeal, hypopharyngeal, oropharyngeal, and oral cavity cancers. Overall, these findings emphasize that anatomical and tumor-related factors, in addition to dosimetric constraints, play a critical role in determining the risk of radiation-induced xerostomia.

In addition to the mean dose, our analysis demonstrated that dose–volume parameters were also significantly associated with xerostomia severity. Specifically, V10, V20, and V30 for both parotid glands, as well as V50 for the submandibular glands, correlated with increased xerostomia symptoms. This underlines the relevance of dose–volume parameters beyond mean dose alone in predicting xerostomia, as radiation exposure of larger gland volumes can significantly contribute to salivary gland dysfunction. Importantly, previous studies have shown that sparing at least one parotid and submandibular gland reduces the risk of xerostomia while improving both stimulated and unstimulated salivary function (3, 4).

Van Dijk et al. (15) demonstrated that textural radiomics features extracted from $^{18}$F-FDG PET images significantly improved the prediction of late xerostomia, particularly one year after RT, highlighting the value of PET-derived image biomarkers for toxicity risk stratification. More recently, Li et al. (16) validated such a PET-based biomarker model in an independent cohort, confirming the independent prognostic value of PET-derived imaging features beyond conventional clinical and dosimetric parameters. In our study, metabolic changes in the salivary glands were evaluated using pretreatment and post-treatment $^{18}$F-FDG PET/CT. SUV values showed significant correlations with both mean gland dose and dose–volume parameters, demonstrating that $^{18}$F-FDG PET/CT can reliably detect the dose-dependent functional impairment of salivary glands following RT. These findings highlight the value of PET-based metabolic imaging as an adjunct to the conventional dose–volume predictor.

The initial decline in salivary flow largely mirrors the intensity of treatment delivery. Among the major salivary glands, the parotids exhibit the highest radiosensitivity, with flow reduction determined by both the radiation dose and the volume of gland tissue encompassed within the treatment field (17). In our study, the parotid glands demonstrated stronger dose-dependent metabolic changes compared with the submandibular glands, as reflected by significant correlations of $^{\Delta}$SUV with both mean dose and low-to-intermediate dose–volume parameters (V10–V30). In contrast, correlations for the submandibular glands were weaker and limited to higher dose exposure (V50). This observation is consistent with the well-established higher radiosensitivity of the parotid glands, which are predominantly composed of serous acinar cells; whereas the mixed serous–mucous composition of the submandibular glands renders them relatively more resistant to radiation-induced injury.

In our cohort, primary tumor sites were relatively homogeneously distributed between the right and left sides, with more than half located in the midline. Tumor lateralization itself was not significantly associated with xerostomia severity. However, nodal involvement was more frequent in left-sided tumors compared with right-sided tumors. Specifically, right-sided tumors more frequently presented as N0 (28.0%) compared with left-sided tumors, (19.2%), whereas higher nodal stages were more common in left-sided tumors. This asymmetry in nodal distribution explains the more pronounced metabolic impairment observed in the left parotid gland, as greater nodal burden on the left side necessitated higher radiation exposure to the ipsilateral salivary gland. Consistent with this clinical observation, significant PET-based metabolic changes were also predominantly seen in the left parotid gland. Both $^{\Delta}SUV_{max}$ and $^{\Delta}SUV_{mean}$ were significantly associated with xerostomia severity and demonstrated dose–response correlations with mean dose and dose–volume parameters (V10–V30). In contrast, the submandibular glands showed weaker associations, which were limited to higher dose exposure (V50). Importantly, correlation strength was greatest in the left parotid gland, in line with its higher radiation burden. Furthermore, patients receiving mean parotid doses above 30 Gy, exhibited significantly greater reductions in $^{\Delta}SUV_{max}$ and $^{\Delta}SUV_{mean}$ in the left parotid, supporting the concept that doses beyond the QUANTEC threshold are linked to persistent metabolic dysfunction (3).

### Study Limitations

Our study has several limitations. First, it was a single-institution, retrospective analysis. Second, although $^{18}$F-FDG PET/CT provided valuable information on salivary gland metabolism, only SUV-based parameters were analyzed, whereas advanced textural features might have offered additional predictive power. Finally, the relatively short follow-up period precluded evaluation of long-term recovery dynamics of salivary gland function beyond the early post-treatment phase.

## Conclusion

Despite widespread adoption of advanced RT techniques such as IMRT and VMAT, xerostomia remains a common and clinically significant late toxicity in HNC. Our findings demonstrate that advanced T and N stage, older age, and tumor location, particularly nasopharyngeal, hypopharyngeal, oropharyngeal, and oral cavity cancers, are associated with a higher risk of moderate-to-severe xerostomia, while laryngeal tumors show substantially

lower rates. Parotid glands exhibited greater radiosensitivity compared with submandibular glands, and $^{18}$F-FDG PET/CT reliably captured dose-dependent metabolic impairment, highlighting its value as a functional biomarker complementing conventional dose–volume metrics.

From a clinical standpoint, careful treatment planning is especially warranted in patients with large tumors, salivary gland–adjacent nodal metastases, and high-risk subsites, where the risk of toxicity is greatest. These results reinforce the need for more personalized toxicity prediction models that go beyond dosimetric constraints alone.

### Ethics

**Ethics Committee Approval:** The study protocol was reviewed and approved by the Health Sciences Ethics Committee of Manisa Celal Bayar University, Faculty of Medicine (number: 20.478.486/3287, date: 16.07.2025).

**Informed Consent:** Written informed consent was obtained from all patients.

### Footnotes

### Authorship Contributions

Surgical and Medical Practices: G.M., B.Ç.B., Ö.K.Ç., G.B., Concept: G.M., B.Ç.B., Ö.K.Ç., G.B., G.G., Design: G.M., B.Ç.B., Ö.K.Ç., Y.P., E.S.B., Data Collection or Processing: G.M., B.Ç.B., E.Ç., Ö.Y., M.K., Analysis or Interpretation: G.M., B.Ç.B., N.A., A.F.S., Y.P., G.B., Literature Search: G.M., B.Ç.B., N.A., Y.P., G.G., E.S.B., Writing: G.M., B.Ç.B., Ö.K.Ç., E.S.B.

**Conflict of Interest:** No conflict of interest was declared by the authors.

**Financial Disclosure:** The authors declared that this study has received no financial support.

## References

1. Porangaba LP, de Melo Garcia F, Rabelo APAA, Andrade AP, de Abreu Alves F, Pellizzon ACA, Jaguar GC. Randomized double-blind placebo-controlled study of salivary substitute with enzymatic system for xerostomia in patients irradiated in head and neck region. Curr Oncol. 2024;31:1102-1112.
2. Hoebers FJP, Wijers OB, van den Hoek JGM, Moons KGM, Reitsma JB, Steenbakkers RJHM, Schuit E, Langendijk JA. Comprehensive toxicity risk profiling in radiation therapy for head and neck cancer: a new concept for individually optimised treatment. Radiother Oncol. 2021;157:147-154.
3. Deasy JO, Moiseenko V, Marks L, Chao KS, Nam J, Eisbruch A. Radiotherapy dose-volume effects on salivary gland function. Int J Radiat Oncol Biol Phys. 2010;76(3 Suppl):S58-63.
4. Moiseenko V, Wu J, Hovan A, Saleh Z, Apte A, Deasy JO, Harrow S, Rabuka C, Muggli A, Thompson A. Treatment planning constraints to avoid xerostomia in head-and-neck radiotherapy: an independent test of QUANTEC criteria using a prospectively collected dataset. Int J Radiat Oncol Biol Phys. 2012;82:1108-1114.
5. Murdoch-Kinch CA, Kim HM, Vineberg KA, Ship JA, Eisbruch A. Dose-effect relationships for the submandibular salivary glands and implications for their sparing by intensity modulated radiotherapy. Int J Radiat Oncol Biol Phys. 2008;72:373-382.
6. Bentzen SM, Constine LS, Deasy JO, Eisbruch A, Jackson A, Marks LB, Ten Haken RK, Yorke ED. Quantitative analyses of normal tissue effects in the clinic (QUANTEC): an introduction to the scientific issues. Int J Radiat Oncol Biol Phys. 2010;76(3 Suppl):S3-9.
7. Cannon B, Schwartz DL, Dong L. Metabolic imaging biomarkers of postradiotherapy xerostomia. Int J Radiat Oncol Biol Phys. 2012;83:1609-1616.
8. Senkal HA, Hayran M, Karakaya E, Yueh B, Weymuller EA Jr, Hoşal AŞ. The validity and reliability of the Turkish version of the University of Washington Quality of Life Questionnaire for patients with head and neck cancer. Am J Otolaryngol. 2012;33:417-426.
9. Le Guevelou J, Palard-Novello X, Kammerer E, Baty M, Perazzi M, Larnaudie A, De Crevoisier R, Castelli J. Assessment and prediction of salivary gland function after head and neck radiotherapy: a systematic review. Cancer Med. 2024;13:e70494.
10. Chambers MS, Garden AS, Rosenthal D, Ahamad A, Schwartz DL, Blanco AI, Chao KS, Morrison WH, Ang KK, Weber RS. Intensity-modulated radiotherapy: is xerostomia still prevalent? Curr Oncol Rep. 2005;7:131-136.
11. Eisbruch A, Dawson LA, Kim HM, Bradford CR, Terrell JE, Chepeha DB, Teknos TN, Anzai Y, Marsh LH, Martel MK, Ten Haken RK, Wolf GT, Ship JA. Conformal and intensity modulated irradiation of head and neck cancer: the potential for improved target irradiation, salivary gland function, and quality of life. Acta Otorhinolaryngol Belg. 1999;53:271-275.
12. Elhalawani H, Cardenas CE, Volpe S, Barua S, Stieb S, Rock CB, Lin T, Yang P, Wu H, Zaveri J, Elgohari B, Abdallah LE, Jethanandani A, Mohamed ASR, Court LE, Hutcheson KA, Brandon Gunn G, Rosenthal DI, Frank SJ, Garden AS, Rao A, Fuller CD. $^{18}$FDG positron emission tomography mining for metabolic imaging biomarkers of radiation-induced xerostomia in patients with oropharyngeal cancer. Clin Transl Radiat Oncol. 2021;29:93-101.
13. Beetz I, Steenbakkers RJ, Chouvalova O, Leemans CR, Doornaert P, van der Laan BF, Christianen ME, Vissink A, Bijl HP, van Luijk P, Langendijk JA. The QUANTEC criteria for parotid gland dose and their efficacy to prevent moderate to severe patient-rated xerostomia. Acta Oncol. 2014;53:597-604.
14. Pan XB, Liu Y, Li L, Qu S, Chen L, Liang SX, Chen KH, Liang ZG, Zhu XD. Prognostic nomogram of xerostomia for patients with nasopharyngeal carcinoma after intensity-modulated radiotherapy. Aging (Albany NY). 2020;12:1857-1866.
15. van Dijk LV, Noordzij W, Brouwer CL, Boellaard R, Burgerhof JGM, Langendijk JA, Sijtsema NM, Steenbakkers RJHM. $^{18}$F-FDG PET image biomarkers improve prediction of late radiation-induced xerostomia. Radiother Oncol. 2018;126:89-95.
16. Li Y, Sijtsema NM, de Vette SPM, Steenbakkers RJHM, Zhang F, Noordzij W, Van den Bosch L, Langendijk JA, van Dijk LV. Validation of the $^{18}$F-FDG PET image biomarker model predicting late xerostomia after head and neck cancer radiotherapy. Radiother Oncol. 2023;180:109458.
17. Leslie MD, Dische S. The early changes in salivary gland function during and after radiotherapy given for head and neck cancer. Radiother Oncol. 1994;30:26-32.

*Interesting Image*

*Mol Imaging Radionucl Ther 2025;34:221-223* *DOI:10.4274/mirt.galenos.2025.32815*

# Penile Metastasis from Prostate Cancer: Detection on $^{18}$F-PSMA-1007 PET/CT

## *Prostat Kanserinden Kaynaklanan Penis Metastazı: $^{18}$F-PSMA-1007 PET/BT ile Saptanması*

***Hend Komber*[1,4], *Ayah Nawwar*[1,2,3], *Julie Searle*[2,4], *Iain Lyburn*[2,4,5]**

[1]*University Hospitals Bristol and Weston NHS Foundation Trust, Clinic of Radiology, Bristol, UK*
[2]*Cobalt Medical Charity, Cheltenham, UK*
[3]*Cairo University Faculty of Medicine, Department of Clinical Oncology and Nuclear Medicine, Cairo, Egypt*
[4]*Gloucestershire Hospitals NHS Foundation Trust, Clinic of Radiology, Gloucestershire, UK*
[5]*Cranfield Forensic Institute, Cranfield University, Wiltshire, UK*

### Abstract

A 74-year-old man with a history of prostate cancer and rising prostate-specific antigen underwent $^{18}$F-prostate specific membrane antigen (PSMA)-1007 positron emission tomography/computed tomography for investigation of oligometastatic disease. There was evidence of PSMA avid local recurrence findings with pelvic and retroperitoneal nodal metastases and skeletal deposits. Although rare and could easily be mistaken for contamination, a small penile metastasis was found. This is associated with poor prognosis and could impact further management. This case highlights the importance of a detailed review of the penis, to ensure differentiation between urinary activity and pathological uptake.

**Keywords:** $^{18}$F-PSMA-1007 positron emission tomography/computed tomography, prostate cancer, penile metastasis

### Öz

Prostat kanseri öyküsü olan ve prostat spesifik antijen düzeyi yükselen 74 yaşında bir erkek hastaya, oligometastatik hastalık araştırması için $^{18}$F-prostat-spesifik membran antijeni (PSMA)-1007 pozitron emisyon tomografi/bilgisayarlı tomografi uygulandı. PSMA avid lokal nüks, pelvik ve retroperitoneal nodal metastazlar ve kemik metastazları ile uyumlu tutulumlar saptandı. Nadir görülse ve kolayca kontaminasyonla karıştırılabilse de, küçük bir penis metastazı tespit edildi. Bu durum kötü prognozla ilişkilidir ve tedaviyi etkileyebilir. Bu olgu, idrar aktivitesi ile patolojik tutulum arasındaki ayrımı sağlamak için penisin detaylı bir şekilde incelenmesinin önemini vurgulamaktadır.

**Anahtar kelimeler:** $^{18}$F-PSMA-1007 pozitron emisyon tomografi/bilgisayarlı tomografi, prostat kanseri, penis metastazı

**Address for Correspondence:** Hend Komber, University Hospitals Bristol and Weston NHS Foundation Trust, Clinic of Radiology, Bristol, UK
**E-mail:** hend.komber@nhs.net **ORCID ID:** orcid.org/0000-0003-1917-9437
**Received:** 03.07.2024 **Accepted:** 20.01.2025 **Epub:** 01.08.2025 **Publication Date:** 08.10.2025

**Cite this article as:** Komber H, Nawwar A, Searle J, Lyburn I. Penile metastasis from prostate cancer: detection on $^{18}$F-PSMA-1007 PET/CT. Mol Imaging Radionucl Ther. 2025;34:221-223.

Copyright© 2025 The Author. Published by Galenos Publishing House on behalf of the Turkish Society of Nuclear Medicine.
This is an open access article under the Creative Commons Attribution-NonCommercial-NoDerivatives 4.0 (CC BY-NC-ND) International License.

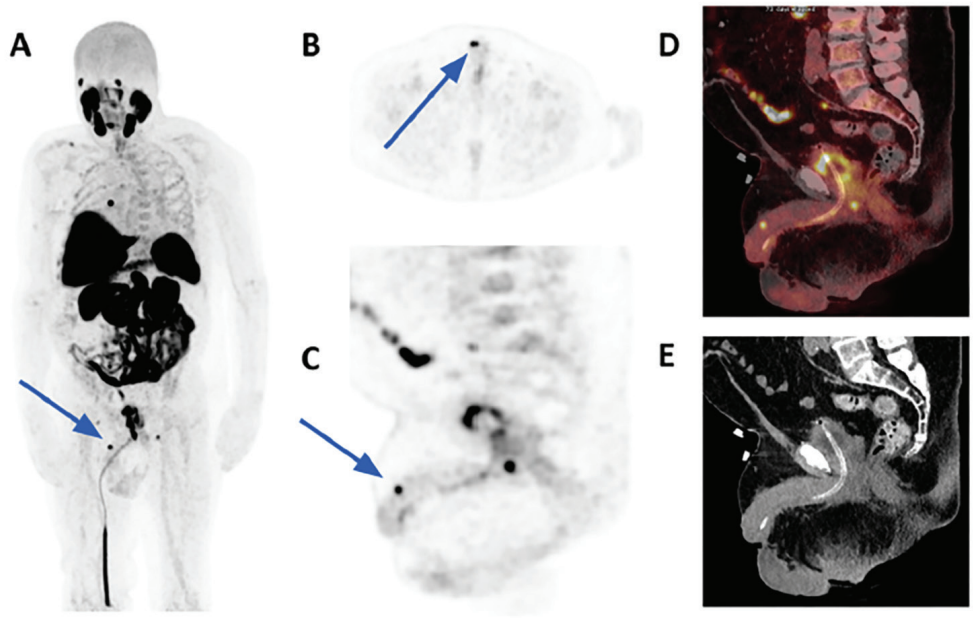



**Figure 1.** A 74-year-old man presents with recurrent prostate cancer and a prostate-specific antigen (PSA) level of 10 ng/mL (A) The left anterior oblique maximal intensity projection of $^{18}$F-fluorodeoxyglucose, positron emission tomography/computed tomography (PET/CT), demonstrates prominent heterogeneous prostatic activity with intense focal activity in the right peripheral zone. A focus of uptake in the distal penile shaft was also seen (arrow). Axial, sagittal $^{18}$F-prostate-specific membrane antigen (PSMA)-1007 PET and sagittal fused PET/CT (B, C and D) demonstrate the subcentimetric focus of tracer uptake in the right side of the penile shaft (arrows), which is not due to urinary contamination. Sagittal low-dose non-contrast CT (E) does not show an appreciable soft tissue lesion. $^{18}$F-PSMA-1007 PET is fast becoming a key imaging modality in the assessment of biochemically recurrent prostate cancer (1), which can occur in up to 27% of patients who are managed by radical prostatectomy, and up to 55% of those managed by radiation therapy (2). A recent meta-analysis found that although the detection rate (DR) of $^{18}$F-PSMA-1007 PET is dependent on serum PSA values, there is a good DR even at low PSA levels (0.5 ng/mL) (1). As expected, local relapse, regional lymph node, distant lymph node, and bone metastases are the most frequent sites of metastases (1), with a significantly higher number of positive findings when compared to conventional CT (3). Penile metastases are rare, usually presenting as part of advanced disease, and indicate poor prognosis, with half of the patients dying within one year of diagnosis (4). The primary malignancies involved are predominantly urological (bladder and prostate cancers), but also, less commonly, gastrointestinal and lung cancers (4). Awareness of the penis as a rare site of metastasis is important to avoid misdiagnosis with other non-malignant conditions (5). Penile metastases can present clinically with malignant priapism and are detectable on PSMA PET/CT (6). Penile metastases from prostate cancer have also been detected on $^{18}$F-choline PET (7,8).

To our knowledge, there has been one case report of a penile metastasis from prostate cancer detected on $^{18}$F-PSMA PET, this was a case of a solitary penile metastasis found on baseline staging in a patient with prostate cancer and PSA>90 ng/mL (9). Our case describes an unexpected example of a $^{18}$F-PSMA avid penile deposit, as part of multifocal recurrence of prostate cancer in a patient with suspected recurrence due to rising PSA. This is associated with extremely poor prognosis, with an average survival of 9 months (10).

## Ethics

**Informed Consent:** The patient has given permission for anonymised imaging and clinical information to be used for teaching, audit, research and publications including social media.

## Footnotes

### Authorship Contributions

Surgical and Medical Practices: A.N., J.S., I.L., Concept: A.N., J.S., I.L., Design: H.K., A.N., J.S., I.L., Data Collection or Processing: H.K., A.N., J.S., I.L., Analysis or Interpretation: H.K., A.N., J.S., I.L., Literature Search: H.K., Writing: H.K., A.N., J.S., I.L.

**Conflict of Interest:** No conflicts of interest were declared by the authors.

**Financial Disclosure:** The authors declare that this study has received no financial support.

## References

1. Ferrari M, Treglia G. $^{18}$F-PSMA-1007 PET in biochemical recurrent prostate cancer: an updated meta-analysis. Contrast Media Mol Imaging. 2021;2021:3502389.
2. Cornford P, van den Bergh RCN, Briers E, Van den Broeck T, Cumberbatch MG, De Santis M, Fanti S, Fossati N, Gandaglia G, Gillessen S, Grivas N, Grummet J, Henry AM, der Kwast THV, Lam TB, Lardas M, Liew M, Mason MD, Moris L, Oprea-Lager DE, der Poel HGV, Rouvière O, Schoots IG, Tilki D, Wiegel T, Willemse PM, Mottet N. EAU-EANM-ESTRO-ESUR-SIOG guidelines on prostate cancer. Part II-2020 update: treatment of relapsing and metastatic prostate cancer. Eur Urol. 2021;79:263-282.

3. Morawitz J, Kirchner J, Lakes J, Bruckmann NM, Mamlins E, Hiester A, Aissa J, Loberg C, Schimmöller L, Arsov C, Antke C, Albers P, Antoch G, Sawicki LM. PSMA PET/CT vs. CT alone in newly diagnosed biochemical recurrence of prostate cancer after radical prostatectomy: comparison of detection rates and therapeutic implications. Eur J Radiol. 2021;136:109556.
4. Zhang K, Da J, Yao HJ, Zheng DC, Cai ZK, Jiang YQ, Xu MX, Wang Z. Metastatic tumors of the penis: a report of 8 cases and review of the literature. Medicine (Baltimore). 2015;94:e132.
5. Dai Y, Shi BL, Zhang J, Liu SN, Jia YT. Penile metastasis from prostate cancer misdiagnosed as Peyronie disease: a case report. Sex Med. 2023;11:qfac011.
6. Kamaleshwaran KK, Balasundararaj BKP, Jose R, Shinto AS. Penile metastasis from prostate cancer presenting as malignant priapism detected using Gallium-68 prostate-specific membrane antigen positron emission tomography/computed tomography. Indian J Nucl Med. 2018;33:57-58.
7. Hodolič M, Fettich J, Cimitan M, Kragelj B, Goldsmith SJ. Unusual F-18 choline uptake in penile metastasis from prostate cancer. Clin Nucl Med. 2012;37:e89-e90.
8. Bianchi D, Rizzo A, Bonacina M, Zaniboni A, Savelli G. penile metastasis from prostate cancer detected by 18f-fluorocholine PET/CT. Clin Nucl Med. 2021;46:e38-e39.
9. Dhull VS, Kshirsagar P, Chowhan M, Patil SC. Solitary penile metastasis from prostate cancer on $^{18}$f-prostate-specific membrane antigen positron emission tomography/computed tomography. Indian J Nucl Med. 2022;37:402-403.
10. Rohan V, Hanji A, Patel J, Goswami J, Tankshali R. Penile metastases from prostate cancer. Urol J. 2009;6:217-219.

*Interesting Image*

*Mol Imaging Radionucl Ther 2025;34:224-227* *DOI:10.4274/mirt.galenos.2025.15870*

# Triple Tumors Uncovered: Insights from $^{68}$Ga PSMA PET-CT

## *Üç Tümörün Ortaya Çıkarılması: $^{68}$Ga PSMA PET-BT'den Elde Edilen Bilgiler*

*Sana Munir Gill[1], Aamna Hassan[1], Waqas Ahmad[2], Islah Ud Din[3]*

[1]*Shaukat Khanum Memorial Cancer Hospital and Research Centre, Clinic of Nuclear Medicine, Lahore, Pakistan*
[2]*The University of British Columbia Faculty of Medicine, Department of Radiology, British Columbia, Canada*
[3]*Shaukat Khanum Memorial Cancer Hospital and Research Centre, Clinic of Radiology, Lahore, Pakistan*

### Abstract

Galium-68 prostate-specific membrane antigen positron emission tomography combined with computed tomography ($^{68}$Ga PSMA PET-CT) is receptor specific imaging, which has increasingly been used in the staging and restaging of prostate carcinoma (PCa). PSMA is type II transmembrane glycoprotein expressed in cytosol of normal prostatic tissue with 100-1000-fold over expression in PCa. It is also expressed in the endothelium of tumor-associated neo vasculature of non-prostatic solid tumor such as transitional cell and renal cell carcinoma, hepatocellular, thyroid, and brain cancers. We hereby present a case where PSMA PET scan showed three tumors proved on follow up imaging.

**Keywords:** $^{68}$Ga PSMA PET-CT, prostate carcinoma, hepatocellular carcinoma, meningioma

### Öz

Galium-68 prostat spesifik membran antijeni pozitron emisyon tomografisi, bilgisayarlı tomografi ($^{68}$Ga PSMA PET-BT), prostat karsinomunun evrelendirilmesinde ve yeniden evrelendirilmesinde giderek daha fazla kullanılan reseptöre özgü bir görüntüleme yöntemidir. PSMA, normal prostat karsinomunda (PCa) sitozolünde eksprese edilen, PCa ise 100-1000 kat fazla eksprese edilen tip II transmembran glikoproteindir. Ayrıca, transizyonel hücreli ve renal hücreli karsinom, hepatoselüler karsinom, tiroid kanseri ve beyin kanseri gibi prostat dışı solid tümörlerin tümörle ilişkili neovasküler endotelinde de eksprese edilir. Burada, PSMA PET taramasının takip görüntülemesinde üç tümör tespit edilen bir olguyu sunuyoruz.

**Anahtar kelimeler:** $^{68}$Ga PSMA PET-BT, prostat karsinomu, hepatosellüler karsinom, menenjiyom

**Address for Correspondence:** Aamna Hassan, Shaukat Khanum Memorial Cancer Hospital and Research Centre, Clinic of Nuclear Medicine, Lahore, Pakistan
**E-mail:** aamnah@skm.org.pk **ORCID ID:** orcid.org/0000-0003-0026-0729
**Received:** 10.12.2024 **Accepted:** 25.02.2025 **Epub:** 12.08.2025 **Publication Date:** 08.10.2025

**Cite this article as:** Gill SM, Hassan A, Ahmad W, Ud Din I. Triple tumors uncovered: insights from $^{68}$Ga PSMA PET-CT. Mol Imaging Radionucl Ther. 2025;34:224-227.

Copyright© 2025 The Author. Published by Galenos Publishing House on behalf of the Turkish Society of Nuclear Medicine.
This is an open access article under the Creative Commons Attribution-NonCommercial-NoDerivatives 4.0 (CC BY-NC-ND) International License.

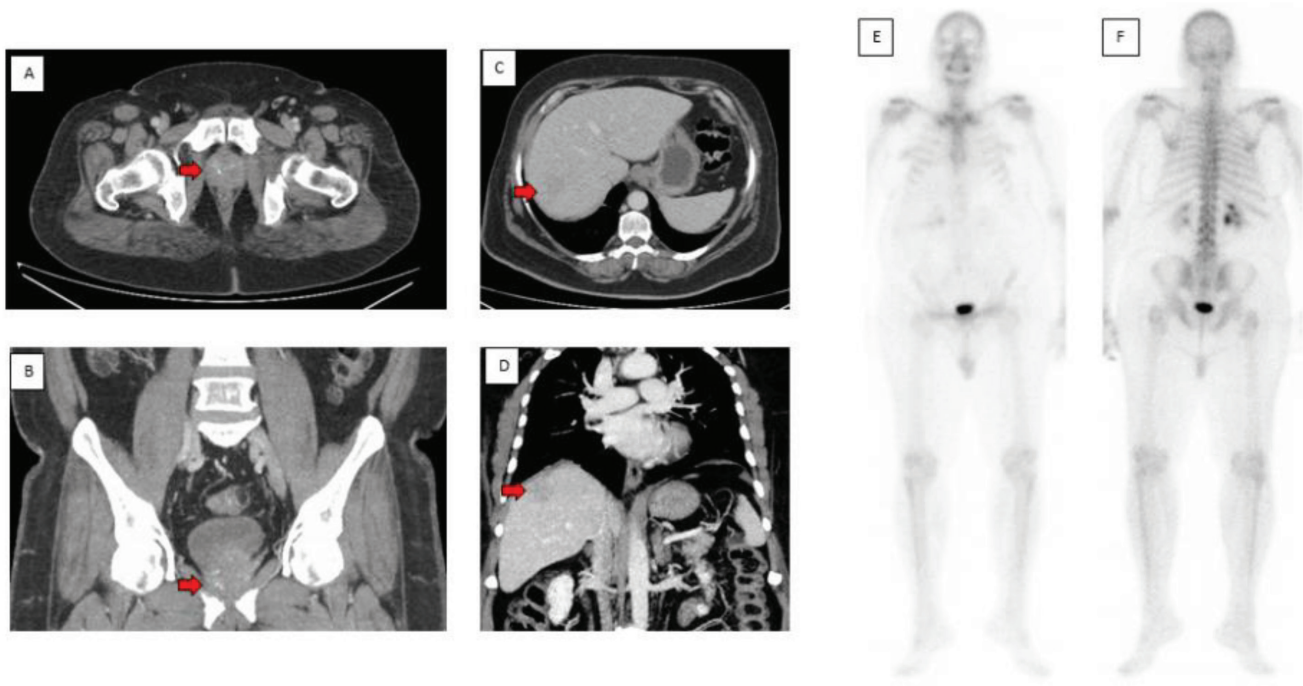



**Figure 1.** A 63-year-old gentleman, known as a diabetic and hypertensive, presented with pain in the right flank. He also had cirrhotic liver against background of hepatitis C virus infection. His ultrasound showed enlarged prostate gland, with prostate-specific antigen of 128 ng/mL and histopathology showed prostatic adenocarcinoma, Gleason score 9/10, and World Health Organization group 5. His computed tomography (CT) chest, abdomen, and pelvis, in addition to the primary prostate carcinoma (PCa) (A, B), showed coarse liver parenchyma with hypodensity in segment VI/VII (C, D); differentials included metastasis or hepatocellular carcinoma. A $^{99}$mTc MDP bone scan was negative for osteoblastic metastasis (E, F). In view of a high Gleason score, the Galium-68 ($^{68}$Ga) prostate-specific membrane antigen (PSMA) positron emission tomography (PET)/CT findings and the tumor board suggested a multiparametric magnetic resonance imaging. $^{68}$Ga PSMA PET/CT, due to its high sensitivity and specificity, is being increasingly used to stage PCa in intermediate - to high- and very high-risk patients when conventional imaging modalities are either negative for distant metastases or show fewer than 5 distant lesions (1,2). PSMA is a type II transmembrane glycoprotein with high expression in PCa and variable expression in neovasculature of some other tumors, such as hepatocellular, lung, thyroid, and renal cell carcinomas (3-5). This allows its potential role in the diagnosis and management of such tumors, which are typically non-avid on $^{18}$F-fluorodeoxyglucose PET/CT ($^{18}$F-FDG) PET/CT which till now is the workhorse in the world of PET/CT (6,7).

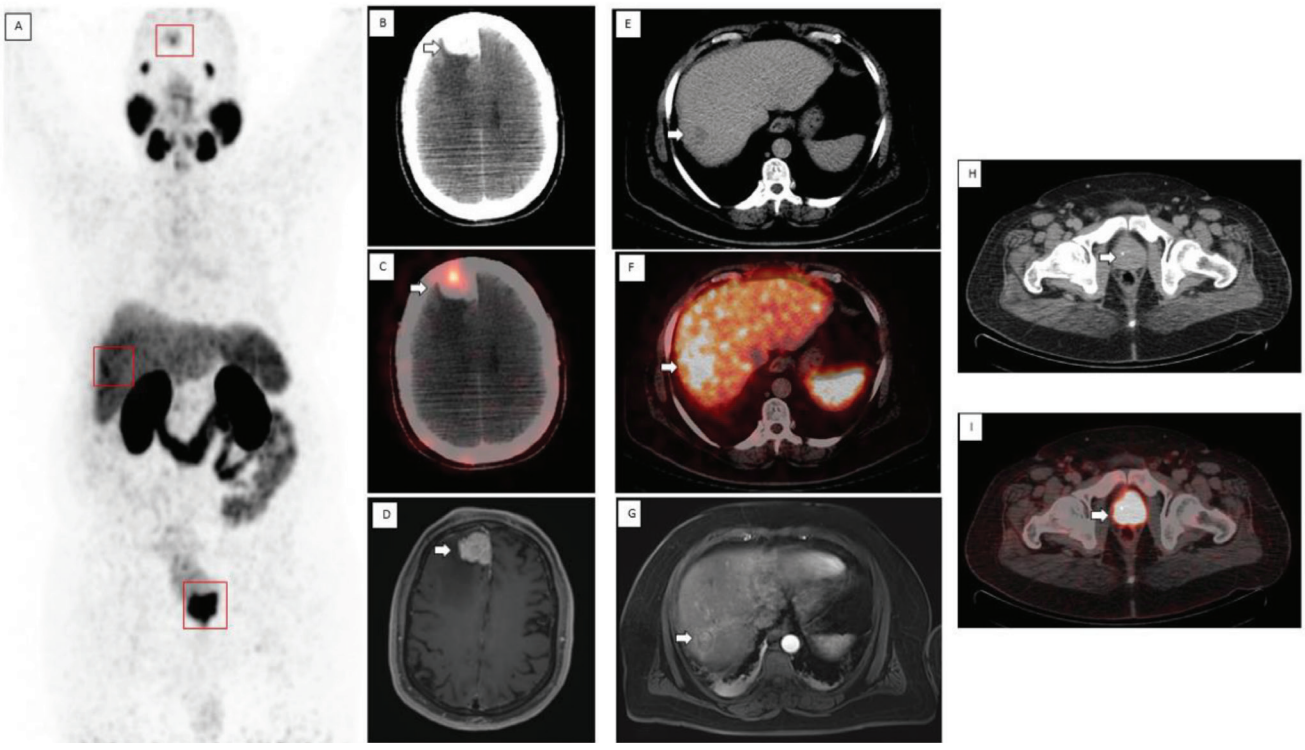



**Figure 2.** Maximum intensity projection image on Galium-68 prostate-specific membrane antigen positron emission tomography combined with computed tomography ($^{68}$Ga PSMA PET/CT) (A) showed avid lesions in the brain, liver and pelvic region (red boxes). There was an enlarged PSMA-avid prostate gland along with an avid enhancing lesion in the right frontal lobe (B, C). His brain magnetic resonance imaging (MRI) with contrast showed an extra-axial mass in the right frontal region adjacent to the falx, suggestive of meningioma (D). In addition, increased PSMA uptake was seen in the known hepatic lesions (E, F). He also had multiparametric MRI with contrast showing pseudocapsular enhancement and early arterial phase enhancement within this lesion, which was highly suggestive of hepatocellular carcinoma (HCC) (G). Also, the primary prostate tumor showed increased PSMA uptake (H-I). Therefore, he was staged as T3N0M0 for prostate cancer and started on androgen deprivation therapy. Hepatobiliary surgeons evaluated his hepatic lesion, which led to resection of segments VI and VII. Histopathology confirmed it to be well-differentiated HCC. After 1.5 years, he received 6000 cGy of radiation in 20 fractions to the prostate gland and seminal vesicles. A few months later, he had stereotactic radiosurgery of 2700 cGy in 3 fractions, to the right frontal lobe meningioma. In our patient, $^{68}$Ga PSMA PET/CT was of paramount importance because it not only helped with the correct initial staging of PCa, but also detected two other tumors, i.e., HCC and meningioma. Therefore, we should be aware of these pitfalls of $^{68}$Ga PSMA PET/CT and be careful in labeling all PSMA avid lesions metastatic because all that glitters is not gold (8).

## Ethics

**Informed Consent:** Exemption of informed consent was sought from the institutional review board (IRB) [Exemption number- EX-29-04-20-04] based on the following points: a) It is a retrospective study, and information in this study is currently in existence in the hospital information system. b) The information is recorded in such a manner that the subjects cannot be identified. c) There would be no contact with the patient.

## Footnotes

### Authorship Contributions

Surgical and Medical Practices: S.M.G., A.H., W.A., I.U.D., Concept: S.M.G., W.A., Design: S.M.G., A.H., Data Collection or Processing: S.M.G., Analysis or Interpretation: S.M.G., A.H., W.A., I.U.D., Literature Search: S.M.G., Writing: S.M.G., A.H., W.A., I.U.D.

**Conflict of Interest:** No conflicts of interest were declared by the authors.

**Financial Disclosure:** The authors declare that this study has received no financial support.

## References

1. Jadvar H, Calais J, Fanti S, Feng F, Greene KL, Gulley JL, Hofman M, Koontz BF, Lin DW, Morris MJ, Rowe SP, Royce TJ, Salami S, Savir-Baruch B, Srinivas S, Hope TA. appropriate use criteria for prostate-specific membrane antigen PET imaging. J Nucl Med. 2022;63:59-68.
2. Jochumsen MR, Bouchelouche K. PSMA PET/CT for primary staging of prostate cancer - an updated overview. Semin Nucl Med. 2024;54:39-45.
3. Kopka K, Benešová M, Bařinka C, Haberkorn U, Babich J. Glu-ureido-based inhibitors of prostate-specific membrane antigen: lessons learned during the development of a novel class of low-molecular-weight theranostic radiotracers. J Nucl Med. 2017;58:17S-26S.
4. Lisney AR, Leitsmann C, Strauß A, Meller B, Bucerius JA, Sahlmann CO. The role of PSMA PET/CT in the primary diagnosis and follow-up of prostate cancer-a practical clinical review. Cancers (Basel). 2022;14:3638.
5. Hangaard L, Jochumsen MR, Vendelbo MH, Bouchelouche K. Metastases from colorectal cancer avid on 68Ga-PSMA PET/CT. Clin Nucl Med. 2017;42:532-533.
6. Tariq A, Pearce A, Rhee H, Kyle S, Raveenthiran S, Pelecanos A, Gan CL, Goh JC, Wong D, McBean R, Marsh P, Goodman S, Dunglison N, Esler R, Navaratnam A, Yaxley JW, Thomas P, Pattison DA, Roberts MJ. The role of prostate-specific membrane antigen positron emission tomography/computed tomography in primary staging of selected renal tumours: initial experience in a multicentre cohort. Eur Urol Focus. 2024;10:770-778.
7. de Galiza Barbosa F, Queiroz MA, Nunes RF, Costa LB, Zaniboni EC, Marin JFG, Cerri GG, Buchpiguel CA. Nonprostatic diseases on PSMA PET imaging: a spectrum of benign and malignant findings. Cancer Imaging. 2020;20:23.
8. Voter AF, Werner RA, Savas H, Gafita A, Ross AE, Gorin MA, Solnes LB, Pomper MG, Rowe SP, Sheikhbahaei S. A practical guide to the pearls and pitfalls of PSMA PET imaging. Semin Nucl Med. 2024;54:119-131.

*Interesting Image*

*Mol Imaging Radionucl Ther 2025;34:228-230* *DOI:10.4274/mirt.galenos.2025.65471*

# The Role of Bone Scintigraphy in Detection of Disseminated Coccidioides Fungemia

## *Dissemine Coccidioidies Fungemisinin Saptanmasında Kemik Sintigrafisinin Rolü*

*Turgut Bora Cengiz,* *Caroline Diane Wilson*

*Atrium Health Wake Forest Baptist Medical Center, Clinic of Nuclear Medicine, Winston-Salem, USA*

**Abstract**

Although extrapulmonary Coccidioides infection is rare, it has been shown to disseminate to the skin and musculoskeletal system, with a strong affinity for bone. We present a case of disseminated Coccidioides infection with bone scintigraphy indicating diffuse fungemia despite equivocal serum assay, leading to appropriate antifungal therapy and a full recovery.

**Keywords:** Mycoses, scintigraphy, Coccidioides

**Öz**

Akciğer dışı Coccidioidies enfeksiyonu nadir görülse de, kemiğe güçlü afinitesi ile deri ve kas-iskelet sistemine yayılabilir. Uygun antifungal tedavi ve tam iyileşme ile sonuçlanan, serum testi belirsiz olmasına rağmen kemik sintigrafisinde dissemine fungemi gösteren ve yaygın Coccidioidies enfeksiyonu olan bir olgu sunulmuştur.

**Anahtar kelimeler:** Mikozlar, sintigrafi, Coccidioides

**Address for Correspondence:** Caroline Diane Wilson, Atrium Health Wake Forest Baptist Medical Center, Clinic of Nuclear Medicine, Winston-Salem, USA
**E-mail:** cdwilson@wakehealth.edu **ORCID ID:** orcid.org/0009-0007-1537-0599

**Received:** 13.01.2025 **Accepted:** 23.03.2025 **Epub:** 01.08.2025 **Publication Date:** 08.10.2025

**Cite this article as:** Cengiz TB, Wilson CD. The role of bone scintigraphy in detection of disseminated coccidioides fungemia. Mol Imaging Radionucl Ther. 2025;34:228-230.

Copyright© 2025 The Author. Published by Galenos Publishing House on behalf of the Turkish Society of Nuclear Medicine.
This is an open access article under the Creative Commons Attribution-NonCommercial-NoDerivatives 4.0 (CC BY-NC-ND) International License.

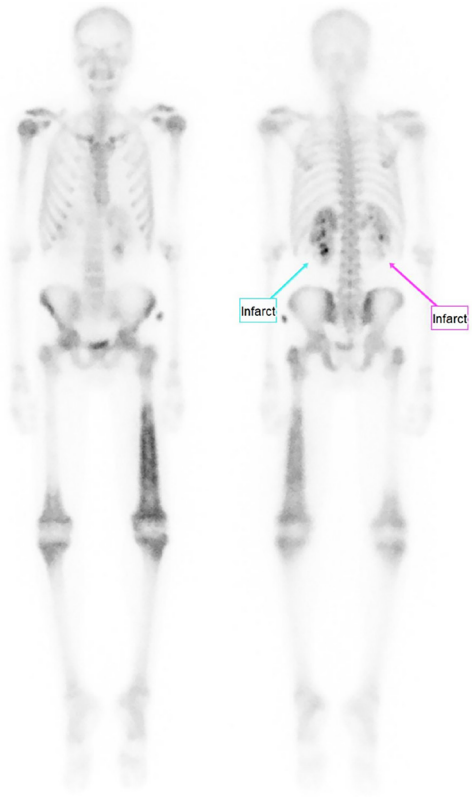



**Figure 1.** A 20-year-old male who had recently emigrated from Venezuela presented to the emergency department with five days of fever, lower abdominal pain, and diarrhea. In triage, he was febrile at 103 degrees, tachycardic at 130 beats per minute, and had scleral icterus. Initial laboratory tests revealed leukocytosis, anemia, thrombocytopenia, elevated bilirubin, and elevated liver enzymes. Initial labs indicated possible *Klebsiella* bacteremia. The patient was started on broad-spectrum antibiotics, but his fever did not resolve.

Infectious disease ordered additional lab work, which revealed positive Coccidioides immunoglobulin G; however, repeat confirmatory testing was negative. Given negative confirmatory tests, a bone scan was ordered for further evaluation; as Coccidioides has high affinity for bone (1,2,3).

Technetium-99m (Tc-99m) methylene diphosphonate (MDP) bone scan showed abnormal radiotracer activity seen in the left femur, bilateral knee joints, distal femurs, proximal tibias, bilateral humeral heads, and bilateral femoral heads. This is concerning for osseous coccidiomycosis with known proclivity for osteoarticular joints (3,4). While osteoarticular Tc-99m MDP uptake is symmetric in the appendicular skeleton, left femoral uptake is very prominent along the left femoral shaft. Bone scintigraphy also showed areas of decreased uptake in bilateral renal cortices, suggestive of infarcts related to septic emboli. Overall, the patient was diagnosed with presumed osseous Coccidioidomycosis after a bone scan. The patient's condition improved after antifungal therapy, leading to a full recovery at the time of discharge.

Although bone scintigraphy is not commonly used to detect fungemia, it can serve as an adjunct imaging modality in cases of equivocal serum assay, as certain species (i.e., Coccidioides) can cause osteoarticular Tc-99m MDP uptake (5). This case depicts the role of bone scintigraphy in disseminated fungemia, especially for the Coccidioides species, and can aid in diagnosis when there is an equivocal serum antibody assay.

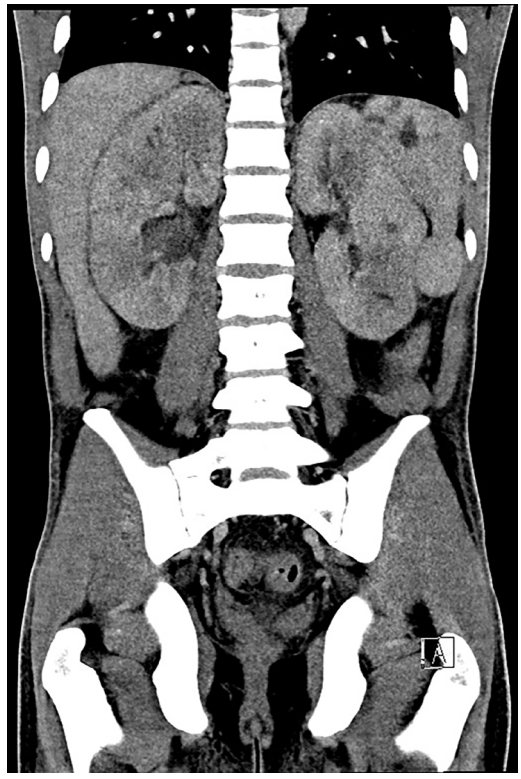


**Figure 2.** (A) A contrast enhanced computed tomography abdomen was ordered revealing wedge-shaped regions of hypoattenuation in the spleen and kidneys matching the pattern seen on bone scintigraphy, confirming renal changes seen on bone scintigraphy and indicating septic emboli.

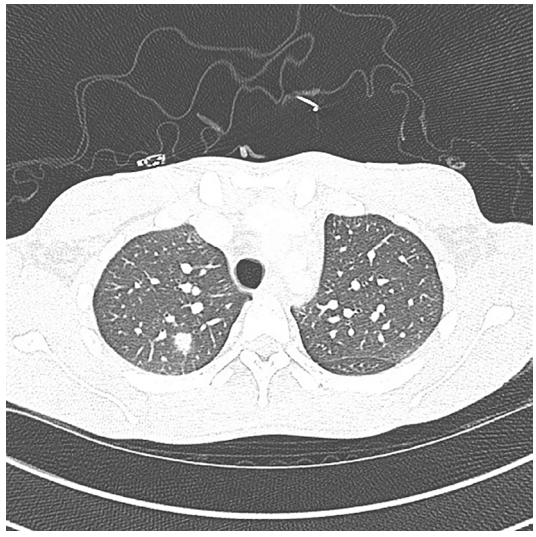


**Figure 3.** A chest computed tomography (CT) was also obtained, which showed scattered pulmonary nodules with surrounding ground glass halos, suggestive of fungal infection.

Given bone scintigraphy and CT scan findings of diffuse fungal infection, the patient was started on itraconazole, which was later switched to fluconazole due to cost.

### Ethics

**Informed Consent:** Our institutional IRB protocol doesn't require documentation of consent for case studies which don't involve protected health data/patient identifiers.

### Footnotes

### Authorship Contributions

Concept: T.B.C., Design: T.B.C., C.W., Data Collection or Processing: T.B.C., C.W., Analysis or Interpretation: T.B.C., C.W., Literature Search: T.B.C., C.W., Writing: T.B.C., C.W.

**Conflict of Interest:** No conflicts of interest were declared by the authors.

**Financial Disclosure:** The authors declare that this study has received no financial support

## References

1. Tsantes AG, Koutserimpas C, Naoum S, Drosopoulou LP, Papadogeorgou E, Petrakis V, Alpantaki K, Samonis G, Veizi E, Papadopoulos DV. Diagnosis, treatment, and outcome of coccidioidal osseous infections: a systematic review. J Fungi (Basel). 2024;10:270.
2. Belthur MV, Blair JE, Shrader MW, Malone JB. Musculoskeletal coccidioidomycosis. Current Orthopaedic Practice. 2018;29:400-406.
3. Deresinski SC. Coccidioidomycosis of bone and joints. Springer eBooks. Published online 1980:195-211.
4. Li YC, Calvert G, Hanrahan CJ, Jones KB, Randall RL. Coccidiomycosis infection of the patella mimicking a neoplasm - two case reports. BMC Med Imaging. 2014;14:8.
5. Moni BM, Wise BL, Loots GG, Weilhammer DR. Coccidioidomycosis osteoarticular dissemination. J Fungi (Basel). 2023;9:1002.

*Interesting Image*

*Mol Imaging Radionucl Ther 2025;34:231-233* *DOI:10.4274/mirt.galenos.2025.15986*

# Extensive Malignant Thrombus Revealed by $^{18}$F-FDG PET/CT in Patient with Papillary Thyroid Cancer

## *Papiller Tiroid Karsinomlu Hastada $^{18}$F-FDG PET/BT ile Saptanan Yaygın Malign Trombüs*

*Merve Nida Calderon Tobar, Lütfü Perktaş, Hasan Önner, Gonca Kara Gedik*

*Selçuk University Faculty of Medicine, Department of Nuclear Medicine, Konya, Türkiye*

**Abstract**

A 59-year-old man admitted to the hospital complained of left arm and neck pain. Magnetic resonance imaging was performed for possible cervical discopathy. It revealed that in the C7 vertebral body, lesions with surrounding bone marrow edema were observed, which were compatible with metastasis that caused cervical stenosis. Cervical stenosis surgery was performed, and the lesion was pathologically diagnosed as a metastasis of thyroid carcinoma. $^{18}$F-fluorodeoxyglucose positron emission tomography/computed tomography ($^{18}$F-FDG PET/CT) scan was ordered for further evaluation. The PET/CT images showed an increased $^{18}$F-FDG uptake from the left internal jugular vein to the right atrium. It was considered a malignant thrombus.

**Keywords:** Malignant thrombus, $^{18}$F-FDG PET/CT, papillary thyroid cancer

**Öz**

Elli dokuz yaşındaki erkek hasta hastanemize, sol kol ve boyun ağrısı şikayetiyle başvurdu. Hastaya servikal diskopati ön tanısı ile manyetik rezonans görüntüleme yapıldı. C7 vertebra korpusunda servikal stenoza neden olan metastaz ile uyumlu, çevresinde kemik iliği ödemi bulunan kitle saptandı. Hasta servikal stenoz nedeniyle opere edildi. Patolojik incelemede tiroid karsinomu metastazı tanısı konuldu. Daha ileri değerlendirme için ile $^{18}$F-florodeoksiglukoz pozitron emisyon tomografisi/bilgisayarlı tomografi ($^{18}$F-FDG PET/BT) taraması istendi. PET/BT görüntülemede sol internal juguler venden sağ atriyuma doğru uzanan $^{18}$F-FDG tutulumu, yaygın malign trombüs olarak değerlendirildi.

**Anahtar kelimeler:** Malign trombüs, $^{18}$F-FDG PET/CT, papiller tiroid kanseri

**Address for Correspondence:** Hasan Önner, Selçuk University Faculty of Medicine, Department of Nuclear Medicine, Konya, Türkiye
**E-mail:** hasanonner_1988@hotmail.com **ORCID ID:** orcid.org/0000-0003-1002-2097
**Received:** 02.02.2024 **Accepted:** 18.04.2025 **Epub:** 01.08.2025 **Publication Date:** 08.10.2025

**Cite this article as:** Calderon Tobar MN, Perktaş L, Önner H, Kara Gedik G. Extensive malignant thrombus revealed by $^{18}$F-FDG PET/CT in patient with papillary thyroid cancer. Mol Imaging Radionucl Ther. 2025;34:231-233.

Copyright© 2025 The Author. Published by Galenos Publishing House on behalf of the Turkish Society of Nuclear Medicine.
This is an open access article under the Creative Commons Attribution-NonCommercial-NoDerivatives 4.0 (CC BY-NC-ND) International License.

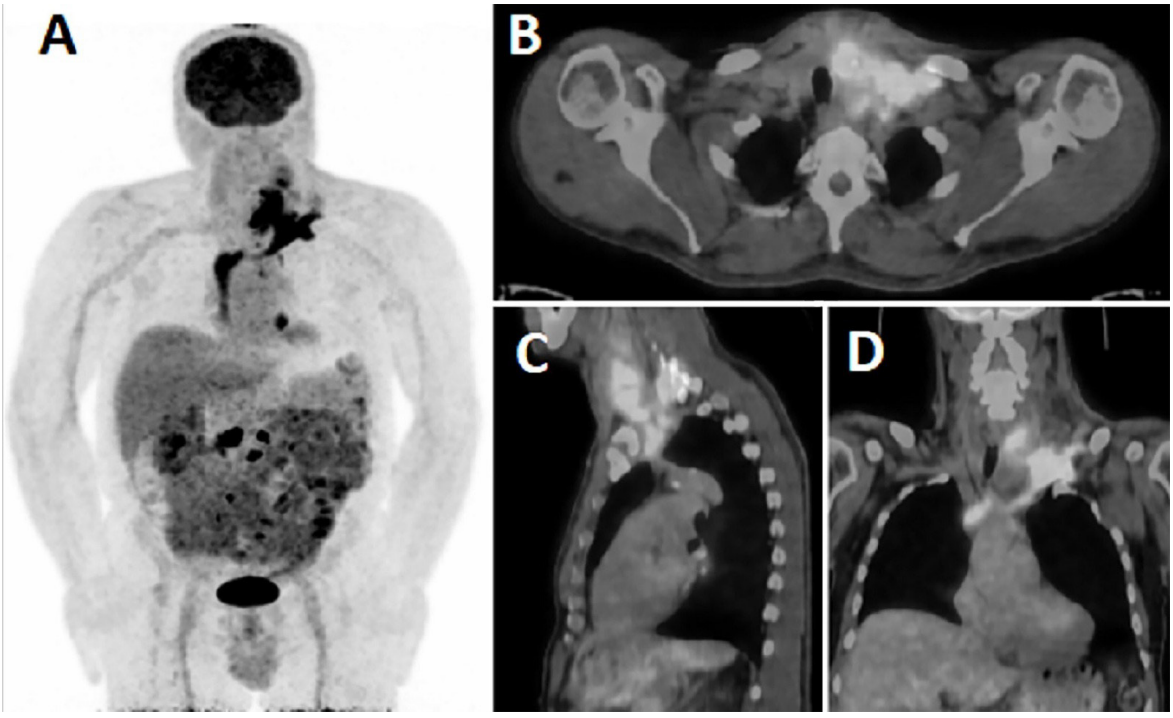



**Figure 1.** A 59-year-old man, who has been operated on for cervical stenosis at the C7 vertebral level, had a lesion that was pathologically positive for CK7, thyroglobulin, and thyroid transcription factor-1, and was diagnosed with thyroid carcinoma metastasis. Ultrasonography revealed a 44x40 mm-sized nodular lesion with irregular borders, that was filling the left lobe of the thyroid. A tru-cut biopsy confirmed the papillary thyroid carcinoma. In this context, $^{18}$F-fluorodeoxyglucose positron emission tomography/computed tomography ($^{18}$F-FDG PET/CT) scan was ordered for further evaluation. Maximum intensity projection (A), transaxial (B), sagittal (C) and, coronal (D) fused PET/CT images showed intense $^{18}$F-FDG uptake in the left internal jugular vein extending to the right atrium ($SUV_{max}$ 12,21) considered as a malignant thrombus. Also, hypermetabolic nodular lesions in the left lobe of the thyroid gland and left hilar, paraaortic, paranasal, and parailiac lymphadenopathies, were observed.

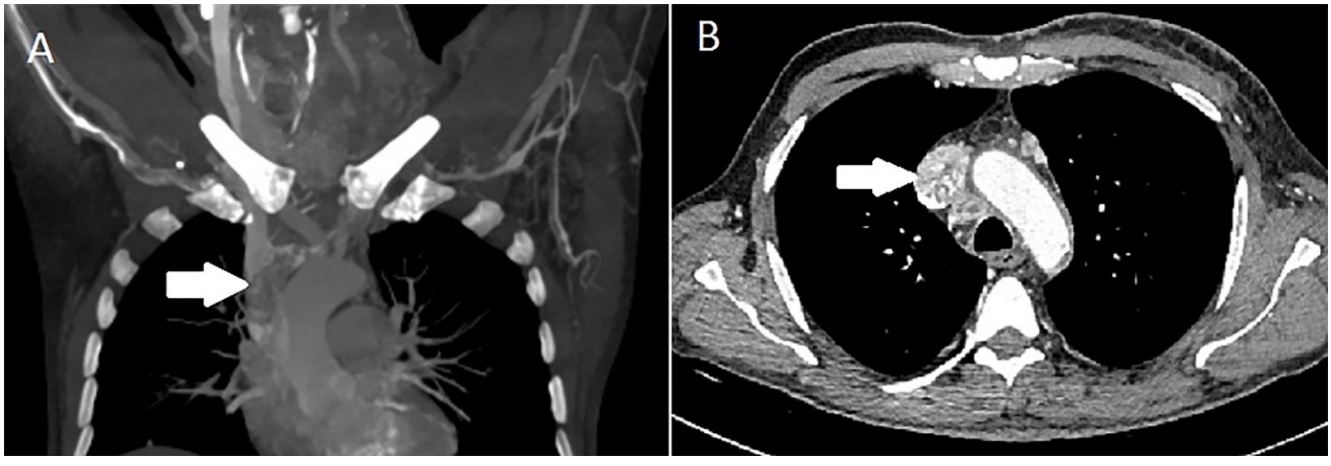



**Figure 2.** Dynamic contrast-enhanced computed tomography showed a massive malignant thrombus in the dilated left internal jugular vein (A) and extending to the right atrium (B). The intense fluoro-D-glucose uptake is considered to be a malignant thrombus in correspondence with these observations. The presence of intravascular tumor thrombus in a vessel is a significant factor that influences the stage, prognosis, and treatment and is commonly observed in a range of malignancies, including renal cell carcinoma, Wilms tumor, adrenal cortical carcinoma, and hepatocellular carcinoma. Thyroid carcinoma with major vascular malignant thrombosis is rare (1). Although regional cervical lymphatic metastasis is expected in papillary thyroid carcinoma patients, the incidence of hematogenous metastasis in these patients is relatively low (2). In this case, there was a notably widespread malignant thrombosis. There have been several reports on malignant thrombosis in major veins in follicular thyroid carcinoma (3,4). Papillary thyroid carcinoma (5) and anaplastic carcinoma (6).

### Ethics

**Informed Consent:** The patient provided written informed consent for the publication of his images.

### Footnotes

### Authorship Contributions

Surgical and Medical Practices: M.N.C.T, L.P, H.Ö, G.K.G, Concept: M.N.C.T, L.P, H.Ö, G.K.G, Design: M.N.C.T, L.P, H.Ö, G.K.G, Data Collection or Processing: M.N.C.T, L.P, H.Ö, G.K.G, Analysis or Interpretation: M.N.C.T, L.P, H.Ö, G.K.G, Literature Search: M.N.C.T, L.P, H.Ö, G.K.G, Writing: M.N.C.T, L.P, H.Ö, G.K.G.

**Conflict of Interest:** No conflicts of interest were declared by the authors.

**Financial Disclosure:** The authors declare that this study has received no financial support.

## References

1. Fotis T, Konstantinou E, Mariolis-Sapsakos T, Mitsos A, Restos S, Katsenis K, Elefsiniotis I, Kapellakis G. Solitary internal jugular vein invasion by thyroid carcinoma: resection and reconstruction. J Vasc Nurs. 2009;27:46-47.
2. Leong JL, Yuen HW, LiVolsi VA, Loevner L, Narula N, Baloch Z, Weber RS. Insular carcinoma of the thyroid with jugular vein invasion. Head Neck. 2004;26:642-646.
3. Taib NA, Hisham AN. Follicular thyroid carcinoma with direct tumour extension into the great cervical veins and right atrium: is transcervical thrombectomy a safe option? Asian J Surg. 2007;30:216-219.
4. Varghese BT, Sebastian P. Internal jugular vein thrombus associated with thyroid carcinoma. Ann Otol Rhinol Laryngol. 2005;114:656.
5. Koike E, Yamashita H, Watanabe S, Yamashita H, Noguchi S. Brachiocephalic vein thrombus of papillary thyroid cancer: report of a case. Surg Today. 2002;32:59-62.
6. Strobel K, Steinert HC, Bhure U, Koma AY, Gassmann N, Stöckli SJ. Tumour thrombus in the superior vena cava from anaplastic carcinoma of the thyroid: FDG-PET/CT imaging findings. Eur J Nucl Med Mol Imaging. 2007;34:813.

*Interesting Image*

*Mol Imaging Radionucl Ther 2025;34:234-238* *DOI:10.4274/mirt.galenos.2025.26937*

# Analysis of Imaging Findings in a Patient with Squamous Cell Carcinoma of the External Auditory Canal Metastatic to the Dura with Trigeminal Nerve Involvement

## *Trigeminal Sinir Tutulumuyla Birlikte Duraya Metastatik Dış Kulak Yolu Skuamöz Hücreli Karsinomu Olan Bir Hastada Görüntüleme Bulgularının Analizi*

**Güler Silov[1], İsmet Miraç Çakır[2], Hande Arslan[3], Asuman Çelik[4], Aslı Ayan[5]**

[1]*Samsun University Faculty of Medicine, Department of Nuclear Medicine, Samsun, Türkiye*
[2]*Samsun University Faculty of Medicine, Department of Radiology, Samsun, Türkiye*
[3]*University of Health Sciences Türkiye, Samsun Training and Research Hospital, Clinic of Otorhinolaryngology, Samsun, Türkiye*
[4]*University of Health Sciences Türkiye, Samsun Training and Research Hospital, Clinic of Pathology, Samsun, Türkiye*
[5]*University of Health Sciences Türkiye, Gülhane Training and Research Hospital, Clinic of Nuclear Medicine, Ankara, Türkiye*

### Abstract

We report the case of a 56-year-old female recently diagnosed with well-differentiated squamous cell carcinoma of the external auditory canal. The patient underwent an $^{18}$F-fluorodeoxyglucose positron emission tomography/computed tomography for staging assessment. This examination revealed intense uptake in the right ear canals, tympanic cavity, eustachian canal, parapharyngeal area, and infratemporal fossa. Notably, we identified intracranial dural metastasis, which represents an uncommon site for metastatic spread in general.

**Keywords:** Squamous cell carcinoma of external auditory canal, dural metastasis, $^{18}$F-fluorodeoxyglucose positron emission tomography/computed tomography

### Öz

Bu yazıda, yakın zamanda dış kulak yolunda iyi diferansiye skuamöz hücreli karsinom tanısı alan 56 yaşında bir kadın hasta sunuldu. Hastaya evreleme değerlendirmesi için $^{18}$F -fluorodeoksiglukoz pozitron emisyon tomografisi/bilgisayarlı tomografi çekildi. Bu incelemede sağ kulak kanallarında, timpanik kavitede, östaki kanalında, parafarengeal alanda ve infratemporal fossada yoğun tutulum saptandı. Özellikle, genel olarak metastatik yayılım için nadir bir bölgeyi temsil eden intrakraniyal dural metastaz tespit ettik.

**Anahtar kelimeler:** Dış kulak yolunun skuamöz hücreli karsinomu, dural metastaz, $^{18}$F-florodeoksiglukoz pozitron emisyon tomografi/bilgisayarlı tomografi

**Address for Correspondence:** Güler Silov, Samsun University Faculty of Medicine, Department of Nuclear Medicine, Samsun, Türkiye
**E-mail:** gulersilov@yahoo.com **ORCID ID:** orcid.org/0000-0002-4658-8634
**Received:** 29.11.2024 **Accepted:** 29.04.2025 **Epub:** 01.08.2025 **Publication Date:** 08.10.2025

**Cite this article as:** Silov G, Çakır İM, Arslan H, Çelik A, Ayan A. Analysis of imaging findings in a patient with squamous cell carcinoma of the external auditory canal metastatic to the dura with trigeminal nerve ınvolvement. Mol Imaging Radionucl Ther. 2025;34:234-238.

Copyright© 2025 The Author. Published by Galenos Publishing House on behalf of the Turkish Society of Nuclear Medicine.
This is an open access article under the Creative Commons Attribution-NonCommercial-NoDerivatives 4.0 (CC BY-NC-ND) International License.

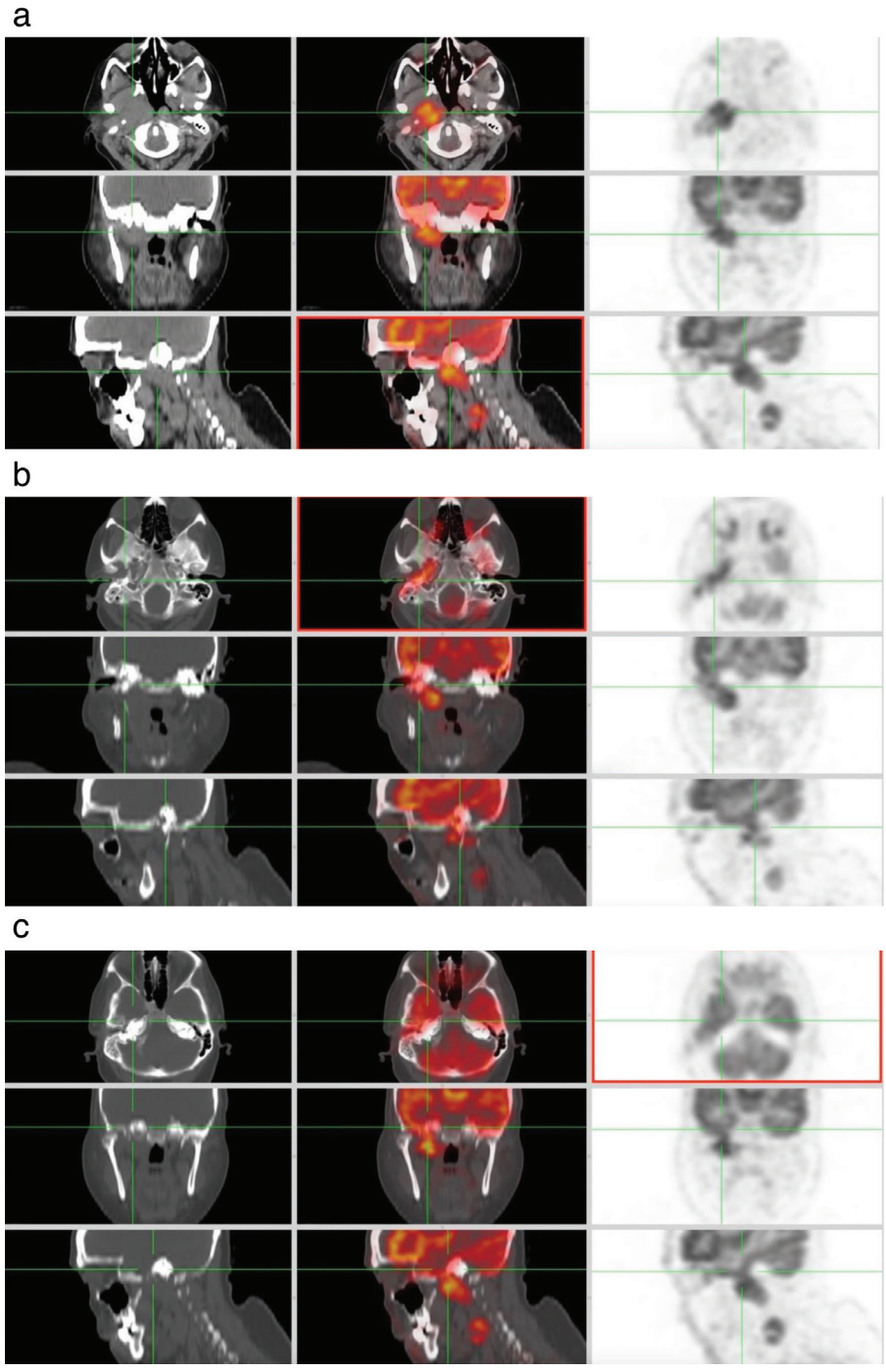



**Figure 1.** In a 56-year-old female patient diagnosed with well-differentiated squamous cell carcinoma of the external auditory canal, initial $^{18}$F-fluorodeoxyglucose positron emission tomography/computed tomography ($^{18}$F-FDG PET/CT) images revealed a hypermetabolic mass standard uptake value maximum ($SUV_{max}$: 10.4, 40x30 mm in size) on the right side extending into the right parapharyngeal and masticator spaces and ipsilateral infratemporal fossa (Figure 1a). Increased $^{18}$F-FDG uptake was also observed extending linearly in the right tympanic cavity, ear canals ($SUV_{max}$: 8.0) and mastoid bone ($SUV_{max}$: 5.7) (Figure 1b). While intense physiological uptake by the brain presents a limitation in the evaluation of skull base lesions, skull base invasion of the tumor was clearly visible in the posteroinferior part of the temporal lobe in this case ($SUV_{max}$: 7.5, contralateral temporal lobe $SUV_{max}$: 5.7). Involvement of the right V3 nerve through the foramen ovale in Meckel's cavity and intracranial spread were observed (Figure 1c). There was increased $^{18}$F-FDG uptake in a right cervical level 2, central hypometabolic peripheral hypermetabolic metastatic lymph node, 28x18 mm in size.

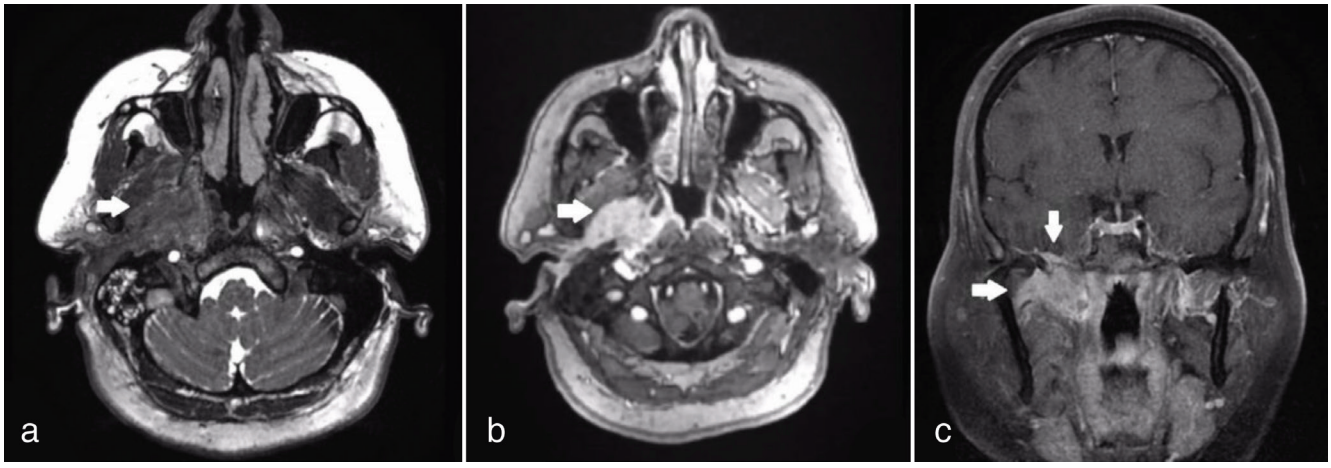



**Figure 2.** Magnetic resonance imaging examination revealed a 39x28 mm lesion, in the right parapharyngeal and masticator area, extending posterolaterally to the carotid sheath and posteriorly to the retropharyngeal area. The lesion appeared hypointense on T2-weighted images (Figure 2a) and exhibited dense heterogeneous contrast enhancement on post-contrast series (Figure 2b). The lesion involved the right pterygoid and masseter muscles, with intracranial extension via the right ınfratemporal fossa. Coronal T1-weighted contrast-enhanced imaging demonstrated skull base invasion through the foramen ovale, resulting in 6.5 mm dural thickening in the posteroinferior aspect of the temporal lobe (Figure 2c). Additionally, the lesion in the right tympanic cavity and external auditory canal (EAC) extended to the nasopharynx via the Eustachian tube, with intense T2 signal increases observed in these areas. Endoscopic nasopharyngeal examination revealed slight fullness in the right rosenmüller fossa. Otoscopic examination demonstrated diffuse maceration and bony erosion in the right EAC, as well as a thickened tympanic membrane. Punch biopsies were obtained from both the nasopharynx and the right EAC.

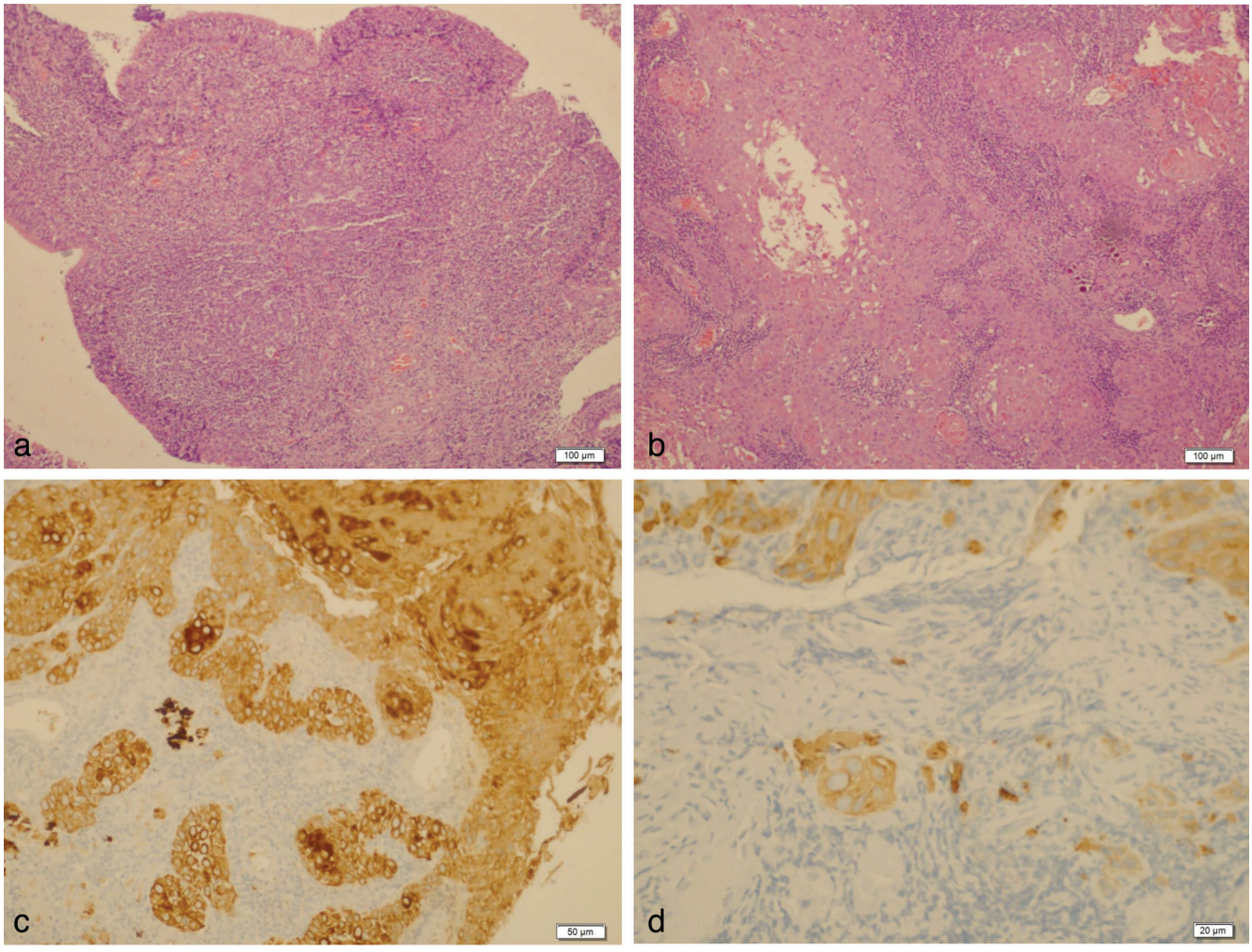



**Figure 3.** Lymphoid hyperplasia, focal squamous metaplasia/reactive cellular changes in the epithelium of the nasopharynx [Figure 3a,10x10 hematoxylin and eosin (HE)] and well-differentiated squamous cell carcinoma of the external auditory canal (EAC-SCC) were diagnosed (Figure 3b, 10x10 HE). Atypical squamous epithelial cells invading the subepithelial stroma of the EAC [(Figure 3c, 20x10 PanK immunohistochemistry (IHC)], (Figure 3d, 40x10 CK5/6 IHC). The patient was classified as T4N1M0 stage, and the tumor was deemed unresectable. Consequently, chemoradiotherapy was administered based on the decision of the multidisciplinary tumor board. Although primary malignant tumors of the EAC are rare (1), T4 stage EAC-SCC exhibits a poor prognosis, with reported two-year survival rates for T4 stage EAC-SCC ranging from 0% to 7% (2). Due to the continuity of the infratemporal fossa with the inferior parapharyngeal space, larger neoplasms can readily extend through the fat in the parapharyngeal space (3). Perineural spread may occur through the foramina and fissures (4). Cross-sectional imaging modalities such as $^{18}$F-FDG PET/CT and MRI play a crucial role in the accurate staging of EAC-SCC.

### Ethics

**Informed Consent:** A consent form allowing the publication of imaging findings and images has been signed by the patient.

### Footnotes

### Authorship Contributions

Surgical and Medical Practices: G.S., İ.M.Ç., H.A., A.Ç., Concept: G.S., Design: G.S., Data Collection or Processing: G.S., İ.M.Ç., H.A., A.Ç., Analysis or Interpretation: G.S., İ.M.Ç., H.A., A.Ç., Literature Search: G.S., İ.M.Ç., H.A., Writing: G.S., İ.M.Ç., H.A., A.Ç., A.A.

**Conflict of Interest:** No conflicts of interest were declared by the authors.

**Financial Disclosure:** The authors declare that this study has received no financial support.

## References

1. Ouaz K, Robier A, Lescanne E, Bobillier C, Morinière S, Bakhos D. Cancer of the external auditory canal. Eur Ann Otorhinolaryngol Head Neck Dis. 2013;130:175-182.
2. Moody SA, Hirsch BE, Myers EN. Squamous cell carcinoma of the external auditory canal: an evaluation of a staging system. Am J Otol. 2000;21:582-588.
3. Sah A, S TG, H CS. Imaging of the ınfratemporal fossa: a comprehensive pictorial essay. Indian J Surg Oncol. 2022;13:868-875.
4. Raut AA, Naphade PS, Chawla A. Imaging of skull base: pictorial essay. Indian J Radiol Imaging. 2012;22:305-316.

*Interesting Image*

*Mol Imaging Radionucl Ther 2025;34:239-241* *DOI:10.4274/mirt.galenos.2025.75875*

# Unveiling the Diagnostic Mystery: $^{18}$F-FDG PET and Bone Scan Negative in Bone Metastases of Lobular Breast Cancer: A Case Report

## *Tanısal Gizemin Çözülmesi: Lobüler Meme Kanseri Kemik Metastazlarında $^{18}$F-FDG PET ve Kemik Taraması Negatif: Bir Olgu Sunumu*

***Sharjeel Usmani[1], Khulood Al Riyami[1], Anjali Jain[1], Asiya Al Busaidi[1], Paul Dumasig[1], Vipin V Jayakrishnan[1], Subhash Kheruka[1], Najeeb Ahmed[2]***

*[1]Sultan Qaboos Comprehensive Cancer Care and Research Centre, Clinic of Radiology and Nuclear Medicine, Maskat, Oman*
*[2]Hull York Medical School, Faculty of Medicine; Castle Hill Hospital, Department of Radiology, Hill, Cottingham, UK*

### Abstract

Identifying osseous metastases by imaging is essential and may be challenging in patients with lobular breast cancer. We present a case of a 66-year-old woman with lobular breast cancer who underwent $^{18}$F- fluorodeoxyglucose positron emission tomography/computed tomography (FDG PET/CT) for staging purposes. $^{18}$F-FDG PET/CT reveals minimal FDG uptake in the primary tumor cells. Prominent sclerotic lesions with low FDG avidity are seen in the spinal and pelvic bones. The subsequent Tc-99m methylene diphosphonate bone scan is unremarkable. The magnetic resonance imaging (MRI) reveals bone metastases. MRI may be beneficial in invasive lobular carcinoma. MRI facilitates improved metastatic evaluation, especially in bone-only and bone-predominant metastatic malignancies, when assessment with $^{18}$F-FDG PET/CT may be difficult and constrained.

**Keywords:** Lobular breast cancer, $^{18}$F-FDG PET/CT, osseous metastases, MRI

### Öz

Lobüler meme kanserli hastalarda kemik metastazlarının görüntüleme ile tespiti önemlidir ve tanısal anlamda zorlayıcı olabilir. Evreleme amacıyla $^{18}$F-fluorodeoksiglukoz pozitron emisyon tomografisi/bilgisayarlı tomografi (FDG PET/BT) taraması yapılan 66 yaşında lobüler meme kanserli bir kadın olguyu sunuyoruz. $^{18}$F-FDG PET/BT, primer tümör hücrelerinde minimal FDG tutulumu göstermiştir. Spinal ve pelvik kemiklerde FDG içermeyen belirgin sklerotik lezyonlar görülmüştür. Ardından yapılan Tc-99m metilen difosfonat kemik taraması normal saptanmıştır. Manyetik rezonans görüntüleme (MRG), çoklu kemik metastazlarını ortaya koymaktadır. MRG, invaziv lobüler karsinomda potansiyel olarak faydalı olabilir. MRG, özellikle sadece kemik ve kemik ağırlıklı metastatik malignitelerde, $^{18}$F-FDG PET/BT ile değerlendirmenin zor ve kısıtlı olabileceği durumlarda, metastazların daha iyi değerlendirilmesine yardımcı olur.

**Anahtar kelimeler:** Lobüler meme kanseri, $^{18}$F-FDG PET/BT, kemik metastazları, MRG

**Address for Correspondence:** Sharjeel Usmani, Sultan Qaboos Comprehensive Cancer Care and Research Centre, Clinic of Radiology and Nuclear Medicine, Maskat, Oman
**E-mail:** dr_shajji@yahoo.com **ORCID ID:** orcid.org/0000-0001-9274-7571
**Received:** 31.10.2024 **Accepted:** 29.04.2025 **Epub:** 01.08.2025 **Publication Date:** 08.10.2025

**Cite this article as:** Usmani S, Al Riyami K, Jain A, Al Busaidi A, Dumasig P, Jayakrishnan VV, Kheruka S, Ahmed N. Unveiling the diagnostic mystery: $^{18}$F-FDG PET and bone scan negative in bone metastases of lobular breast cancer: a case report. Mol Imaging Radionucl Ther. 2025;34:239-241.

Copyright© 2025 The Author. Published by Galenos Publishing House on behalf of the Turkish Society of Nuclear Medicine.
This is an open access article under the Creative Commons Attribution-NonCommercial-NoDerivatives 4.0 (CC BY-NC-ND) International License.

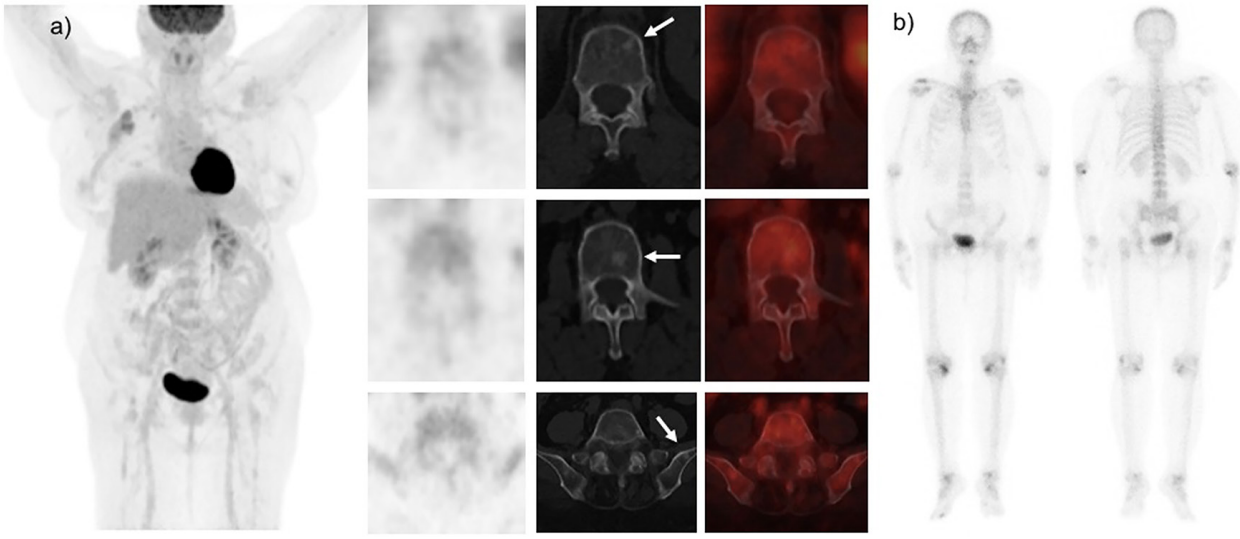



**Figure 1.** A 66-year-old female has a documented diagnosis of locally advanced grade 2 right lobular breast cancer, which is estrogen receptor-positive; progesterone receptor-positive; and human epidermal growth factor receptor 2-negative. [18]F-fluorodeoxyglucose positron emission tomography/computed tomography (FDG PET/CT) performed for preliminary staging. (a) Mild FDG uptake is seen in the primary tumor of the right breast. Diffuse heterogeneous [18]F-FDG uptake is seen in the skeleton, matching CT reveals ill-defined sclerotic lesions, most noticeable at the body of T12, L2 vertebrae, and bilateral iliac bones (white arrow) with no significant [18]F-FDG avidity. (b) The whole body Tc-99m methylene diphosphonate bone scan is unremarkable.

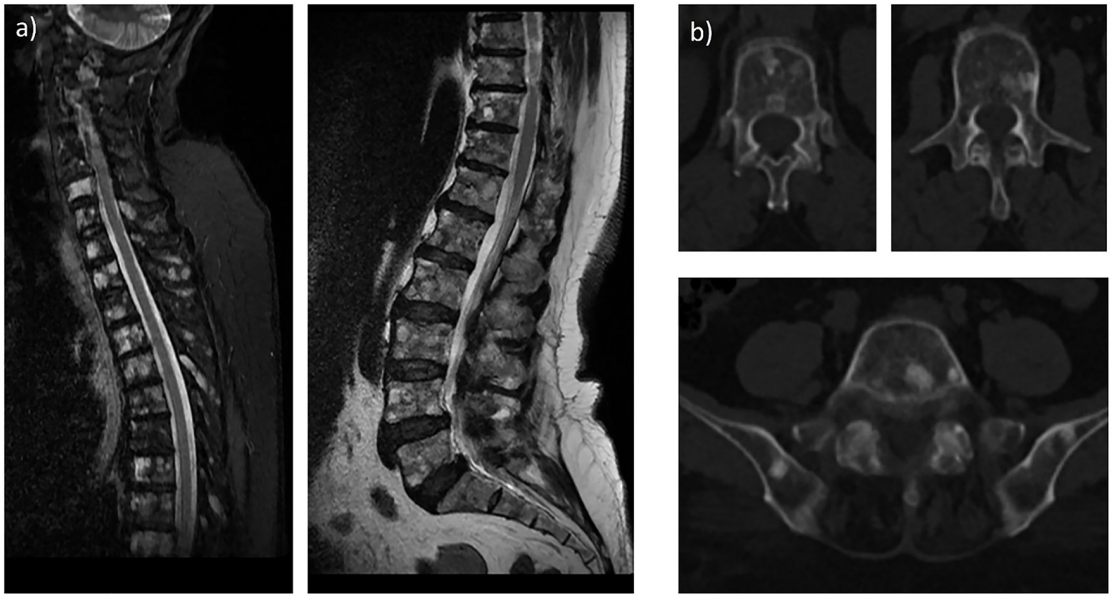



**Figure 2.** (a) The contrast-enhanced T2 images of magnetic resonance imaging (MRI) showed abnormal bone marrow signals across almost the entire spine, ribs, shoulder blades, hips, and pelvis, suggestive of widely spread bone metastases. (b) Follow-up computed tomography (CT) imaging demonstrates that several bony lesions have become denser (increased sclerosis), suggesting the healing response. Invasive lobular carcinoma (ILC) accounts for a notable portion of invasive breast carcinomas, developing insidiously in roughly 10-15% of cases.

[18]F-fluorodeoxyglucose positron emission tomography/CT(FDG PET) plays a meaningful role in the staging and restaging of breast cancer. However, its sensitivity and detection rates are lower in lobular carcinoma, attributable to the lessened FDG-avidity of malignant cells (1). ILC demonstrates lower maximum standardized uptake values standardized uptake value than invasive ductal carcinoma (IDC) on account of multiple mechanisms, such as lower tumor cell density, reduced proliferation rates, diffuse infiltration into encompassing tissues, and diminished GLUT-1 expression (2).

In women with breast cancer, bone is the principal site of distant metastasis. It is also the primary site of metastasis in 50% of patients (3). Individuals

diagnosed with lobular breast cancer display a greater tendency for bone metastases compared to those with ductal malignancies and more often appear sclerotic on CT scans than those with IDC. $^{18}$F-FDG PET/CT is more sensitive in detecting lytic bone metastases in breast cancer patients, while Tc-99m methylene diphosphonate bone scintigraphy demonstrates greater sensitivity for detecting sclerotic bone metastases. Recently, a study by Usmani et al. (4) showed low sensitivity and precision of $^{18}$F-FDG PET/CT in identifying bone metastases in patients with lobular breast cancer. The absence of uptake on whole body bone scan despite the presence of sclerotic lesions presents an intriguing diagnostic phenomenon. This discordance may be attributed to several factors, including the subtle nature and small size of the sclerotic lesions, which could fall below the resolution threshold of bone scintigraphy. Additionally, these findings might represent very early metastatic disease that is currently undetectable. Another consideration is the possibility of low osteoblastic activity despite the sclerotic appearance on CT, suggesting a unique biological behavior of these metastatic lesions. MRI demonstrates superior accuracy in the diagnosis of bone metastasis associated with lobular breast cancer. It detects bone metastases at an earlier stage than other imaging techniques. It can identify subtle changes in bone marrow that may not be visible on bone scan, $^{18}$F-FDG PET or CT scans. The rate of misdiagnosis associated with MRI in identifying bone metastasis in lobular breast cancer is comparatively low (5). In untreated patients with ILC, non-FDG-avid sclerotic osseous metastases were found to be significantly more prevalent than in those with IDC. The diagnostic confidence is lower in $^{18}$F-FDG PET/CT in ILC when evaluating for osseous metastases and consideration given to performing a biopsy/MRI or obtaining follow-up imaging before excluding metastatic disease. Our case highlights the need for careful evaluation of any sclerotic lesion in lobular breast cancer patients, even if negative on $^{18}$F-FDG PET/CT, and to consider alternative imaging modalities or more specific PET tracers such as $^{18}$F-fluoroestradiol and $^{68}$Ga-fibroblast activation protein inhibitor-04 as alternative options for comprehensive evaluation of lobular breast cancer metastases (6,7). Furthermore, PET/MRI emerges as a promising hybrid modality that could enhance diagnostic accuracy in such cases. This hybrid technology demonstrates higher sensitivity for detecting bone metastases compared to PET/CT, making it particularly valuable in cases of ILC where metabolic activity is characteristically low. The integration of PET/MRI into the diagnostic algorithm for ILC could potentially bridge the current imaging gaps, though availability and cost considerations may influence its implementation in clinical practice.

## Ethics

**Informed Consent:** The consent was obtained for image use.

## Footnotes

## Authorship Contributions

Surgical and Medical Practices: S.U., K.A.R., A.J., A.A.B., N.A., Concept: S.U., K.A.R., A.J., Design: S.U., V.V.J., S.K., Data Collection or Processing: S.U., K.A.R., A.J., A.A.B., P.D., V.V.J., S.K., N.A., Analysis or Interpretation: S.U., A.J., A.A.B., Literature Search: S.U., N.A., Writing: S.U., K.A.R., N.A.

**Conflict of Interest:** No conflicts of interest were declared by the authors.

**Financial Disclosure:** The authors declare that this study has received no financial support.

## References

1. Hogan MP, Goldman DA, Dashevsky B, Riedl CC, Gönen M, Osborne JR, Jochelson M, Hudis C, Morrow M, Ulaner GA. Comparison of 18F-FDG PET/CT for systemic staging of newly diagnosed invasive lobular carcinoma versus invasive ductal carcinoma. J Nucl Med. 2015;56:1674-1680.
2. Bos R, van Der Hoeven JJ, van Der Wall E, van Der Groep P, van Diest PJ, Comans EF, Joshi U, Semenza GL, Hoekstra OS, Lammertsma AA, Molthoff CF. Biologic correlates of (18)fluorodeoxyglucose uptake in human breast cancer measured by positron emission tomography. J Clin Oncol. 2002;20:379-387.
3. Hamaoka T, Madewell JE, Podoloff DA, Hortobagyi GN, Ueno NT. Bone imaging in metastatic breast cancer. J Clin Oncol. 2004;22:2942-2953.
4. Usmani S, Al Riyami K, Jain A, Alajmi AA, AlBaimani K, Dumasig P, Al Busaidi A, Al Sukati R. Enhancing precision in bone metastasis diagnosis for lobular breast cancer: reassessing the role of 18 F-FDG PET/CT. Nucl Med Commun. 2024;45:858-864.
5. Rong Y, Ren H, Ding X. MRI and bone scintigraphy for breast cancer bone metastase: a meta-analysis. Open Med (Wars). 2019;14:317-323.
6. Sahin E, Kus T, Aytekin A, Uzun E, Elboga U, Yilmaz L, Cayirli YB, Okuyan M, Cimen V, Cimen U. $^{68}$Ga-FAPI PET/CT as an alternative to $^{18}$F-FDG PET/CT in the imaging of invasive lobular breast carcinoma. J Nucl Med. 2024;65:512-519.
7. Ulaner GA, Jhaveri K, Chandarlapaty S, Hatzoglou V, Riedl CC, Lewis JS, Mauguen A. Head-to-head evaluation of $^{18}$F-FES and $^{18}$F-FDG PET/CT in metastatic invasive lobular breast cancer. J Nucl Med. 2021;62:326-331.

*Interesting Image*

*Mol Imaging Radionucl Ther 2025;34:242-245* *DOI:10.4274/mirt.galenos.2025.89847*

# Gluteal Muscle Metastasis of Papillary Thyroid Cancer with Increased Somatostatin Receptor Expression in $^{68}$Ga-DOTATATE PET/MRI

## *Papiller Tiroit Kanserinin Gluteal Kas Metastazında Artmış Somatostatin Ekspresyonunun $^{68}$Ga-DOTATATE PET/MR Görüntüsü*

*Ali Kibar[1], Sertaç Asa[1], Lebriz Uslu-Beşli[1], Mine Önenerk[2], Sait Sağer[1], Kerim Sönmezoğlu[1], Haluk Burçak Sayman[1]*

[1]*İstanbul University-Cerrahpaşa, Cerrahpaşa Faculty of Medicine, Department of Nuclear Medicine, İstanbul, Türkiye*
[2]*İstanbul University-Cerrahpaşa, Cerrahpaşa Faculty of Medicine, Department of Pathology, İstanbul, Türkiye*

### Abstract

A 56-year-old male patient underwent total thyroidectomy, and pathology revealed multicentric papillary thyroid cancer. His post-operative stimulated thyroglobulin value was >500 ng/mL. $^{18}$F-fluorodeoxyglucose positron emission tomography (PET) computed tomography revealed hypermetabolic metastatic pulmonary nodules, cervical, and mediastinal lymph nodes. There was also a hypermetabolic lesion in the left gluteal muscle. Due to the patient's history of a pilonidal cyst in the same region, the possibility of an abscess was also considered, and due to the absence of radioactive iodine (RAI) uptake in the lesion, follow-up was deemed appropriate. During follow-up, as the patient progressed to RAI-refractory state, $^{68}$Ga-DOTATATE PET/magnetic resonance imaging, which was done for radionuclide therapy planning, revealed heterogeneously increased uptake in the gluteal lesion. A subsequent biopsy confirmed the diagnosis of PTC metastasis.

**Keywords:** PET/MRI, FDG, $^{68}$Ga, DOTATATE, thyroid cancer, muscle, metastasis

### Öz

Elli altı yaşında erkek hasta total tiroidektomi sonucunda multifokal papiller tiroid kanseri (PTK) tanısı almıştır. Postoperatif stimüle tiroglobulin değeri >500 ng/mL olarak ölçülmüş olup yapılan $^{18}$F-florodeoksiglukoz pozitron emisyon tomografisi (PET) bilgisayarlı tomografi hipermetabolik metastatik pulmoner nodüller, servikal ve mediastinal lenf nodları saptanmıştır. Ayrıca sol gluteal bölgede kastahipermetabolik bir lezyon saptanmıştır. Aynı bölgede pilonidal kist öyküsü de olan hastada abse ihtimali de değerlendirilmiş olup lezyonda radyoaktif iyot (RAİ) tutulumu da olmaması üzerine takip uygun görülmüştür. RAİ refrakter duruma geçen hastaya yapılan $^{68}$Ga-DOTATATE-PET/manyetik rezonans görüntülemesinde gluteal lezyonda heterojen artmış aktivite tutulumu gözlenmesiyle birlikte yapılan biyopsi PTK metastazı tanısını doğrulamıştır.

**Anahtar kelimeler:** PET/MRI, FDG, $^{68}$Ga DOTATATE, tiroit kanseri, kas, metastaz

**Address for Correspondence:** Ali Kibar, İstanbul University-Cerrahpaşa, Cerrahpaşa Faculty of Medicine, Department of Nuclear Medicine, İstanbul, Türkiye
**E-mail:** alikibar01@gmail.com **ORCID ID:** orcid.org/0000-0003-0073-2343
**Received:** 18.02.2025 **Accepted:** 08.06.2025 **Epub:** 01.08.2025 **Publication Date:** 08.10.2025

**Cite this article as:** Kibar A, Asa S, Uslu-Beşli L, Önenerk M, Sait Sağer S, Sönmezoğlu K, Sayman HB. Gluteal muscle metastasis of papillary thyroid cancer with increased somatostatin receptor expression in $^{68}$Ga-DOTATATE PET/MRI. Mol Imaging Radionucl Ther. 2025;34:242-245.

Copyright© 2025 The Author. Published by Galenos Publishing House on behalf of the Turkish Society of Nuclear Medicine.
This is an open access article under the Creative Commons Attribution-NonCommercial-NoDerivatives 4.0 (CC BY-NC-ND) International License.

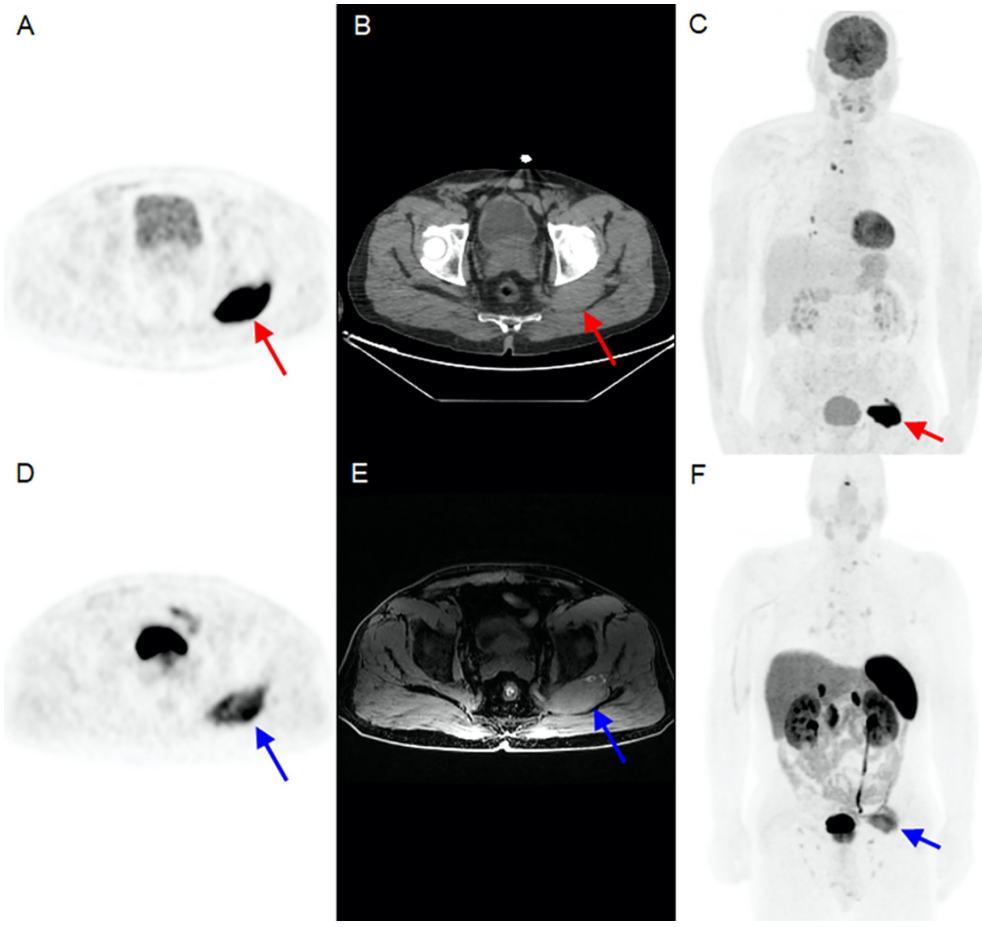



**Figure 1.** $^{18}$F-fluorodeoxyglucose-positron emission tomography ($^{18}$F-FDG PET) is beneficial in high-risk thyroid cancer patients who have increased thyroglobulin (Tg) levels (>10 ng/mL) for both metastasis detection and prognostication (1,2,3). $^{68}$Ga-DOTATATE PET can also be performed for metastasis detection and for $^{177}$Lu DOTATATE treatment planning (4,5,6). While cervical lymph nodes, lungs, and bones are the most common sites of metastasis, papillary thyroid carcinoma (PTC) can also metastasize to the brain, kidneys, liver, and adrenal glands (7). Skeletal muscle metastases are extremely rare (8). Our patient had a bilateral total thyroidectomy operation, and the pathology result revealed multicentric (R: 1.1, 0.3, 0.2 cm; L: 7 cm) PTC (follicular, oncocytic follicular, classical variants, and diffuse sclerosing variant containing tall cell areas) and 1/1 central lymph node metastasis. His post-operative stimulated Tg value was >500 ng/dL, and $^{18}$F-FDG PET/computed tomography was performed to detect metastasis, which revealed cervical and mediastinal lymph nodes, and pulmonary metastases. Moreover, a 75x36x44 mm hypermetabolic lesion was detected inside the left gluteal muscle [maximum standardized uptake value ($SUV_{max}$)=40.08]. After receiving a total of 750 mCi of radioactive iodine (RAI) therapy, the patient was considered RAI-refractory because of sustained high serum Tg levels. The gluteal lesion did not show radioiodine uptake. The patient underwent $^{68}$Ga-DOTATATE PET for radionuclide therapy planning due to a state refractory to RAI. The gluteal lesion showed increased DOTATATE uptake (73x38x40 mm, $SUV_{max}$=10.43), which increased suspicion for the lesion. A biopsy was performed to rule out a second primary malignancy, and it confirmed thyroid cancer metastasis. Besides being extremely rare, this is the first report of a $^{68}$Ga-DOTATATE PET/magnetic resonance imaging (MRI) of thyroid cancer muscle metastasis, to our knowledge. $^{18}$F-FDG PET (A), computed tomography (B), and maximum intensity projection (MIP) (C) images of the patient showed a well-circumscribed left gluteal lesion, which had an intense FDG uptake (red arrows). $^{68}$Ga-DOTATATE PET (D), T1-weighted MRI (E), and MIP (F) images showed heterogeneously increased $^{68}$Ga-DOTATATE uptake (blue arrows).

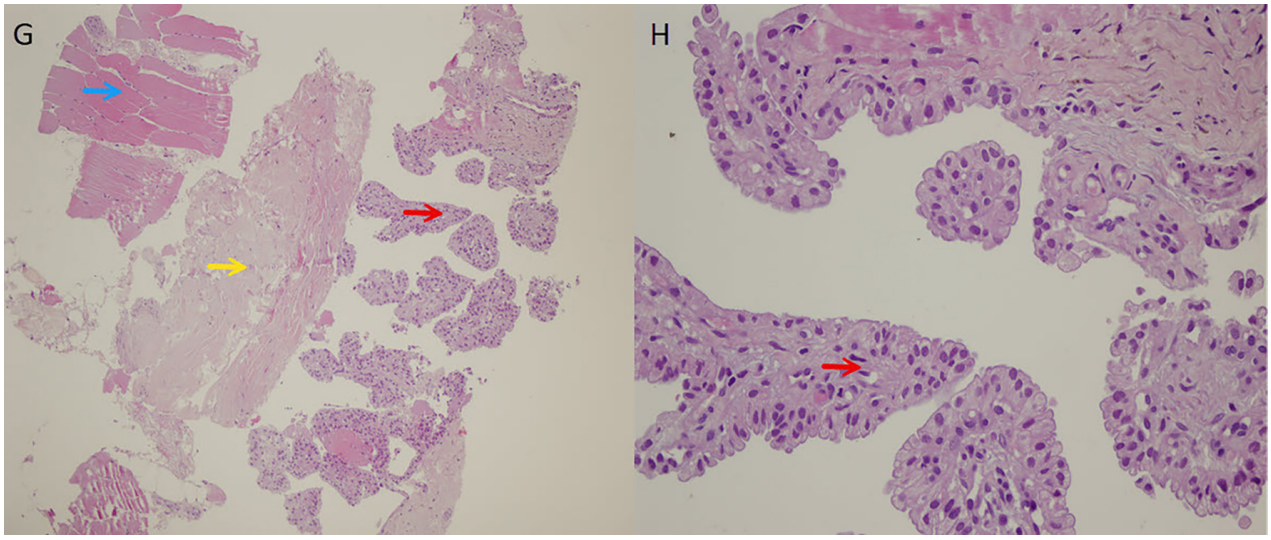



**Figure 2.** Biopsy histological image. Papillary thyroid carcinoma within skeletal muscle and collagenous tissue [H&E, x40 (G) and x400 (H) magnification], skeletal muscle tissue (blue arrow), collagenous fibrous tissue (yellow arrow), thyroid cancer cells (red arrows).

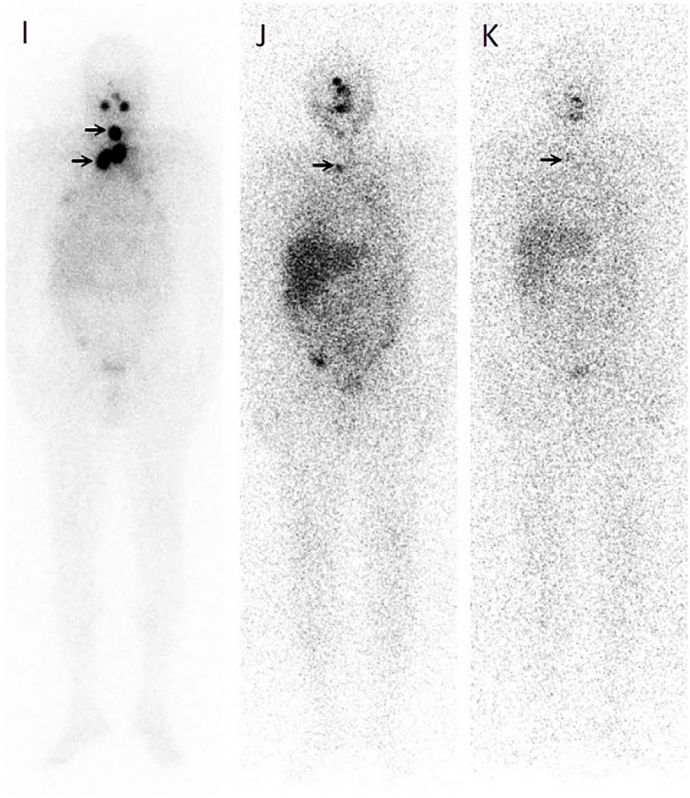



**Figure 3.** Post-RAI MIP images: the first 250 mCi image (I) shows thyroid bed and mediastinal lymph node uptake (black arrows). The second 250 mCi image (J) shows a lymph node uptake (black arrow). The third 250 mCi image (K) shows a more faint lymph node uptake (black arrow). The gluteal lesion did not show uptake.
RAI: Radioactive iodine, MIP: Maximum intensity projection

## Ethics

**Informed Consent:** Informed consent was obtained from the patient for the use of their imaging data.

## Footnotes

## Authorship Contributions

Surgical and Medical Practices: A.K., Concept: A.K., S.A., L-U.B., M.Ö., S.S., K.S., H.B.S., Design: A.K., S.A., Data Collection or Processing: A.K., S.A., L-U.B., M.Ö., S.S., K.S., H.B.S., Analysis or Interpretation: A.K., S.A., L-U.B., M.Ö., S.S., K.S., H.B. S., Literature Search: A.K., Writing: A.K.

**Conflict of Interest:** No conflicts of interest were declared by the authors.

**Financial Disclosure:** The authors declare that this study has received no financial support.

## References

1. Haugen BR, Alexander EK, Bible KC, Doherty GM, Mandel SJ, Nikiforov YE, Pacini F, Randolph GW, Sawka AM, Schlumberger M, Schuff KG, Sherman SI, Sosa JA, Steward DL, Tuttle RM, Wartofsky L. 2015 American thyroid association management guidelines for adult patients with thyroid nodules and differentiated thyroid cancer: the American Thyroid Association Guidelines task force on thyroid nodules and differentiated thyroid cancer. Thyroid. 2016;26:1-133.
2. Haslerud T, Brauckhoff K, Reisæter L, Küfner Lein R, Heinecke A, Varhaug JE, Biermann M. F18-FDG-PET for recurrent differentiated thyroid cancer: a systematic meta-analysis. Acta Radiol. 2016;57:1193-1200.
3. Manohar PM, Beesley LJ, Bellile EL, Worden FP, Avram AM. Prognostic value of FDG-PET/CT metabolic parameters in metastatic radioiodine-refractory differentiated thyroid cancer. Clin Nucl Med. 2018;43:641-647.
4. Roll W, Riemann B, Schäfers M, Stegger L, Vrachimis A. 177Lu-DOTATATE Therapy in radioiodine-refractory differentiated thyroid cancer: a single center experience. Clin Nucl Med. 2018;43:e346-e351.
5. Vrachimis A, Stegger L, Wenning C, Noto B, Burg MC, Konnert JR, Allkemper T, Heindel W, Riemann B, Schäfers M, Weckesser M. [(68) Ga]DOTATATE PET/MRI and [(18)F]FDG PET/CT are complementary and superior to diffusion-weighted MR imaging for radioactive-iodine-refractory differentiated thyroid cancer. Eur J Nucl Med Mol Imaging. 2016;43:1765-1772.
6. Versari A, Sollini M, Frasoldati A, Fraternali A, Filice A, Froio A, Asti M, Fioroni F, Cremonini N, Putzer D, Erba PA. Differentiated thyroid cancer: a new perspective with radiolabeled somatostatin analogues for imaging and treatment of patients. Thyroid. 2014;24:715-726.
7. UpToDate. https://www.uptodate.com/contents/papillary-thyroid-cancer-clinical-features-and-prognosis (2025, accessed February 2025)
8. Herbowski L. Skeletal muscle metastases from papillary and follicular thyroid carcinomas: An extensive review of the literature. Oncol Lett. 2018;15:7083-7089.

*Mol Imaging Radionucl Ther 2025;34:246-248* *DOI:10.4274/mirt.galenos.2025.43402*

# An Interesting Case of Fornix Rupture Discovered Accidentally on Bone Scintigraphy

## *Kemik Sintigrafisinde Tesadüfen Saptanan İlginç Bir Forniks Rüptürü Olgusu*

***Salah Nabih Oueriagli, Ayoub Dribla, Omar Ait Sahel, Yassir Benameur, Abderrahim Doudouh***

*Military University Hospital, Clinic of Nuclear Medicine, Rabat, Morocco*

**Abstract**

A 62-year-old male patient, with bladder carcinoma, was referred to our institution for Technetium-99m methylene diphosphonate bone scintigraphy to assess for bone metastasis. While the bone scan showed no abnormal uptake, extraosseous uptake was detected in the left perirenal and pelvic regions on the whole body scan. Computed tomography showed fornix rupture and demonstrated tracer pooling in the perirenal collection. Our diagnosis was very consistent, and oriented the therapeutic attitude towards a percutaneous drainage for the perinephric urinary leak.

**Keywords:** Urinoma, bone scintigraphy, bladder carcinoma

**Öz**

Mesane karsinomu olan 62 yaşında bir erkek hasta, kemik metastazını değerlendirmek üzere Teknesyum-99m metilen difosfonat kemik sintigrafisi için kurumumuza sevk edildi. Kemik taramasında anormal tutulum görülmezken, tüm vücut taramasında sol perirenal ve pelvik bölgelerde ekstraosseöz tutulum tespit edildi. Bilgisayarlı tomografi, forniks rüptürü ve perirenal koleksiyonda radyoaktivite birikimi gösterdi. Tanımız oldukça tutarlıydı ve tedavi yaklaşımımızı perinefrik idrar kaçağı için perkütan drenaja yönlendirdi.

**Anahtar kelimeler:** Ürinom, kemik sintigrafisi, mesane karsinomu

**Address for Correspondence:** Salah Nabih Oueriagli, Military University Hospital, Clinic of Nuclear Medicine, Rabat, Morocco
**E-mail:** salah.nabihoueriagli@gmail.com **ORCID ID:** orcid.org/0000-0001-7824-3158
**Received:** 18.02.2025 **Accepted:** 15.06.2025 **Epub:** 01.08.2025 **Publication Date:** 08.10.2025

**Cite this article as:** Oueriagli SN, Dribla A, Sahel OA, Benameur Y, Doudouh A. An interesting case of fornix rupture discovered accidentally on bone scintigraphy. Mol Imaging Radionucl Ther. 2025;34:246-248.

Copyright© 2025 The Author. Published by Galenos Publishing House on behalf of the Turkish Society of Nuclear Medicine.
This is an open access article under the Creative Commons Attribution-NonCommercial-NoDerivatives 4.0 (CC BY-NC-ND) International License.

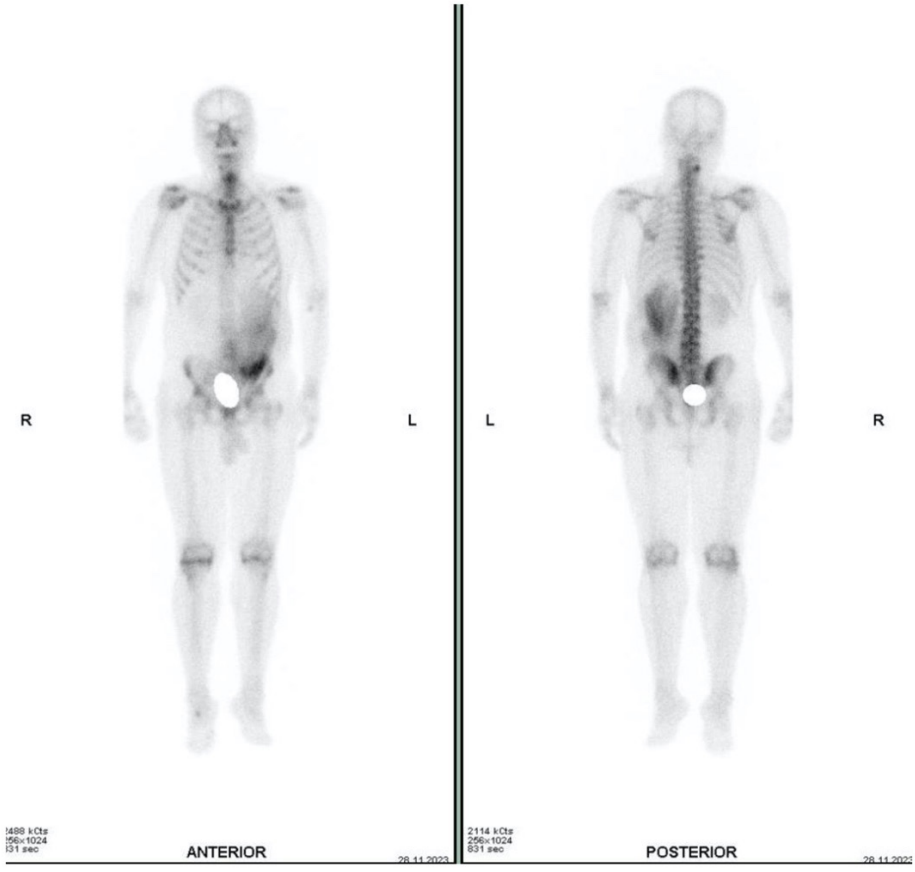



**Figure 1.** Urinary collecting system rupture, leading to perirenal or retroperitoneal urine extravasation, is a rare complication often associated with urinary tract obstruction. A urinoma refers to a localized accumulation of urine in the retroperitoneum, outside the urinary tract, and typically occurs due to injury to the urinary system wall. Ureteral obstruction caused by a bladder tumor represents a rare cause of urinoma (1). We report an interesting case of a 62-year-old man with a history of bladder carcinoma, referred to our institution for bone scintigraphy as part of the initial staging of his neoplastic disease. Bone scintigraphy with Technetium-99m hydroxymethylene diphosphate in planar anterior and posterior views revealed an area of extraosseous uptake in the left perirenal and pelvic regions, likely related to fornix rupture, with no suspicious hypermetabolic foci suggestive of bone metastasis.

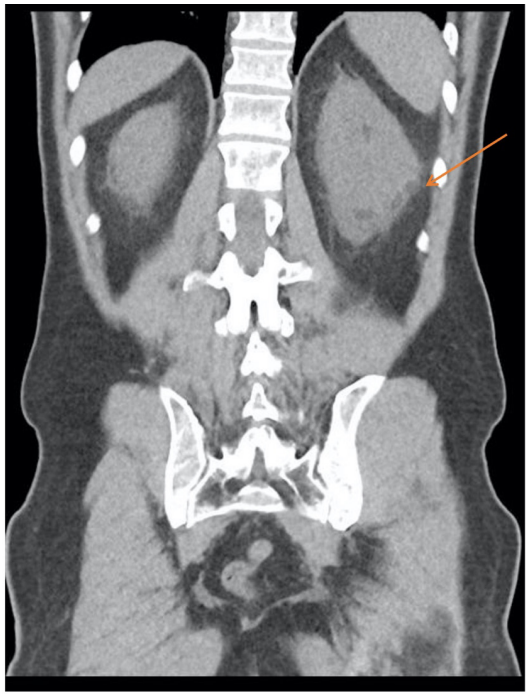


**Figure 2.** A history of mild abdominal pain in the left flank was reported. Our diagnosis was confirmed by an abdominopelvic computed tomography scan, showing fornix rupture with perirenal collection consistent with perirenal leak. Next day, the therapeutic approach towards percutaneous drainage was indicated for our patient.

Urinoma is a rare pathology linked to ureteral obstruction (commonly due to calculi) (2). It may also result from retroperitoneal fibrosis, pelvic mass, ureteropelvic junction obstruction, and pregnancy (1). Ureteric obstruction by neoplasm is a rare cause of spontaneous urinary leak and it is not typically detected via bone scintigraphy (3). However, the presence of radiotracer excretion outside the genitourinary tract can help in diagnosing urinary leaks (4). Incidental findings of urinary leaks have been reported in literature with others radiotracers which are normally excreted by the kidneys such as: Fluorine-18 fluorodeoxyglucose and iodine-123 metaiodobenzylguanidine, (5). The significance of this case lies in the unexpected discovery of a urinary leak during oncologic evaluation via bone scintigraphy.

### Ethics

**Informed Consent:** The institutional review board of our institute "Med V Military Teaching Hospital" approved this publication, and the requirement to obtain informed consent was waived.

### Footnotes

### Authorship Contributions

Concept: S.N.O., A.D., A.D., Design: S.N.O., A.D., A.D., Data Collection or Processing: S.N.O., A.D., A.D., Analysis or Interpretation: S.N.O., Y.B., A.D., Literature Search: S.N.O., O.A.S., Writing: S.N.O.

**Conflict of Interest:** No conflicts of interest were declared by the authors.

**Financial Disclosure:** The authors declare that this study has received no financial support.

## References

1. Doehn C, Fiola L, Peter M, Jocham D. Ursachen und verlauf bei fornixruptur [causes and course of fornix rupture]. Aktuelle Urol. 2010;41:119-121.
2. Wimpissinger F, Türk C, Kheyfets O, Stackl W. The silence of the stones: asymptomatic ureteral calculi. J Urol. 2007;178:1341-1344.
3. Grosse A, Grosse C. Bildgebungsmodalitäten und therapieoptionen bei patienten mit akutem flankenschmerz [imaging modalities and therapy options in patients with acute flank pain]. Radiologe. 2014;54:700-714.
4. Vadi SK, Dasagrandhi V, Bhattacharya A, Singh SK, Mittal BR. Incidental detection of perinephric urinary leak on bone scintigraphy in a patient with urinary bladder carcinoma. Indian J Nucl Med. 2018;33:68-70.
5. Banzo I, Martinez-Rodriguez I, Quirce R, Jimenez-Bonilla J, Sainz-Esteban A, Barragán J, Portilla-Quattocciochi H, Medina-Quiroz P, Carril JM. Incidental detection of renal transplantation urinary leakage on FDG-PET/CT imaging for evaluation of lung metastases. Clin Nucl Med. 2009;34:924-926.

*Interesting Image*

*Mol Imaging Radionucl Ther 2025;34:249-251* *DOI:10.4274/mirt.galenos.2025.03764*

# Rare Acute Polyarticular Gout Disease Detected with $^{18}$F-FDG PET/CT

## *$^{18}$F-FDG PET/BT ile Tespit Edilen Nadir Akut Poliartiküler Gut Hastalığı*

***Zehranur Tosunoğlu[1], Ayşe Nur Toksöz Yıldırım[2], Esra Arslan[1], Göksel Alçın[1], Elife Akgün[1]***

*[1]University of Health Sciences Türkiye, İstanbul Training and Research Hospital, Clinic of Nuclear Medicine, İstanbul, Türkiye*
*[2]Göztepe Prof. Dr. Süleyman Yalçın City Hospital, Clinic of Pathology, İstanbul, Türkiye*

**Abstract**

Gout is an inflammatory arthropathy that develops due to the accumulation of monosodium urate crystals in the joints in adults. In approximately half of the cases, it presents as monoarthritis with an acute attack involving the first metatarsophalangeal joint. The first attack is rarely polyarticular. Herein, we present a male patient who presented with swelling and acute pain in the 5$^{th}$ toe but $^{18}$F-fluorodeoxyglucose positron emission tomography/computed tomography showed symmetric polyarticular involvement which was mimicking arthritis.

**Keywords:** Gout disease, $^{18}$F-FDG PET/CT, arthritis

**Öz**

Gut, yetişkinlerde eklemlerde monosodyum ürat kristallerinin birikmesi nedeniyle gelişen bir enflamatuvar artropatidir. Olguların yaklaşık yarısında, birinci metatarsofalangeal eklemi içeren akut atakla monoartrit olarak ortaya çıkar. İlk atak nadiren poliartikülerdir. Burada, 5. ayak parmağında şişlik ve akut ağrı ile başvuran ancak $^{18}$F-fluorodeoksiglukoz pozitron emisyon tomografisi/bilgisayarlı tomografi'de artriti taklit eden simetrik poliartiküler tutulum gösteren bir erkek hastayı sunuyoruz.

**Anahtar kelimeler:** Gut, hastalık, $^{18}$F-FDG PET/BT, artrit

**Address for Correspondence:** Elife Akgün, University of Health Sciences Türkiye, İstanbul Training and Research Hospital, Clinic of Nuclear Medicine, İstanbul, Türkiye
**E-mail:** elifekaymak@hotmail.com **ORCID ID:** orcid.org/0000-0001-5625-9749
**Received:** 27.04.2025 **Accepted:** 19.06.2025 **Epub:** 01.08.2025 **Publication Date:** 08.10.2025

**Cite this article as:** Tosunoğlu Z, Toksöz Yıldırım AN, Arslan E, Alçın G, Akgün E. Rare acute polyarticular gout disease detected with $^{18}$F-FDG PET/CT. Mol Imaging Radionucl Ther. 2025;34:249-251.

Copyright© 2025 The Author. Published by Galenos Publishing House on behalf of the Turkish Society of Nuclear Medicine.
This is an open access article under the Creative Commons Attribution-NonCommercial-NoDerivatives 4.0 (CC BY-NC-ND) International License.

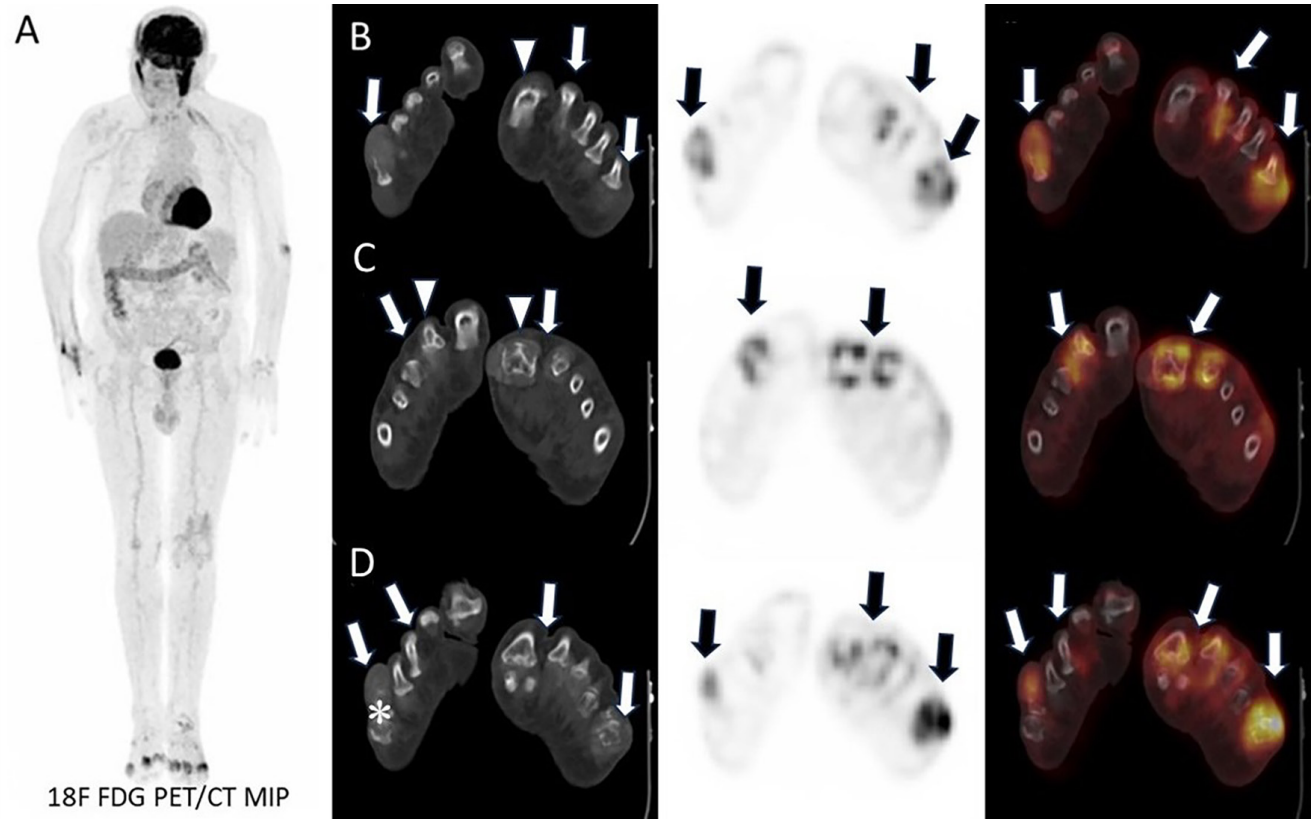



**Figure 1.** An 84-year-old man, with a known history of hypertension, asthma, and coronary artery disease, presented to the orthopedics clinic with complaints of acute swelling and pain in the right fifth toe. The patient had not experienced similar complaints previously. Magnetic resonance imaging revealed T2 hyperintense nodular images on the articular surfaces of the 1st and 2nd metatarsophalangeal joints of the right foot. A hyperintense mass was observed on imaging distal to the 2nd metatarsal, extending to the phalanx, disrupting the cortex, and spreading into the soft tissue. Additionally, a mass was detected in the distal phalanx of the 5th toe which destroys the bone cortex and extends into the soft tissue. To rule out malignancy, $^{18}$F-fluorodeoxyglucose positron emission tomography/computed tomography ($^{18}$F-FDG PET/CT) was performed (A). Significant increased $^{18}$F-FDG uptake was detected in bilateral intertarsal, tarsometatarsal, metatarsophalangeal, and interphalangeal joints which was more pronounced on the left side (line B, C, and D: arrows). CT images revealed destruction of the cortices of the bones adjacent to the metatarsophalangeal joint surfaces (line B, C: arrowhead), and soft tissues around the joints (line D: asterix) While active symmetric bilateral arthritis was primarily considered, no findings suggestive of malignancy were found in the other parts of the body.
$^{18}$F-FDG PET/CT: $^{18}$F-fluorodeoxyglucose positron emission tomography/computed tomography, MIP: Maximum intensity projection

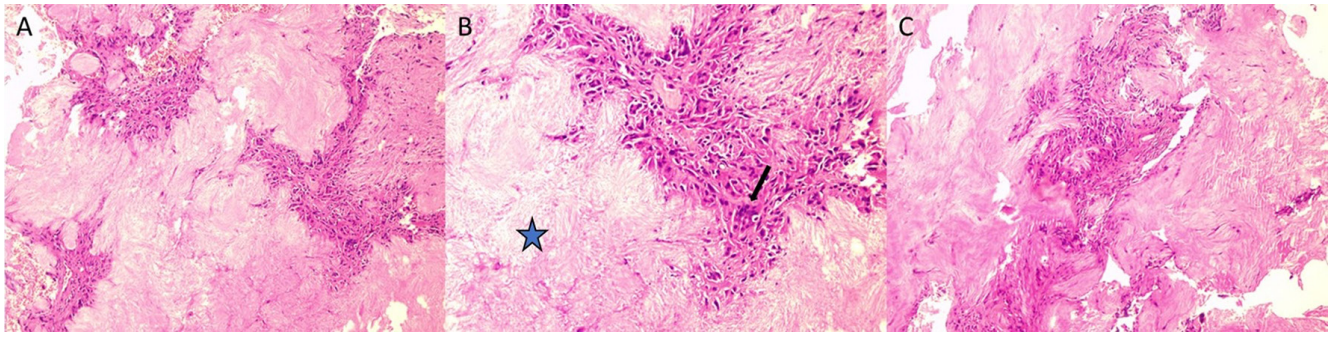



**Figure 2.** A biopsy was performed from the distal left 5$^{th}$ metatarsal and the right 5$^{th}$ interphalangeal joints (A, B, C: hematoxylin and eosin x 100). Amorphous, pale eosinophilic material with a nodular appearance (B: star) was observed within the fibrous tissue, surrounded by palisade-arranged histiocytes and multinucleated giant cells, (B: arrow). The biopsy result was reported as consistent with gout involvement.

$^{18}$F-fluorodeoxyglucose ($^{18}$F-FDG) is not specific to cancer. Increased $^{18}$F-FDG uptake can be detected in cells involved in inflammation due to increased glucose metabolism (1). Therefore, $^{18}$F-FDG is an ideal biological marker for evaluating arthritic disorders (2). In gout arthritis, moderate $^{18}$F-FDG uptake can be observed in tophi, adjacent joints, and soft tissues (2,3). $^{18}$F-FDG uptake is generally lower than that seen in malignant lesions (4). Polyarticular involvement of gout disease is unusual. It can mimic other rheumatological arthritis or more rarely metastatic disease on $^{18}$F-FDG positron emission tomography/computed tomography (PET/CT) (1,5). Arthritic symptoms can also be caused by paraneoplastic events, such as carcinoma polyarthritis (6). However, periarticular localization observed on CT, along with juxta-articular erosive lesions that have sclerotic and protruding borders, suggests gout (7,8). In elderly men who undergo $^{18}$F-FDG PET/CT imaging to rule out malignancy, as in our case, focal $^{18}$F-FDG uptake due to gouty arthropathy should be considered. There are limited data in the literature showing the benefits of functional imaging in gouty arthropathy. Excluding malignancy and early detection of the disease with $^{18}$F-FDG PET/CT can lead to earlier treatment and improved patient outcomes.

## Ethics

**Informed Consent:** The written and verbal informed consent was obtained from the patient.

## Footnotes

## Authorship Contributions

Surgical and Medical Practices: Z.N.T., E.A., Concept: A.N.T.Y., E.A., E.A., Design: G.A., E.A., Data Collection or Processing: Z.N.T., E.A., Analysis or Interpretation: A.N.T.Y., E.A., G.A., Literature Search: Z.N.T., G.A., E.A., Writing: E.A.

**Conflict of Interest:** No conflicts of interest were declared by the authors.

**Financial Disclosure:** The authors declare that this study has received no financial support.

## References

1. Kwee TC, de Klerk JMH, Nix M, Heggelman BGF, Dubois SV, Adams HJA. Benign bone conditions that may be FDG-avid and mimic malignancy. Semin Nucl Med. 2017;47:322-351.
2. Carey K, Saboury B, Basu S, Brothers A, Ogdie A, Werner T, Torigian DA, Alavi A. Evolving role of FDG PET imaging in assessing joint disorders: a systematic review. Eur J Nucl Med Mol Imaging. 2011;38:1939-1955.
3. Davies J, Riede P, van Langevelde K, Teh J. Recent developments in advanced imaging in gout. Ther Adv Musculoskelet Dis. 2019;11:1759720X19844429.
4. Parathithasan N, Lee WK, Pianta M, Oon S, Perera W. Gouty arthropathy: review of clinico-pathologic and imaging features. J Med Imaging Radiat Oncol. 2016;60:9-20.
5. Jamar F, van der Laken CJ, Panagiotidis E, Steinz MM, van der Geest KSM, Graham RNJ, Gheysens O. Update on imaging of ınflammatory arthritis and related disorders. Semin Nucl Med. 2023;53:287-300.
6. Rybak LD, Rosenthal DI. Radiological imaging for the diagnosis of bone metastases. Q J Nucl Med. 2001;45:53-64.
7. Ito K, Minamimoto R, Morooka M, Kubota K. A case of gouty arthritis to tophi on 18F-FDG PET/CT imaging. Clin Nucl Med. 2012;37:614-617.
8. Weaver JS, Vina ER, Munk PL, Klauser AS, Elifritz JM, Taljanovic MS. Gouty arthropathy: review of clinical manifestations and treatment, with emphasis on ımaging. J Clin Med. 2021;11:166.

*Interesting Image*

*Mol Imaging Radionucl Ther 2025;34:252-254* *DOI:10.4274/mirt.galenos.2025.80947*

# $^{18}$F-FDG PET/CT Detection of Extensive Pleural Metastasis in Rare Malignancy Thymoma

## *Nadir Bir Malignite Olan Timomada Yaygın Plevral Metastazın $^{18}$F-FDG PET/BT ile Tespiti*

*Mehmet Oğuz Kartal[1], Berna Okudan[2]*

[1]*University of Health Sciences Türkiye, Elazığ Fethi Sekin City Hospital, Clinic of Nuclear Medicine, Elazığ, Türkiye*
[2]*Ankara Bilkent City Hospital, Clinic of Nuclear Medicine, Ankara, Türkiye*

**Abstract**

The majority of metastatic pleural lesions are caused by malignancies such as bronchogenic carcinoma (40%), breast cancer (20%), lymphoma (10%), and ovarian or gastric carcinomas (5%). However, pleural metastases from thymoma are extremely rare. In this report, we present the $^{18}$F-fluorodeoxyglucose ($^{18}$F-FDG) positron emission tomography/computed tomography (PET/CT) imaging findings of a patient with thymoma and extensive pleural metastases. Although biopsy remains the gold standard for diagnosis, it is important to consider high grade thymoma in the differential diagnosis, as extensive pleural involvement observed on $^{18}$F-FDG PET/CT imaging can mimic both primary and metastatic pleural malignancies. Recognizing this possibility can assist in more accurate interpretation of imaging findings.

**Keywords:** Thymoma, pleura, metastasis, $^{18}$FDG, PET/CT

**Öz**

Metastatik plevral lezyonların büyük çoğunluğunu bronkojenik karsinom (%40), meme kanseri (%20), lenfoma (%10), over ve gastrik kanserler (%5) gibi malignitelerden kaynaklanmaktadır. Timomanın plevral metastazları ise oldukça nadir görülmektedir. Bu olguda yaygın plevral metastaz saptanan timoma hastasına ait $^{18}$F-florodeoksiglukoz ($^{18}$F-FDG) pozitron emisyon tomografi/bilgisayarlı tomografi (PET/BT) görüntülerini paylaşıyoruz. Her ne kadar altın standart biyopsi tanısı olsa da, yaygın plevral tutulumların $^{18}$F-FDG PET/CT görüntüsü itibarı ile primer ve metastatik plevral maligniteleri taklit edebileceğinden ayırıcı tanıda yüksek grade timomayı hatırlamak görüntüyü daha doğru yorumlamaya yardımcı olacaktır.

**Anahtar kelimeler:** Timoma, plevral, metastaz, $^{18}$FDG, PET/BT

**Address for Correspondence:** Mehmet Oğuz Kartal, University of Health Sciences Türkiye, Elazığ Fethi Sekin City Hospital, Clinic of Nuclear Medicine, Elazığ, Türkiye
**E-mail:** m.oguzkartal@gmail.com **ORCID ID:** orcid.org/0009-0009-6440-4219
**Received:** 09.01.2025 **Accepted:** 29.06.2025 **Publication Date:** 08.10.2025

**Cite this article as:** Kartal MO, Okudan B. $^{18}$F-FDG PET/CT detection of extensive pleural metastasis in rare malignancy thymoma. Mol Imaging Radionucl Ther. 2025;34:252-254.

Copyright© 2025 The Author. Published by Galenos Publishing House on behalf of the Turkish Society of Nuclear Medicine.
This is an open access article under the Creative Commons Attribution-NonCommercial-NoDerivatives 4.0 (CC BY-NC-ND) International License.

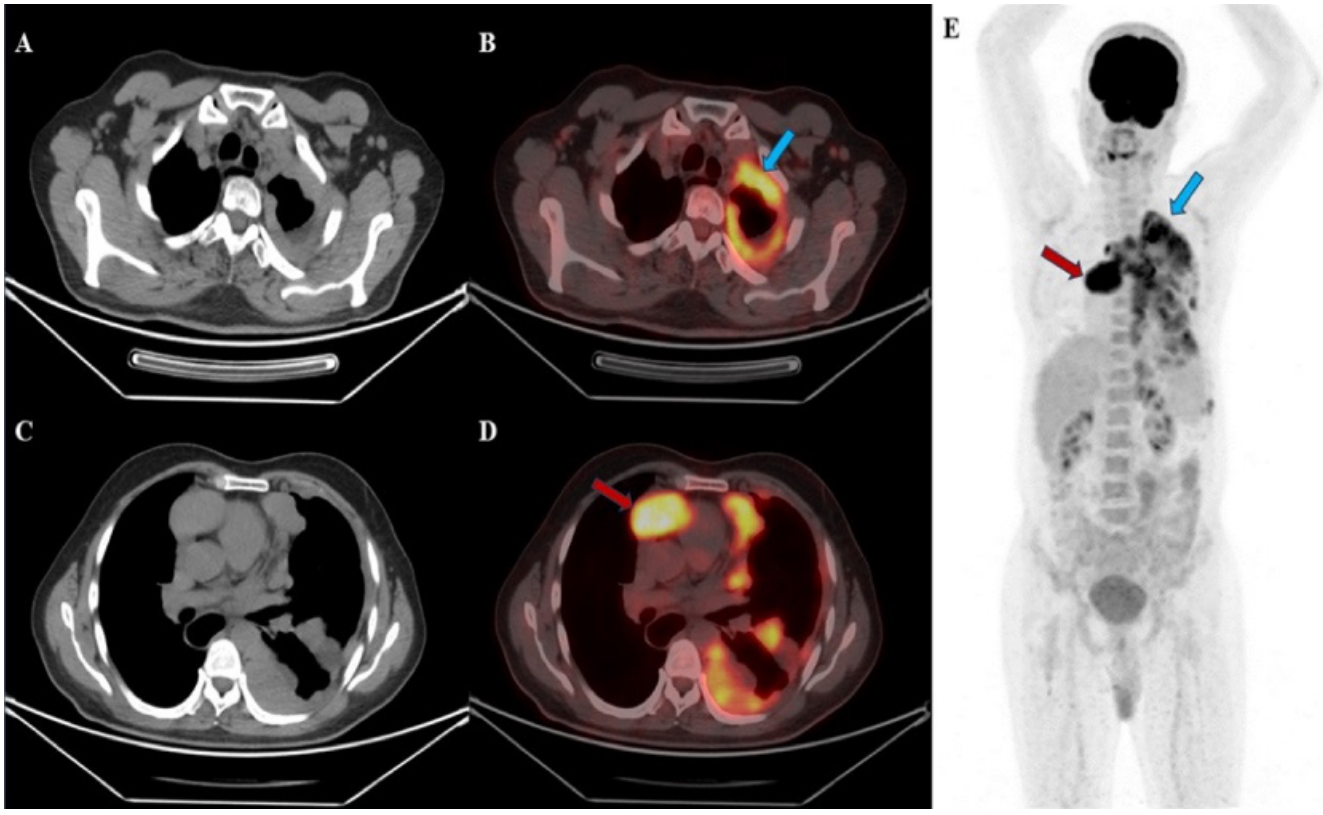



**Figure 1.** A 49-year-old male presented to the outpatient clinic with progressive shortness of breath and a persistent cough. Thoracic computed tomography (CT) demonstrated multiple nodular masses, measuring up to 4 cm, involving the mediastinal, costal, and diaphragmatic pleura (Figures A, C). Additional conglomerated nodular lesions were identified in the anterior mediastinum. Histopathological evaluation of a tru-cut biopsy from a suspected primary pleural malignancy confirmed the presence of a malignant thymic epithelial neoplasm, consistent with thymoma. Immunohistochemical staining showed neoplastic cells positive for TdT, PanCK, and p63, while calretinin and thyroid transcription factor-1 were negative. Due to limited biopsy material, precise World Health Organization (WHO) subtype classification could not be performed.
$^{18}$F-fluorodeoxyglucose ($^{18}$F-FDG) positron emission tomography (PET))/CT imaging provided further diagnostic confirmation, revealing increased $^{18}$F-FDG uptake in a soft tissue lesion located in the anterior mediastinum measuring 64 × 44 mm (Figures D, E, red arrow) with a maximum standardized uptake value ($SUV_{max}$) of 11.11. Additional elevated FDG uptake was observed in pleural masses in the left hemithorax (Figures B, D, blue arrow) with an $SUV_{max}$ of 7.99. No pleural effusion was identified, and physiological FDG distribution was noted in other regions of the body (Figure E).
Thymomas are classified into five histological subtypes (A, AB, B1, B2, and B3) based on the WHO classification. Subtypes A, AB, and B1 are considered low risk for recurrence, whereas subtypes B2 and B3 are categorized as high-risk, with a greater propensity for metastasis and recurrence (1). Thymomas are rare neoplasms that generally grow slowly and exhibit local spread. Common metastatic sites include the pleura, pericardium, and diaphragm, while extrathoracic metastases are uncommon (2).
Although pleural metastases of high-risk thymoma are rare, they can mimic the imaging features of primary pleural malignancies or metastatic pleural disease (3). Therefore, it is important to consider high-grade thymoma in the differential diagnosis when pleural involvement is observed. Careful evaluation of the anterior mediastinum in such cases may facilitate accurate diagnosis and significantly impact treatment planning. This case highlights the diagnostic value of $^{18}$F-FDG PET/CT and underscores its critical role in differentiating thymomas with pleural involvement (4,5).

### Ethics

**Informed Consent:** The patient consent was obtained.

### Footnotes

### Authorship Contributions

Surgical and Medical Practices: M.O.K., B.O.T., Concept: M.O.K., B.O.T., Design: M.O.K., B.O.T., Data Collection or Processing: M.O.K., B.O.T., Analysis or Interpretation: M.O.K., B.O.T., Literature Search: M.O.K., B.O.T., Writing: M.O.K., B.O.T.

**Conflict of Interest:** No conflicts of interest were declared by the authors.

**Financial Disclosure:** The authors declare that this study has received no financial support.

## References

1. Sandri A, Cusumano G, Lococo F, Alifano M, Granone P, Margaritora S, Cesario A, Oliaro A, Filosso P, Regnard JF, Ruffini E. Long-term results after treatment for recurrent thymoma: a multicenter analysis. J Thorac Oncol. 2014;9:1796-1804.
2. Falkson CB, Bezjak A, Darling G, Gregg R, Malthaner R, Maziak DE, Yu E, Smith CA, McNair S, Ung YC, Evans WK; Lung Cancer Disease Site Group of Cancer Care Ontario's Program in Evidence-Based Care. The management of thymoma: a systematic review and practice guideline. J Thorac Oncol. 2009;4:911-919.
3. Qureshi NR, Gleeson FV. Imaging of pleural disease. Clin Chest Med. 2006;27:193-213.
4. Tumapon D, Kim EE. Recurrent Thymoma with lung, pleural, and splenic metastases demonstrated on F-18 FDG PET/CT. OALib. 2023;10:1-6.
5. Gajendra S, Sahoo MK. (18)F FDG-PET/CT of malignant thymoma with pleural and diaphragmatic metastases. Lung India. 2016;33:116-177.

*Letter to the Editor*

*Mol Imaging Radionucl Ther 2025;34:255* *DOI:10.4274/mirt.galenos.2025.29577*

# Comment on the Use of the ThyPRO Questionnaire in Turkish Populations: Methodological Consideration

## *ThyPRO Anketinin Türk Popülasyonlarında Kullanımına İlişkin Yorum: Metodolojik Değerlendirme*

*Aziz Gültekin*

*Pamukkale University Faculty of Medicine, Department of Nuclear Medicine, Denizli, Türkiye*

**Keywords:** Health-related quality of life (HRQoL), questionnaire validity, hyperthyroidism
**Anahtar kelimeler:** Sağlıkla ilişkili yaşam kalitesi (HRQoL), anket geçerliliği, hipertiroidizm

**Dear Editor,**

I have read with great interest the article by Afşin and Çalışkan (1) titled "Quality of Life Outcomes Following Radioactive Iodine-131 Therapy in Hyperthyroid Patients: Insights from the Thyroid Patient-Reported Outcome Questionnaire," recently published in Molecular Imaging and Radionuclide Therapy.

While the topic is undoubtedly relevant and the study presents promising findings regarding the impact of radioactive iodine (RAI) therapy on quality of life (QoL) in hyperthyroid patients, I would like to raise a methodological concern that may impact the interpretability of the results.

The authors have utilized the thyroid patient-reported outcome (ThyPRO) questionnaire to assess QoL changes before and after RAI therapy. However, to the best of my knowledge, no formal validity and reliability study has yet been conducted for the Turkish version of the ThyPRO instrument. The absence of a culturally and linguistically validated version of the tool may introduce bias, limit interpretability, and compromise the internal validity of the results.

Given the importance of using psychometrically robust instruments, especially in studies relying on patient-reported outcomes, this issue should be acknowledged as a limitation in the manuscript. I respectfully suggest that future studies using the ThyPRO in Turkish-speaking populations should ensure proper cross-cultural adaptation and psychometric validation in accordance with established guidelines.

Thank you for considering this comment in the spirit of constructive academic discourse.

Sincerely,

### Footnotes

**Conflict of Interest:** No conflict of interest was declared by the authors.

**Financial Disclosure:** The authors declared that this study has received no financial support.

### References

1. Afşin H, Çalışkan B. Quality of life outcomes following radioactive iodine 131 therapy in hyperthyroid patients: insights from the thyroid patient-reported outcome questionnaire. Mol Imaging Radionucl Ther. 2025;34:38-47.

**Address for Correspondence:** Aziz Gültekin, Pamukkale University Faculty of Medicine, Department of Nuclear Medicine, Denizli, Türkiye
**E-mail:** agultekin@pau.edu.tr **ORCID ID:** orcid.org/0000-0002-0311-8077
**Received:** 15.05.2025 **Accepted:** 18.06.2025 **Epub:** 04.08.2025 **Publication Date:** 08.10.2025

**Cite this article as:** Gültekin A. Comment on the use of the ThyPRO questionnaire in Turkish populations: methodological consideration. Mol Imaging Radionucl Ther. 2025;34:255.

Copyright© 2025 The Author. Published by Galenos Publishing House on behalf of the Turkish Society of Nuclear Medicine.
This is an open access article under the Creative Commons Attribution-NonCommercial-NoDerivatives 4.0 (CC BY-NC-ND) International License.

*Review*

*Mol Imaging Radionucl Ther 2025;34:256-266* *DOI:10.4274/mirt.galenos.2025.44452*

# False Positive Findings of $^{68}$Ga-DOTATOC PET/CT: A Systematic Review

## *$^{68}$Ga-DOTATOC PET/BT'nin Yanlış Pozitif Bulguları: Sistematik Derleme*

***Dhuha Al-Adhami[1], Ahmed Saad Abdlkadir[1], Sze Ting Lee[2], Punit Sharma[3], Naser Obeidat[4], Hassan Al-Alawi[1], Mai Hong Son[5], Aysar Khalaf[6], Akram Naif Al-Ibraheem[1]***

[1]*King Hussein Cancer Center (KHCC), Clinic of Nuclear Medicine and PET/CT, Amman, Jordan*
[2]*Austin Health, Clinic of Molecular Imaging and Therapy, Melbourne, Australia*
[3]*Apollo Multispecialty Hospital, Clinic of Nuclear Medicine and PET-CT, Kolkata, India*
[4]*Jordan University of Science and Technology, Faculty of Medicine, Department of Diagnostic Radiology and Nuclear Medicine, Irbid, Jordan*
[5]*Warith International Cancer Institute, Department of Nuclear Medicine, Karbala, Iraq*
[6]*Hospital 108, Clinic of Nuclear Medicine, Hanoi, Vietnam*

### Abstract

This systematic review aimed to explore the currently reported false positive findings of Gallium-68 ($^{68}$Ga)-1, 4, 7, 10-tetraazacyclododecane-1, 4, 7, 10-tetraacetic acid Tyr3-octreotide ($^{68}$Ga-DOTATOC). PubMed, Web of Science, and Scopus databases were used to conduct a systematic search and were updated until March 4, 2024. Three authors independently screened the titles and abstracts of the retrieved articles and selected the articles based on the inclusion and exclusion criteria. In a qualitative analysis of 42 included research articles involving 601 patients, 219 false positive findings were identified and categorized. Non-oncologic etiologies predominated, constituting 50.2% of pitfalls, followed by benign oncologic (27.4%) and malignant neoplasms (22.4%). Anatomically, the abdomen was the most common site for pitfalls (30.6%), followed by the musculoskeletal (22.4%), head and neck (20.5%), and pelvic (14.6%) regions. Chest region findings were least frequent, accounting for only 11.9%. This study elucidates potential false positive findings, predominantly occurring in the abdominal and head-neck regions—primary sites for meningiomas and neuroendocrine tumors (NETs). Understanding these false-positive findings is crucial for accurate diagnosis. Furthermore, recognizing these pitfalls may lead to novel applications of $^{68}$Ga-DOTATOC beyond its conventional use in evaluating NETs and meningiomas, potentially expanding its current utility.

**Keywords:** $^{68}$Ga-DOTATOC, SSTR, PET/CT, false positive findings, false positive uptake, diagnostic pitfalls, pitfalls, systematic review

### Öz

Bu sistematik derlemenin amacı, Galyum-68 ($^{68}$Ga)-1, 4, 7, 10-tetraazasilododeskan-1, 4, 7, 10-tetraasetik asit Tyr3-oktreotid ($^{68}$Ga-DOTATOC) ile bildirilen yanlış pozitif bulguları incelemektir. Sistematik tarama için PubMed, Web of Science ve Scopus veritabanları kullanıldı ve aramalar 4 Mart 2024 tarihine kadar güncellendi. Üç yazar, elde edilen makalelerin başlık ve özetlerini bağımsız olarak tarayarak dahil etme ve dışlama kriterlerine göre seçim yaptı. Altı yüz bir hastayı kapsayan 42 araştırma makalesinin nitel analizinde 219 yanlış pozitif bulgu saptandı ve kategorize edildi.

**Address for Correspondence:** Akram Naif Al-Ibraheem, King Hussein Cancer Center (KHCC), Clinic of Nuclear Medicine and PET/CT, Amman, Jordan
**E-mail:** akramalibrahim@gmail.com **ORCID ID:** orcid.org/0000-0002-0978-4716
**Received:** 21.02.2025 **Accepted:** 29.08.2025 **Publication Date:** 08.10.2025

**Cite this article as:** Al-Adhami D, Abdlkadir AS, Lee ST, Sharma P, Obeidat N, Al-Alawi H, Son MH, Khalaf A, Al-Ibraheem AN. False positive findings of $^{68}$Ga-DOTATOC PET/CT: a systematic review. Mol Imaging Radionucl Ther. 2025;34:256-266.

Copyright© 2025 The Author. Published by Galenos Publishing House on behalf of the Turkish Society of Nuclear Medicine.
This is an open access article under the Creative Commons Attribution-NonCommercial-NoDerivatives 4.0 (CC BY-NC-ND) International License.

Onkolojik olmayan etiyolojiler baskındı ve hataların %50,2'sini oluşturdu; bunu iyi huylu onkolojik (%27,4) ve kötü huylu neoplazmlar (%22,4) izledi. Anatomik olarak en sık hatalar karın bölgesinde (%30,6) görüldü; bunu kas-iskelet sistemi (%22,4), baş-boyun (%20,5) ve pelvik (%14,6) bölgeler takip etti. Göğüs bölgesi bulguları en az sıklıkla görüldü ve yalnızca %11,9 oranında raporlandı. Bu çalışma, yanlış pozitif bulguların çoğunlukla karın ve baş-boyun bölgelerinde ortaya çıktığını ve bunların menenjiyomlar ile nöroendokrin tümörlerin (NET'ler) primer bölgeleri olduğunu göstermektedir. Bu yanlış pozitif bulguların anlaşılması, doğru tanı için kritik öneme sahiptir. Ayrıca bu hataların tanınması, $^{68}$Ga-DOTATOC'un NET'ler ve menenjiyomların değerlendirilmesindeki geleneksel kullanımının ötesinde, potansiyel olarak yeni uygulama alanlarına genişletilmesine katkı sağlayabilir.

**Anahtar kelimeler:** $^{68}$Ga-DOTATOC, SSTR, PET/BT, yanlış pozitif bulgular, yanlış pozitif tutulum, tanısal tuzaklar, tuzaklar, sistematik derleme

## Introduction

Gallium-68 ($^{68}$Ga)-1, 4, 7, 10-tetraazacyclododecane-1, 4, 7, 10-tetraacetic acid Tyr3-octreotide ($^{68}$Ga-DOTATOC) is a positron emission tomography (PET) imaging agent that is expressed primarily in neuroendocrine tumor pathologies and meningiomas and contains abundant somatostatin receptor (SSTR) type 2 (1). In 2001, the first study on this promising PET tracer targeting SSTRs was published, introducing DOTATOC labeled with $^{68}$Ga (2). Multiple comparative studies have been subsequently conducted to benchmark its reliability against the traditionally used $^{111}$In-octreotide single photon emission computed tomography (CT) ovel SSTR imaging agent in different neuroendocrine tumor subtypes (3,4,5). $^{68}$Ga-DOTATOC has generally demonstrated superiority to $^{111}$In-octreotide regarding detection rate, sensitivity, and image resolution (3,4,5).

$^{68}$Ga-DOTATOC is utilized not only for imaging purposes but also for a theranostic approach, a concept that has become increasingly relevant in recent years (6). Radiotheranostics, involving the use of $^{68}$Ga-DOTATOC for quantitative imaging of tumor-related biomarkers, is considered the pinnacle of personalized nuclear medicine (6). Initial evaluation with $^{68}$Ga-DOTATOC aids in identifying individuals suitable for SSTR-based peptide radionuclide receptor therapy (PRRT) (7). Patients who demonstrate positive accumulation of the radiolabeled molecule in tumor lesions are deemed eligible for PRRT, which involves intravenous administration of a SSTR targeting molecule labeled with a therapeutic radionuclide such as lutetium-177-DOTA peptides (7). The increasing use of radiotheranostics in nuclear medicine is currently widely recognized (6).

Although the sensitivity of $^{68}$Ga-DOTATOC PET/CT compared to that of other imaging modalities has been well studied, the cancer specificity and positive predictive value of $^{68}$Ga-DOTATOC-avid PET/CT findings are currently understudied. Pitfalls have been observed to affect various anatomic sites and are linked to various disease entities, potentially limiting optimal diagnostic accuracy (8). With the increasing number of SSTR PET imaging studies performed worldwide, there are consequently many reported cases of false-positive $^{68}$Ga-DOTATOC-avid findings, but most of these findings have been published as case reports.

The objective of this systematic review was to explore the currently reported false positive findings of $^{68}$Ga-DOTATOC and study their relative prevalence, aiming to provide an up-to-date overview relevant for the interpretation of clinical $^{68}$Ga-DOTATOC PET/CT findings.

## Materials and Methods

### Search Strategy

This systematic review adapted its methodology from the guidelines of the preferred reporting items for systematic reviews and meta-analyses (9). The study has not been registered in PROSPERO or any other registration domains. Three authors—DAA, ASA, and AA-I—conducted a systematic search of PubMed, Web of Science, and Scopus-indexed articles to identify research publications exploring SSTR-positive findings beyond physiologic distribution, NETs and meningiomas using $^{68}$Ga-DOTATOC as the primary radiotracer.

The search algorithm combined key terms of interest and their related Medical Subject Headings terms (10). No language or date filters were applied during the data retrieval. The systematic literature search and extraction methods were updated until March 4, 2024. Studies were included if they clearly specified false positive findings and provided patient demographics for individuals with the pitfall of interest. All research papers, except meeting abstracts, were considered eligible for inclusion. Preclinical, simulation, and animal studies were excluded from the analysis.

The same three authors reviewed the titles and abstracts of the retrieved articles using the aforementioned search algorithm. They applied the previously mentioned inclusion and exclusion criteria, eliminating articles that were clearly ineligible.

### Data Extraction

This systematic review extracted comprehensive datasets from the included studies. General extracted information

encompassed the primary author's name, publication year, total study sample size, study language, patient characteristics (such as gender and age), journal name, and article subtype. Additionally, specific qualitative data related to false positive findings were collected, including the name of each diagnostic pitfall, its anatomical site, and its etiology. Microsoft Excel Version 2016 was utilized for data organization and collection.

### Assessment of Methodological Quality and Risk of Bias

The methodological quality of the original articles included in this systematic review, which examine the diagnostic utilities of $^{68}$Ga-DOTATOC PET/CT, was independently evaluated utilizing the standardized Quality Assessment of Diagnostic Accuracy Studies-2 (QUADAS-2) protocol (11). QUADAS-2 scores were analyzed to ascertain the risk of bias and the methodological applicability of the studies (11).

For single reported instances, we employed an adapted version of the CAse REport (CARE) scoring system to evaluate the credibility of the presented data. This methodology utilizes a comprehensive set of 13 parameters outlined in the CARE checklist (12). Adapted CARE quality assessment framework categorizes manuscripts based on criteria adherence: high-quality papers meet at least 10 criteria, intermediate-quality 5-9, and low-quality no more than 4 (13).

## Results

### Study Inclusion

Overall, 42 research articles met the eligibility criteria for the systematic review (Figure 1A) (4,5,6,7,8,14,15,16,17,18, 19,20,21,22,23,24,25,26,27,28,29,30,31,32,33,34,35, 36,37,38,39,40,41,42,43,44,45,46,47,48,49,50,51,52, 53). These studies included a total of 601 patients, with a slight male predominance, constituting approximately 54% of the total patient population. Nearly two third of the included studies were published in journals specializing in nuclear medicine (4,8,14,15,16,17,21,24,25,27,28, 29,31,32,33,34,35,37,38,39,43,45,46,49). The majority of the studies were conducted in European countries, which accounted for the correspondence in 34 studies, representing 81% of the total. Most of the research articles were case reports or interesting images, comprising 60% of the total publications (8,14,16,18,21,23,25,26, 29,31,32,33,34,35,37,39,40,42,43,44,46,48-50,52,53). Original research studies followed in frequency, making up one-third of the total publications and were mostly retrospective in nature (4,15,17,19,20,22,24,27,28,30, 36,38,41,45,51).

Finally, a single review article was identified that showcased a diagnostic pitfall in single reported case (Table 1) (47).

### Methodological Quality

The QUADAS-2 qualitative assessment of original studies (Figure 1B), revealed a high risk of bias and high applicability concerns in the patient selection domain for four studies, primarily due to small sample sizes and suboptimal recruitment strategies (17,19,20,38). An additional study exhibited high patient selection bias risk owing to its limited sample size (30). Two studies demonstrated unclear biases and applicability concerns stemming from retrospective recruitment (27,51). One prospective study showed unclear patient selection applicability due to its limited sample size, potentially affecting generalizability (45). A single study presented unclear applicability concerns due to ambiguous blinding of readers to clinical information (38). Furthermore, one study displayed unclear applicability in reference standards, which were absent for a subset of included patients (19).

Regarding case reports, two-thirds of the reported cases demonstrated high quality according to adapted CARE criteria, while the remaining one-third was of intermediate quality (Figure 1C). Notably, no low-quality case reports were observed. A more comprehensive qualitative assessment is provided in the Supplementary Tables 1 and 2.

### Overview of False Positive Findings

A total of 219 false positive findings were detected, with the most commonly encountered finding being uptake in the pancreatic uncinate process (23.7%), followed by uptake in the vertebral hemangioma (15.9%), uptake in the head and neck squamous cell carcinoma (HNSCC) (14.1%), and non-specific uptake in the prostate (11.4%). All other pitfalls were reported less frequently. All false positive findings were subsequently classified based on their anatomic location and etiology (Table 2).

### Head and Neck Region

The head and neck region ranked third in terms of frequency of false positive findings. HNSCC with avidity for $^{68}$Ga-DOTATOC was the predominant finding in this region. It is noteworthy that malignant causes were more common in this region, with only a small percentage of benign oncologic conditions identified and no non-oncologic causes noted (Table 3).

### Chest Region

The chest region exhibited the lowest frequency of false positive findings. Notably, subacute myocardial infarction was the most commonly observed condition in this area. Subsequently, there were five instances of immunotherapy-

**Table 1. General characteristics of included studies**

| First author, year | Country | Study | Total sample (Gender) | Age | Journal |
|---|---|---|---|---|---|
| Al-Ibraheem, 2022 (16) | Jordan | CR | 1 (1M) | 64 | Nuclear Medicine and Molecular Imaging |
| Al-Ibraheem, 2016 (14) | Jordan | CR | 1 (1M) | 49 | Nuklearmedizin |
| Al-Ibraheem, 2011 (15) | Jordan | OR | 43 (13M, 30F) | 64 | European Journal of Nuclear Medicine and Molecular Imaging |
| Bashir, 2021 (8) | Denmark | CR | 15 (3M, 12F) | 67 | European Journal of Nuclear Medicine and Molecular Imaging |
| Höög, 2018 (26) | Sweden | CR | 2 (2M) | 71 | Clinical Genitourinary Cancer |
| Khalaf, 2020 (29) | Jordan | CR | 1 (1M) | 13 | Nuclear Medicine and Molecular Imaging |
| Johnbeck, 2017 (28) | Denmark | OP | 59 (35M, 24F) | 61 | Journal of Nuclear Medicine |
| Lapa, 2015 (30) | Germany | OP | 12 (7M, 5F) | 52 | International Journal of Cardiology |
| Richard, 2023 (42) | France | CR | 1 (1F) | 73 | Clinical Nuclear Medicine |
| Werner, 2016 (53) | Germany | CR | 5 (3M, 2F) | 61 | Journal of Medical Imaging and Radiation Oncology |
| Putzer, 2009 (41) | Austria | OR | 51 (29M, 22F) | 60 | Journal of Nuclear Medicine |
| Bollano, 2022 (18) | Sweden | CR | 1 (1M) | 20 | European Heart Journal |
| Trevisi, 2022 (50) | Italy | CR | 1 (1F) | 82 | Journal of Cancer Research and Therapeutics |
| Vandekerckhove, 2021 (52) | Belgium | CR | 1 (1M) | 66 | Acta Clinica Belgica |
| Ceccato, 2020 (20) | Italy | OR | 16 (7M, 9F) | 66 | Endocrine Connections |
| Gossili, 2020 (24) | Denmark | OR | 8 (8M) | 67 | Hellenic Journal of Nuclear Medicine |
| Lococo, 2017 (33) | Italy | CR | 1 (1M) | 77 | Clinical Nuclear Medicine |
| Lococo, 2021 (34) | Italy | CR | 5 (1M, 4F) | 67 | Clinical Nuclear Medicine |
| Pinot, 2021 (40) | France | CR | 1 (1M) | 67 | Clinical Nuclear Medicine |
| Umana, 2022 (51) | Italy | OR | 67 (33M, 34F) | 69 | Anticancer Research |
| Treglia, 2014 (49) | Switzerland | CR | 1 (1F) | 48 | Nuclear Medicine and Molecular Imaging |
| Ryoo, 2020 (43) | Korea | CR | 1 (1F) | 55 | Nuclear Medicine and Molecular Imaging |
| Jacobsson, 2012 (27) | Sweden | OR | 50 (26M, 24F) | 59 | Clinical Nuclear Medicine |
| Binse, 2016 (17) | Germany | OR | 15 (8M, 7F) | 59 | Journal of Nuclear Medicine |
| Gilardi, 2017 (23) | Italy | CR | 1 (1F) | 68 | Endocrine |
| Peter, 2014 (39) | Germany | CR | 1 (1M) | 77 | Clinical Nuclear Medicine |
| Gabriel, 2007 (4) | Austria | OP | 84 (48M, 36F) | 58 | Journal of Nuclear Medicine |
| Gauthé, 2018 (22) | Spain | OR | 79 (40M, 39F) | 65 | European Radiology |
| Lorusso, 2021 (35) | Italy | CR | 1 (1M) | 58 | Clinical Nuclear Medicine |
| Fabritius, 2021 (21) | Germany | CR | 1 (1F) | 74 | Clinical Nuclear Medicine |
| Paquet, 2018 (38) | France | OR | 15 (10M, 5F) | 53 | European Journal of Nuclear Medicine and Molecular Imaging |
| Schmidt, 2019 (46) | USA | CR | 1 (1M) | 60 | World Journal of Nuclear Medicine |
| Takesh, 2011 (48) | Germany | CR | 1 (1F) | 59 | Radiology Case Reports |
| Guglielmo, 2022 (25) | Italy | CR | 1 (1M) | 81 | Clinical Nuclear Medicine |
| Sharma, 2013 (47) | India | RA | 7 (2M, 5F) | 38 | American Journal of Roentgenology |
| Boughdad, 2021 (19) | Switzerland | OR | 11 (10M, 1F) | 71 | Journal for ImmunoTherapy of Cancer |
| Mahajan, 2019 (37) | USA | CR | 1 (1M) | 70 | Clinical Nuclear Medicine |
| Saeed, 2022 (44) | Germany | CR | 1 (1M) | 73 | RöFo |

| Table 1. Continued | | | | | |
|---|---|---|---|---|---|
| **First Author, Year** | **Country** | **Study** | **Total sample (Gender)** | **Age** | **Journal** |
| Laurens, 2018 (31) | Netherlands | CR | 1 (1M) | 56 | Clinical Nuclear Medicine |
| Schartinger, 2013 (45) | Austria | OP | 15 (13M, 2F) | 55 | European Journal of Nuclear Medicine and Molecular Imaging |
| Liberini, 2019 (32) | Italy | CR | 1 (1M) | 42 | Clinical Nuclear Medicine |
| Luboldt, 2010 (36) | Germany | OR | 20 (20M) | 67 | Molecular Imaging and Biology |
| CR: Case reports, F: Female, M: Male, OP: Original prospective studies, OR: Original retrospective studies, RA: Review article | | | | | |

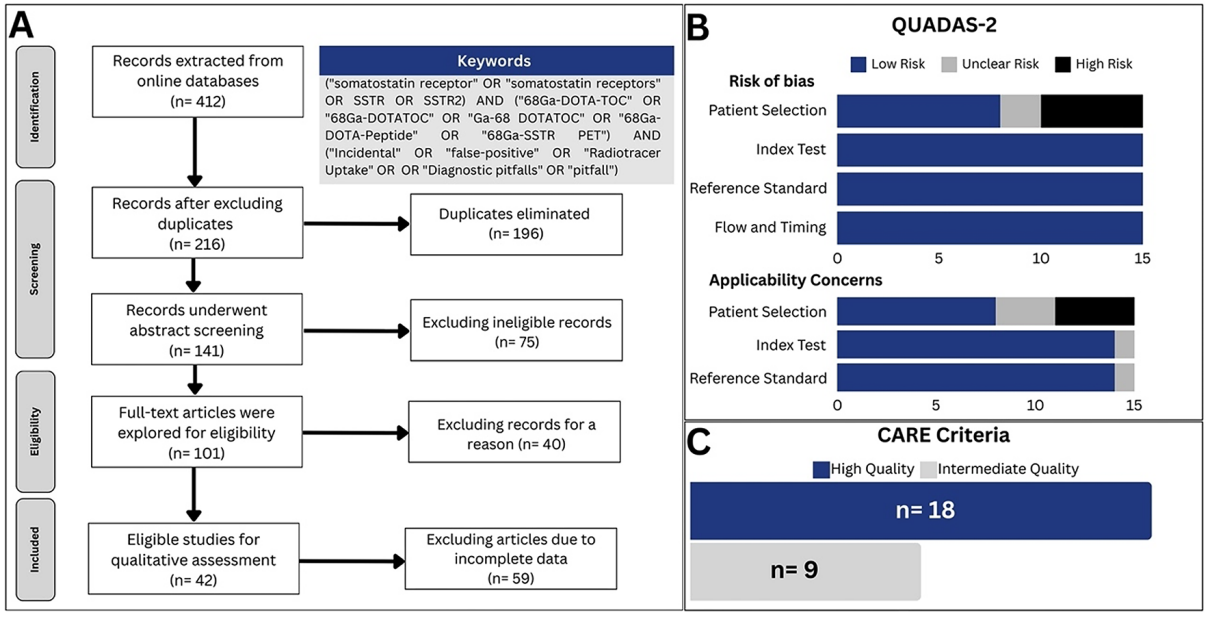



**Figure 1.** (A) A flowchart demonstrating the process of data acquisition, duplicate removal, screening, and final inclusion. (B) Results from standardized Quality Assessment of Diagnostic Accuracy Studies-2 (QUADAS-2) protocol assessment. (C) Results from the adapted CAse REport (CARE) scoring system, OR: Original retrospective studies, SSTR: Somatostatin receptor, 68GA: Gallium-68 PET: Positron emission tomography

induced myocarditis (Figure 2), and five instances of a pleural solitary fibrous tumor. Furthermore, several diagnostic challenges were recorded and categorized (Table 4).

### Abdomen and Pelvis

The abdomen and pelvis are areas in which false positive findings commonly occur. Together, these regions account for approximately 45% of all false positive findings. Pitfalls in the abdomen are more prevalent, representing 30.6%, while pelvic pitfalls make up 14.6% (Figure 3). Within the abdomen, uptake in the pancreatic uncinate process is the most frequently encountered pitfall (23.7%). Whereas, pelvic pitfalls were mostly due to non-specific uptake in the prostate. Additional findings are detailed in Table 5.

| Table 2. Classification of false positive findings based on anatomical location and underlying cause | | |
|---|---|---|
| **Region-based analysis** | | |
| **Anatomic site** | **Number of observations** | **Percentage** |
| Head and neck | 45 | 20.5% |
| Chest | 26 | 11.9% |
| Abdomen | 67 | 30.6% |
| Pelvis | 32 | 14.6% |
| Musculoskeletal | 49 | 22.4% |
| **Etiology-based analysis** | | |
| **Etiology** | **Number of observations** | **Percentage** |
| Non-oncologic etiology | 110 | 50.2% |
| Benign oncologic etiology | 60 | 27.4% |
| Malignant oncologic etiology | 49 | 22.4% |

### Musculoskeletal Region

The musculoskeletal region is the anatomic site where benign oncologic findings are commonly found. Among these findings, vertebral hemangioma was the most frequently observed entity compared to other conditions (Table 6).

### Etiology-based Analysis

Etiology-based analysis revealed that non-oncologic etiologies predominated, constituting 50.2% of pitfalls, followed by benign oncologic etiologies (27.4%) and malignant neoplasms (22.4%). Non-specific $^{68}$Ga-DOTATOC uptake within the pancreatic uncinate process or prostate was the most common cause of non-oncologic findings. Benign oncologic findings were primarily due to vascular tumors (n=38; 63.3% of all benign oncologic findings). HNSCC was the most prevalent malignant oncologic finding (n=31; 63.4% of observed malignancies). A detailed etiology-based analysis is summarized in Supplementary Table 3.

**Table 3. False positive findings in head and neck region**

| Etiology | Finding | Number | Percentage |
|---|---|---|---|
| Malignant oncologic (n=38; 84.5%) | HNSCC | 31 | 68.8% |
| | Poorly differentiated thyroid cancer | 4 | 9% |
| | Papillary thyroid cancer | 1 | 2.22% |
| | CNS lymphoma | 1 | 2.22% |
| | Intracranial metastasis from breast cancer | 1 | 2.22% |
| Benign oncologic (n=7; 15.5%) | Vestibular schwannoma | 3 | 6.7% |
| | Pituitary adenoma | 1 | 2.2% |
| | Parotid basal cell adenoma | 1 | 2.2% |
| | Parotid pleomorphic adenoma | 1 | 2.2% |
| | Intracranial hemangioblastoma | 1 | 2.2% |

CNS: Central nervous system, HNSCC: Head and neck squamous cell carcinoma

## Discussion

A full systematic review of literature exploring false positive findings in $^{68}$Ga-DOTATOC PET/CT imaging is highly relevant, especially given the increased demand and investment following its Food and Drug Administration approval in 2019 (54,55). Understanding the pitfalls, common findings, and physiological uptake of $^{68}$Ga-DOTATOC is essential for accurate interpretation of imaging results, yet these topics have not been adequately studied. This is evident from the fact that the majority of current literature consists merely of case reports shared in isolated instances (8,14,16,18,21,23,25,26,29,31,32,33,34,35,37,39,40,42,43,44,46,48,49,50,52,53). There is also a lack of prospective original studies primarily aimed at identifying false-positive findings (4,30,45).

Overall, 219 false positive findings were observed, with the abdomen being the most frequent site for pitfall occurrence. For instance, pancreatic uncinate process uptake was the most prevalent finding in this systematic

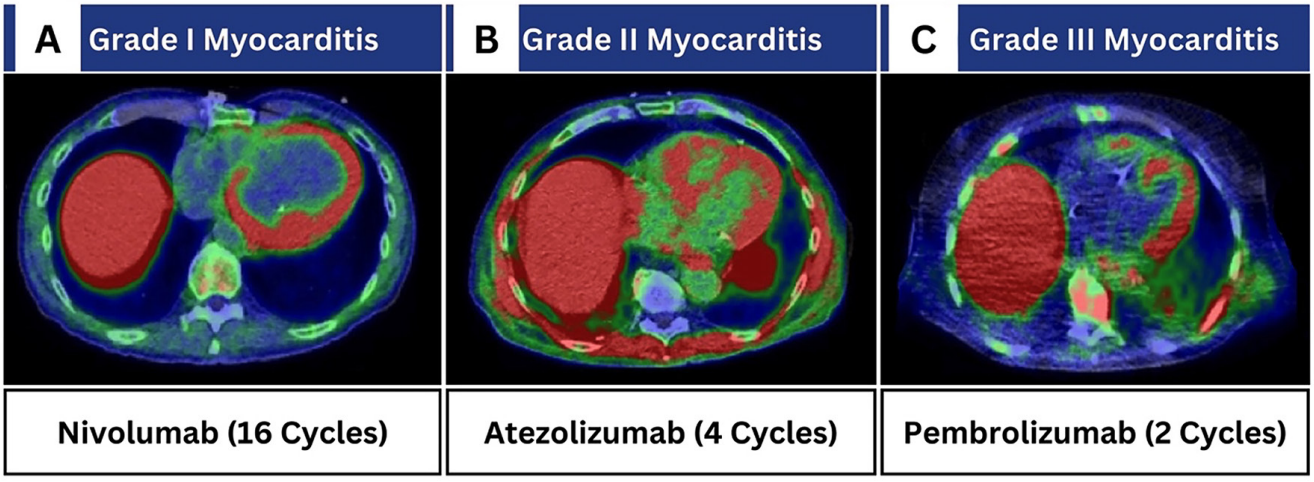



**Figure 2.** (A-C) Fused Gallium-68 ($^{68}$Ga)-1,4,7,10-tetraazacyclododecane-1, 4,7,10-tetraacetic acid Tyr3-octreotide ($^{68}$Ga-DOTATOC) positron emission tomography/computed tomography (PET/CT) images were performed for three cancer patients treated with immune checkpoint inhibitors. The fused axial cardiac PET/CT views reveal (A) diffuse ventricular wall $^{68}$Ga-DOTATOC expression, or (B, C) patchy ventricular wall $^{68}$Ga-DOTATOC expression correlating with clinically confirmed immunotherapy-induced myocarditis. All figure subpanels were reproduced from Figure 1 of previous original research by Boughdad under the Creative Commons license (CC BY 4.0) (19)

review, highlighting significant challenges in evaluating primary and locoregional gastroenteropancreatic neuroendocrine tumors. Historically, pancreatic uncinate process uptake in SSTR imaging was initially thought to be solely part of physiological distribution (56).

**Table 4. False positive findings in the chest region**

| Etiology | Finding | Number | Percentage |
|---|---|---|---|
| Non-oncologic (n=21; 80.8%) | Subacute myocardial infarction | 6 | 23% |
| | Immunotherapy-induced myocarditis | 5 | 19.2% |
| | Acute myocarditis | 3 | 11.5% |
| | Cardiac sarcoidosis | 2 | 7.6% |
| | Acute pericarditis | 1 | 3.9% |
| | Myocarditis post COVID-19 vaccination | 1 | 3.9% |
| | Radiotracer embolus | 1 | 3.9% |
| | Mediastinal lymphadenitis | 1 | 3.9% |
| | Post-surgical chest wall inflammation | 1 | 3.9% |
| Benign oncologic (n=5; 19.2%) | Pleural solitary fibrous tumor | 5 | 19.2% |

COVID-19: Coronavirus disease 2019

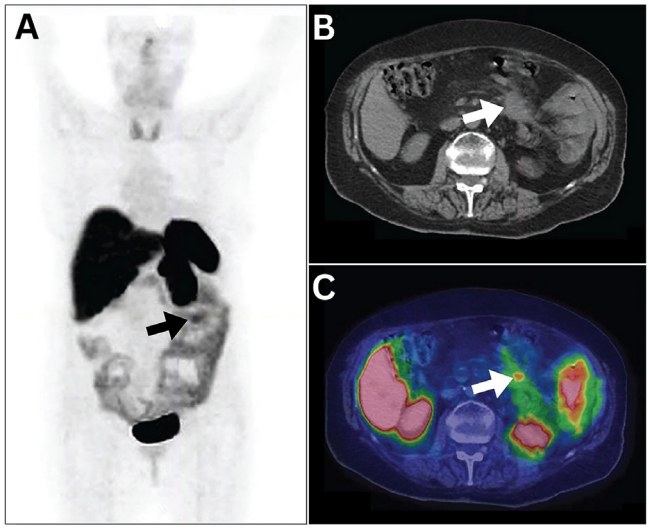



**Figure 3.** (A-C) Maximum intensity projection, axial computed tomography (CT), and fused Gallium-68 ($^{68}$Ga)-DOTATOC positron emission tomography (PET)/CT images performed in an 82-year-old woman with history of resected pancreatic neuroendocrine tumor. A mildly $^{68}$Ga-DOTATOC-avid focus in the proximal jejunum was detected, ultimately diagnosed as mesenteric fibromatosis on histopathology. The figure was reproduced from Figure 1 primary supplied by Trevisi et al. (50) under a Creative Commons license (CC BY-NC-SA 3.0)

However, further research has linked its occurrence to various entities such as pancreatic head polypeptide hyperplasia, insulin resistance, and diabetes (57,58). Current European association of nuclear medicine guidelines advise a thorough assessment of $^{68}$Ga-DOTATOC uptake in the uncinate pancreatic process, emphasizing the importance of comparing PET/CT findings with diagnostic CT images to exclude the presence of any visually identifiable lesions that may necessitate further examination (59). The evaluation of conventional imaging holds significant importance during the reporting process, and it is crucial to consider clinical correlation with underlying chronic conditions to recognize relevant contributing factors. Abdominal splenule also presents a significant diagnostic challenge and is often misattributed to lymph node metastasis or pancreatic neoplasm (43,44,48,49,52,53). Recent reports have marked the successful definitive diagnosis of splenosis through the utilization of technetium-99m-macroaggregated albumin-red blood cell or abdominal magnetic resonance imaging (43,44).

The second most common site for false positive findings was the musculoskeletal system, where vascular tumors, mostly vertebral hemangiomas, predominate and can mimic skeletal metastatic lesions, necessitating imaging correlation for optimal diagnosis (22,23). Third, pitfalls were found in the head and neck regions, mostly due to tumorous etiologies. With the low physiological $^{68}$Ga-DOTATOC uptake in the brain, $^{68}$Ga-DOTATOC might help evaluate various neuro-oncological conditions beyond meningiomas (60). While Schartinger et al. (45) found $^{68}$Ga-DOTATOC expression in therapy-naive HNSCC patients, their uptake was variable, limiting accurate evaluation. However, this study highlighted that more than 93% of studied HNSCC patients had positive SSTR2 expressions on immunohistochemistry (45). Therefore, detection of $^{68}$Ga-DOTATOC-avid focus within the head and neck region should not be automatically attributed to NETs, as many other etiologies can overlap when assessing this challenging region (61).

Another area of potential interest is the thoracic cavity, where myocardial uptake has been predominantly linked to myocardial infarction, inflammation, and immunotherapy adverse effects (18,19,30). Such findings have stimulated many physicians to explore the potential utility of $^{68}$Ga-DOTATOC in these vital conditions, with several clinical trials ongoing to investigate its potential in infective endocarditis (NCT05432427), acute myocarditis (NCT03347760), and cardiac sarcoidosis (NCT04206163).

| Table 5. False positive findings in the abdomen and pelvis | | | |
|---|---|---|---|
| **Abdomen (n=67; 30.6%)** | | | |
| **Etiology** | **Finding** | **Number** | **Percentage** |
| Non-oncologic (n=62; 92.5%) | Pancreatic uncinate process | 52 | 77.6% |
| | Abdominal splenule | 6 | 8.9% |
| | Mesenteric lymphadenitis | 2 | 3% |
| | Acute gastritis | 1 | 1.5% |
| | Chronic pancreatitis | 1 | 1.5% |
| Malignant oncologic (n=4; 6%) | Metastatic pancreatic lesion from RCC | 2 | 3.0% |
| | Primary left RCC | 1 | 1.5% |
| | Abdominal leiomyosarcoma | 1 | 1.5% |
| Benign oncologic (n=1; 1.5%) | Mesenteric fibromatosis (desmoid tumor) | 1 | 1.5% |
| **Pelvis (n=32; 14.6%)** | | | |
| Non-oncologic (n=25; 78.1%) | Non-specific prostatic uptake | 25 | 78.1% |
| Malignant oncologic (n=7; 21.9%) | Primary advanced prostate cancer | 7 | 21.9% |
| RCC: Renal cell carcinoma | | | |

| Table 6. False positive findings in the musculoskeletal system | | | |
|---|---|---|---|
| **Musculoskeletal system (n=49; 22.4%)** | | | |
| **Etiology** | **Finding** | **Number** | **Percentage** |
| Benign oncologic (n=47; 95.9%) | Vertebral hemangioma | 35 | 71.4% |
| | Tumor-induced osteomalacia | 6 | 12.2% |
| | Solitary fibrous tumor | 2 | 4.1% |
| | Capillary angioma | 1 | 2.05% |
| | Non-ossifying fibroma | 1 | 2.05% |
| | Tibial enchondroma | 1 | 2.05% |
| | Spinal hemangioblastoma | 1 | 2.05% |
| Non-oncologic (n=2; 4.1%) | Vertebral osteophyte | 1 | 2.05% |
| | Periarticular vertebral inflammation | 1 | 2.05% |

Within the pelvic region, non-specific prostatic uptake was remarkably prevalent. Gossili et al. (24) reported that 4.5% of men exhibited incidental prostate $^{68}$Ga-DOTATOC uptake during the examination of 178 male patients who underwent 193 $^{68}$Ga-DOTATOC PET/CT studies. After confirming that no malignancy was found in the examined prostate in this population, the authors hypothesized that such incidental $^{68}$Ga-DOTATOC findings are best labeled as non-specific (24). However, this evidence is singular and requires further investigation to explore various factors that may affect such observations. In such circumstances, biochemical correlation can help exclude prostatic malignancies, which can also present as false-positive findings (36).

This study has several limitations, primarily due to the sole reliance on qualitative assessment, while many other important factors such as lesion uptake kinetics and lesion-to-background ratios were not recorded and analyzed. Such datasets were not evenly reported or addressed in the included publications, which were mostly case reports.

## Conclusion

This systematic review explores the potential false positive findings that may arise during $^{68}$Ga-DOTATOC PET imaging. These false positive findings are often seen in the abdominal and head-neck regions, which are common locations for primary meningiomas and neuroendocrine tumor occurrences. Acknowledging these findings serves multiple purposes. Firstly, it raises awareness about possible locations and causes of diagnostic errors in order to prevent misinterpretation and improve reporting. Secondly, identifying these pitfalls may open up new possibilities for the use of $^{68}$Ga-DOTATOC beyond its traditional role in treating NETs and meningiomas, potentially broadening its current applications.

## Footnotes

### Authorship Contributions

Surgical and Medical Practices: D.A-A., A.S.A., S.T.L., N.O., H.A., A.K., M.H.S., A.AI., Concept: D.A-A.,, A.S.A., S.T.L., A.AI., Design: D.A-A., A.S.A., N.O., A.K., M.H.S., Data Collection or Processing: D.A-A., A.S.A., S.T.L., A.AI., Analysis or Interpretation: D.A-A., S.T.L., N.O., A.AI., Literature Search: D.A-A., A.S.A., H.A., Writing: D.A-A., A.S.A., N.O., A.AI.

**Conflict of Interest:** No conflict of interest was declared by the authors.

**Financial Disclosure:** The authors declared that this study received no financial support.

## References

1. Graham MM, Gu X, Ginader T, Breheny P, Sunderland JJ. $^{68}$Ga-DOTATOC imaging of neuroendocrine tumors: a systematic review and metaanalysis. J Nucl Med. 2017;58:1452-1458. Epub 2017 Mar 9. Erratum in: J Nucl Med. 2017;58:1707.
2. Hofmann M, Maecke H, Börner R, Weckesser E, Schöffski P, Oei L, Schumacher J, Henze M, Heppeler A, Meyer J, Knapp H. Biokinetics and imaging with the somatostatin receptor PET radioligand (68)Ga-DOTATOC: preliminary data. Eur J Nucl Med. 2001;28:1751-1757.
3. Van Binnebeek S, Vanbilloen B, Baete K, Terwinghe C, Koole M, Mottaghy FM, Clement PM, Mortelmans L, Bogaerts K, Haustermans K, Nackaerts K, Van Cutsem E, Verslype C, Verbruggen A, Deroose CM. Comparison of diagnostic accuracy of (111) in-pentetreotide SPECT and (68)Ga-DOTATOC PET/CT: a lesion-by-lesion analysis in patients with metastatic neuroendocrine tumours. Eur Radiol. 2016;26:900-909. Epub 2015 Jul 12.
4. Gabriel M, Decristoforo C, Kendler D, Dobrozemsky G, Heute D, Uprimny C, Kovacs P, Von Guggenberg E, Bale R, Virgolini IJ. 68Ga-DOTA-Tyr3-octreotide PET in neuroendocrine tumors: comparison with somatostatin receptor scintigraphy and CT. J Nucl Med. 2007;48:508-518.
5. Buchmann I, Henze M, Engelbrecht S, Eisenhut M, Runz A, Schäfer M, Schilling T, Haufe S, Herrmann T, Haberkorn U. Comparison of 68Ga-DOTATOC PET and 111In-DTPAOC (Octreoscan) SPECT in patients with neuroendocrine tumours. Eur J Nucl Med Mol Imaging. 2007;34:1617-1626. Epub 2007 May 23.
6. Al-Ibraheem A, Zimmermann R, Abdlkadir AS, Herrmann K. Radiotheranostics global market and future developments. Semin Nucl Med. 2024;54:622-633. Epub 2024 Mar 13.
7. Basu S, Parghane RV, Kamaldeep, Chakrabarty S. Peptide receptor radionuclide therapy of neuroendocrine tumors. Semin Nucl Med. 2020;50:447-464. Epub 2020 Jul 3.
8. Bashir A, Broholm H, Clasen-Linde E, Vestergaard MB, Law I. Pearls and pitfalls in interpretation of 68Ga-DOTATOC PET Imaging. Clin Nucl Med. 2020;45:e279-e280.
9. Page MJ, McKenzie JE, Bossuyt PM, Boutron I, Hoffmann TC, Mulrow CD, Shamseer L, Tetzlaff JM, Akl EA, Brennan SE, Chou R, Glanville J, Grimshaw JM, Hróbjartsson A, Lalu MM, Li T, Loder EW, Mayo-Wilson E, McDonald S, McGuinness LA, Stewart LA, Thomas J, Tricco AC, Welch VA, Whiting P, Moher D. The PRISMA 2020 statement: an updated guideline for reporting systematic reviews. BMJ. 2021;372:n71.
10. DeMars MM, Perruso C. MeSH and text-word search strategies: precision, recall, and their implications for library instruction. J Med Libr Assoc. 2022;110:23-33.
11. Whiting PF, Rutjes AW, Westwood ME, Mallett S, Deeks JJ, Reitsma JB, Leeflang MM, Sterne JA, Bossuyt PM; QUADAS-2 Group. QUADAS-2: a revised tool for the quality assessment of diagnostic accuracy studies. Ann Intern Med. 2011;155:529-536.
12. Gagnier JJ, Kienle G, Altman DG, Moher D, Sox H, Riley D; CARE Group. The CARE guidelines: consensus-based clinical case reporting guideline development. Headache. 2013;53:1541-1547.
13. Al-Ibraheem A, Abdlkadir AS, Lopci E, Allouzi S, Paez D, Alkuwari M, Makoseh M, Novruzov F, Usmani S, Al-Rabi K, Mansour A. FDG-PET in chimeric antigen receptor T-cell (CAR T-cell) therapy toxicity: a systematic review. Cancers (Basel). 2024;16:1728.
14. Al-Ibraheem A, Al-Hussaini M, AlSharif A, Abdulelah H. Synchronous presentation of nasopharyngeal carcinoma and abdominal paraganglioma with avid 18F-FDG and 68Ga-DOTA-TOC uptake in PET/CT by both tumours. Nuklearmedizin. 2016;55:N34-5.
15. Al-Ibraheem A, Bundschuh RA, Notni J, Buck A, Winter A, Wester HJ, Schwaiger M, Scheidhauer K. Focal uptake of 68Ga-DOTATOC in the pancreas: pathological or physiological correlate in patients with neuroendocrine tumours? Eur J Nucl Med Mol Imaging. 2011;38:2005-2013. Epub 2011 Jul 27.
16. Al-Ibraheem A, Sweedat DA, Anwer F, Istatieh F, Juweid ME. $^{68}$Ga-dotatoc embolus manifestation and spontaneous resolution by PET/CT. Nucl Med Mol Imaging. 2022;56:208-210. Epub 2022 May 12.
17. Binse I, Poeppel TD, Ruhlmann M, Ezziddin S, Görges R, Sabet A, Beiderwellen K, Bockisch A, Rosenbaum-Krumme SJ. 68Ga-DOTATOC PET/CT in patients with Iodine- and 18F-FDG-negative differentiated thyroid carcinoma and elevated serum thyroglobulin. J Nucl Med. 2016;57:1512-1517. Epub 2016 Mar 31.
18. Bollano E, Bergh N, Dudás A, Bobbio E, Polte CL. Somatostatin receptor positron emission tomography/computed tomography in myocarditis following mRNA COVID-19 vaccination. Eur Heart J Case Rep. 2022;6:ytac117.
19. Boughdad S, Latifyan S, Fenwick C, Bouchaab H, Suffiotti M, Moslehi JJ, Salem JE, Schaefer N, Nicod-Lalonde M, Costes J, Perreau M, Michielin O, Peters S, Prior JO, Obeid M. $^{68}$Ga-DOTATOC PET/CT to detect immune checkpoint inhibitor-related myocarditis. J Immunother Cancer. 2021;9:e003594. Erratum in: J Immunother Cancer. 2022;10:e003594corr1.
20. Ceccato F, Cecchin D, Gregianin M, Ricci G, Campi C, Crimì F, Bergamo M, Versari A, Lacognata C, Rea F, Barbot M, Scaroni C. The role of 68Ga-DOTA derivatives PET-CT in patients with ectopic ACTH syndrome. Endocr Connect. 2020;9:337-345.
21. Fabritius MP, Geyer T, Ahmaddy F, Albert NL, Bartenstein P, Tiling R, Rübenthaler J, Holzgreve A. Breast cancer metastasis mimicking meningioma in 68Ga-DOTATOC PET/CT. Clin Nucl Med. 2021;46:922-923.
22. Gauthé M, Testart Dardel N, Ruiz Santiago F, Ohnona J, Nataf V, Montravers F, Talbot JN. Vertebral metastases from neuroendocrine tumours: how to avoid false positives on $^{68}$Ga-DOTA-TOC PET using CT pattern analysis? Eur Radiol. 2018;28:3943-3952. Epub 2018 Mar 12.
23. Gilardi L, Vadrucci M, Grana CM. Multiple vertebral hemangiomas: a potential pitfall in $^{68}$Ga-DOTATOC PET/CT interpretation. Endocrine. 2017;55:992-993. Epub 2016 Aug 12
24. Gossili F, Almasi CE, Zacho HD, Petersen LMJ. Clinical significance of 68Ga-DOTATOC prostatic uptake on PET/CT: a ten-year review. Eur J Nucl Med Mol Imaging. 2020;47(Suppl 1):S26.
25. Guglielmo P, Pesella F, Sartorello A, El Khouzai B, Berti S, Muccioli S, Gregianin M. metastasis from clear cell renal cell carcinoma mimicking well-differentiated pancreatic neuroendocrine tumor at 18F-FDG and 68Ga-DOTATOC PET/CT. Clin Nucl Med. 2022;47:e498-e499. Epub 2022 Apr 5.
26. Höög A, Kjellman M, Mattsson P, Juhlin CC, Shabo I. Somatostatin receptor expression in renal cell carcinoma-a new front in the diagnostics

and treatment of renal cell carcinoma. Clin Genitourin Cancer. 2018;16:e517-e520. Epub 2018 Mar 27.

27. Jacobsson H, Larsson P, Jonsson C, Jussing E, Grybäck P. Normal uptake of 68Ga-DOTA-TOC by the pancreas uncinate process mimicking malignancy at somatostatin receptor PET. Clin Nucl Med. 2012;37:362-365.
28. Johnbeck CB, Knigge U, Loft A, Berthelsen AK, Mortensen J, Oturai P, Langer SW, Elema DR, Kjaer A. Head-to-head comparison of $^{64}$Cu-DOTATATE and $^{68}$Ga-DOTATOC PET/CT: a prospective study of 59 patients with neuroendocrine tumors. J Nucl Med. 2017;58:451-457. Epub 2016 Sep 22.
29. Khalaf A, Hirmas N, Anwer F, Al-Ibraheem A. $^{68}$Ga DOTA-TOC uptake in non-ossifying fibroma: a case report. Nucl Med Mol Imaging. 2020;54:199-203. Epub 2020 Jul 6.
30. Lapa C, Reiter T, Li X, Werner RA, Samnick S, Jahns R, Buck AK, Ertl G, Bauer WR. Imaging of myocardial inflammation with somatostatin receptor based PET/CT - a comparison to cardiac MRI. Int J Cardiol. 2015;194:44-49. Epub 2015 May 16.
31. Laurens ST, Netea-Maier RT, Aarntzen EJHG. 68Ga-DOTA-TOC uptake in pleomorphic adenoma. Clin Nucl Med. 2018;43:524-525.
32. Liberini V, Nicolotti DG, Maccario M, Finessi M, Deandreis D. 68Ga-DOTA-TOC PET/CT of von Hippel-lindau disease. Clin Nucl Med. 2019;44:125-126.
33. Lococo F, Rapicetta C, Casali M, Bellafiore S, Rossi G, Treglia G, Gasparini E, Paci M. 68Ga-DOTATOC PET/CT imaging in solitary fibrous tumor of the pleura. Clin Nucl Med. 2017;42:e294-e296.
34. Lococo F, Rufini V, Filice A, Paci M, Rindi G. 68Ga-DOTATOC PET/CT in pleural solitary fibrous tumors. Clin Nucl Med. 2021;46:e336-e338.
35. Lorusso M, Angelico G, Quirino M, Scolozzi V, Calcagni ML. 18F-FDG and 68Ga-DOTATOC PET/CT findings in a case of abdominal leiomyosarcoma. Clin Nucl Med. 2021;46:e270-e272.
36. Luboldt W, Zöphel K, Wunderlich G, Abramyuk A, Luboldt HJ, Kotzerke J. Visualization of somatostatin receptors in prostate cancer and its bone metastases with Ga-68-DOTATOC PET/CT. Mol Imaging Biol. 2010;12:78-84. Epub 2009 May 7.
37. Mahajan S, Bodei L, Huicochea Castellanos S, Grewal RK. Enchondroma of tibia as potential false-positive finding on 68Ga-DOTATOC PET/CT scan. Clin Nucl Med. 2019;44:e57-e59.
38. Paquet M, Gauthé M, Zhang Yin J, Nataf V, Bélissant O, Orcel P, Roux C, Talbot JN, Montravers F. Diagnostic performance and impact on patient management of $^{68}$Ga-DOTA-TOC PET/CT for detecting osteomalacia-associated tumours. Eur J Nucl Med Mol Imaging. 2018;45:1710-1720. Epub 2018 Mar 12.
39. Peter L, Sänger J, Hommann M, Baum RP, Kaemmerer D. Molecular imaging of late somatostatin receptor-positive metastases of renal cell carcinoma in the pancreas by 68Ga DOTATOC PET/CT: a rare differential diagnosis to multiple primary pancreatic neuroendocrine tumors. Clin Nucl Med. 2014;39:713-716.
40. Pinot F, Uguen A, Leclere JC, Thuillier P, Abgral R. Incidental finding of a parotid basal cell adenoma with high tracer uptake on 68Ga-DOTATOC PET/CT. Clin Nucl Med. 2021;46:e381-e383.
41. Putzer D, Gabriel M, Henninger B, Kendler D, Uprimny C, Dobrozemsky G, Decristoforo C, Bale RJ, Jaschke W, Virgolini IJ. Bone metastases in patients with neuroendocrine tumor: 68Ga-DOTA-Tyr3-octreotide PET in comparison to CT and bone scintigraphy. J Nucl Med. 2009;50:1214-1221. Epub 2009 Jul 17.
42. Richard C, Cros J, Seban RD, Champion L, Hescot S. 68 Ga-DOTATOC PET/CT imaging of a muscular solitary fibrous tumor. Clin Nucl Med. 2023 May 1;48:e228-e229. Epub 2023 Mar 1.
43. Ryoo HG, Choi H, Cheon GJ. Spleen scan for $^{68}$Ga-DOTATOC PET-positive pancreatic tail lesion: differential diagnosis of neuroendocrine tumor from accessory spleen. Nucl Med Mol Imaging. 2020;54:43-47. Epub 2019 Dec 9.
44. Saeed S, Dimopoulos I, Begum N, Kröger JR. Intrapankreatische Nebenmilz imitiert NET mit falsch positivem somatostatin-rezeptor-PET/CT (68Ga-DOTA-TOC-PET/CT). Rofo. 2022;194:549-552. Epub 2022 Jan 26.
45. Schartinger VH, Dudás J, Url C, Reinold S, Virgolini IJ, Kroiss A, Riechelmann H, Uprimny C. (68)Ga-DOTA (0)-Tyr (3)-octreotide positron emission tomography in nasopharyngeal carcinoma. Eur J Nucl Med Mol Imaging. 2015;42:20-24.
46. Schmidt MQ, Trenbeath Z, Chin BB. Neuroendocrine prostate cancer or prostatitis? An unusual false positive on gallium-68 DOTA-Tyr3-octreotate positron emission tomography/computed tomography in a patient with known metastatic neuroendocrine tumor. World J Nucl Med. 2019;18:304-306.
47. Sharma P, Mukherjee A, Bal C, Malhotra A, Kumar R. Somatostatin receptor-based PET/CT of intracranial tumors: a potential area of application for 68 Ga-DOTA peptides? AJR Am J Roentgenol. 2013;201:1340-1347.
48. Takesh M, Zechmann CM, Kratochwil C, Sahli H, Zein M. Positive somatostatin receptor scintigraphy in accessory spleen mimicking recurrent neuroendocrine tumor. Radiol Case Rep. 2015;6:513.
49. Treglia G, Giovanella L, Muoio B, Caldarella C. Splenosis mimicking relapse of a neuroendocrine tumor at gallium-68-DOTATOC PET/CT. Nucl Med Mol Imaging. 2014;48:163-165. Epub 2013 Nov 26.
50. Trevisi E, Facilissimo I, Taraglio S, Brizzi MP. Fibromatosis mimicking relapse of a neuroendocrine tumor at 68Ga-DOTATOC positron-emission tomography/computed tomography. J Cancer Res Ther. 2022;18:1171-1173.
51. Umana GE, Ferini G, Harikar MM, Venkataram T, Costanzo R, Scalia G, Palmisciano P, Brunasso L, Paolini F, Sciortino A. Detection of "incidentalomas" on brain and body 68Ga-DOTATOC-PET scans: a retrospective study and case illustration. Anticancer Res. 2022;42:5867-5873.
52. Vandekerckhove E, Ameloot E, Hoorens A, De Man K, Berrevoet F, Geboes K. Intrapancreatic accessory spleen mimicking pancreatic NET: can unnecessary surgery be avoided? Acta Clin Belg. 2021;76:492-495. Epub 2020 May 12.
53. Werner C, Winkens T, Freesmeyer M. Splenic scintigraphy for further differentiation of unclear (68) Ga-DOTATOC-PET/CT findings: strengths and limitations. J Med Imaging Radiat Oncol. 2016;60:365-369.
54. Hennrich U, Benešová M. [$^{68}$Ga]Ga-DOTA-TOC: The First FDA-Approved $^{68}$Ga-radiopharmaceutical for pet imaging. Pharmaceuticals (Basel). 2020;13:38.
55. Tabacchi E, Fortunati E, Argalia G, Zanoni L, Calabrò D, Telo S, Campana D, Lamberti G, Ricci C, Casadei R, Fanti S, Ambrosini V. [68Ga]Ga-DOTANOC Uptake at pancreatic head/uncinate process: is it a persistent diagnostic pitfall over time? Cancers (Basel). 2022;14:3541.
56. Brabander T, Teunissen J, Kwekkeboom D. Physiological uptake in the pancreatic head on somatostatin receptor scintigraphy using [111In-DTPA]octreotide: incidence and mechanism. Clin Nucl Med. 2017;42:15-19.
57. Wang X, Zielinski MC, Misawa R, Wen P, Wang TY, Wang CZ, Witkowski P, Hara M. Quantitative analysis of pancreatic polypeptide cell distribution in the human pancreas. PLoS One. 2013;8:e55501. Epub 2013 Jan 31.
58. Bozkurt MF, Virgolini I, Balogova S, Beheshti M, Rubello D, Decristoforo C, Ambrosini V, Kjaer A, Delgado-Bolton R, Kunikowska J, Oyen WJG, Chiti A, Giammarile F, Sundin A, Fanti S. Guideline for PET/CT imaging of neuroendocrine neoplasms with $^{68}$Ga-DOTA-conjugated somatostatin receptor targeting peptides and $^{18}$F-DOPA. Eur J Nucl Med Mol Imaging. 2017;44:1588-1601. 2017 May 25.

59. Bozkurt MF, Virgolini I, Balogova S, Beheshti M, Rubello D, Decristoforo C, Ambrosini V, Kjaer A, Delgado-Bolton R, Kunikowska J, Oyen WJG, Chiti A, Giammarile F, Sundin A, Fanti S. Guideline for PET/CT imaging of neuroendocrine neoplasms with $^{68}$Ga-DOTA-conjugated somatostatin receptor targeting peptides and $^{18}$F-DOPA. Eur J Nucl Med Mol Imaging. 2017;44:1588-1601. Epub 2017 May 25. Erratum in: Eur J Nucl Med Mol Imaging. 2017;44:2150-2151.

60. Abdlkadir AS, Amarin R, Estrada-Lobato E, Al-Ibraheem A. Recurrent sinonasal meningioma: insights from somatostatin receptor imaging. Rev Esp Med Nucl Imagen Mol (Engl Ed). 2024;43:500014. Epub 2024 May 4.

**Supplementary Tables 1-3**

https://d2v96fxpocvxx.cloudfront.net/e851a139-2bc3-493d-b78f-b505df823ad8/content-images/d5f4fc33-c40e-4416-a315-609ff0f178d7.pdf

## 2025 Referee Index - 2025 Hakem Dizini

A. Cahid Civelek
Ahmet Tutuş
Akın Yıldız
Ali Fuat Yapar
Ali Ozan Öner
Ali Sarıkaya
Anil Kumar Pandey
Antonio Italiano
Ayşe Aktaş
Ayşe Mavi
Ayşegül Akgün
Bedri Seven
Bengül Günalp
Berna Okudan Tekin
Bilal Kovan
Billur Çalışkan
Bircan Sönmez
Burçak Yılmaz
Bülent Turgut
Cengiz Taşcı
Claudine Als
Corinna Altini
Cristina Ferrari
Cüneyt Türkmen
Çiğdem Soydal
Doğangün Yüksel
Dr Nosheen Fatima
Dragana Sobic Saranovic
Elgin Özkan
Emre Entok
Eser Lay Ergün
Fatma Suna Kıraç
Fatma Yurt Lambrecht
Feyza Çağlıyan
Fikriye Gül Gümüşer
Fuat Dede
Funda Aydın
Funda Üstün
Gamze Çapa Kaya
Georgios Spyridon Limouris
Giuseppe Rubini
Gonca G. Bural
Gonca Kara Gedik
Gözde Dağlıöz Görür
Guevork A. Kevorkıan
Gülay Durmuş Altun
Hamid Amer
Hanife Aslı Ayan Eke
Hatice Sınav Uslu
Hülya Peker
Irena Dimitrova Kostadinova
İlknur Ak Sivrikoz
İnanç Karapolat
İrfan Peksoy
İsmail Doğan
Jorgen Frockier
Levent Kabasakal
Lieselotte Hojgaard
Lorenzo Biassoni
Mahmut Yüksel
Majid Assadi
Maria Lyra Georgosopoulou
Mehmet Çabuk
Mehmet Emin Mavi
Mehmet Reyhan
Meliha Korkmaz
Meryem Kaya
Metin Halac
Mike Sathekge
Mine Araz
Mustafa Demir
Mustafa Serdengeçti
Nedim C. M. Gülaldı
Neşe Torun
Nilüfer Yıldırım
Nurhan Ergül
Nuri Arslan
Özgül Ekmekçioğlu
Patrick Bourguet
Pelin Arıcan
Pınar Pelin Özcan Kara
Rabia Lebriz Uslu Beşli
Sait M. Sağer
Salih Ozguven
Serdar Savaş Gül
Serkan İşgören
Serkan Kuyumcu
Seval Erhamamcı
Sevin Coşar Ayaz
Seyfettin Ilgan
Tamer Atasever
Tamer Özülker
Tarık Şengöz
Ümmühan Abdülrezzak
Yakup Yürekli
Yasemin Şanlı
Yavuz Narin
Yusuf Demir
Zehra Özcan
Zekiye Hasbek
Zeynep Burak
Zeynep Yapar